Development of Antimalarial Human Monoclonal Antibodies against *Plasmodium falciparum*

A thesis submitted in fulfilment of the requirements for the degree of Doctor of Philosophy

Lawrence T. Wang

Hertford College

Department of Biochemistry, University of Oxford

NIH Oxford-Cambridge Scholars Program

Vaccine Research Center, National Institutes of Health

March 2022

Word Count: ~42,000 words (excluding appendices, references, and figure/table legends)

Abstract

Development of Antimalarial Human Monoclonal Antibodies against *Plasmodium falciparum*

By Lawrence T. Wang

Advances in high-throughput isolation of neutralizing human monoclonal antibodies (mAbs) have enabled development of mAb-based therapeutics for many viruses (e.g., HIV-1, Ebola, SARS-CoV-2). This approach has recently been applied to isolate antimalarial human mAbs against the *Plasmodium falciparum* circumsporozoite protein (CSP) on sporozoites (SPZ) and reticulocyte-binding protein homolog 5 (RH5) on merozoites (MZ). CSP and RH5 are leading malaria vaccine targets because they are respectively required for the SPZ and MZ stages of malaria parasites to invade host hepatocytes and erythrocytes. CSP has three domains: an N-terminus, a central region composed of repeating NPDP/NVDP/NANP tetrapeptides, and a C-terminus. A truncated form of CSP containing 19 NANP repeats and the C-terminus is the antigenic target of the world's only approved malaria vaccine (RTS,S). RTS,S formulated with the adjuvant AS01 elicited protective CSP antibodies but was only 30-50% effective at preventing malaria in a phase III trial. The focus of this Thesis is the isolation of potent human mAbs that bind new sites of vulnerability on CSP (and RH5) in order to facilitate clinical development of promising antimalarial mAbs and improve designs of vaccines targeting these antigens.

Here, and in a Report featured on the cover of *Immunity*, I describe the first human NVDP-specific CSP mAb (L9) that preferentially binds two adjacent NVDP repeats while cross-reacting with NANP repeats. L9 was more potently protective against SPZ challenge in mice than seven published neutralizing human NPDP- and NANP-specific CSP mAbs. Isothermal titration calorimetry and multiphoton microscopy showed that L9 and the other most protective

mAbs bound CSP with a unique "two-step" binding phenotype and mediated protection by killing SPZ in the liver and preventing their egress from sinusoids to invade hepatocytes. This study defined the subdominant NVDP repeats as protective CSP epitopes not included in RTS,S, identified an *in vitro* correlate of mAb-mediated SPZ neutralization, and showed that the liver is an important site for CSP-specific antibodies to prevent malaria. Based on its high potency, a half-life extended version of L9 (L9LS) was clinically developed and completed Phase I testing at the NIH in December 2021 (NCT05019729).

Here, and in a Report published in *Cell Reports*, I show that L9 lineage B cells have baseline NVDP affinity and evolve to acquire NANP reactivity. Pairing the L9 light chain with clonally-related heavy chains resulted in chimeric mAbs that preferentially bound two adjacent NVDP with high affinity, cross-reacted with NANP, and more potently neutralized SPZ compared to their original light chain. X-ray crystal structures of these chimeric mAbs revealed that they bound NANP and NVDP in a similar type-1 β-turn. These data provide insight into the ontogeny and binding mechanisms of the potent NVDP-specific mAb L9 and suggest that RTS,S might be improved by presenting ≥2 adjacent NVDP minor repeats.

Here, and in a Research Article published in *PLOS Pathogens*, I demonstrate that combining two neutralizing "repeat" mAbs against the NPDP/NVDP/NANP tetrapeptides in the central repeat region of CSP, or combining a repeat mAb with mAbs against the C-terminus of CSP, did not provide improved protection against SPZ challenge in mice compared to a single repeat mAb. However, passive transfer of a repeat mAb (e.g., L9) into mice immunized with a RTS,S-like vaccine (which induces polyclonal antibodies against the repeat region and C-terminus of CSP) provided superior protection compared to the mAb or vaccine alone. These data show that, while combining two mAbs against the repeat region and C-terminus of CSP was

ineffective at enhancing SPZ neutralization *in vivo*, protection was enhanced when a mAb was combined with vaccine-induced polyclonal antibodies. Given that RTS,S was recently recommended for widespread usage by the World Health Organization and CSP mAbs like L9 are scheduled to begin Phase II testing in Africa in 2022, these data suggest that combining RTS,S vaccination with passive transfer of potent CSP mAbs should provide even greater protection against malaria.

Additionally, I isolated a panel of >200 human mAbs against RH5 (and its two accessory proteins, CyRPA and Ripr) from naturally infected subjects living in a malaria endemic region of Mali and from naïve subjects in the UK immunized with a RH5 vaccine. Only one study has reported the isolation of 17 RH5 human mAbs, while no CyRPA and Ripr human mAbs have been isolated to date. Determination of the epitopes bound by these mAbs, as well as their potency, is ongoing. If a potent RH5-CyRPA-Ripr-specific mAb is identified, it can potentially be combined with L9 in a multi-stage antimalarial mAb cocktail against both SPZ and MZ.

Acknowledgments

I would like to thank my official principal investigators, Bob Seder and Simon Draper, for providing me with expert scientific mentorship over the last few years. I am particularly grateful for how approachable you have been, the responsibilities and opportunities you bestowed upon me, and your thoughtful nurturing of the skills and credentials I will need to succeed as an aspiring young investigator. Your abilities to quickly provide incisive scientific insights, effectively communicate science, and muster expert collaborators around the world have been particularly inspiring, and I hope to emulate these qualities in my future career. Learning from you and working in both of your labs has provided me with a collection of expert scientists to learn from and a wealth of resources to utilize, all of which have been instrumental in my success as a graduate student.

I would also like to thank my unofficial principal investigator, Josh Tan, for taking me on as an impromptu visiting student in his lab. It has been an incredibly rewarding experience to work alongside and learn from such a hands-on research mentor. I am particularly grateful for the privilege of observing how you have built your lab up as an early-stage investigator and getting to run so many expensive experiments on cutting-edge platforms like the Beacon and Carterra.

I would also like to thank Joe Francica and Azza Idris for their superb leadership of the VRC Malaria Unit, their mentorship over the years, and their companionship at meetings. Thanks for steering me towards certain projects that ended up being more fruitful and answering all my stupid questions over the years. I would also like to thank Barbara Flynn for patiently teaching me so many laboratory techniques; Rachel Vistein and Neville Kisalu for being great lab mates and helping me around the lab; and Lais Pereira, Marlon Dillon, and Brian

Bonilla for undertaking the herculean task of testing the functional effects of my antibodies by challenging mice with sporozoites. I would also like to thank Alexandra Mullen, Kristina Gonzalez-Wartz, and Lauren Purser for making sure I was never in want of reagents, as well as David Ambrozak and Ludmila Krymskaya for running tight ships at the flow core and helping me sort literally hundreds of millions of B cells.

In terms of my colleagues at Oxford, I would like to thank Carolyn Nielsen for her companionship and mentorship over the years, especially for providing me with intelligence on the situation at Oxford when I was at the NIH. Special thanks to Kirsty McHugh, Martino Bardelli, and Dimitra Pipini for taking me under your wings and showing me the ropes in the Draper lab. I am also very grateful to Francesca Donnellan and Barney Williams for answering all my questions about being an Oxford DPhil student and for their companionship in the lab.

Last, but certainly not least, thanks to my mom for always being there for me and wanting to hear about what I was up to in the lab. Being able to count on your unconditional support throughout my life has been an incredible gift I can never repay.

Table of Contents

List of Figures

List of Tables

List of Appendices

List of Acronyms and Abbreviations

AA: amino acid

Abs: absorbance

AF: Alexa Fluor™

AFM: atomic force microscopy

ALF-Q: army liposomal formula Q

ALS: Advanced Light Source

AMA1: apical membrane antigen 1

Apo-L9: L9 Fab alone

AS01: Adjuvant System 01

AUC: area under the curve

BCR: B cell receptors

BLI: biolayer interferometry

BSA: bovine serum albumin

BSA: buried surface area

C-CSP: C-terminus of circumsporozoite protein

C-region: constant region

CD: cytochalasin D

$CD4^+$: cluster of differentiation 4

CF: absorbance correction factor

ChAd63: chimpanzee adenovirus 63

CHMI: controlled human malaria infection

C_H: constant region of heavy chain

C_L: constant region of light chain

CSP: circumsporozoite protein

CSPR: circumsporozoite protein precipitation reaction

CyRPA: cysteine-rich protective antigen

D: diversity

DMEM: Dulbecco's modified eagle medium

Dpi: days post-infection

DsbC: disulfide bond C protein

EC_{50}: effective concentration to mediate 50% inhibition

EC_{80}: effective concentration that elicits 80% protection

ED_{50}: effective dose that elicits 50% protection

ED_{80}: effective dose that elicits 80% protection

EDTA: ethylenediamine tetra acetic acid

EEFs: exoerythrocytic forms

EGF: epidermal growth factor-like

ELISA: enzyme-linked immunosorbent assay

Fab: fragment antigen-binding

FBS: fetal bovine serum

Fc: fragment crystallizable region

FcRn: neonatal fragment crystallizable region receptor

FDA: Food and Drug Administration

FL-rCSP: full-length recombinant *Plasmodium falciparum* circumsporozoite protein

FL: full-length

gDNA: genomic DNA

GFP: green fluorescent protein

GIA: growth inhibition activity

gp120: envelope glycoprotein 120

GPI: glycosylphosphatidylinositol

H: heavy

H.W52: tryptophan at position 52

HCDR3: heavy complementarity-determining region 3

Hpi: hours post-infection

HRP: horse radish peroxidase

HSPGs: heparan sulfate proteoglycans

IC_{50}: half maximal inhibitory concentration

ID: intradermal

Ig: immunoglobulins

IL: interleukin

IMGT: International Immunogenetics Information System

IND: investigational new drug

ITC: isothermal titration calorimetry

IV: intravenous

IVIS: *in vivo* imaging system

J: joining

KCDR3:8: 8–amino-acid–long Vκ complementarity-determining region 3

K_D: dissociation constant

$K_{D(app.)}$: apparent avidity

LS: M451L/N457S mutation

mAbs: monoclonal antibodies

Mali2: Mali subject 2

MBC: memory B cell

MFI: median fluorescence intensity

MG: midgut

MG: midgut

ML: mother liquor

MMS: Mali multiple subjects

MPCCs: micropatterned hepatocyte-fibroblast co-cultures

MR: molecular replacement

MRCA: most recent common ancestor

MSP1: merozoite surface protein 1

MVA: modified vaccinia Ankara

MW: molecular weight

MZ: merozoites

N-CSP: N-terminus of circumsporozoite protein

N: stoichiometry

NHP: non-human primate

NIH: National Institutes of Health

NK cells: natural killer cells

ns: not significant

nt: nucleotide

OD_{450}: optical density at 450 nm

OEP: opto-electropositioning

OR: odds ratio

Pb-PfCSP-SPZ: *Plasmodium berghei* sporozoites expressing *Plasmodium falciparum* circumsporozoite protein

Pb: *Plasmodium berghei*

PBMCs: peripheral blood mononuclear cells

PBS-FBS: phosphate-buffered saline + fetal bovine serum

PBS-PFA: phosphate-buffered saline + paraformaldehyde

PBS: phosphate-buffered saline

PEXEL: Plasmodium export element

Pf_3D7: *Plasmodium falciparum* 3D7 isolate

Pf: *Plasmodium falciparum*

PK: pharmacokinetics

Py: *Plasmodium yoelii*

Q: heat flow

R: correlation coefficient

RCR: RH5, CyRPA, Ripr trimeric protein complex

RH5: reticulocyte-binding protein homolog 5

RI: region I

RII+: region II+

RIII+: region III+

Ripr: RH5-interacting protein

RMSD: root mean square deviation

RONs: rhoptry neck proteins

rPfCSP, rPfCSP_FL, $rPfCSP_{FL}$, FL-rCSP: full-length recombinant Pf circumsporozoite protein

rRNA: ribosomal RNA

RT-PCR: reverse transcription polymerase chain reaction

SA: streptavidin

SD: standard deviation

SEC: size exclusion chromatography

SG: salivary gland

SG: salivary gland

SHM: somatic hypermutation

SP: signal peptide

SPR: surface plasmon resonance

SPZ: sporozoites

t: time

V-region: variable region

V: variable

V_H: variable region of heavy chain

V_L: variable region of light chain

VRC: Vaccine Research Center

WHO: World Health Organization

WT: wild-type

αTSR: α-thrombospondin type-1 repeat

ΔC_p: change in heat capacity

ΔG: change in Gibbs free energy

ΔH: change in enthalpy

ε: extinction coefficient

$-T\Delta S$: change in entropy contribution to Gibbs free energy

2PL: two-parameter logistic

Chapter I: Introduction

1.1 Antibodies

Antibodies (or immunoglobulins, Ig) are soluble proteins that bind to foreign substances called antigens (e.g., proteins, polysaccharides, and glycoproteins)[1]. First described in 1890 by Emil von Behring and Kitasato Shibasaburō as protective bloodborne antitoxins in animals exposed to tetanus or diphtheria toxins[2], antibodies are mainly responsible for binding and neutralizing foreign invaders (e.g., viruses, bacteria, parasites) in extracellular spaces before they invade cells. The structure of antibodies can be broadly subdivided into the variable and constant regions (V- and C-regions), which are composed of two heavy and two light chains (**Figure 1.1**). Heavy chains come in five varieties (IgG, IgA, IgM, IgD, and IgE), while light chains come in two varieties (Igκ and Igλ). The type of heavy chain determines the isotype (or class) of a particular immunoglobulin[1].

The V-region is composed of two fragment antigen-binding (Fab) domains that bind epitopes on antigens and therefore determines the antibody's antigen specificity. The C-region is composed of the fragment crystallizable region (Fc) domain, which binds to receptors on immune cells and thereby mediates effector functions (e.g., recruitment of immune cells to destroy the pathogen). Together, these two regions enable antibodies to perform four basic immunological functions: 1) neutralize pathogens and toxins by directly binding them, 2) opsonize pathogens and recruit immune cells like macrophages to phagocytose the pathogens, 3) fix complement to pathogens and mediate the formation of the membrane attack complex to lyse their membranes, and 4) recruit natural killer (NK) cells to degranulate and kill infected cells.

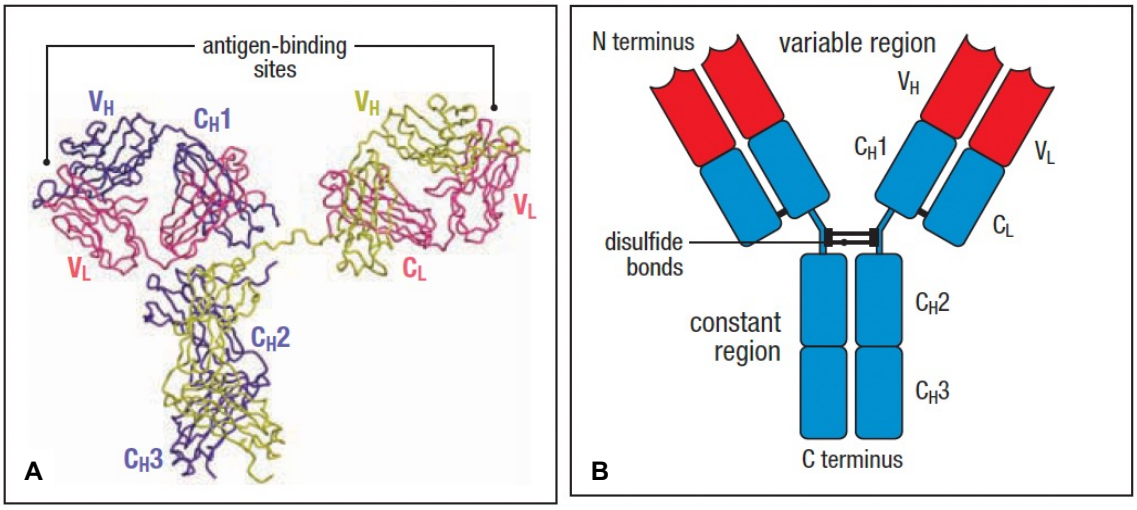

Figure 1.1: Structure of an IgG antibody. A) IgG X-ray crystallographic structure expressed as a ribbon diagram. The two heavy chains (purple and yellow) and two light chains (red) form three globular regions that together approximate a Y shape. The variable regions of the heavy and light chains (V_H and V_L, respectively) form the antibody's antigen-binding sites at the two tips of the Y and are tethered to the trunk of the Y by a flexible hinge region. The heavy and light chain constant regions (C_H1-3 and C_L) are shown. **B)** A simplified schematic of the IgG structure respectively showing the variable and constant regions in red and blue. The two heavy chains are linked by a disulfide bond. Figure and legend adapted from Janeway's Immunobiology (9th edition)[1].

1.1.1 Antibody Diversity

Antibodies are secreted by B cells (or B lymphocytes), which also bear membrane-bound antibodies on their surface called B cell receptors (BCR). B cells are major components of the adaptive immune system's humoral response because the antibodies they produce can recognize and bind essentially any substance[1]. This immunological diversity is a defining feature of the adaptive immune system and is exemplified by B cells being able to produce a theoretical repertoire of a quintillion (~10^{18}) unique antibodies[3]. This massive degree of antibody diversity enables the immune system to respond to the myriad array of microbes and other foreign substances that the body encounters throughout its lifespan.

The adaptive immune system's ability to respond to foreign invaders is attributed to the theory of clonal selection (**Figure 1.2**). In the context of mature naïve B cells, high-affinity

interaction of the B cell's unique BCR with its cognate antigen activates the B cell causing it to proliferate into clones identical to itself. These effector cells all bear the same unique BCR and secrete the same antibody to eliminate the source of the antigen that activated the parental B cell. Once these effector cells eliminate the threat, most of them die upon contraction of the immune response; however, a few persist to mediate immunological memory in case the same antigen is re-encountered. Thus, multiple distinct B cell lineages each clonally proliferate and produce different antibodies when a new antigen is encountered, resulting in a diverse polyclonal B cell and antibody response that binds multiple epitopes on the same antigen[1].

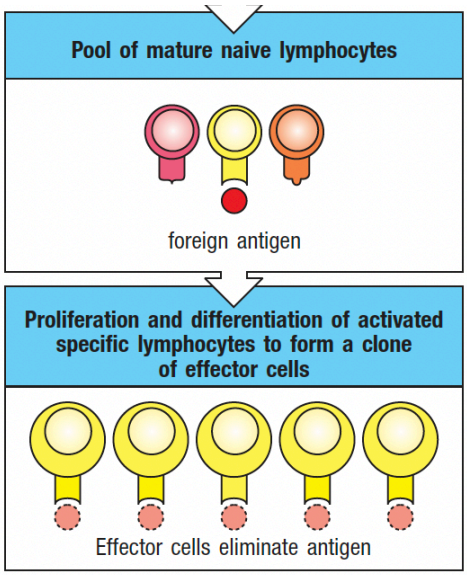

Figure 1.2: Clonal selection of lymphocytes. A foreign antigen (red dot) binds to the receptor on a mature naïve lymphocyte (i.e., B cell), which activates that cell and causes it to begin proliferating and differentiating into identical clones of itself which all bear the same BCR. Figure and legend adapted from Janeway's Immunobiology (9th edition)[1].

1.1.2 Monoclonal Antibodies

Given the reductionism at the core of biological investigation, it was necessary to parse the complexity of polyclonal antibodies by isolating and studying monoclonal antibodies (mAbs) that originate from a single B cell lineage and bind a single epitope on an antigen. In 1975, Georges Köhler and César Milstein reported the first protocol for producing mAbs by fusing

antibody-producing splenocytes from immunized mice with immortalized myeloma cell lines. These so-called "hybridomas" formed colonies of identical cells that could be continuously cultured and would secrete the same mouse mAb for scientists to harvest[4]. This seminal discovery showed that mAbs against any desired antigen could be produced in the lab, which revolutionized biomedical research and led to the development of countless antibody-based laboratory reagents, diagnostic tests, and therapeutics[5].

Since the invention of hybridoma technology, several more high-throughput techniques have been developed to isolate fully human mAbs for use as drugs because human mAbs are generally safer and better tolerated than non-human mAbs. These technological advances include phage display, transgenic mice, B cell immortalization, and single B cell cloning (**Figure 1.3**)[6] and have led to the isolation of human mAbs that are being used as prophylactic or therapeutic drugs against various pathogens, mainly viruses (e.g., HIV, Ebola, SARS-CoV-2)[7–9].

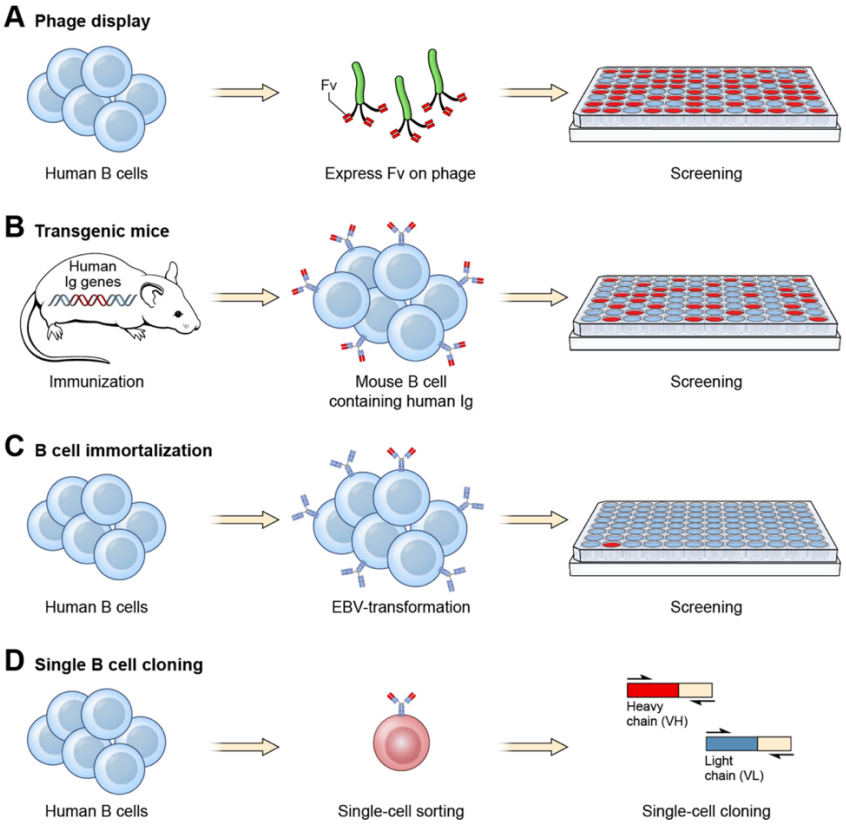

Figure 1.3: Four techniques for isolating human mAbs. (A) Single-chain variable fragment or Fabs from human B cells are expressed on phages and used to create huge phage display libraries that are screened for antigen-specific phage clones. **(B)** Transgenic mice with human Ig genes are immunized with an antigen and used to produce stable mouse B cell lines that secrete fully human mAbs. Antigen-specific mAbs can be identified by screening. **(C)** Human B cells are immortalized by transformation with Epstein-Barr virus and screened for binding to the desired antigen. **(D)** Single antigen-specific human B cells are sorted by flow cytometry and their immunoglobulin genes are amplified using reverse transcription polymerase chain reaction (RT-PCR). These gene sequences are cloned into vectors, expressed as antibodies using cell lines, and screened for antigen specificity. Figure and legend adapted from Ho et al[6].

1.2 Malaria

Malaria is an ancient scourge of mankind, having afflicted humanity throughout much of our evolutionary history. The earliest recorded references of this parasitic mosquito-borne disease are found in Chinese texts dating from ~2700 BC, while parasite DNA has been detected in Egyptian mummies from ~2000 BC[10]. Over the millennia, these parasites have exerted more evolutionary pressure on humanity than any other pathogen and may have killed nearly half of all humans that ever lived (though this startling statistic is difficult to definitively prove)[11,12]. There are six species of *Plasmodium* parasites that infect humans (*P. falciparum, vivax, malariae, ovale curtisi*, *ovale wallikeri*, and *knowelsi*), with *P. falciparum* (Pf) being the deadliest species responsible for the most malaria-associated mortality and *P. vivax* being the most geographically widespread[13].

The clinical symptoms of Pf malaria begin ~10-14 days after a human is bitten by a Pf-infected mosquito and include fever, chills, myalgia, sweating, malaise, headaches, nausea, vomiting, and diarrhea. Severe malaria can lead to anemia, pulmonary edema, kidney failure, and cerebral malaria (i.e., the deadliest consequence of this disease). Malaria inflicts the greatest harm on infants, children, and pregnant women; specifically, ~67% of malaria-associated deaths

occur in children under 5 years of age and malaria can cause severe complications (e.g., stillbirths, low birthweights, premature deliveries) in pregnant women[14,15].

Much progress has been made in limiting malaria-associated morbidity and mortality. For instance, between 2000-2015 the implementation of public health interventions (e.g., antimalarial drugs, insecticide-treated bed nets, and indoor residual spraying of insecticides) halved global malaria deaths[16]. However, progress towards eliminating malaria has stalled in many areas since 2015 coincident with a rise in resistance to drugs and insecticides[17]. These worrying trends have been further exacerbated by the COVID-19 pandemic's deleterious effects on health systems and economies worldwide[18]. The latest World Health Organization (WHO) World Malaria Report reported that 241 million people were infected with malaria and 627,000 people died of malaria in 2020[19]. These data underscore the need for new tools to control malaria.

1.2.1 The life cycle of *Plasmodium falciparum* in humans

Pf parasites have a complex life cycle split between human and mosquito hosts (**Figure 1.4**). The asymptomatic "pre-erythrocytic stage" of Pf pathogenesis begins when a female *Anopheles* mosquito inoculates 0-1,000 sporozoites (SPZ) from its salivary gland into the human's skin as it salivates while probing for a blood vessel[20,21]. SPZ are motile and use their locomotory apparatus to migrate from the skin into blood vessels[22]. Upon entering the vasculature, SPZ ride the bloodstream to the liver[23] where each SPZ infects a hepatocyte and quiescently multiplies over ~7-10 days into 30,000 – 90,000 merozoites (MZ), the next stage of the parasite's life cycle[24]. The "blood-stage" commences when these MZ exit hepatocytes and enter the bloodstream in vesicles called merosomes[25], infect erythrocytes, and asexually replicate until the erythrocytes lyse, releasing more MZ that continuously replicate until there are billions

of MZ in the bloodstream[26,27]. It is during this "blood-stage" that human hosts begin experiencing the symptoms associated with malaria. The Pf life cycle in humans concludes with the "transmission stage," where <10% of MZ sexually differentiate into male/female gametocytes that perpetuate malaria by re-infecting additional mosquitoes upon ingestion during a blood meal[28,29]. Importantly, of the parasite's three stages in humans, SPZ are the clear bottleneck in terms of parasite numbers and stopping SPZ from developing into MZ can completely abrogate malaria infection.

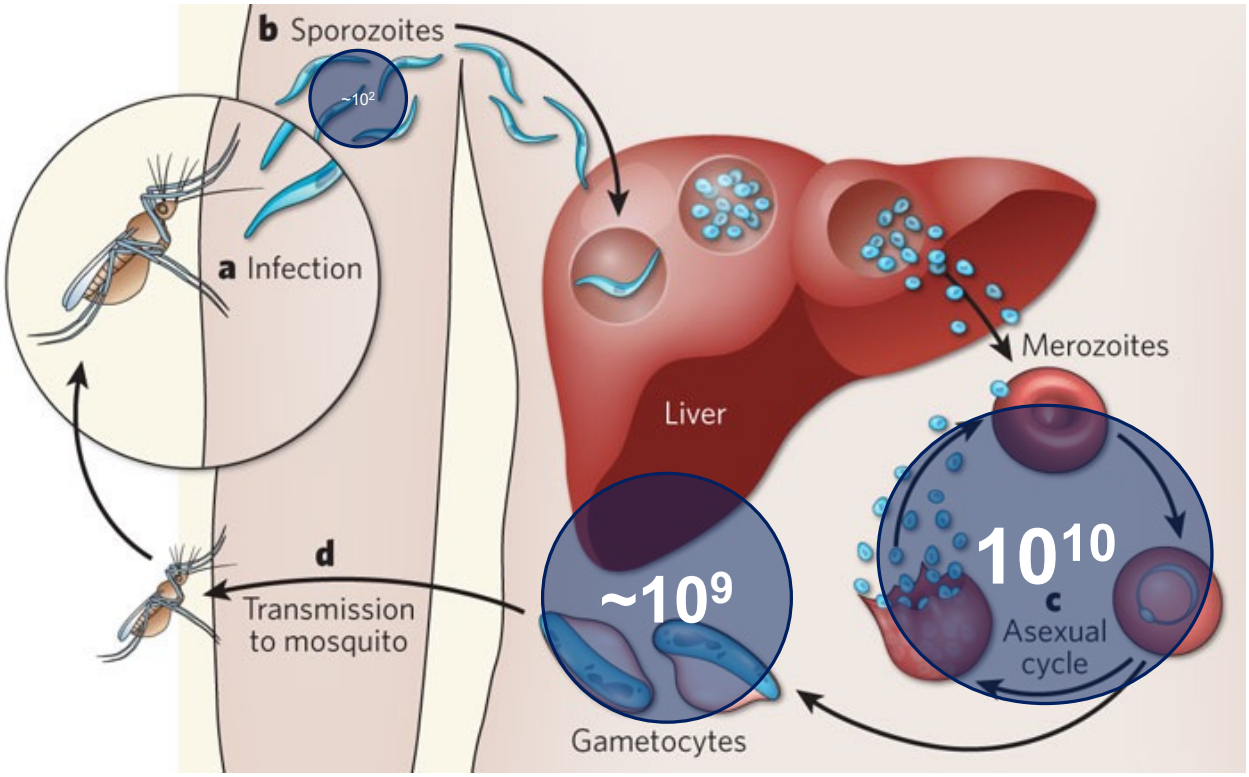

Figure 1.4: Pf life cycle and force of infection in humans. The force of infection (i.e., approximate parasite numbers) of SPZ, MZ, and gametocytes during the three stages of the Pf life cycle in humans. Figure adapted from Michalakis et al[30].

1.3 Antibodies against *P. falciparum* CSP on sporozoites

First described in 1969, the circumsporozoite protein (CSP) is the most abundant surface protein on SPZ[31,32]. CSP is required for SPZ to invade the liver and is thus a leading target for

pre-erythrocytic stage malaria vaccines[33]. Several seminal studies in the 1960s-80s showed that mice could be sterilely protected from challenge with *P. berghei* (Pb, which cause murine malaria) SPZ challenge by immunizing them with radiation-attenuated PbSPZ or by incubating PbSPZ with mAbs targeting PbCSP prior to challenge[34,35]. Subsequent studies showed that humans could also be protected from PfSPZ challenge following immunization with radiation-attenuated PfSPZ[36]. These proof-of-concept studies led to the development and clinical testing of multiple vaccines based on whole PfSPZ and recombinant PfCSP to prevent malaria infection in humans[37,38].

1.3.1 PfCSP structure and function

PfCSP has three domains: an N-terminus (N-CSP), a central domain composed of repeating tetrapeptides (1 NPDP, 4 NVDP minor repeats, and 38 NANP major repeats in the Pf reference isolate 3D7), and a C-terminus (C-CSP) containing a glycosylphosphatidylinositol (GPI) anchor that tethers PfCSP to the SPZ membrane[37–39] (**Figure 1.5**). Of the three domains, the PfCSP C-terminus has the greatest degree of genetic variability in global Pf field isolates. Most of these polymorphisms occur in the cluster of differentiation 4 ($CD4^+$) helper T cell epitopes in the C-terminus, suggesting that these epitopes undergo high levels of recombination from immunological pressure[40–43]. Of note, the C-terminus does contain two regions called region II+ and III+ that are highly conserved between different human-tropic *Plasmodium* species[44,45]. The PfCSP N-terminus has low genetic variation and notably contains a pentapeptide sequence called region I that is completely conserved in CSP from all known *Plasmodium* species[46–49]. The PfCSP central repeat domain has limited genetic variability in that the single NPDP is conserved in 99.8% of Pf isolates along with NVDP and NANP repeating

tetrapeptides[50]. However, the number and order of NVDP and NANP repeats varies widely between different isolates and there are occasional nonsynonymous mutations in the NANP/NVDP repeats[46–49].

In the Pf reference isolate 3D7 (Pf_3D7), the "junctional region" at the end of N-CSP and start of the repeat domain begins with NPDP followed by 3 interspersed NANP and NVDP repeats. This junctional region is then followed by 35 NANP repeats, with the fourth NVDP inserted after the twentieth NANP[51,52] (**Figure 1.5A**). Importantly, the full structure of PfCSP has not yet been solved despite decades of effort by structural biologists. The only empirically-solved structures reported to date are a C-CSP construct[45] and a PfCSP construct with a truncated repeat region in complex with Fabs directed against the NANP repeats[53]. A computationally-predicted structure of PfCSP was recently generated on AlphaFold, which shows that all domains of PfCSP are disordered except for C-CSP[54] (**Figure 1.5B**).

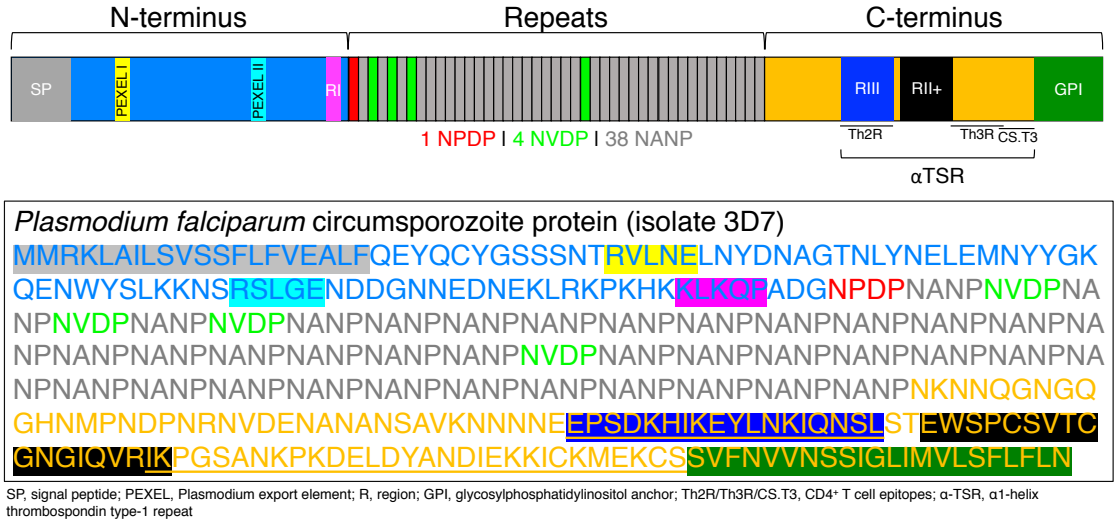

SP, signal peptide; PEXEL, Plasmodium export element; R, region; GPI, glycosylphosphatidylinositol anchor; Th2R/Th3R/CS.T3, CD4+ T cell epitopes; α-TSR, α1-helix thrombospondin type-1 repeat

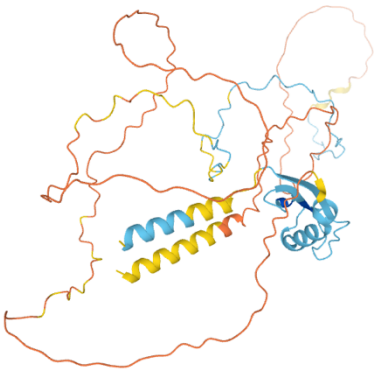

Figure 1.5: PfCSP schematic, amino acid sequence, and predicted structure. Top) color-coded schematic illustrating the N-terminus, repeat region, and C-terminus of PfCSP from the 3D7 reference isolate. N-CSP contains a signal peptide (SP), two Plasmodium export element (PEXEL) sites, and the conserved region I (RI). The repeat region is composed of three types of tetrapeptides (1 NPDP, 4 NVDP, and 38 NANP). C-CSP has a linker to the repeat region, an α-thrombospondin type-1 repeat (αTSR) domain that contains two conserved motifs (region III and region II+, RIII and RII+) and several cluster of differentiation 4 ($CD4^+$) helper T cell epitopes (Th2R, Th3R, CS.T3), and a GPI anchor sequence. **Middle)** sequence of PfCSP_3D7, color-coded to match the schematic. The sequences of the $CD4^+$ T cell epitopes are underlined. **Bottom)** structure of PfCSP_3D7 predicted by AlphaFold.

There are two conserved motifs in CSP, region I (RI) and region II+ (RII+), that are essential for SPZ to migrate through their hosts and invade mosquito salivary glands and mammalian hepatocytes[55,56]. RI in N-CSP and a cluster of positively-charged lysine residues directly upstream of RI are believed to mediate the initial electrostatic interaction of CSP with salivary glands and negatively-charged heparan sulfate proteoglycans (HSPGs) on the surface of hepatocytes[57–60]. Subsequently, RII+ in C-CSP (which folds into the αTSR domain) and lysines downstream of RII+ strengthen the attachment of CSP to hepatocytes[61–63]. Besides mediating invasion of salivary glands and hepatocytes, RII+ is also essential for SPZ motility, as disruption of this motif dramatically abolishes these phenotypes[64]. Thus, N-CSP and C-CSP respectively act as primary and secondary SPZ binding ligands and are essential for SPZ pathogenesis.

PfCSP undergoes several post-translational modifications to modulate adhesion, including proteolytic cleavage of N-CSP[65,66] and conformational changes to mask C-CSP[67,68]

(**Figure 1.6**). N-CSP is post-translationally cleaved three times: twice at each of two PEXEL (Plasmodium export element) sites that facilitate export of PfCSP from the endoplasmic reticulum to the plasma membrane[69–72] and once at RI when SPZ binds HSPGs on hepatocytes[65]. One study proposed that native CSP on SPZ exists in an "open" conformation (wherein C-CSP is exposed) when SPZ are developing in the mosquito midgut (MG) and shifts to a "collapsed" conformation (wherein N-CSP is cleaved at RI and the repeats mask C-CSP) when SPZ migrate into the salivary gland (SG) (**Figure 1.6A**). When SG SPZ are inoculated into the skin, PfCSP remains "collapsed" as SPZ migrate through the skin/vasculature and flips "open" (thereby exposing C-CSP) directly before hepatocyte invasion when SPZ contact HSPGs in the liver[67]. Another study proposed a different model (**Figure 1.6B**) wherein N-CSP, not the repeats, masks C-CSP and is cleaved at RI upon contact with HSPGs on hepatocytes, which exposes C-CSP[68]. While these models differ in when N-CSP is cleaved and which domain(s) mask C-CSP, they both concur that native CSP on SPZ adopts two conformations (an adhesive conformation in which C-CSP is exposed and a non-adhesive conformation in which C-CSP is masked) and that SG SPZ mask C-CSP to protect this critical domain from antibody recognition whilst migrating through the host.

Several studies of recombinant PfCSP (rPfCSP) and peptides corroborate the existence of two PfCSP conformations. The intrinsically disordered repeat region was predicted to adopt two energetically favorable helical conformations[73,74]. These computational predictions were later confirmed by atomic force microscopy (AFM) studies showing that rPfCSP adopts two conformations: an open monomer with a filamentous shape and a collapsed monomer with a compact shape[67]. Further AFM studies confirmed the bimodal distribution of rPfCSP molecules (with 40/60% having no/low mechanical resistance) and showed that the mechanically pliable

repeats forms a flexible rod-like structure that likely acts as an entropic spring and may provide lubrication for the SPZ during motility and invasion[75,76].

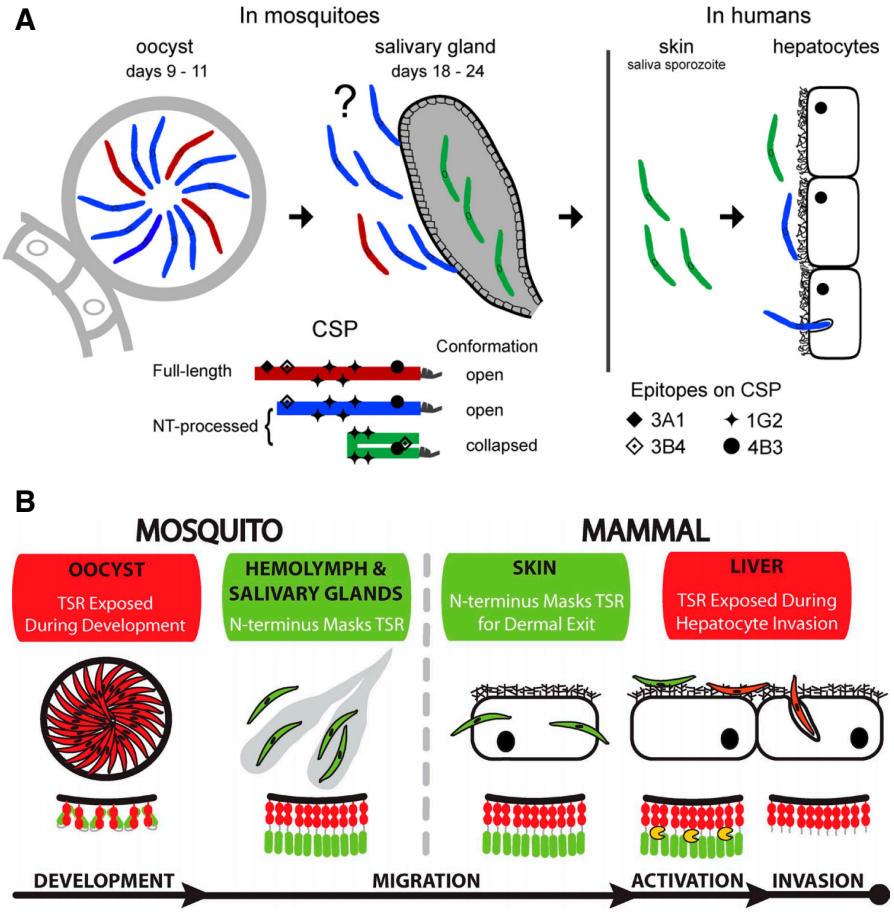

Figure 1.6: Two models for post-translational modifications of native PfCSP on SPZ. (A) Model proposed by Herrera et al[67] of the biochemical and biophysical changes in PfCSP and its role during the journey of SPZ through their hosts. The key at the bottom represents the different forms and conformations observed for PfCSP and the locations of various epitopes bound by PfCSP mouse mAbs (N-CSP: 3A1, 3B4; repeats, 1G2; C-CSP, 4B3). The question mark denotes that the conformation of PfCSP is speculative. **(B)** Model proposed by Coppi et al[68] showing the correlation between the conformation of PfCSP on SPZ and their location/developmental stage in both mosquito and mammalian hosts. Green SPZ have N-CSP exposed and red SPZ have C-CSP exposed. Below each group of SPZ is a schematic of PfCSP, in which green shows N-CSP, red shows C-CSP, and gray shows the repeats. The protease that cleaves PfCSP is marked yellow.

1.3.2 Antibody responses against PfCSP

The first anti-CSP mAb, a mouse mAb called 3D11 produced by hybridoma technology that bound PbCSP, was published in 1980[35]. Subsequently, the first protective PfCSP-specific

mouse mAb (2A10) was reported in 1983[77]. Since these studies, hundreds of mouse and human mAbs against all domains of PfCSP have been characterized. Most neutralizing PfCSP mAbs isolated to date (including 2A10) target the immunodominant NANP repeats in the central repeat region[78]. Importantly, structural studies indicate that the anti-repeat motifs recognized by PfCSP repeat-specific mAbs are actually DPNA, NPNV, and NPNA, derived from the joining of the three different tetrapeptides[53,76,79–81].

A critical tool for studying protective antibodies is a simple, reliable, and high-throughput *in vitro* assay to measure mAb neutralization that correlates with *in vivo* protection in animal models (or ideally humans). A widely used *in vitro* assay for assessing antibody-mediated neutralization of SPZ involves incubating freshly dissected SPZ with antibodies prior to inoculating the antibody-bound SPZ onto a monolayer of cultured hepatocytes (primary or cell lines), incubating them for several hours, and then assessing hepatocyte infection via microscopy or flow cytometry[82,83]. Unfortunately, this *in vitro* assay has been shown to poorly correlate with *in vivo* protection in normal mice challenged with transgenic rodent malaria-causing Pb expressing PfCSP (Pb-PfCSP-SPZ) or in liver-humanized mice challenged with wild-type PfSPZ[84,85]. Notably, the liver-humanized mice are prohibitively expensive and require highly specialized skills to produce and utilize. Thus, the current state-of-the-art tool for down-selecting potent PfCSP mAbs is the transgenic Pb-PfCSP-SPZ model in normal mice.

Based on quantitative studies of rodent-tropic Pb and *P. yoelii* (Py) in normal mice, only ~30% of SPZ inoculated into the skin during a mosquito's blood meal successfully migrate into dermal capillaries over several hours while the remainder are trapped in the skin or lymph nodes and mostly destroyed[23,86]. Notably, a minority of SPZ are injected directly into the vasculature from the mosquito's proboscis[87–89] and migrate to the liver within minutes[90]. These migratory

SPZ use CSP to adhere to highly sulfated HSPGs protruding into liver sinusoids through endothelial fenestrations[91] and secrete pore-forming proteins[92,93] that enable their passage through or between Kupffer cells or endothelial cells lining liver sinusoids into the liver parenchyma[94,95], where they traverse through several hepatocytes[96,97]. Eventually, the HSPGs on hepatocytes trigger SPZ to switch from their migratory phenotype to an invasive phenotype and proteolytically cleave N-CSP, which mediates their invasion of hepatocytes[65,66]. CSP-specific antibodies inhibit SPZ throughout these physiological sites via multiple mechanisms broadly subdivided into two categories: direct neutralization by the Fab region and Fc-mediated effector functions.

The Fab region of CSP antibodies directly neutralize SPZ via a cytotoxic process called "dotty death" observed *in vivo* in the skin, vasculature, and liver that is complement- and Fc-independent[85,98]. Specifically, SPZ undergo dotty death when antibodies cross-link CSP molecules on their surface, which triggers the rapid posterior shedding of antibody-bound CSP in a process called the CSP precipitation reaction (CSPR)[99,100] and the over-secretion of new CSP from the parasite's anterior pole to replenish the shed CSP. Both processes eventually deprive SPZ of their protective CSP coat, rendering the parasite's own membrane vulnerable to the permeabilizing effects of their secreted pore-forming proteins[98]. Furthermore, CSP antibodies impair the critical SPZ phenotype of gliding motility *in vivo*[101,102], which limits the parasite's abilities to migrate out of the dermis into the vasculature[103,104], exit liver sinusoids to access the parenchyma[85], and traverse through hepatocytes[83,85]. CSP antibodies can also decrease the number of SPZ inoculated by mosquitoes by forming immune complexes with soluble CSP in mosquito saliva and blocking the egress of SPZ through the mosquito's proboscis[105]. Nearly all these insights were derived from intravital imaging of wild-type or transgenic PbSPZ/PySPZ

expressing PfCSP and confirmed with *in vitro* studies of PfSPZ. Lastly, there is *in vitro* evidence that antibodies sterically hinder the proteolytic cleavage of PfCSP and thereby block PfSPZ invasion of hepatocytes[84,106].

In terms of Fc-mediated effector functions, the Fc region of CSP antibodies can fix C1q on PfSPZ and activate the classical complement pathway, resulting in the slowing and lysis of SPZ *in vitro*[107–110]. Furthermore, opsonization of SPZ by CSP antibodies enhances their phagocytosis by skin-resident macrophages[111], bloodborne neutrophils and monocytes and NK cells[112,113], and liver-resident Kupffer and NK cells *in vitro*[113,114]. CSP antibodies can also trigger NK cells to degranulate and kill opsonized SPZ *in vitro*[112,113].

Collectively, these studies indicate that CSP antibodies inhibit SPZ via multiple mechanisms across several physiological sites. This complexity has hindered the development of a single simple, reliable, and high-throughput *in vitro* assay for down-selecting highly protective PfCSP mAbs. It is clear that CSP antibodies exert a significant proportion of their inhibitory effects on SPZ in the skin, where these parasites are most vulnerable[98,102–104]. However, as a single SPZ can initiate a symptomatic malaria infection and a small number of SPZ are directly inoculated into the vasculature through the mosquito's proboscis and thus bypass the skin[87–89], it is likely that the most protective CSP mAbs must efficiently inhibit SPZ in the vasculature and liver in order to prevent these parasites from infecting hepatocytes and developing into MZ[85].

1.4 Antibodies against *P. falciparum* RH5-CyRPA-Ripr on merozoites

If even a single SPZ successfully infects a hepatocyte and multiples into ~30,000 MZ, these MZ begin exiting the infected hepatocyte to enter the bloodstream and invade erythrocytes. The trimeric protein complex PfRH5-PfCyRPA-PfRipr (RCR) on the surface of MZ is critical

for these parasites to bind basigin (an erythrocyte surface protein) and invade erythrocytes. The RCR complex is composed of three proteins (RH5, reticulocyte-binding protein homolog 5; CyRPA, cysteine-rich protective antigen; and Ripr, RH5-interacting protein), all of which were identified relatively recently (RH5 in 2008[115], Ripr in 2011[116], and CyRPA in 2012[117]) and are leading Pf malaria blood-stage vaccine targets[118]. Importantly, RH5 is only expressed by *P. falciparum* while orthologues of CyRPA and Ripr are present in all other human-tropic *Plasmodium* species[119]. Of the three proteins, RH5 is the most advanced malaria vaccine target with Phase I/II clinical trials having been completed or currently underway[38].

1.4.1 Structure and function of RH5-CyRPA-Ripr

RH5 is a diamond-shaped protein whose structure was solved in 2014[120]. RH5 is proteolytically processed before being secreted by MZ[116] and is critically important for erythrocyte invasion due to its role as the MZ ligand that physically binds basigin[121]. CyRPA is a protein shaped like a six-bladed β-propeller with five disulfide bonds whose structure was solved in 2017[122,123] and is located between RH5 and Ripr[124]. Ripr is a protein composed of ten epidermal growth factor-like (EGF) domains, eighty-seven cysteines, and putatively unstructured regions. Ripr is proteolytically processed into two similarly-sized fragments: an N-terminal fragment (EGF 1-2) and a C-terminal fragment (EGF 3-10)[116]. The RCR complex assembles into a trimer whose structure was solved in 2019[124]. Importantly, the role of CyRPA and Ripr in MZ invasion of erythrocytes is still unknown.

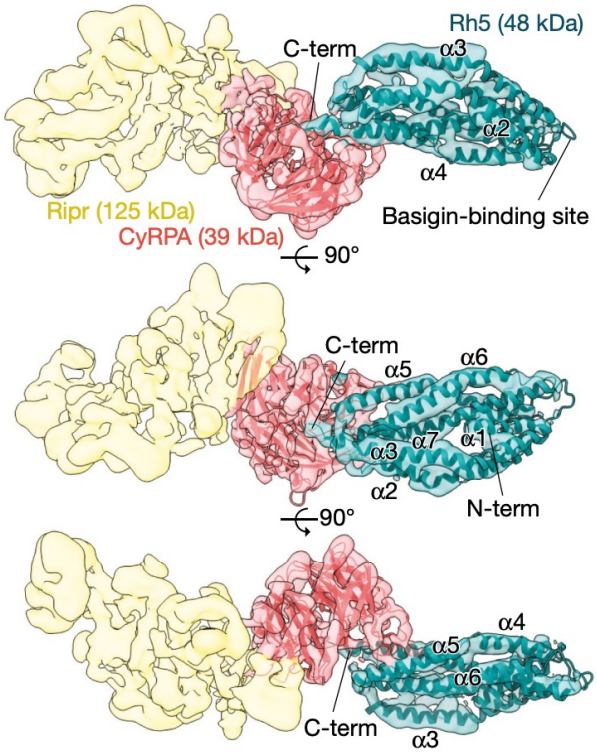

Figure 1.7: Structure of the RH5-CyRPA-Ripr trimeric complex. 3D reconstruction at 7.17 angstrom resolution based on cryogenic electron microscopy. Figure taken from Wong et al[124].

RH5, CyRPA, and Ripr are all highly conserved and essential for invading erythrocytes[118], a rapid process that only lasts ~30 seconds[125]. The process of MZ invasion begins when various merozoite surface proteins (MSP; e.g., MSP1) attach with low affinity to the erythrocyte membrane. Higher-affinity interactions with reticulocyte-binding-like homolog and erythrocyte-binding-like proteins enable the MZ to firmly attach itself to erythrocytes[126]. MZ subsequently reorient themselves so that their apical ends are facing the erythrocyte membrane. It is at this point that the RCR complex assembles on the MZ surface[127,128] and RH5 binds to basigin, which triggers an intracellular calcium spike in the erythrocyte[121,128] (**Figure 1.8**). Subsequently, the parasite inserts several rhoptry neck proteins (RONs) and apical membrane antigen 1 (AMA1) into the erythrocyte membrane to form a tight junction[129,130]. The MZ then

activates an actin-myosin motor to propel the nascent tight junction at its apex to its distal end, resulting in the formation of a parasitophorous vacuole and eventually the complete entry of the MZ into the erythrocyte's interior[131]. The MZ then divides into 16-32 MZ over ~48 hours, which are released to invade other erythrocytes[132].

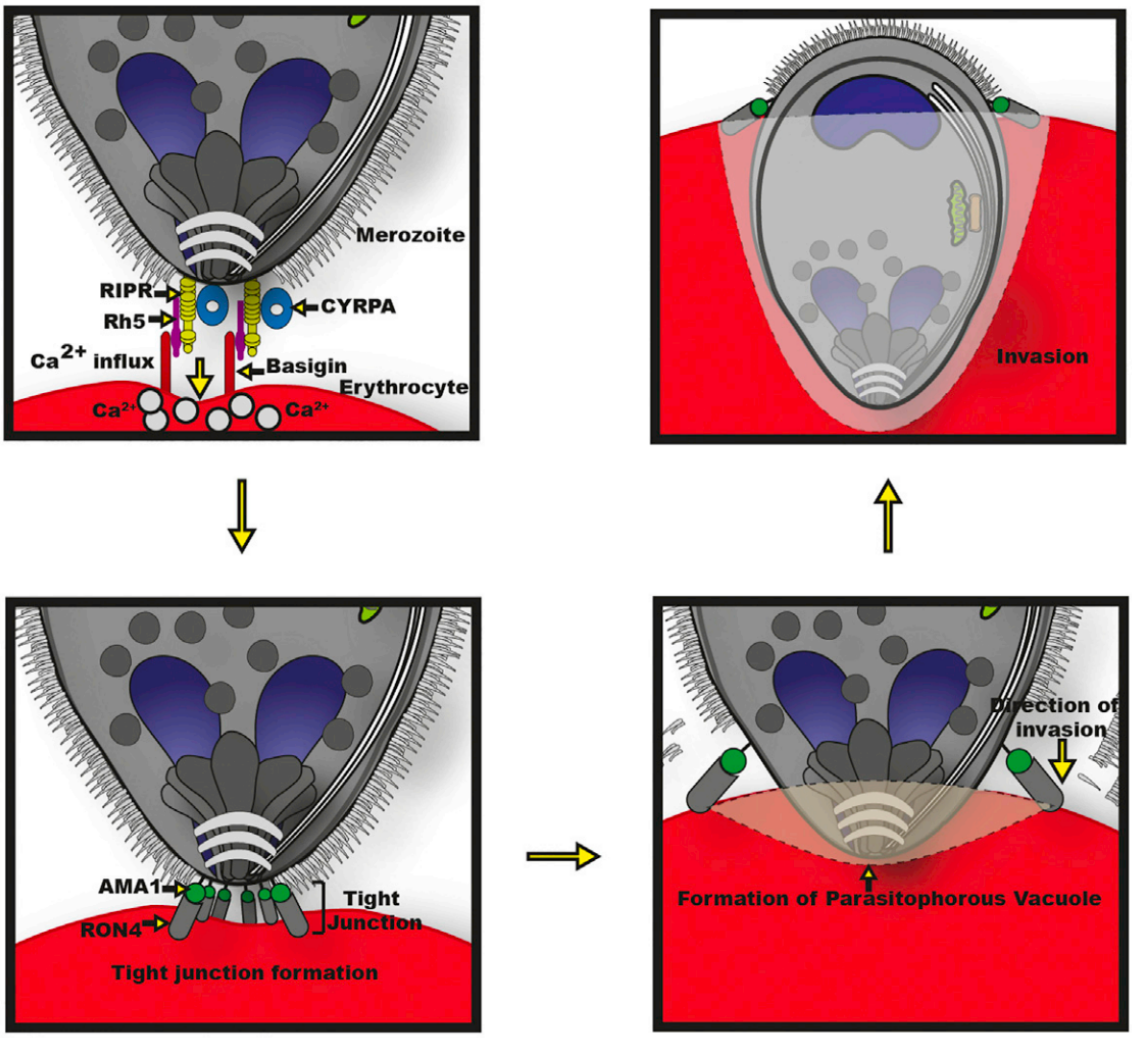

Figure 1.8: Model for the role of the RCR complex in MZ erythrocyte invasion. RH5, CyRPA, and Ripr are secreted by the MZ and form a trimeric complex at the interface between the MZ apex and the erythrocyte membrane. The binding of RH5 to basigin on the erythrocyte surface triggers intracellular release of calcium within the erythrocyte, a necessary step for the MZ to form a tight junction with the erythrocyte membrane. Figure and legend adapted from Volz et al[128].

1.4.2 Antibody responses against RH5-CyRPA-Ripr

Antibodies directed against RH5, CyRPA, and Ripr are being actively investigated because of their ability to neutralize nearly all Pf strains tested so far (i.e., "strain-transcending" neutralization). This attribute is particularly promising and interesting because MZ have evolved multiple mechanisms (e.g., mutating or switching surface proteins, employing multiple redundant invasion pathways) to hamper the effectiveness of antibodies in blocking their invasion of erythrocytes. Thus, the RCR complex appears to be a unique vulnerability for MZ because all three proteins are highly conserved and absolutely essential for erythrocyte invasion[118]. Indeed, RH5-specific antibodies induced by natural malaria exposure have been associated with protection against malaria in children in Papua New Guinea and Mali[133–135]. This protective correlation is potentially blunted by the low anti-RCR reactivity observed in serum from malaria-exposed subjects. Specifically, RH5-, CyRPA-, and Ripr-specific antibody titers were significantly lower than all other merozoite antigens targeted by historical vaccine candidates (e.g., MSP1, AMA1)[117,133,136–139]. The intrinsically low natural immunogenicity of the RCR complex is likely due to its lower antigen abundance compared to other merozoite surface proteins[118].

Unlike for SPZ and anti-SPZ antibodies, a relatively simple, reliable, and high-throughput *in vitro* assay exists for assessing MZ neutralization by anti-MZ antibodies. This growth inhibition activity (GIA) assay was first reported in 2005[140] and has since been shown to strongly correlate with protection mediated by MSP1-, AMA1-, and RH5-based vaccines as well as RH5-specific mAbs in non-human primates (NHPs) challenged with *P. falciparum* or *P. knowlesi*[141–144]. The standardized GIA assay, run out of the GIA Reference Center at the National Institutes of Health (NIH), involves culturing MZ-infected erythrocytes with antibodies and

determining the degree to which these antibodies inhibit reinvasion of uninfected erythrocytes (measured by parasite lactate dehydrogenase).

Some progress has been made in isolating and characterizing mAbs against the RCR complex; however, the dozens of RCR-specific mAbs published so far pales in comparison to the hundreds of published CSP mAbs[78]. To date, only seventeen human RH5-specific mAbs have been published[145] while no human CyRPA- or Ripr-specific mAbs have been reported. In terms of mouse mAbs, ten RH5[122,123,146], twenty-seven CyRPA[117,122,147], and five Ripr mAbs[135] have been isolated so far. The most potent RH5 mAb reported to date is R5.016, which has an effective concentration to mediate 50% inhibition (EC_{50}) of 9.6 µg/mL in the GIA assay[145]. All potent RH5-specific mAbs characterized so far bind at or near the tip of the RH5 diamond that contacts basigin. Most inhibitory RH5 mAbs bind directly to the tip of RH5 and thus sterically block RH5 from contacting basigin. However, some rare and highly potent mAbs (including R5.016) bind near the tip of RH5 but do not directly hinder binding of RH5 to basigin *in vitro*; thus, the neutralization mechanism of mAbs like R5.016 is still unclear[120,145]. The most potent CyRPA mAb reported to date is SB1.6 (~64% growth inhibition at 500 µg/mL), which binds a conformational epitope and whose neutralization mechanism was not reported[147]. Manuscripts that described other comparably protective CyRPA mAbs speculated that these mAbs may neutralize invasion by disrupting the CyRPA-RH5 interface[122] or by binding CyRPA and sterically hindering the RCR complex from accessing basigin by directing their bulky Fc region towards the erythrocyte membrane. The most potent Ripr mAb reported to date is 1G12 (EC_{50} = 350 µg/mL), which binds an epitope in EGF-7 that is located away from the CyRPA-Ripr interface and thus does not interfere with RCR complex assembly.

Of the three antigens in the RCR complex, mAbs against RH5 are the most potent neutralizers of MZ erythrocyte invasion *in vitro*[118]. Despite the relatively greater potency of RH5 mAbs, enormous mAb doses of 100 mg/kg were required to provide the high titers (600-900 µg/mL) needed to protect NHPs challenged with Pf-infected erythrocytes[144]. These requisite mAb titers are orders of magnitude higher than those required to protect NHPs from challenge against viruses like the human immunodeficiency virus (HIV-1) (3-6 µg/mL of the mAb VRC01)[148] and bacteria like *Borrelia burgdorferi* (35-45 µg/mL of the mAb 2217)[149]. The high antibody titers required to ameliorate the symptoms of blood-stage malaria are one of the greatest barriers to implementing potent RCR-specific mAbs as antimalarial therapeutics.

Improving the potency of RCR-specific mAbs will facilitate their translation into clinical products. This can be accomplished via three methods: 1) identifying even more potent RH5, CyRPA, or Ripr mAbs, 2) combining mAbs targeting different epitopes within each antigen, or 3) combining mAbs specific for each of the three antigens. Indeed, several *in vitro* and *in vivo* protection studies have shown that mixing mouse mAbs against RH5, CyRPA, and Ripr (method 3) additively or even synergistically neutralize MZ[123,127,135,150,151]. Furthermore, it was recently shown that non-neutralizing RH5 human mAbs slowed down parasite invasion and thus acted synergistically when combined with neutralizing RH5, CyRPA, and Ripr mAbs (method 2+3)[145]. Collectively, these data suggest that the high RCR-specific antibody titers required to neutralize MZ can be lowered by isolating more potent individual mAbs or identifying synergistic mAb combinations.

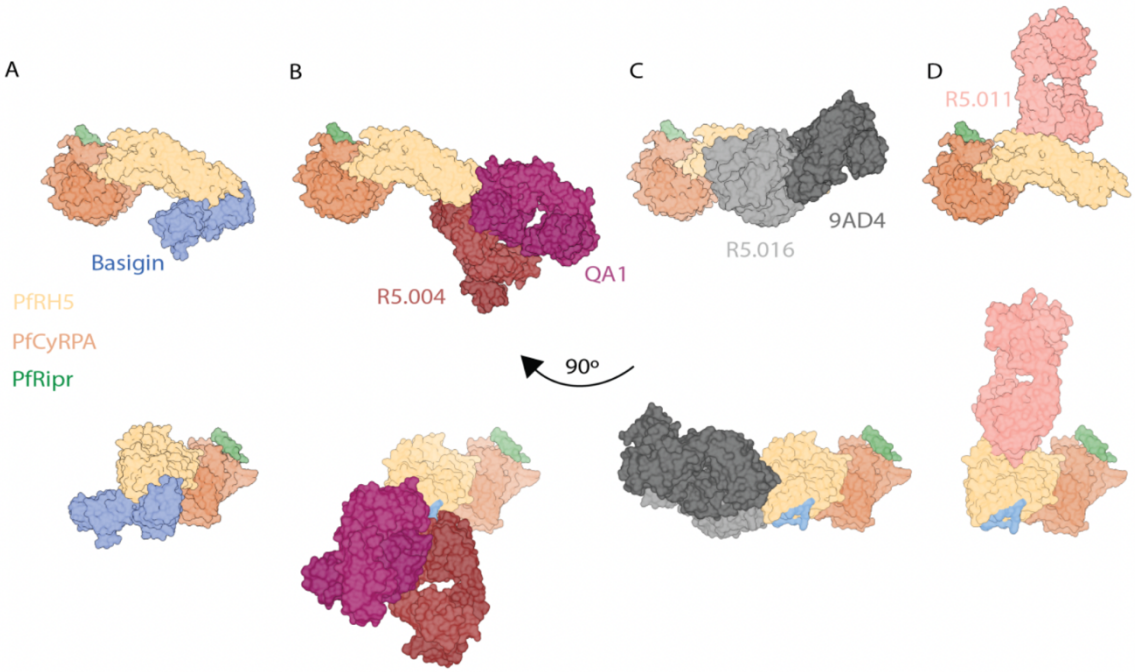

Figure 1.9: Binding of mAbs to the RCR complex. (A) Illustration of RCR bound to basigin. **(B)** RCR bound by neutralizing Fabs QA1 and R5.004, which bind directly to the basigin binding site on RH5. **(C)** RCR bound by neutralizing Fabs R5.016 and 9AD4, which bind near the basigin binding site on RH5. **(D)** RCR bound by non-neutralizing Fab R5.011. Figure and legend adapted from Ragotte et al[118].

1.5 Passive transfer of antimalarial antibodies in humans

A long-sought goal for curbing malaria is the development of a highly effective vaccine against Pf. The world's most advanced malaria vaccine (RTS,S), which was recently approved by the WHO, is a protein subunit vaccine that induces protective anti-PfCSP antibody and $CD4^+$ T cell responses by presenting a portion of PfCSP fused to hepatitis B surface antigen[152,153]. In a phase III clinical trial, three immunizations of RTS,S formulated with the Adjuvant System 01 (AS01) conferred ~50% protection against clinical malaria at one year and ~30% protection over four years in 5-17 month-old infants who received a fourth booster dose[154]. The limited efficacy of RTS,S/AS01 is attributed to the rapid waning of anti-CSP antibodies below the high levels required for protection, thus necessitating additional boosters[155–157]. An alternative intervention

that could mediate higher levels of protection for defined periods of time is passive transfer of potent antimalarial mAbs.

1.5.1 Convalescent plasma therapy for treating acute malaria

Passive transfer of antimalarial antibodies is sufficient to protect against malaria. This phenomenon was first reported in a case study from 1917, when Sotiriades observed clinical improvement in a patient suffering from acute malaria who was inoculated with 10 mL of serum from a convalescent subject who had been chronically exposed to malaria[158]. The antimalarial effect of convalescent plasma therapy was definitively demonstrated in 1961 when Gambian children with high parasitemia and acute malaria symptoms were treated with purified immunoglobulins from malaria-exposed Gambian adults, which reduced their parasitemia and improved their clinical presentation; however, protection only lasted ~3 months due to waning antibody levels[159]. The antimalarial effects of convalescent plasma therapy were substantiated in subsequent clinical studies in Nigeria[160], Tanzania[161], Thailand[162], and Malawi[163]. Importantly, these patients were already in the symptomatic blood-stage of malaria and the immunoglobulins mediated their therapeutic effects by targeting bloodborne MZ and/or infected erythrocytes. Overall, these studies demonstrated that malaria can be treated with antibodies targeting blood-stage parasites.

1.5.2 Monoclonal antibodies for passive malaria prophylaxis

Passive transfer of potent human mAbs has recently emerged as a new modality for treating or preventing infectious diseases for which no highly effective vaccine exists, like malaria[37]. Like all drugs, concentrations of passively administered mAbs wane over time below a

protective threshold; thus, maximizing the pharmacokinetic half-life of anti-infective mAbs is vital to optimizing their feasibility because it decreases the amount and frequency of mAb administrations required to achieve high-level protection[164]. One strategy to extend the half-life of mAbs is to introduce mutations in their Fc regions that enhance their affinity for the neonatal Fc receptor (FcRn), which saves antibodies from lysosomal degradation and recycles them back into circulation[165]. Specifically, mutating M428L/N434S (LS) in the Fc of the anti-HIV-1 mAb VRC01 increased this mAbs' affinity for FcRn by 12-fold[157], which resulted in a 2.5-fold longer serum half-life in NHPs (4.65 days for VRC01 vs. 11.80 days for VRC01LS)[166] and a 4-fold longer serum half-life in humans (15 days for VRC01 vs. 71 days for VRC01LS).[167]

In 2021, it was shown for the first time that malaria can be prevented with a mAb instead of antimalarial drugs or vaccines. Specifically, passive transfer of a potent long-acting PfCSP-specific human mAb called CIS43LS (which targets the junctional epitope NPDP and the immunodominant NANP repeats) sterilely prevented malaria in malaria-naïve volunteers (including yours truly!) exposed to five bites from Pf-infected mosquitoes up to nine months following mAb administration[168]. Passive transfer of CIS43LS provided distinct advantages to the earlier convalescent plasma therapies. Firstly, by targeting the infective SPZ stage CIS43LS was able to sterilely prevent malaria while the plasma therapies are only effective once recipients have entered the symptomatic blood-stage. Secondly, the LS mutation increased the protective duration of CIS43LS. Thirdly, CIS43LS is a more targeted antimalarial intervention because it is a single mAb that binds a defined epitope whereas the plasma therapies contain a mix of polyclonal antibodies (many of which are not malaria-specific). Collectively, these proof-of-principle studies showed that malaria can be prevented or treated with antibodies alone.

1.6 Thesis outline and aims

The initial aims of my DPhil research were to: 1) isolate and characterize potent PfCSP-specific human mAbs against PfSPZ, 2) isolate and characterize potent PfRH5-CyRPA-Ripr-specific human mAbs against PfMZ, and 3) assess the protective efficacy of a multi-stage mAb cocktail against PfCSP and PfRH5 (or CyRPA or Ripr). Aim 1 has been fully achieved (Chapters III-IV); additionally, a number of side projects (Chapters V-VI) have yielded additional interesting insights into PfCSP mAb immunology. Aim 2 has been partially achieved in that the largest known panel of PfRH5-CyRPA-Ripr human mAbs has been isolated (Chapter VII); characterization of these mAbs' potency, target epitopes, and neutralization mechanisms are ongoing. Aim 3 was not achieved as I am still working to identify the most potent PfRH5-CyRPA-Ripr mAbs from the aforementioned panel. If/when a potent PfRH5-CyRPA-Ripr mAb is identified, it will be interesting to determine whether combining PfCSP and PfRH5-CyRPA-Ripr mAbs in a multi-stage mAb cocktail provides enhanced protection against malaria.

Specifically, the following Chapters present the work done to achieve Aims 1 and 2:

- Chapter II describes the materials and methods used to collect the data in Chapters III-VII
- Chapter III describes the isolation, characterization, and preclinical development of a highly potent PfCSP human mAb called L9 that is the first reported to preferentially bind the subdominant NVDP minor repeats of PfCSP
- Chapter IV describes insights into the binding properties and neutralization mechanisms of potent PfCSP mAbs gleaned by comparing L9 to seven other published protective PfCSP human mAbs using an array of biochemical, biophysical, and functional assays

- Chapter V describes the isolation and biophysical/structural characterization of mAbs clonally related to L9 and provides insight into the ontogeny and evolution of this rare NVDP-preferring B cell lineage
- Chapter VI describes the binding and protection of mAb cocktails targeting the three domains of PfCSP (i.e., N-CSP, repeat region, and C-CSP) as well as combining active-and-passive immunization with PfCSP-based vaccines and PfCSP mAbs
- Chapter VII describes the isolation and preliminary binding/genetic characterization of a large panel of >200 human mAbs specific for PfRH5, CyRPA, and Ripr from malaria-exposed and vaccinated subjects

Chapter II: Materials and Methods

2.1 Chapter III-VII shared methods

Human clinical specimens (VRC 312 and 314 Study Teams)

Clinical specimens for Chapters III-VI were derived from malaria-naive, healthy adults (18-45 years of age) in the Vaccine Research Center (VRC) 314 clinical trial (https://clinicaltrials.gov/; NCT02015091) after obtaining written informed consent. Briefly, VRC 314 was a multi-institution, phase 1, open-label, dose-escalation trial with controlled human malaria infection (CHMI) that was designed to assess the safety, immunogenicity, and protective efficacy of the Sanaria PfSPZ Vaccine administered by intravenous or intramuscular injection[169]. The Sanaria PfSPZ Vaccine is composed of radiation-attenuated, aseptic, purified, cryopreserved PfSPZ derived from the NF54 strain[170]. Clinical specimens for Chapter VII were derived from either a cohort study of 1,187 malaria-exposed subjects aged 1 month to 43 years (50.8% female) in the rural village of Kalifabougou, Mali as previously described[171,172] or the VAC063 study conducted in the UK by the University of Oxford (NCT02927145) as previously described[173]. Briefly, malaria episodes in Malian subjects were prospectively diagnosed by referral and biweekly/monthly visits. Peripheral blood mononuclear cells (PBMCs) and plasma were isolated from venous blood at the following timepoints: before and after each malaria season, when a clinical malaria episode was diagnosed, and 7-10 days after the diagnosis. mAbs were isolated from PBMCs collected at all these timepoints. VAC063 was a multi-center, non-randomized, open-label, dose escalation Phase I/IIa clinical trial evaluating the safety, immunogenicity, and efficacy of RH5.1 formulated with the adjuvant $AS01_B$ in 88 healthy, malaria-naïve UK volunteers 18-45 years of age (62.5% female). I focused my attention on subjects in Groups 1

and 4, which respectively received three vaccinations of 2 and 50 μg of RH5.1/AS01$_B$ at days 0, 28 and 56. mAbs were cloned from PBMCs collected at Day 140 (i.e., 12 weeks after the final immunization).

Mice (L. Pereira, VRC; Y. Flores-Garcia, JHU; A.S.P. Yang, Radboud Univ.; J. O'Connor, ANU)

Female 6- to 8-week old B6(Cg)-Tyrc-2J/J albino mice and female 6- to 12-week old C57BL/6 mice were obtained from The Jackson Laboratory. Female 6- to 8-week old C57BL/6 mice and female 8-week old Swiss Webster mice were obtained from Charles River Laboratories. Female 8-9 month old FRG-huHep human liver-chimeric mice were obtained from Yecuris Corp. All mouse research was performed according to NIH guidelines for use and care of live animals approved by the institutional animal care and use ethics committees of the VRC (Animal Study Protocol VRC-17-702), Johns Hopkins University (Approved protocol permit no. MO18H419), Radboud University Medical Center (ADV103002016452), and Australia National University (A2016/17 & A2019/36).

Sporozoites (L. Pereira, M. Dillon, B. Bonilla, VRC; A. Molina-Cruz, NIAID)

Green fluorescent protein (GFP) labeled *P. berghei* SPZ expressing PfCSP (Pb-PfCSP-GFP-SPZ) were generated by crossing the parental Pb-PfCSP-SPZ line[174] with the previously described *P. berghei*-ConF parasite line that expresses GFP under the control of a heat shock protein 70 (HSP70) promotor[97]. Briefly, C57BL/6 mice were co-infected with Pb-PfCSP-SPZ and *P. berghei*-ConF at a ratio of 10:1. *Anopheles stephensi* mosquitoes were allowed to feed on the mice; subsequently, SPZ dissected from these mosquitoes were used to infect naïve animals.

Parasites expressing the GFP transgene were sorted from the blood of these mice by use of a FACSAria cell sorter and used to infect mice. GFP^+ progeny were cloned, and the clones were screened for the insertion of the PfCSP knock-in via measurement of anti-PfCSP antibody binding to progeny SPZ. *P. falciparum* NF54 sporozoites were isolated from an individual near Schiphol Airport (The Netherlands)[175]. Transgenic *P. berghei* (strain ANKA 676m1c11, MRA-868) expressing full-length *P. falciparum* CSP and a GFP/luciferase fusion protein (Pb-PfCSP-GFP/Luc-SPZ) were obtained as previously described[176]. *Anopheles stephensi* Nijmegen strain mosquitoes were infected with *P. berghei* malaria-infected Balb/c mice or with *P. falciparum* NF54 gametocytes using membrane feeding. Pb-PfCSP-GFP/Luc-SPZ were dissected from salivary glands 20-24 days post-infection; PfSPZ were dissected from salivary glands 16-18 days post-infection. SPZ were isolated into either ice-cold phosphate-buffered saline (PBS) with or without 10 μM E-64 protease inhibitor (Sigma-Aldrich) to prevent PfCSP proteolytic cleavage or Leibovitz's L-15 medium (Sigma-Aldrich). The infected salivary glands were homogenized gently by passing them 15 times through a syringe with a 28G needle or grinder with pestles for tissue. The salivary gland homogenate was passed through a 40 μm cell strainer (Pluriselect, USA) by gravity. The SPZ were counted in a hemocytometer and placed on ice.

Cell Lines

Expi293 and 293F cells used were from Thermo Fisher Scientific. The human hepatoma cell line HC-04 (MRA-965, deposited by Jetsumon Sattabongkot)[177] was obtained through the Malaria Research and Reference Reagent Resource Center as part of the Biodefense and Emerging Infections Research Resources Repository.

Production of rPfCSP constructs

The amino acid sequence of PfCSP in the 3D7 clone of the NF54 isolate (PlasmoDB ID: PF3D7_0304600.1) was used to generate a codon-optimized synthetic gene for expression in mammalian cells (GenScript). The DNA construct corresponding to the full-length (FL) rPfCSP, in which the leader peptide residues 1–20 were replaced with a mammalian secretory signal peptide derived from the modified bovine prolactin (MDSKGSSQKGSRLLLLLVVSNLLLPQGVLA) and the GPI anchor residues 376–397 were excluded, was cloned into a CMV/R-expression vector with a C-terminal AviTag, HRV3C-processing tag, and a 6X histidine tag. This construct, termed PfCSP_SAmut_C5S, encodes the N-terminal domain (with four amino acid mutations that removed processing sites and prevented dimerization upon solubilization to increase yield and facilitate consistent analyses), the central domain consisting of 38 NANP tandem repeats interspersed with 4 NVDP repeats, and the C-terminal domain. Truncated[53] and NVDP repeat mutant rPfCSP synthetic constructs were created in the same expression vector with identical N- and C-termini to PfCSP_SAmut_C5S, expressed through transient transfection in 293F cells using the Freestyle 293F expression system (Thermo Fisher Scientific) at 37°C, 8% CO_2 for 6 days, and purified from culture supernatants through polyhistidine-tag affinity chromatography followed by size-exclusion chromatography on an ÄKTA™ Start (GE Healthcare). Monomer-containing fractions were pooled, concentrated, snap frozen, and stored at −80°C. N-CSP was created by GenScript, as previously described[84,178]. For the recombinant C-CSP construct, a codon-optimized sequence encoding PfCSP_3D7 amino acids 295–374 was cloned in-frame with a sequence encoding tissue plasminogen activator leader peptide[179] on the 5’ end and a GlySerGlySerGly linker followed by a His8 tag on the 3’ end. The construct was inserted into the pTT3 vector[180] for expression in FreeStyle 293F cells

(Thermo Fisher Scientific), which were cultured and processed as previously described[181]. Briefly, cells were transfected using PEI MAX (Polysciences, Inc) and subsequently cultured for 5 days. Upon harvesting by centrifugation, the supernatant was treated by addition of NaN_3 (0.02%, final concentration) and NaCl (+350 mM), and protein was purified by immobilized metal affinity chromatography followed by size-exclusion chromatography over a calibrated HiLoad 16/600 Superdex 200 pg column (GE Healthcare). Peak fractions were pooled, flash-frozen in liquid nitrogen, and stored at -20°C until use.

Production of PfCSP peptides (GenScript)

Peptides were produced by direct synthesis and biotinylated by GenScript. These include 15mer peptides numbered 20-88 that were 15 amino acids in length and overlapped by 4 residues spanning the central repeat region of PfCSP, a 36mer peptide $(NANP)_9$, a 31mer junctional peptide 21-25 (NPDPNANPNVDPNANPNVDPNANPNVDPNAN), 16mer peptides $(NPNV)_4$ and $(NPNA)_4$, and an 8mer peptide NANPNVDP.

Production of recombinant immunoglobulins

Following single cell sorting of B cells into lysis buffer, all RNA transcripts were reverse transcribed to cDNA (SuperScript III First-Strand Synthesis System; Thermo Fisher Scientific). Amplification of the genes encoding the immunoglobulin variable regions heavy chains, as well as kappa or lambda light chains, was performed using a cocktail of primers followed by sequencing (ACGT) and cloning into the pVRC8400 huIgG1, pVRC8400 huIgK, or SBShuLambda expression vectors (GenScript) containing the relevant constant region. Sequences of previously published PfCSP mAbs were retrieved from the Protein Data Bank and

cloned into the aforementioned plasmids. Sequence analysis (e.g., determination of heavy and light chain sequences and somatic mutations) and phylogenetic tree generation was performed using the International Immunogenetics Information System (IMGT, http://www.imgt.org/) and Geneious Prime (Geneious), with clonality being defined as having the same V/J genes, heavy complementarity-determining region (HCDR) 3 length, and HCDR3 sequence with >80% identity. Matched heavy and light chain constructs were co-transfected into Expi293 cells using the ExpiFectamine^{TM} 293 Transfection Kit (Thermo Fisher Scientific) and cultures were incubated at 37°C, 8% CO_2 for 6 days. Supernatants were harvested and purified using rProtein A Sepharose Fast Flow resin (GE Healthcare) and buffer exchanged with 1X PBS (pH 7.4) before being concentrated using Amicon Centrifugal Filters (Millipore). Purified mAb concentrations were determined using a Nanodrop spectrophotometer.

Enzyme-linked immunosorbent assay (ELISA) for binding of mAbs to rPfCSP constructs

Immulon 4HBX flat bottom microtiter plates (Thermo Fisher Scientific) were coated with 100 µL per well of rPfCSP (FL, 0.5 µg/mL; 5/3, 0.337 µg/mL; $\Delta(NVDP)_4$, 0.499 µg/mL; N-CSP, 0.5 µg/mL; C-CSP, 0.5 µg/mL) in bicarbonate buffer overnight at 4ºC. Coated plates were blocked with 200 µL of 10% PBS + fetal bovine serum (FBS) for 2 h at room temp, followed by incubation for 2 h at 37°C with 100 µL of PfCSP or control mAbs at varying concentrations ($5x10^{-7}$ – 5.0 µg/mL, 10-fold serial dilutions in 10% PBS-FBS. Plates were incubated with 100 µL/well of 0.1 µg/mL horse radish peroxidase (HRP) conjugated goat anti–human IgG (Bethyl Laboratories). Plates were washed six times with PBS + 0.05% Tween-20 between each step. After a final wash, samples were incubated for 10 min with 1-Step Ultra TMB-ELISA Substrate (Thermo Fisher Scientific). The optical density at 450 nm (OD_{450}) was read after addition of

stopping solution (2N sulfuric acid, 100 µL/well). To generate area under the curve (AUC) heat maps, OD_{450} values were plotted against log-transformed mAb concentrations in GraphPad Prism (version 7.0) and the AUC analysis function was used to calculate the Peak Area with a baseline of Y (OD_{450}) = 0.2. The average AUC values for binding to each antigen from 2-4 replicate experiments were plotted as a Heat Map in Prism. Endpoint titers for the serum ELISAs were determined by nonlinear regression and interpolation of the log-transformed serum dilutions (GraphPad Prism, version 7.0).

ELISA for binding of mAbs to PfCSP peptides

Pierce™ Streptavidin Coated High Capacity Plates (Thermo Fisher Scientific) were coated with 100 µL per well of indicated peptides (0.01 µg/mL) diluted in wash buffer (Tris-buffered saline [25mM Tris, 150mM NaCl; pH 7.2], 0.1% BSA, 0.05% Tween-20) for 2 h at room temp, followed by incubation for 2 h at 37°C with 100 µL of PfCSP or control mAbs at varying concentrations ($5x10^{-7}$ – 5.0 µg/mL, 10-fold serial dilutions in wash buffer). Plates were incubated with 100 µL/well of 0.1 µg/mL HRP-conjugated goat anti–human IgG (Bethyl Laboratories) in wash buffer. Plates were washed three times with 200 µL wash buffer between each step. After a final wash, samples were incubated for 10 min with 1-Step Ultra TMB-ELISA Substrate (Thermo Fisher Scientific). OD_{450} was read after addition of stopping solution (2N sulfuric acid, 100 µL/well).

Epitope mapping and competition ELISAs (B. Flynn, VRC)

Epitope mapping was performed using PfCSP overlapping peptides (peptides 20-61) that were 15 amino acids in length (GenScript) and overlapped by 11 residues spanning the central repeat

region of PfCSP using the MSD U-Plex Assay platform (MSD) according to the manufacturer's instructions, with all mAb concentrations at 0.01 μg/mL. Competitive ELISA was also performed using peptides 20-61, $(NPNA)_4$, and $(NPNV)_4$. Briefly, ELISA plates were coated with 10 μl of rPfCSP (200 ng/mL) for 1 h at room temperature. After coating, PfCSP-specific mAbs (10 ng/mL) preincubated overnight with varying concentrations (0 – 1,000 μg/mL) of selected PfCSP peptides in PBS + 1% bovine serum albumin (BSA) were added to the rPfCSP-coated plates, and ELISA was performed on the MSD platform as described above. For the alanine scanning mutagenesis experiments, competitive ELISA was performed as described above using peptide 22 variants where each residue was mutated to an alanine or a serine if the original residue was an alanine (GenScript).

ELISA for quantitation of mAb serum titers (B. Flynn, VRC)

ELISA was performed on serum from mice passively transferred human PfCSP mAbs as previously described[84] using rPfCSP-coated plates (200 ng/mL). A standard curve for each mAb was generated using eight two-fold serial dilutions of mAb starting at 10 ng/mL. Serum samples were applied at various dilutions in dilution/blocking buffer. For datapoints in the linear range of the standard curve, the average of the calculated concentration values was used for each individual sample.

Fluorescent antibody labeling

Antibodies were conjugated to Alexa Fluor™ (AF) 405 or 750 molecules using a SAIVI Antibody Labeling Kit according to the manufacturers' directions but using AF405 NHS ester (Thermo Fisher Scientific), which was mixed with each mAb at an 8:1 molar ratio for 1 h at

room temperature. The reaction was then purified over the SAIVI column, with fractions collected to determine the location of the conjugate. mAbs were fluorescently labeled with the AF647 Antibody Labeling Kit according to the manufacturers' instructions (Thermo Fisher Scientific). Purified mAbs were mixed with reconstituted kit components, incubated for 1 h at room temperature, and purified over a column packed with the kit's purification resin. For determination of concentration and degree of labeling: AF405 conjugates: absorbance correction factor (CF) = 0.7; extinction coefficient (ε) = 34,500; AF647 conjugates: CF = 0.03, ε = 203,000; AF750 conjugates: CF = 0.034, ε = 270,000. Resulting PfCSP mAb conjugates had degree of labeling ratios between 1-4. Prior to use, conjugate binding was compared to unlabeled mAbs by rPfCSP ELISA and/or Pb-PfCSP-SPZ flow cytometry to confirm binding was not dramatically altered.

Biolayer interferometry (BLI) kinetic binding assay

Antibody binding kinetics were measured using BLI on an Octet HTX instrument (FortéBio) using streptavidin-capture biosensors (fortéBio). PfCSP mAb solutions were plated in black tilted-bottom 384-well microplates (fortéBio); assays were performed with agitation at 30°C. mAb serial concentrations used are as follow: 1.25, 0.625, 0.3125, and 0.15625 μg/mL. Loading of biotinylated peptides 21, peptide 22, and peptide 29 (GenScript) was performed for 300 sec, followed by dipping of biosensors into buffer (1% PBS-BSA) for 60 s to assess baseline assay drift. Association with whole IgG (serially diluted from 16.67 to 1.04 μM) was done for 300 sec, followed by a dissociation step in buffer for 600 sec. Background subtraction of nonspecific binding was performed through measurement of association in buffer alone. Data analysis and curve fitting were performed using Octet software, version 7.0. Experimental data were fitted

with the binding equations describing a 1:1 analyte-ligand interaction. Global analyses of the complete data sets, assuming binding was reversible (full dissociation), were carried out using nonlinear least-squares fitting allowing a single set of binding parameters to be obtained simultaneously for all concentrations of a given mAb dilution series.

Isothermal titration calorimetry (ITC) (A. Schön, JHU)

ITC was carried out using a VP-ITC microcalorimeter (Malvern Panalytical). In all titration experiments, the rPfCSP constructs and mAbs were prepared in PBS, pH 7.4. Each antibody solution, prepared at a concentration of ~40 µM (expressed per antigen binding site), was injected in 5 or 7 µl aliquots into the calorimetric cell containing the respective rPfCSP construct at a concentration of ~0.4 µM except for rPfCSP_5/3, which was prepared at 0.8 µM, at the specified temperatures (15-35°C). The concentration of either of the peptides 22, 25, 29 and NANPNVDP was ~2.5 µM. The exact concentrations of the reactants in each experiment were determined from the absorbance at 280 nm. The heat evolved upon each injection of antibody was obtained from the integral of the calorimetric signal. The heat associated with binding to the different rPfCSP constructs was obtained by subtracting the heat of dilution from the heat of reaction. The individual heats were plotted against the molar ratio, and the enthalpy change, ΔH, the association constant, K_a (the dissociation constant, $K_d = 1/K_a$) and the stoichiometry (valency of antigen binding sites), N, were obtained by nonlinear regression of the data to a model that takes into account the binding to either one or two sets of sites with different binding affinities. Gibbs energy, ΔG, was calculated from the relation $\Delta G = -RT\ln K_a$, where R is the universal gas constant, (1.987 cal/(K × mol)) and T the absolute temperature in Kelvin. The entropy contribution to Gibbs energy, $-T\Delta S$, was calculated from the known relation $\Delta G = \Delta H - T\Delta S$. The results were expressed per mole of antigen

binding sites and the stoichiometry, *N*, denotes the number of antigen binding sites per mole of the respective rPfCSP construct.

Measurement of PfCSP mAb binding to SPZ

Salivary glands containing SPZ were dissected as previously described (Flores-Garcia et al., 2019) into PBS containing the protease inhibitor E-64 (Millipore-Sigma). Freshly isolated Pb-PfCSP-GFP/Luc-SPZ were purified across an Accudenz density gradient (Accurate Chemical) to remove mosquito debris as previously described[182] and resuspended in PBS containing the protease inhibitor E-64 (Sigma-Aldrich) to prevent proteolytic processing of PfCSP. SPZ were stained with SYBR Green (10,000X concentrate; Thermo Fisher Scientific) diluted 1:2,000 in PBS for 30 min at 4ºC, washed twice, and ~8,000 SPZ were aliquoted to each well of a 96-well V-bottom plate (50 µl/well). SPZ were incubated for 30 min at 4ºC with PfCSP mAbs or isotype control in 10% PBS-FBS, washed twice with 200 µl PBS-FBS, stained for 20 minutes at 4ºC with goat anti-human IgG-AF647 secondary antibody (Thermo Fisher Scientific) diluted 1:1,000 in PBS-FBS, washed once with 200 µl PBS-FBS, and fixed in 200 µL 0.5% PBS + paraformaldehyde (PFA). Following fixation, events were acquired on a modified LSR II (BD Biosciences) and analyzed using FlowJo v.10.

Intravenous (IV) and intradermal (ID) mouse challenge studies with Pb-PfCSP-SPZ (L. Pereira, M. Dillon, B. Bonilla, VRC)

Specified amounts of anti-PfCSP or control mAbs diluted in sterile-filtered PBS (200 µl/mouse) were injected into the tail veins of female 6- to 8-week-old B6(Cg)-Tyrc-2J/J albino mice. For IV challenge, 2,000 freshly harvested Pb-PfCSP-GFP/Luc-SPZ in Leibovitz's L-15 medium

(Sigma-Aldrich) were injected into the tail vein 2 hours after mAb administration. For ID challenge, 5,000 freshly harvested Pb-PfCSP-GFP/Luc-SPZ in L-15 medium were injected into the paw either 24 or 72 hours after mAb administration. Liver burden (40-42 hours post-challenge) or parasitemia (days 5 or 7 post-challenge) were respectively quantified by intraperitoneally injecting mice with 150 µl of D-Luciferin (30 mg/mL), anesthetizing them with isoflurane, and measuring the bioluminescent radiance (total flux; photons/sec) expressed by Pb-PfCSP-GFP/Luc-SPZ using the *in vivo* imaging system (IVIS) Spectrum (PerkinElmer) 10 min after luciferin injection. Total flux in regions of interest were quantified using Living Image 4.5 software (PerkinElmer).

Mosquito bite challenge with Pb-PfCSP-SPZ (Y. Flores-Garcia, JHU)

Female *Anopheles stephensi* mosquitoes were allowed to feed on female 8-week old Swiss Webster mice infected with blood-stage Pb-PfCSP-SPZ. Twenty days after infected bloodmeal, the proportion of infected mosquitoes was between 70-80%, as assessed by microscopic observation of 20 salivary glands. Based on this observation, 6-7 mosquitoes were needed to expose mice to the bites of ~5 infected mosquitoes. Female 6-8 week old C57BL/6 mice were injected IV with specified doses of PfCSP mAbs diluted in 1X PBS (pH 7.4) in a total volume of 200 µL. At specified timepoint after mAb administration, mice were subjected to a small tail vein bleed to ascertain pre-challenge mAb serum titers. At specified timepoint after mAb administration, test and control mice were anesthetized with 2% Avertin (Alfa Aesar, Ward Hill, MA). Mosquitoes were allowed to feed on mice for 10 min. Following feeding, mosquito abdomens were inspected to confirm blood meals. Mouse parasitemia was assessed daily through Giemsa staining of blood smears starting on day 4 and up to day 12 post-challenge.

Growth inhibition activity assay (K. Miura, NIAID)

GIA of PfMZ was performed by the GIA Reference Center, NIH, USA as previously described[140]. Briefly, plasma or purified IgG_1 (10 mg/mL and 1-2.5 mg/mL, respectively) were incubated with human erythrocytes infected with synchronized Pf_3D7 parasites (40 µL) at 37°C for 40 h. Parasitemia was quantified by biochemical determination of Pf lactate dehydrogenase. To determine GIA EC_{50}, select mAbs were diluted in specified dilution ranges.

Quantification and statistical analysis (B. Mayer, M. Gerber, R. Gottardo, VISC)

Statistical tests used, exact value of n, what n represents, and precision measures can be found in figure legends. Unless otherwise indicated, all data were plotted using GraphPad Prism, version 7.0. For >3 comparisons, all mAbs were compared for significance to untreated/isotype control or to each other using the Kruskal-Wallis test with Dunn's post-hoc correction for multiple comparisons. For 2 comparisons, the two-tailed Mann-Whitney test was used. For the *in vitro* hepatocyte invasion assay, two-way analysis of variance (ANOVA) was used to compare each mAb to the isotype control at each respective concentration and adjusted for multiple comparisons using Bonferroni's post-hoc test. For the intravital liver imaging data (locations, traversal, CSPR, and dotty death), all mAbs were first compared to each other using an omnibus chi-squared test; if the distribution varied significantly, then each individual mAb was compared to isotype control (or the best performing mAb) and adjusted for multiple comparisons using Bonferroni's post-hoc test. For measurement of PfCSP mAbs in mouse serum, standard curves were fitted with a hyperbolic parameter curve, and concentration values in the linear range of the standard curve were interpolated. For the ITC stoichiometry data, errors with 95% confidence

were estimated from the fits of the data. For the mosquito bite challenge experiments in Chapter IV, L9 was tested for superiority against the other mAbs (one-sided tests) and *P*-values were corrected using the Holm method[183]. For the Kaplan–Meier curves, comparisons were tested using the log-rank test; an exact *P*-value was calculated when the sample size did not exceed 15 in either group[184]. The relationship between dose or circulating serum mAb concentration prior to challenge and protection were modeled using two-parameter logistic (2PL) models with the following functional form: $y = 1/1 + (x/ED_{50})^{h})$[185]. The ED_{50} (or EC_{50} for concentration) is the effective dose that elicits 50% protection and the hill slope, h, determines the steepness of the logistic curve. The 2PL model was fit to the data using logistic regression with a log-transformed dose or concentration covariate. For mAbs eliciting at least 50% protection, a single model was fit assuming a common hill slope and a mixed model was used with a random intercept specified for each experiment. ED_{50}, EC_{50}, ED_{80}, and ED_{80} with 95% confidence intervals were estimated from these fitted models using parametric simulation. Protection was compared between L9 and the other mAbs using the dose-adjusted or concentration-adjusted odds ratio (OR) from these models. For mAbs eliciting less than 50% protection, separate logistic models with small-sample size corrections (Firth-correction) were fit for each paired adjusted OR comparison[186]. *P*-values of OR were corrected together within dose or concentration comparisons. Protection analyses were conducted in R programming language (CRAN)[187]. Mixed effects logistic regression models were implemented with the lme4 package[188], simulations were implemented with the arm package[189], and data manipulation and visualization were implemented with the tidyverse packages[190,191]. Statistics for X-ray crystal structures were calculated by Phenix and MolProbity[192].

2.2 Chapter III methods

Generation of junctional probe (J. Nelson and N. King, IPD)

S02, a 43-residue structurally stabilized peptide mimicking the junctional epitope (MPESSSNPDCNANPNVDPNEDLIKKCEKINVPTEEIKKEIEEKK), was designed using Rosetta[193] by modifying the junctional peptide 21 with flanking sequences to stabilize the peptide in a conformation that retains binding by the neutralizing junctional antibody CIS43, but which is unfavorable to binding by the poorly neutralizing junctional antibody CIS42[84]. Sera from 14 protected subjects in group 6 of VRC 314 who received a total of three doses of radiation-attenuated PfSPZ (9.0×10^5) IV at weeks 0, 8, and 16 were screened for antibody titers against S02 using ELISA. A subject whose sera demonstrated the highest reactivity against S02 at the week 20 timepoint, 4 weeks after the last immunization, was chosen for memory B cell (MBC) sorting and mAb isolation.

rPfCSP and S02 probe generation (J. Francica, VRC)

For tetramer probe generation, rPfCSP or S02-DsbC (S02 fused to the disulfide bond C protein) were first biotinylated and then respectively conjugated to the fluorophores fluorescein isothiocyanate (FITC) and Brilliant Violet™ (BV605) (BD Biosciences). Biotinylation was performed using ligase Bir A (Avidity) at 30°C for 4 h prior to buffer exchange with 1X PBS (pH 7.4) over a 30-kDa Centricon Plus-70 Centrifugal Filter (Millipore) to remove excess free biotin. Biotinylated rPfCSP and S02-DsbC were fluorescently labeled through sequential addition of streptavidin conjugated to FITC (SA-FITC) or BV605 (SA-BV605), respectively, in a 4:1 molar ratio.

Isolation of PfCSP-specific MBCs by probe sorting (J. Francica and D. Ambrozak, VRC)

Probe-specific MBCs were isolated from cryopreserved PBMCs stained with the following panel: Aqua LIVE/DEAD (Thermo Fisher Scientific), rPfCSP-FITC and S02-BV605 tetramer probes, and antibodies against CD3-APC/Cy7 (BioLegend), CD8-V450 (BD Biosciences), CD14-BV785 (BioLegend), CD20-Alexa Fluor 700/PE (BioLegend), IgM-PE/Cy5 (BD Biosciences), and IgG-APC (BD Biosciences). Cells were sorted using a BD FACS Aria II (BD Immunocytometry Systems), and flow cytometry data were analyzed using FlowJo software (Tree Star). PfCSP-reactive (rPfCSP^{+} and/or S02^{+}) CD20^{+}CD3^{-}CD14^{-} MBCs were single-cell sorted into 96-well PCR plates containing lysis buffer (RNase OUT, 5X First-Strand buffer, DTT, IgePAL, and water; SuperScript III First-Strand Synthesis System, Thermo Fisher Scientific).

IV challenge with PfSPZ (A.S.P. Yang and R. Sauerwein, Radboud Univ.)

Female 8-9 month old FRG-huHep mice with engrafted human hepatocytes from two different donors (HHM19027 and HHM13022) were purchased from Yecuris Corp. Repopulation of human hepatocytes were confirmed by the level of serum albumin and ranged between 4,000-8,000 μg/mL, evenly divided between the different experimental groups. Mice were intravenously injected with the indicated dose of VRC01 or PfCSP mAbs (100 μL per mouse) 24 hours before PfSPZ challenge. On the day of PfSPZ challenge, *Anopheles stephensi* mosquitoes infected with Pf NF54 (on day 14-18 post blood meal) were harvested into Dutch modified RPMI 1640 media (Thermo Fisher Scientific). 100,000 PfSPZ (in a total volume of 100 μl) were injected IV in the tail vein of each mouse. Six days following challenge, serum was collected via cardiac bleed and livers of each mice were harvested as previously described[96,194]. Briefly, lobes were pooled and

emulsified to obtain single-cell suspensions for subsequent genomic DNA (gDNA) extraction. gDNA were extracted from roughly 25% of the chimeric livers and used to quantify parasite load using oligonucleotides specific for Pf 18S ribosomal RNA (rRNA) as previously described[96,195]. PCR was used to quantify the relative amount of human hepatocytes engrafted onto the mouse liver, as previously described[196].

NVDP conservation in global field isolates

PfCSP sequences and country in which the sequences were isolated were retrieved from GenBank. N- and C-terminal sequences were trimmed in Geneious Prime (Geneious) and the central repeat region sequences was exported into Microsoft Excel. All NPDP tetrapeptides were transformed into 0, NANP repeats into 1, and NVDP repeats into 2; sequences were numerically ordered based on number of NVDP repeats and the geographic region in which they were isolated was indicated.

Generation of mAb L9LS

The L9 Fc heavy chain was modified to include a LS mutation (L9LS) to extend its serum half-life. Restriction enzymes (NEB) were used to digest plasmids carrying the L9 heavy chain and the VRC01LS heavy chain (W. Shi, VRC). The variable region of the L9 heavy chain was ligated to the Fc heavy chain containing the LS mutation and a kanamycin selection marker using the Quick Ligation Kit (NEB). The resultant ligation mix was transformed into DH5α cells (Thermo Fisher), grown under antibiotic selection, and sequenced to confirm that the L9LS variable regions was identical to the L9 WT parent and that the LS mutation was present in the

Fc. The L9LS heavy chain plasmid and the L9 kappa chain were co-transfected into Expi293 cells (Thermo Fisher Scientific) and purified over protein A (GE Healthcare).

Generation of anti-idiotypic antibody against L9 Fab (W.P. Kong and W. Shi, VRC)

Mouse mAbs specific for the L9 idiotype were generated as previously described[197]. Briefly, L9 Fab was generated by LysC digestion and female Balb/c mice (Jackson Laboratory) were intramuscularly immunized twice with 20 μg of L9 Fab in 100 μL PBS and Ribi adjuvant (Millipore Sigma) at 0 and 4 weeks. Ten days post-boost, ELISA was used to test serum reactivity against L9 Fab and mice with high L9 reactivity were selected for cell fusion. Three days before cell fusion, L9-reactive mice were boosted IV with 20 μg of L9 Fab in 100 μL PBS prior to spleen excision. Splenocytes were purified and fused with myeloma cells Sp2/0 (ATCC) in a 2:1 ratio according to established fusion protocols[198]. Ten days post-fusion, triplicate hybridoma supernatants were screened for L9 Fab reactivity. PCR was performed to amplify the heavy and light chain antibody genes of positive hybridomas, which were cloned into mouse IgG2a expression vectors (Gene Synthesis), expressed in Expi293 cells (Thermo Fisher Scientific), and purified over protein A (GE Healthcare). ELISA was performed with plates coated with L9 or CIS43 IgG.

Pharmacokinetics studies in non-human primates (J.P. Todd and TRP, VRC)

Nine healthy, naïve rhesus macaques (one male and two females/group) from the VRC NHP program were randomized into three study groups and dosed once IV with 10 mg/kg of CIS43LS, L9LS, and L9 in a volume of 8 mL/monkey administered into the right saphenous vein via slow hand push over 3-4 min. Detailed observations at dosing included body weight and

temperature, while temperature, pulse, and respiration were noted 4 hours post-dosing. Pre-dose and at each blood collection, detailed observations (e.g., body weight, body temperature, pulse rate, and respiration rate) were measured. For dosing and blood collection, all animals were sedated with injectable anesthetic agents and the infusion site or blood draw site was disinfected. Blood samples were obtained from the femoral veins according to facility standard operating procedures at 12 post-dose time points: day 1 (i.e., 24 hours post-dose), 2, 7, 14, 28, 42, 56, 70, 84, 98, 112 and 126. Upon completion of the infusion and each phlebotomy, the animals were closely monitored until fully recovered from anesthesia. After the day 126 blood collection, the health of each macaque was re-verified prior to return of the animal to the NHP program. The monkeys were made available for reuse and have been subsequently used for other research projects.

2.3 Chapter IV methods

ELISA for binding of mAbs to $NANP_9$ (B. Flynn, VRC)

Gold microtiter plates (MSD) were blocked with 5% PBS-BSA (20 µl/well). Blocked plates were coated with 10 µl/well of NANP biotinylated peptides (240 pmol, GenScript) in 1% PBS-BSA for 1 h at room temperature. The coated plates were incubated for 2 h at room temperature with 10 µl of PfCSP or control mAbs at varying concentrations ($5x10^{-7}$ – 5.0 µg/mL, 5-fold serial dilutions). Plates were then incubated with 10 µl/well of 1.0 µg/mL Sulfo-tag goat anti–human IgG (MSD) for 1 h at room temperature. Plates were washed six times with PBS-Tween between each step. After a final wash, 35 µl of 1X Read T Buffer (MSD) was added to each well and plates were analyzed on a Sector Image 2400 instrument (MSD).

Measuring mAb concentrations in the skin (B. Flynn, VRC)

Mouse skin punches were weighed and homogenized for 2 min in 1.5 mL tubes containing 400 µL PBS supplemented with cOmplete, EDTA-free Protease Inhibitor (Roche). Homogenates were centrifuged at 14,000 RPM for 15 minutes at 4°C and supernatants were filtered through 0.22 µm spin filters and stored at –80°C until ELISA measurement. mAb amounts were normalized to the weight of skin biopsies.

***In vitro* inhibition of Pf invasion of HC-04 hepatocytes (A. Fabra-Garcia, Radboud Univ.)**

The human hepatoma cell line HC-04 was used to evaluate the *in vitro* capacity of the PfCSP mAbs to block hepatocyte invasion by PfSPZ NF54. HC-04 cells were seeded at 50,000 cells/well in rat tail collagen pre-treated 96-well plates for 16-24 h. Salivary gland PfSPZ were pre-mixed with heat-inactivated human serum and varying concentrations of PfCSP mAbs (10, 1 or 0.1 µg/mL)

for 30 min on ice and then seeded in triplicate (50,000 sporozoites/well) onto the HC-04 cells. Plates were centrifuged for 10 min at 3000 xg and incubated for 3 h at 37°C with 5% CO_2. Cells were washed with PBS (Gibco) and treated with trypsin (0.05% Trypsin-ethylenediamine tetra acetic acid (EDTA); Gibco) to generate a single-cell suspension. Subsequently, cells were fixed and permeabilized (eBioscience) for 30 min at 4°C. The staining was done with a cell viability dye (1:2,000; Fixable viability dye eFluor 780, eBioscience, Thermo Fisher Scientific) and a fluorescently-labelled mouse anti-PfCSP antibody (1:400; 3SP2-FITC) for 30 min at 4°C. After washing with 2% PBS-FBS, cells were fixed with 1% PBS-PFA and analyzed by flow cytometry using Gallios (Beckman Coulter) and FlowJo software (version 10.0.8, Tree Star).

***In vitro* inhibition of Pf invasion of primary hepatocytes (A. Idris and M. Marquette, MIT)**

In vitro infection of micropatterned hepatocyte-fibroblast co-cultures (MPCCs) was carried out as previously described[82,84,199]. Briefly, soft lithography techniques were used to pattern rat tail type I collagen (Corning) into 500 μm diameter islands on the surface of glass bottom 96-well plates (Greiner Bio). Cryopreserved primary human hepatocytes (Bioreclamation IVT) were thawed and 10,000 hepatocytes were seeded onto the collagen islands in serum-free Dulbecco's Modified Eagle Medium (DMEM) with 1% PenStrep. One day after hepatocyte seeding, PfCSP mAbs were added to the MPCCs in triplicate at three concentrations (10, 1.0, and 0.1 μg/ml) 30 min prior to infection with 7×10^4 fresh PfSPZ per well. Plates were incubated for 3 h at 37°C with 5% CO_2. Cells were then washed with hepatocyte culture medium containing 3% PenStrep and 0.1% Fungizone, and 7,000 3T3-J2 fibroblasts were added to create the coculture. Medium was replaced daily until samples were fixed with methanol at 4°C on day 3.5 post infection. Plates were kept at 4°C until staining. To visualize the exoerythrocytic forms (EEFs) of the

parasite, PfHSP70 (mouse 4C9 clone) was used with a fluorescently-labelled secondary antibody (donkey anti-mouse IgG, AF594, Thermo Fisher Scientific) coupled with a nuclear stain Hoechst (Thermo Fisher Scientific). Liver-stage parasites or EEFs were enumerated using a Nikon Eclipse Ti fluorescence microscope.

Intravital liver imaging of Pb-PfCSP-SPZ (J. O'Connor and I. Cockburn, ANU)

Female 6- to 12-week old C57BL/6 mice (The Jackson Laboratory) received sequential IV injections of AF405-labeled mAbs (30 µg, blinded), 1 x 10^5 Pb-PfCSP-GFP-SPZ, and rhodamine-labeled dextran (20 µg/mL, 50 µL). Mice were immediately prepared for multiphoton microscopy as previously described[200]. Briefly, mice were anaesthetized with a mix of Ketamine (100 mg/kg) and Xylazine (10 mg/kg). The mouse temperature was maintained at 37ºC using a heating mat attached to a feedback probe inserted in the mouse rectum throughout the surgery and imaging procedure. A lateral incision was made over the left lobe of the liver and any vessels cauterized by applying light pressure to the vessel until clotting occurred naturally. The mouse was then placed in a custom-made holder. The liver was exposed and directly adhered to a coverslip that was secured in the holder. Once stable, the preparation was transferred to a Fluoview FVMPE-RS multiphoton microscope system (Olympus) equipped with a XLPLN25XWMP2 objective (25x; NA1.05; water immersion; 2mm working distance). For quantification of parasites, damaged hepatocytes, and shedding of PfCSP, a single 50 µm Z-stack (2 µm/slice) was acquired using a resonance scanner. Fluorescence of AF405, GFP and rhodamine were detected using an 860 nm wavelength laser. For videos of traversal or shedding, a sequence of between 1,000-2,000 50 µm Z-stacks (2 µm/slice) was acquired using a resonance scanner. Images were acquired using FV30 software (Olympus) and exported to Imaris

(Bitplane) for downstream processing. SPZ and shed PfCSP were measured using the measurement function on Imaris. SPZ were classified as either sinusoid-bound, traversing hepatocytes, or having infected a hepatocyte based on the following criteria. Any SPZ located within a sinusoid and not within 40 μm (i.e., diameter of a hepatocyte) of a rhodamine$^+$ hepatocyte was considered to be vessel bound in the sinusoid. Any SPZ within 40 μm of at least one rhodamine$^+$ hepatocyte and still in contact with the traversed hepatocyte was considered to be traversing. Any sporozoite within 40 μm of at least one rhodamine$^+$ hepatocyte, but not in a sinusoid nor in contact with a rhodamine$^+$ hepatocyte, was considered to have established infection. Additionally, any SPZ with a discontinuation (i.e., fragmentation) of GFP along its length was classified as undergoing "dotty death", and any sporozoite with a length of AF405 not colocalized with GFP was considered to be shedding its mAb-bound PfCSP coat and undergoing a CSPR. Parasite death in any of the resonance videos was characterized as bursting if a sudden loss of membrane integrity and release of GFP into the surrounding tissue was observed.

2.4 Chapter V methods

Isolation of plasmablasts (PBs) (A. Idris and B. Flynn, VRC)

PBs were isolated from freshly isolated PBMCs collected seven days after Sanaria PfSPZ Vaccine immunization as previously described[84]. Briefly, PBMCs were stained for viability with Aqua LIVE/DEAD (Thermo Fisher Scientific) followed by surface staining of the following markers: CD3-PE/Cy7 (BD Bioscience), CD19-FITC (BD Bioscience), CD20-APC/Cy7 (BD Bioscience), CD27-APC (Thermo Fisher Scientific), and CD38-PE (BD Bioscience). PBs were gated as live $CD3^-CD20^-CD19^+CD27^+CD38^+$ and single cell sorted using a BD FACS Aria II (BD Immunocytometry Systems) into 96-well PCR plates containing 20 µL/well of RT reaction buffer from the SuperScript™ First-Strand Synthesis System for RT-PCR (Thermo Fisher Scientific). Plates were snap frozen on dry ice and stored at -80°C.

Determination of $L9_{MRCA}$ (most recent common ancestor) sequence (C.H. Shen, VRC)

The heavy chain and kappa chain sequence of $L9_{MRCA}$ were determined using a previously described informatics pipeline for antibodyome analysis[201]. The variable (V), diversity (D), joining (J), and V(D)J gene recombination were assigned and analyzed by IgBLAST[202]. Multiple sequence alignments of the germline gene and sequences related to L9 were aligned by mafft[203] and the MRCA was computed using dnaml with default parameters[204].

Fab production and size exclusion chromatography (SEC) (N. Hurlburt, Fred Hutch)

Purified recombinant IgGs were mixed with LysC (NEB) at a ratio of 1 µg LysC per 10 mg of IgG and incubated at 37°C for 18 h with nutation. The cleaved product was incubated with Protein A resin (GoldBio) at a ratio of 1 mL resin per 10 mg of initial IgG and incubated at room

temperature for 1 h to bind any uncleaved IgG and digested Fc. The purified Fab was further purified by SEC using a HiLoad 16/600 Superdex 200 pg column (GE Healthcare). Purified Fabs were incubated with 2-fold molar excess of peptide 22 and incubated at room temp for 1 hr. Fab-peptide complexes were run on a HiLoad 16/600 Superdex 200 pg column (GE Healthcare).

Crystal screening and structure determination (N. Hurlburt, Fred Hutch)

Purified Fabs were incubated with 1.5 molar excess of the synthetic NANPNVDP peptide (GenScript). Initial crystal screening was performed by sitting-drop vapor-diffusion in the MCSG Crystallization Suite (Anatrace) and ProPlex (Molecular Dimensions) using a NT8 drop setter (Formulatrix). For apo-L9, crystals grew in ProPlex E5 and diffracting crystals were harvested directly from screen and cryoprotected using Paratone-N. Data was collected at Advanced Light Source (ALS) beamline 5.0.2 at 12.398 keV. For $F10_HL9_K$-NANPNVDP, diffracting crystals were grown in a mother liquor (ML) containing 0.1 M sodium citrate, pH 3.5, 1.5 M $(NH_4)_2SO_4$. Crystals were cryoprotected in ML supplemented with 30% ethylene glycol. Diffraction data was collected at ALS beamline 5.0.2 at 12.286 keV. For $L9_HF10_K$-NANPNVDP, diffracting crystals were grown in a ML containing 0.1 M MES, pH 6.5, 18% PEG 4K, and 0.6 M NaCl. Crystals were cryoprotected in ML supplemented with 30% ethylene glycol. Diffraction data was collected at ALS beamline 19-ID at 12.669 keV. All datasets were processed using XDS[205] and data reduction was performed using AIMLESS in CCP4[206] to a resolution of 2.98, 1.89, and 2.23 Å for apo-L9, $F10_HL9_K$-NANPNVDP, and $L9_HF10_K$-NANPNVDP, respectively. Initial phases for apo-L9 were solved by molecular replacement (MR) using Phaser in Phenix[207] with a search model of 1210 Fab (PDBid: 6D01) divided into Fab and Fc portions. The model of L9 was used as the search model for the MR of the chimera structures using Phaser. Model

building was completed using Coot[208] and refinement was performed in Phenix. The data collection and refinement statistics are summarized in Appendix 3. Structural figures were made in PyMOL (Schrodinger, LLC).

Competitive ELISA (B. Flynn, VRC)

For competition of binding to rPfCSP (FL, 5/3, $\Delta(NVDP)_4$) by junctional peptide 21-25 and $(NANP)_9$, Immulon 4HBX flat bottom microtiter plates (Thermo Fisher Scientific) were coated with rPfCSP (FL, 5/3, or $\Delta(NVDP)_4$; 9 nM) for 1 h at 37°C and then blocked with 5% BSA. PfCSP mAbs were preincubated for 2 h at 37°C with varying concentrations (0 – 1,000 μg/mL) of either the junctional peptide 21-25 or the $(NANP)_9$ peptide before being added to the coated plates. Plates were then incubated for 1 h at room temperature with 1:20,000 dilution of HRP-conjugated goat anti–human IgG (Thermo Fisher Scientific). The plates were washed five times with PBS-Tween between each step. After a final wash, samples were incubated for 10 min with 1-Step Ultra TMB-ELISA Substrate (Thermo Fisher Scientific). OD_{450} was read after addition of stopping solution (2N sulfuric acid). Competition of binding to $rPfCSP_{FL}$ by peptides 20-61, was performed as described above, with plates coated with 200 ng/mL of $rPfCSP_{FL}$ and peptide concentrations ranging from 0 – 1,000 μg/mL.

PfCSP mAb-mediated immobilization and CSPR induction of Pb-PfCSP-SPZ (Y. Flores-Garcia, JHU)

The *in vitro* motility assays were performed as previously described[209]. Briefly, freshly harvested SPZ suspended in Hank's balanced salt solution containing 2% FBS (HBSS-FBS) were adjusted to a concentration of 10,000 SPZ/μL and 20 μL were allowed to settle on a 35 mm glass bottom

Mattek dish for 10 min on ice. Motility was subsequently assayed using time-lapse microscopy at 37ºC, with recordings made using an Olympus IX-71 inverted wide-field fluorescence microscope with a PCO complementary metal-oxide-semiconductor (CMOS) camera driven by DeltaVision software (Applied Precision, Seattle, WA). SPZ were imaged using an LED light source and FITC filter to visualize GFP expressed by the parasite. A field of view containing approximately 30 SPZ was chosen, and a video was taken using a 5 s time-lapse for 15 min total. mAbs diluted in HBSS-FBS were added directly to the dish containing the SPZ suspension to a final concentration of 25 μg/mL. Parasites continuously moving in a circle before mAb addition were identified as motile and as non-motile only if their circular movement came to a complete stop 15 min after mAb exposure. Motility was assessed with the assistance of ImageJ software. Percentage of non-motile parasites were calculated as follows: non-motile SPZ x 100 / total SPZ. For the *in vitro* CSPR assay, 50 μl of freshly harvested SPZ in HBSS-FBS (10,000 SPZ/μL) were incubated at 37°C in a microtube with 50 μg/mL of PfCSP mAb. After 15 min, an aliquot of the parasite suspension was placed in a hemocytometer and observed by light microscopy using a 40X magnifying lens. The number of parasites with or without a CSPR-induced tail were recorded. Percentage of CSPR positive and negative parasites were calculated as follows: CSPR SPZ x 100 / total SPZ.

2.5 Chapter VI methods

Flow cytometric measurement of AF647-labeled mAb SPZ binding

Freshly isolated Pb-PfCSP-GFP/Luc-SPZ or PfSPZ in PBS ± 10 μM E-64 were stained with SYBR Green (10,000X concentrate; Thermo Fisher Scientific) diluted 1:2,000 in PBS for 30 min at 4ºC, washed twice, and ~8,000 SPZ were aliquoted to each well of a 96-well V-bottom plate (50 μl/well). For measurement of single mAb binding, SPZ were incubated for 30 min at 28ºC with anti-PfCSP or control mAbs in DMEM or PBS (Thermo Fisher Scientific), washed twice with 200 μl PBS, stained for 20 minutes at 4ºC with goat anti-human IgG-AF647 secondary antibody (Thermo Fisher Scientific) diluted 1:1,000 in PBS, washed once with 200 μl PBS, and fixed in 200 μL 0.5% PBS-PFA. For measurement of 5D5-AF647 binding, SPZ were incubated with specified concentrations of unlabeled mAbs for 1 h at 28ºC in DMEM ± 0.5 μM cytochalasin D (Millipore Sigma) followed by 20 μg/mL of 5D5-AF647 for 10 min at 28ºC. Subsequently, SPZ were washed twice with 200 μl PBS and fixed in 200 μL 0.5% PBS-PFA. Following fixation, events were acquired on a modified LSR II (BD Biosciences). FlowJo v.10 was used to determine the percentage in AF647 of SYBR Green-positive events corresponding to SPZ that were in a gate drawn to exclude background unstained events; median fluorescence intensity of AF647 events was also analyzed.

ELISA measurement of N-CSP mAb 5D5 binding to rPfCSP in presence of heparin

Immulon 4HBX flat bottom microtiter plates (Thermo Fisher Scientific) were coated with 100 μl per well of 0.5 μg/mL rPfCSP in bicarbonate buffer overnight at 4ºC. Coated plates were blocked with 200 μl of 10% PBS-FBS for 2 h at room temperature, followed by incubation with 100 μl of 5D5 at varying concentrations ($5x10^{-7}$ – 5.0 μg/mL, 10-fold serial dilutions) in PBS-FBS

containing 5 μg/mL heparin (Millipore Sigma) for 2 h at 37°C and incubation with 100 μl/well of 0.1 μg/mL HRP-conjugated goat anti–human IgG (Bethyl Laboratories) for 1 h at room temperature. Plates were washed six times with PBS-Tween between each step. Samples were then incubated for 10 min with 100 μL 1-Step Ultra TMB-ELISA Substrate (Thermo Fisher Scientific) prior to the addition of stopping solution (2N sulfuric acid, 100 μl/well). OD_{450} was measured for each plate.

Epitope binning

Epitope binning experiments were performed with the Carterra LSA. A HC30M chip (Carterra) was primed with filtered and degassed 25 mM 2-(N-morpholino)ethanesulfonic acid buffer supplemented with 0.05% Tween-20 (Thermo Fisher Scientific). The chip was activated with a mixture of 400 mM 1-ethyl-3- (3-dimethylaminopropyl)carbodiimide hydrochloride and 100 mM N-hydroxysuccinimide (Thermo Fisher Scientific). Next, 10 μg/mL of each mAb in pH 4.5 acetate buffer was directly coupled to discrete spots on the chip, followed by blocking with 1M ethanolamine (pH 8.5). The chip was then primed with HEPES-buffered saline Tris-EDTA + 0.05% BSA. Monomeric 200 nM FL-rCSP was added to the antibody spots, followed by addition of 10 μg/mL of the sandwiching mAb. Regeneration after incubation with each sandwiching antibody was performed with 10 mM glycine pH 2.0. Binning data were analyzed using the Epitope Software (Carterra).

Flow cytometric measurement of AF750-labeled mAb sporozoite binding

Freshly isolated Pb-PfCSP-GFP/Luc-SPZ or PfSPZ were stained with SYBR Green and aliquoted as above. For measurement of single mAb binding, SPZ were incubated for 30 min at

28°C with anti-PfCSP or control mAbs in 10% PBS-FBS, washed twice with 200 µl PBS-FBS, stained for 20 minutes at 4°C with goat anti-human IgG-AF647 secondary antibody (Thermo Fisher Scientific) diluted 1:1,000 in PBS-FBS, washed once with 200 µl PBS-FBS, and fixed in 200 µL 0.5% PBS-PFA. For measurement of co-incubated AF750-labeled and unlabeled mAbs, SPZ were incubated with specified concentrations of both mAbs for 30 min at 28°C, washed twice with 200 µl PBS-FBS, and fixed in 200 µL 0.5% PBS-PFA. For measurement of co-incubated AF750-labeled mAbs and serum, SPZ were incubated with 0.2 µg/mL of AF750-labeled mAbs and serum diluted 1:5 in PBS-FBS for 30 min at 28°C, washed twice with 200 µl PBS-FBS, and fixed in 200 µL 0.5% PBS-PFA. Following fixation, events were acquired on a modified LSR II (BD Biosciences). FlowJo v.10 was used to determine the median fluorescence intensity in AF750 of SYBR Green-positive events corresponding to SPZ.

R21 immunizations in mice (M. Dillon, VRC)

R21 immunogen[210] was diluted in sterile PBS to 1 µg with 33.3 µL of army liposomal formula Q (ALFQ; liposomal adjuvant formulation containing monophosphoryl lipid A and QS-21[211]) in a final volume of 50 µL. Female 6- to 8-week-old B6(Cg)-Tyrc-2J/J albino mice were immunized intramuscularly in the quadriceps at 3 week intervals with 50 µL of R21 + ALFQ. Passive transfer of mAbs prior to Pb-PfCSP-SPZ challenge was performed 3 weeks following the last immunization (i.e., week 6), as described below.

2.6 Chapter VII methods

Plasma and mAb binding to antigen-coated beads

Streptavidin beads (Spherotech) were incubated with biotinylated RH5 (50 µg/mL), Ripr (50 µg/mL), CyRPA (10 µg/mL), RCR (3 µg/mL), MSP1 (10 µg/mL), and PfCSP (10 µg/mL) for 30 min at room temperature, washed with 0.5% PBS+BSA, blocked with CD4 (10 µg/ml; negative control antigen) for 30 min at room temperature, washed, mixed, aliquoted, and frozen at -80^{o}C. 1:20 diluted Malian plasma was incubated with thawed beads 1:1 for 30 min at room temperature, washed, and stained with 2.5 µg/mL goat anti-human IgG-AF647 (Jackson Immunoresearch). Twelve mAb dilutions were incubated with antigen-coated beads 1:1 for 30 min at room temperature, washed, and incubated with IgG-AF647 secondary. Following a wash, plasma- or mAb-bound beads were read with the iQue Screener Plus (Intellicyt) high-throughput flow cytometer and data were analyzed with FlowJo (Tree Star). Malian plasma data were normalized by dividing antigen median fluorescence intensity (MFI) by CD4 MFI. For mAb titrations, AUC values were calculated using GraphPad Prism and normalized to control mAbs run with each experiment.

Isolation of RH5-CyRPA-Ripr mAbs by MBC culture

Antigen-specific MBCs were identified by MBC culture as previously described[171]. Briefly, cryopreserved PBMCs were stained for 20 min at 4°C in PBS with LIVE/DEAD Fixable Aqua (Thermo Fisher Scientific) prior to staining for 20 min at 4°C in 1% PBS-FBS with the following panel: CD3-BV510, CD14-BV510, CD56-BV510 (BioLegend), CD19-ECD (Beckman Coulter), IgA-AF647 (Jackson Immunoresearch), IgM-PerCP-Cy5.5 (BD Biosciences) and IgD-PECy7 (BD Biosciences). Live single IgG^{+} MBCs were sorted using a BD FACSAria III by gating on

$CD3^-CD14^-CD56^-CD19^+IgD^-IgM^-IgA^-$ cells and 2 MBCs/well were plated into 384-well plates containing 10,000 cells/well irradiated 3T3-CD40L feeder cells (N. Doria-Rose, VRC) in I10 media (Iscove's modified Dulbecco's Medium, 10% FBS, 1:1000 MycoZap; Thermo Fisher and Lonza) supplemented with 100 U/ml interleukin (IL)-2 (Roche) and 50 ng/ml IL-21 (Thermo Fisher Scientific). After culturing at 37°C for 2 weeks, supernatants were harvested and incubated for 30 min at 4°C with streptavidin beads (Spherotech) coated with biotinylated RH5, CyRPA, Ripr, MSP1 (Wright lab, University of York), RCR (Higgins lab, University of Oxford), and PfCSP (Seder lab). Unwashed beads were then incubated with 1 µg/mL goat anti-human IgG-AF647 (Jackson Immunoresearch) for 30 min at 4°C and read with the iQue Screener Plus high-throughput flow cytometer; data were analyzed on the Forecyt program (Intellicyt).

Isolation of RH5-CyRPA-Ripr mAbs using the Beacon Optofluidic System

Antigen-specific MBCs were identified using the Beacon Optofluidic System as previously described[212]. Cryopreserved PBMCs were stained as above, except with the addition of CD27-AF488 (BioLegend) and CD38-APC/Cy7 (BioLegend). Single $CD3^-CD14^-CD56^-CD19^+CD27^+CD38^+$ PBs were sorted into Plasma Cell Survival Medium (Berkeley Lights), loaded onto an OptoSelect 11k chip, and individually moved into nanoliter-volume pens using opto-electropositioning (OEP) light cages drawn by the Beacon's Cell Analysis Suite (Berkeley Lights). 7 µm streptavidin beads (Spherotech) coated with 10 µg/mL of biotinylated RH5+CyRPA+Ripr were co-incubated with 2.5 µg/ml of goat anti-human IgG-AF647 (Jackson Immunoresearch) above the penned B cells and a 30 min time course was performed to measure secretion of IgG that bound the antigen-coated beads. Antigen-specific B cells were exported individually from the chip using OEP light cages (Cell Unload protocol, Berkeley Lights) and

transferred into 96-well plates containing lysis buffer. Alternatively, sorted single $CD3^{-}CD14^{-}CD56^{-}CD19^{+}IgD^{-}IgM^{-}IgA^{-}IgG^{+}$ MBCs were cultured via two methods: 1) 2,500 MBCs/well cultured in a proprietary cytokine cocktail (Berkeley Lights) for 6 days in 96-well U-bottom plates or, 2) 100 MBCs/well and 10,000 feeder cells/well cultured in I10 supplemented with 100 ng/mL IL-21 (Gibco), 0.5 µg/mL R848 (Mabtech), and 1 µg/mL human CD40L (R&D Systems) for 6 days in 384-well plates. After stimulation, culture supernatants were screened for binding to RH5/CyRPA/Ripr/RCR/MSP1/PfCSP-coated streptavidin beads (Spherotech) as above. MBCs of interest were loaded onto the Beacon, screened for antigen specificity, and exported as above.

Chapter III: Isolation and preclinical development of a potent PfCSP human mAb

3.1 Authorship statement

Sections of this Chapter were published in Wang et al., *Immunity* 2020 (10.1016/j.immuni.2020.08.014). Jorgen Nelson and Neil King created the junctional probe S02; Barbara Flynn screened the VRC 314 serum, performed detailed epitope mapping of CIS43 and L9, and measured serum mAb concentrations in macaques; Joe Francica and David Ambrozak stained and sorted MBCs; Rosemarie Mason, Nicole Cavett, and Reid Ballard optimized the human Ig PCR protocols; Alvaro Molina-Cruz provided infected mosquitoes for SPZ isolation; Azza Idris and Lais Pereira dissected SPZ and optimized the mouse model for assessing antibody-mediated protection against SPZ challenge; Marlon Dillon assisted with mouse experiments; Annie S.P. Yang performed the FRG-huHep mouse protection studies with PfSPZ; Arne Schön performed the ITC; Kazutoyo Miura performed the GIA assay; John-Paul Todd and the VRC Translational Research Program infused human mAbs and collected specimens from NHPs; Wei Shi and Wing-Pui Kong generated the L9 anti-idiotypic hybridomas.

3.2 Introduction

Shortly before I began my DPhil studies in 2018, two manuscripts were published that reported the isolation of rare potent neutralizing human PfCSP mAbs that exhibited dual specificity for NANP repeats and the unique tetrapeptide NPDP at the junction of the N-terminus and repeat region[84,213]. These data identified the subdominant junctional tetrapeptide NPDP as a

new site of vulnerability[214] and generated ongoing efforts to characterize new and more potent PfCSP mAbs against epitopes in the junctional region[215].

One of these rare junctional mAbs, CIS43, was cloned at the VRC from a subject in VRC 312 (https://clinicaltrials.gov/ct2/show/NCT01441167). VRC 312 was a phase 1, open-label, dose-escalation study investigating the safety, immunogenicity, and protective efficacy of IV administration of radiation-attenuated, aseptic, purified, cryopreserved PfSPZ derived from the NF54 strain (Sanaria PfSPZ Vaccine) in healthy malaria-naïve adults. VRC 312 subjects received five doses of 1.35×10^5 PfSPZ, which is a 1,000-fold greater challenge dose than the ~100 SPZ inoculated into humans from a single mosquito bite[88]. The exponentially increased antigen exposure in recipients of the PfSPZ Vaccine compared to naturally infected individuals likely generated higher-magnitude B cell responses against subdominant epitopes like NPDP and contributed to the successful isolation of a rare junctional mAb like CIS43.

Upon discovering that CIS43 was highly effective at preventing Pf malaria in mice[84], the VRC began developing CIS43 with a LS mutation to extend serum half-life (CIS43LS) for a Phase I clinical trial to assess its safety and efficacy in preventing malaria infection in humans[216,217]. As part of this preclinical development process, a pharmacokinetics (PK) study was performed in NHPs to ensure that CIS43LS had greater serum half-life than wild-type CIS43. Furthermore, anti-idiotypic mAbs that recognize the unique idiotope (i.e., variable region) of CIS43 with high specificity[218] were generated for use as reagents to accurately measure serum concentrations of CIS43LS in trial participants.

This Chapter details the isolation, initial characterization, and initial preclinical development of a PfCSP human mAb called L9 that binds a previously uncharacterized site of vulnerability in the PfCSP junctional region and is even more potently protective than CIS43.

3.3 Isolation of a new panel of human PfCSP mAbs from VRC 314

The initial goal of my research was to isolate a PfCSP human mAb that was more potent than CIS43, the VRC's best first-generation PfCSP mAb. In order to isolate mAbs more potent than CIS43, I focused my attention on clinical specimens from subjects in VRC 314 who received three IV doses of 9.0 x 10^5 PfSPZ at weeks 0, 8, and 16. VRC 314 (https://clinicaltrials.gov/; NCT02015091) was a Phase 1, open-label, dose-escalation clinical trial that assessed safety, immunogenicity, and durability of protection following IV and intramuscular administration of the PfSPZ Vaccine in healthy malaria-naïve adults. Notably, VRC 314 subjects were immunized with ~7-fold higher PfSPZ doses than the VRC 312 subjects from which CIS43 was isolated.

3.3.1 Screening of human serum from VRC 314 for junctional reactivity

Structural analysis and molecular dynamics simulations demonstrated that CIS43 bound at a specific angle to a rare conformation of the junctional peptide 21 (NPDPNANPNVDPNAN)[84]. To facilitate isolation of new junctional-reactive PfCSP human mAbs, collaborators at the Institute for Protein Design created a structurally and conformationally stabilized mimic of peptide 21 termed S02 (MPESSSNPDCNANPNVDPNEDLIKKCEKINVPTEEIKKEIEEKK) that was designed to select for CIS43-like mAbs. S02 was fused to the *Escherichia coli* DsbC, which stabilizes S02 by acting as a chaperone to facilitate disulfide bond formation.

Sera from fourteen malaria-naïve subjects in group 6 of VRC 314 were screened for S02 reactivity (**Figure 3.1**). The serum of subject 611, who was protected following CHMI,

demonstrated the highest S02 reactivity at week 20. This subject/timepoint were selected for MBC isolation.

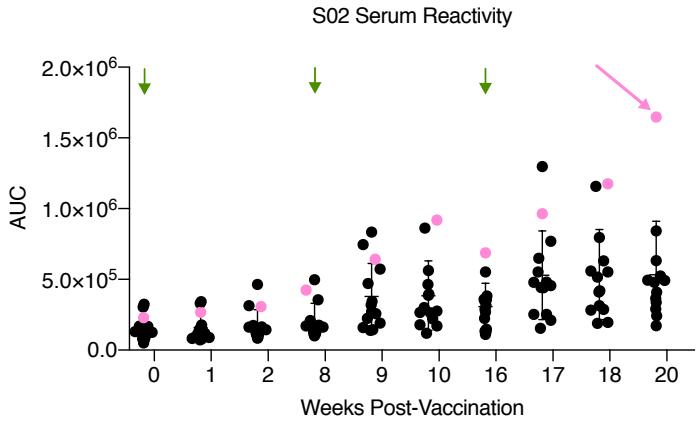

Figure 3.1: **S02 serum reactivity in VRC 314 subjects.** Fourteen malaria-naïve subjects (circles) were immunized with PfSPZ at 0, 8, and 16 weeks (green arrows). Serum was collected at the indicated timepoints and S02 reactivity was measured by ELISA and plotted as AUC. S02 serum reactivity of the subject (611) selected for mAb isolation is indicated by the pink circles; the timepoint selected for cloning is indicated by the pink arrow.

3.3.2 MBC isolation

Single PfCSP-reactive MBCs were sorted from PBMCs collected at the indicated timepoint using fluorescently-labeled rPfCSP and S02-DsbC as probes (**Figure 3.2**). 186 live MBCs were successfully sorted into two 96-well plates. My colleague Rachel Vistein processed the first plate with 96 MBCs, while I processed the second plate with 90 MBCs. Of these 90 MBCs, 13 were IgG^+ and 77 were IgM^+. Here, I will only present data from the plate I processed.

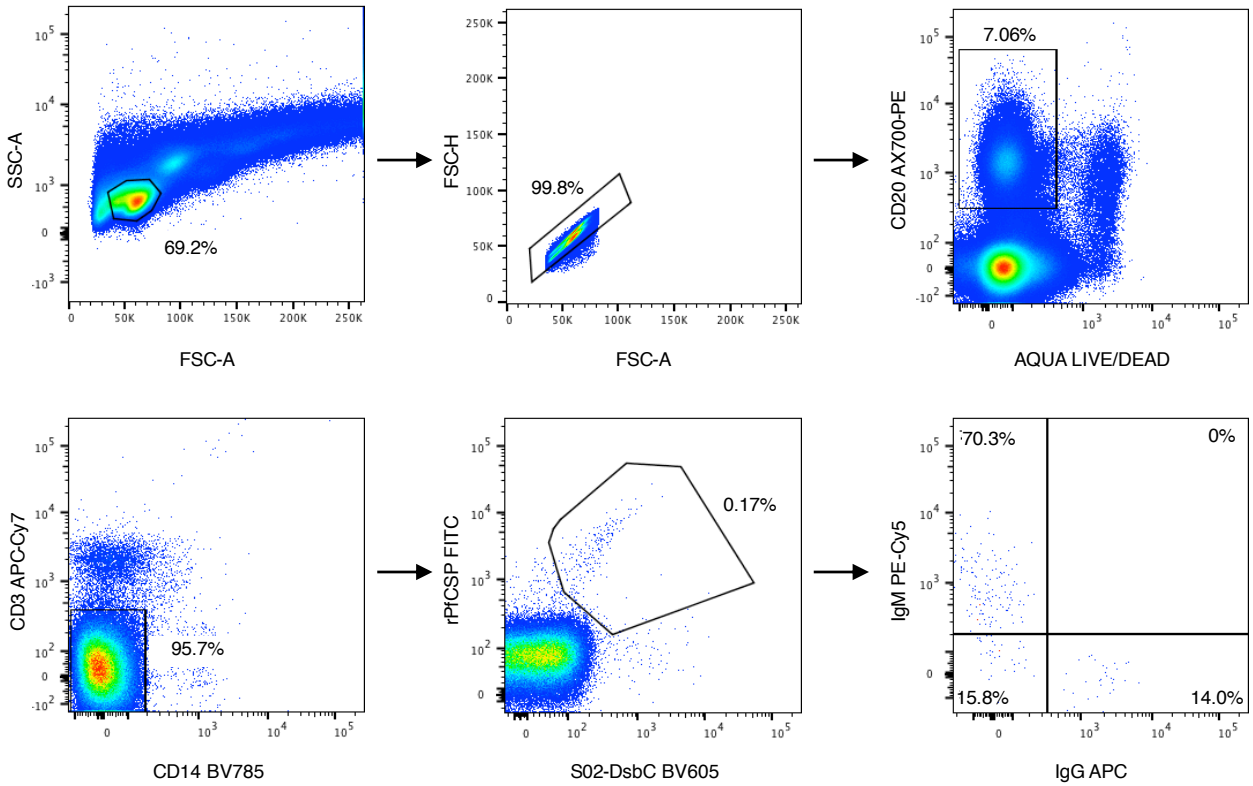

Figure 3.2: Isolation of S02-reactive MBCs. Gating strategy to isolate single, live $CD20^{+}CD3^{-}CD14^{-}$ MBCs. rPfCSP and S02-DsbC, respectively labeled with FITC and BV605, were used as probes to sort junctional-reactive MBCs. Anti-IgG and IgM markers were included to segregate sorted MBCs based on isotype. The probe sort gate did not include single-positive $rPfCSP^{-}S02^{+}$ or $rPfCSP^{+}S02^{-}$ MBCs due to the likelihood of the former being false-positives and the latter being non-junctional PfCSP mAbs.

3.3.3 V_H/V_L gene amplification and cloning

The 90 MBCs were directly sorted into lysis buffer. Immediately after sorting, RNA in the MBC lysates was reverse-transcribed into cDNA and PCR was performed to amplify antibody V-genes using standardized protocols and primers optimized at the VRC. Amplicons were recovered for 69 V_H genes and 88 V_L genes (77% and 88% recovery, respectively), resulting in a V_H/V_L matched pair efficiency of 77% (69 of 90 mAb sequences amplified) (**Figure 3.3**). Sequences were recovered for 59 V_H genes and 76 V_L genes (86% efficiency for both). This ultimately resulted in 48 matched V_H/V_L pairs and a final matched pair efficiency of

53% (48 of 90 complete mAb sequences recovered). 10 of the 13 IgG mAbs and 38 of the 77 IgM mAbs were recovered (77% and 47% efficiency, respectively).

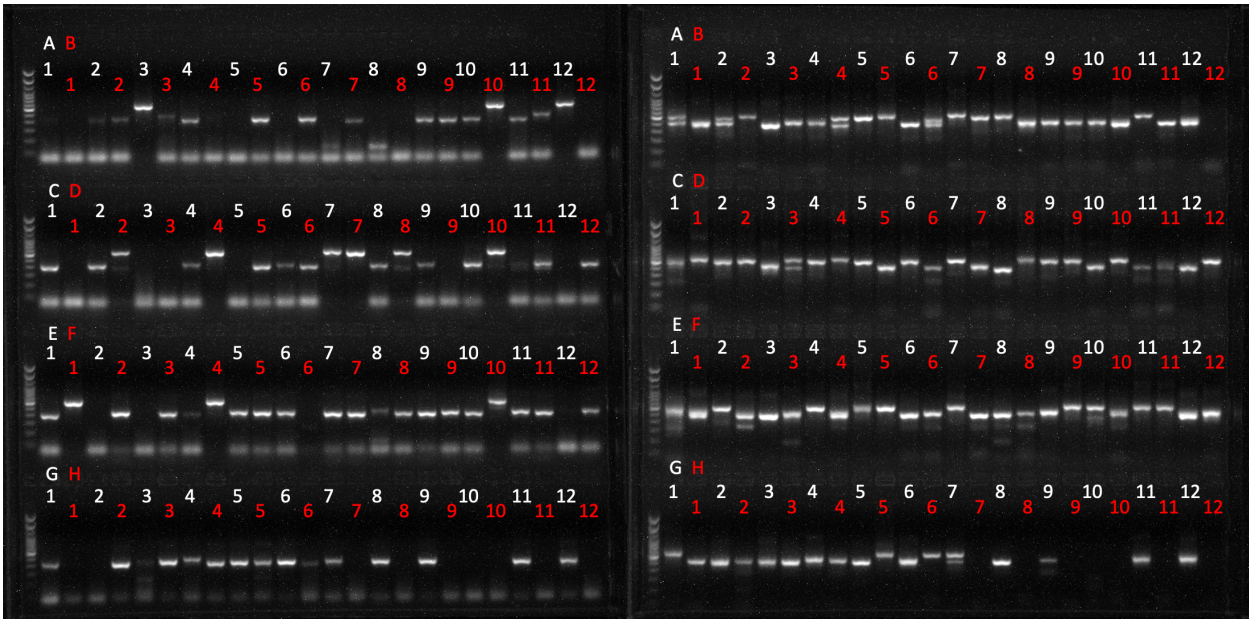

Figure 3.3: PCR amplification of antibody V_H and V_L genes from subject 611. Each lane represents a PCR amplicon from a single MBC run on a 1% agarose gel. Left, V_H amplicons (expected size ~500bp); right, $V_L\kappa$ and $V_L\lambda$ amplicons (expected size ~1,000bp). Numbers and letters indicate well designation in the 96-well plate.

3.3.4 mAb expression and screening

The 48 matched pair V_H/V_L sequences were sent to GenScript for gene synthesis and cloning into human IgG_1 plasmid vectors (**Figure 3.4**) regardless of original isotype (IgG or IgM). The mAbs I cloned were designated FAA (for 611) and L (for Lawrence); the mAbs cloned by my colleague Rachel Vistein were designated FAA-R (for Rachel). Henceforth, all mAbs cloned from subject 611 will be referred to as the L-series (L#) or R-series (R#) mAbs.

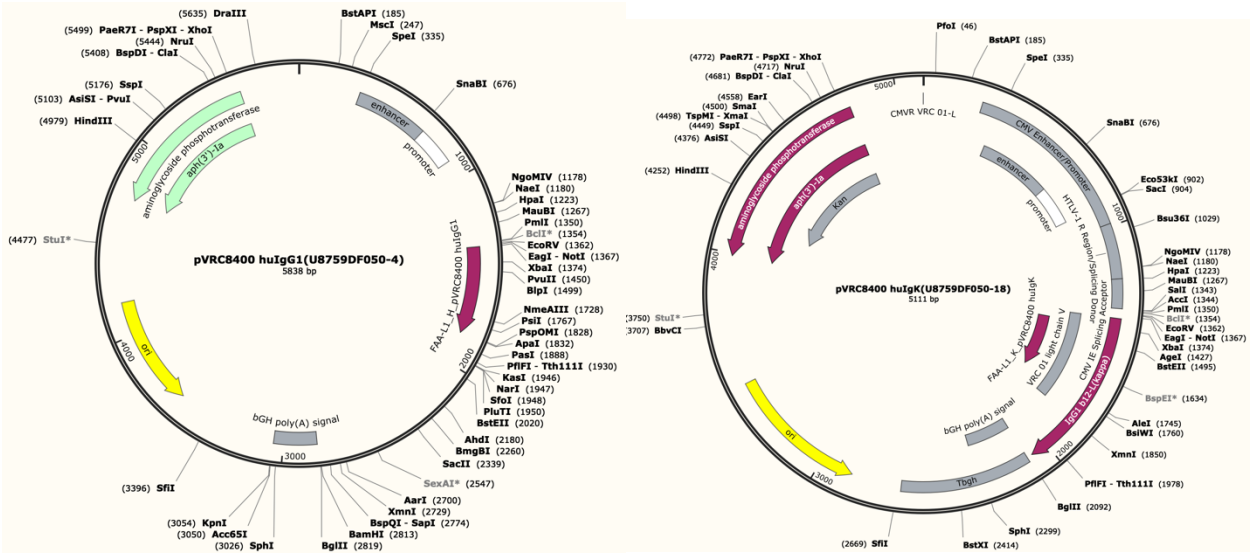

Figure 3.4: Plasmids used for recombinant mAb expression. Example plasmid maps used by the VRC for expression of human IgG_1 V_H (left) and Vκ (right) genes for mAb FAA-L1 (or L1).

3.4 *In vitro* binding characteristics of the mAb panel from VRC 314

Upon receipt of plasmids from GenScript, all mAbs were expressed as recombinant IgG_1, purified from supernatant, and screened for binding to rPfCSP and peptides, binding to Pb-PfCSP-SPZ, and *in vivo* functional activity.

3.4.1 Binding to rPfCSP and select peptides

Of the 48 L-series human IgG_1 expressed, 34 bound to rPfCSP by ELISA (**Figure 3.5A**). 9 of these 34 PfCSP mAbs bound the junctional peptide 21, with L9 demonstrating the greatest peptide 21 binding. Of these 9 junctional-reactive mAbs, none bound S02 (**Figure 3.5B**). All 34 mAbs were also tested for binding to peptide 29 (NANPNANPNANPNAN), which is composed of only NANP repeats (**Figure 3.5C**). Six of the nine junctional mAbs bound peptide 29, with L35 demonstrating the greatest peptide 29 binding. The peptide cross-reactivity of L2, L3, L8,

L9, L24, and L35 recapitulates the dual specificity for the junctional epitope (peptide 21) and pure NANP repeats (peptide 29) seen in some junctional mAbs[84,213].

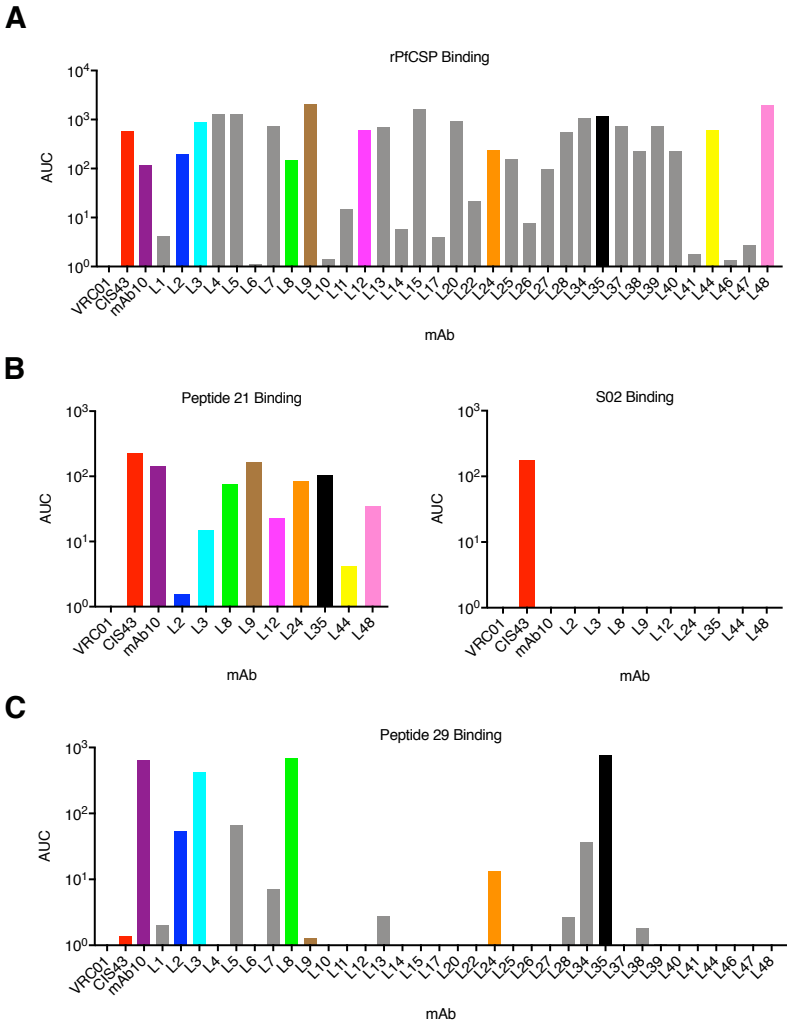

Figure 3.5: L-series mAb binding to rPfCSP and peptides. Binding of varying concentrations of L-series mAbs to **(A)** rPfCSP, **(B)** the junctional peptide 21 and S02, **(C)** and peptide 29, which is composed of only NANP repeats. VRC01 was included as a negative control; CIS43 (a junctional NPDP-preferring IgG that cross-reacts with NANP) and mAb10 (an NANP-preferring IgG that cross-reacts with NPDP) were included as positive controls. CIS43, mAb10, and the 9 L-series mAbs that bound peptide 21 are colored.

To extend the binding analysis of the L-series mAbs, BLI was used to measure the apparent avidity ($K_{D(app.)}$) of four mAbs' (L2, L3, L8, and L9) binding to rPfCSP, peptide 21, and peptide 29 (**Figure 3.6**). CIS43 and mAb10 were included as positive controls for peptide 21 and

29 binding, respectively. None of the four L-series mAbs demonstrated peptide 21 binding comparable to CIS43 ($K_{D(app.)}$ <0.001 nM for peptide 21). Furthermore, none of the L-series mAbs demonstrated peptide 29 binding comparable to mAb10 ($K_{D(app.)}$ <0.001 nM for peptide 29).

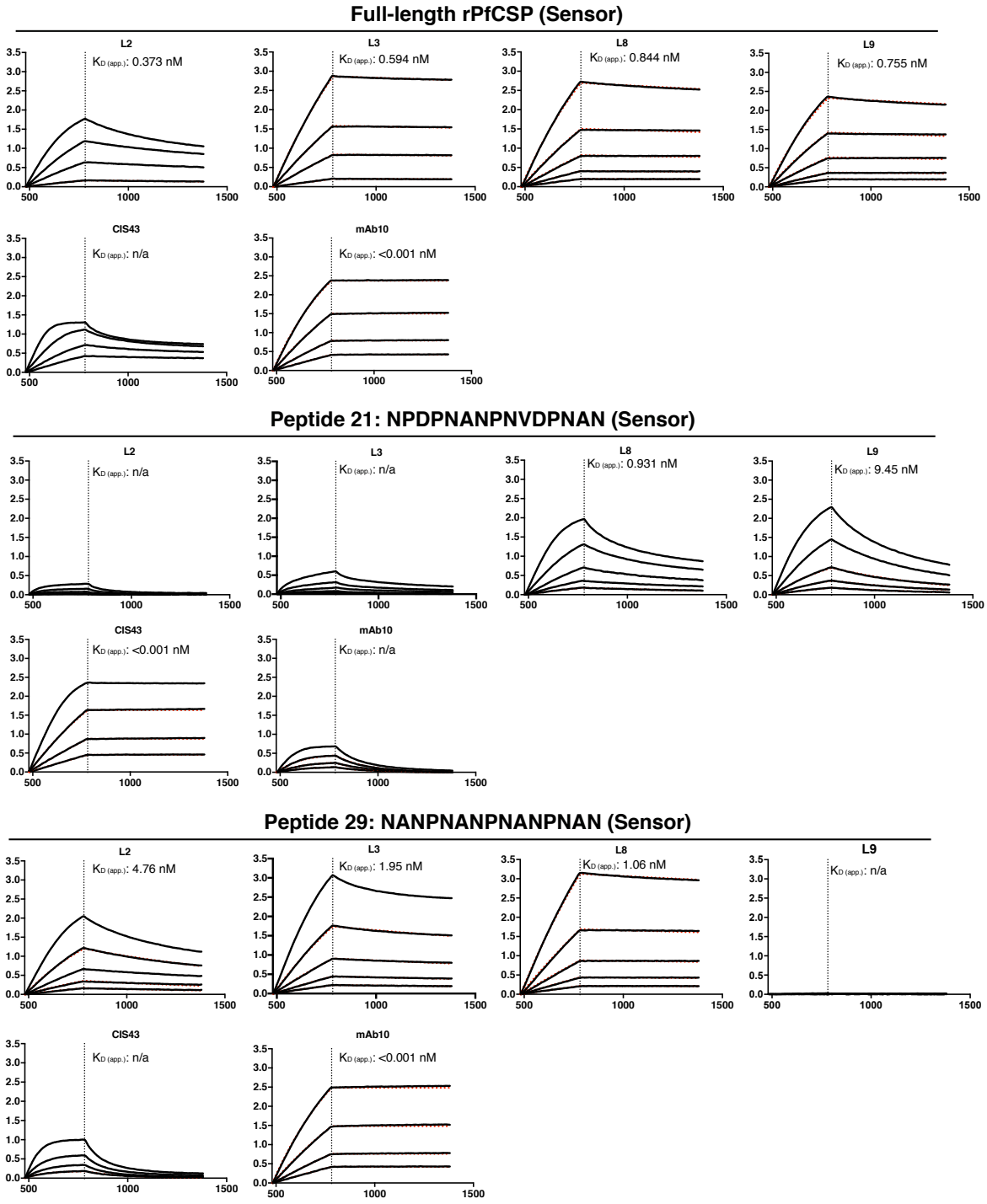

Figure 3.6: BLI of four L-series mAbs binding to rPfCSP, peptide 21, and peptide 29. Antibody binding curves are shown in black (raw data). Data were fitted (dotted red lines) with the binding equations describing a 1:1 analyte-ligand binding model. Serial concentrations of antibodies used are as follow: 1.25, 0.625, 0.3125, and 0.15625 µg/mL. Apparent avidity, $K_{D(app.)}$, of each mAb is shown. CIS43 and mAb10 were included as controls.

3.4.2 Binding to Pb-PfCSP-SPZ

The 34 mAbs that bound rPfCSP were tested for binding to native PfCSP on the surface of Pb-PfCSP-SPZ by flow cytometry. Of these 34 PfCSP mAbs, 27 bound SPZ (**Figure 3.7**). The seven mAbs that displayed low MFI values comparable to the negative control VRC01 were L4, L7, L10, L15, L20, L37, and L40.

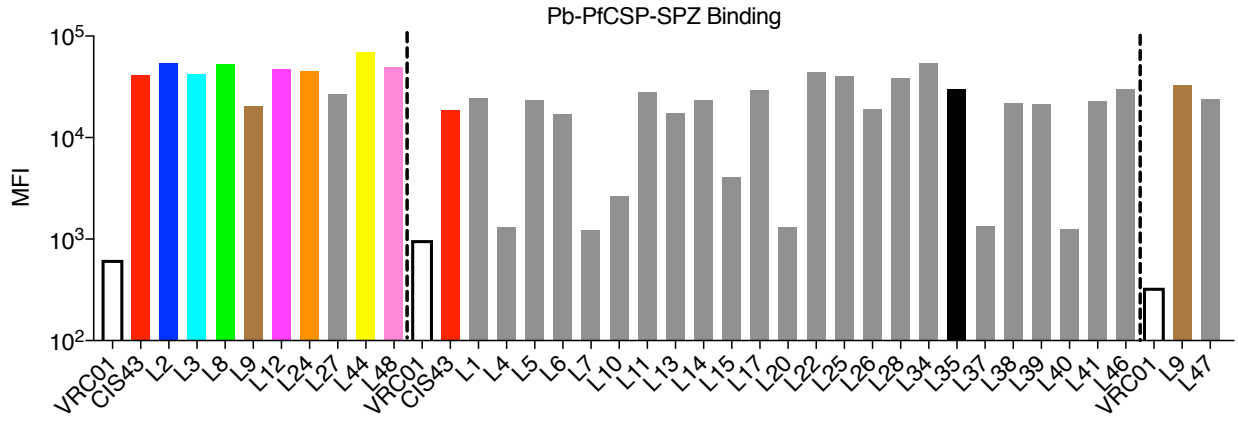

Figure 3.7: Binding of L-series mAbs to Pb-PfCSP-SPZ. MFI values for mAb-bound SPZ determined by flow cytometry. Dotted lines separate independent experiments. VRC01 and CIS43 were respectively included as negative and positive controls.

3.4.3 Antibody gene usage

The antibody variable region gene usage of these 34 mAbs were determined (**Figure 3.8** and **Table 3.1**). The majority (20 of 34, 71%) were IgM. Nearly all (32 of 34, 94%) belonged to the Ig variable heavy chain gene family 3 (IGV_H3), particularly IGV_H3-33 (15 of 34, 44%) and IGV_H3-30 (6 of 34, 18%), consistent with previous reports of the enrichment of this public antibody lineage in PfSPZ-immunized subjects[79,213,219,220].

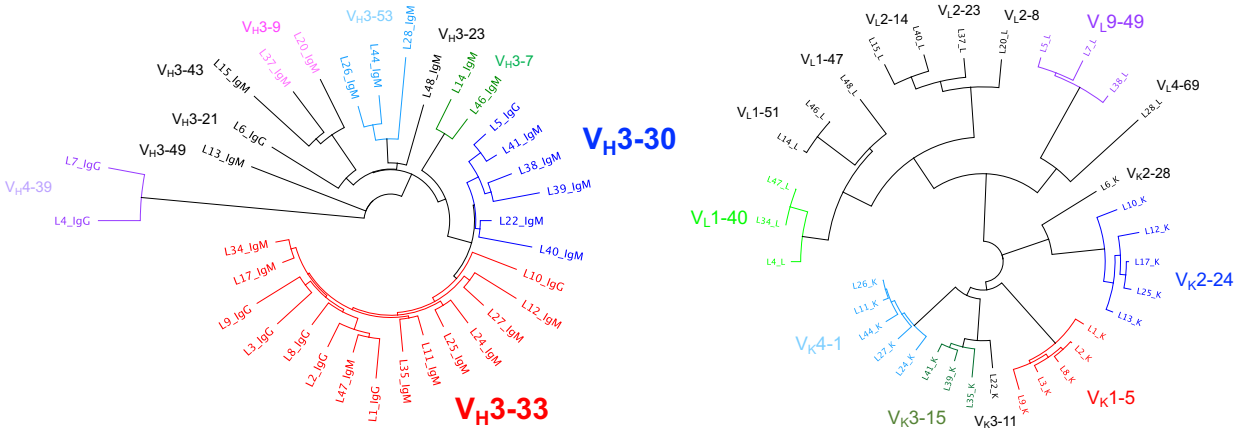

Figure 3.8: Phylogenetic trees of L-series antibody gene usage. Left: V_H gene usage; right: V_L gene usage. Antibodies are color-coded by genes.

mAb	V_H	V_H maturation (nt, %)	J_H	HCDR3 length (aa)	V_L	V_L maturation (%)	J_L	KCDR3 Length (aa)
L1	VH3-33*01	2.8	JH3*02	18	Vκ1-5*03	2.2	Vκ1*01	8
L2	VH3-33*01	1.0	JH3*02	20	Vκ1-5*03	0.4	Vκ1*01	8
L3	VH3-33*01	4.5	JH4*02	16	Vκ1-5*03	1.8	Vκ1*01	8
L4	VH4-39*01	5.5	JH5*02	17	Vλ1-40*01	1.7	Vλ2*01	11
L5	VH3-30-3*01	1.0	JH4*02	17	Vλ9-49*01	1.4	Vλ3*02	13
L6	VH3-21*04	31.6	JH6*02	14	Vκ2-28*01	2.7	Vκ1*01	9
L7	VH4-39*01	2.1	JH5*02	16	Vλ9-49*01	1.4	Vλ1*01	13
L8	VH3-33*01	2.8	JH4*02	11	Vκ1-5*03	1.1	Vκ1*01	8
L9	VH3-33*01	4.2	JH4*02	13	Vκ1-5*03	3.9	Vκ1*01	9
L10	VH3-33*01	4.9	JH4*02	11	Vκ2-24*01	3.7	Vκ4*01	8
L11	VH3-33*01	1.7	JH4*02	13	Vκ4-1*01	0.7	Vκ4*01	9
L12	VH3-33*01	4.9	JH1*01	13	Vκ2-24*01	3.4	Vκ2*03	9
L13	VH3-49*05	2.4	JH4*02	11	Vκ2-24*01	1.0	Vκ1*01	8
L14	VH3-7*01	2.8	JH4*02	11	Vλ1-51*01	0.4	Vλ2*01	11
L15	VH3-43*01	1.0	JH6*02	19	Vλ2-14*01	2.4	Vλ2*01	10
L17	VH3-33*01	0.7	JH4*02	11	Vκ2-24*01	0.3	Vκ2*01	8
L20	VH3-9*01	1.4	JH1*01	19	Vλ2-8*01	1.0	Vλ2*01	10
L22	VH3-30*03	0.7	JH4*02	14	Vκ3-11*01	0.0	Vκ4*01	8
L24	VH3-33*01	2.4	JH4*02	17	Vκ4-1*01	2.0	Vκ2*01	9
L25	VH3-33*01	3.8	JH4*02	8	Vκ2-24*01	1.0	Vκ2*02	8
L26	VH3-53*01	1.1	JH6*02	10	Vκ4-1*01	0.0	Vκ4*01	8
L27	VH3-33*01	3.1	JH4*02	18	Vκ4-1*01	2.4	Vκ1*01	9
L28	VH3-53*01	7.0	JH4*02	13	Vλ4-69*01	3.1	Vλ2*01	10

L34	VH3-33*01	0.7	JH4*02	19	Vλ1-40*01	0.0	Vλ1*01	12
L35	VH3-33*01	3.1	JH4*02	13	Vκ3-15*01	2.5	Vκ2*01	8
L37	VH3-9*01	1.7	JH6*02	21	Vλ2-23*01	1.0	Vλ1*01	10
L38	VH3-30*01	1.0	JH1*01	16	Vλ9-49*03	1.4	Vλ3*02	13
L39	VH3-30*16	2.8	JH3*02	16	Vκ3-15*01	2.2	Vκ1*01	9
L40	VH3-30*03	3.8	JH6*02	22	Vλ2-14*01	0.7	Vλ1*01	11
L41	VH3-30-3*01	1.4	JH4*02	20	Vκ3-15*01	0.7	Vκ1*01	9
L44	VH3-53*01	5.3	JH6*02	10	Vκ4-1*01	1.7	Vκ4*01	8
L46	VH3-7*01	1.0	JH4*02	11	Vλ1-51*01	0.0	Vλ2*01	11
L47	VH3-33*01	0.7	JH3*02	18	Vλ1-40*01	0.0	Vλ1*01	11
L48	VH3-23*01	2.8	JH4*02	14	Vλ1-47*01	1.1	Vλ2*01	11

Table 3.1: Ig V-gene family usage of the L-series mAbs. V-gene family, somatic hypermutation (maturation, %) and CDR3 length for the heavy and light chains of the 34 PfCSP mAbs cloned in this study. nt = nucleotides, H = heavy, L = light, J = joining, aa = amino acids.

3.5 *In vivo* functional activity of the mAb panel from VRC 314

The 34 PfCSP mAbs were assessed for their ability to reduce parasite liver burden in mice challenged IV with Pb-PfCSP-SPZ 2 hours after mAb administration (**Figure 3.9**). The IV challenge model is widely used to screen PfCSP mAbs for *in vivo* functional activity[84,106,185]. All mAbs were benchmarked against 300 µg/mouse of CIS43, a dose which confers maximum protection in this assay. Only one of these new mAbs, L9, reduced liver burden comparably to CIS43 at 300 µg/mouse. The 37 R-series mAbs cloned by my colleague Rachel Vistein were also tested at 300 µg/mouse, but none lowered liver burden comparably to L9 or CIS43 (data not shown).

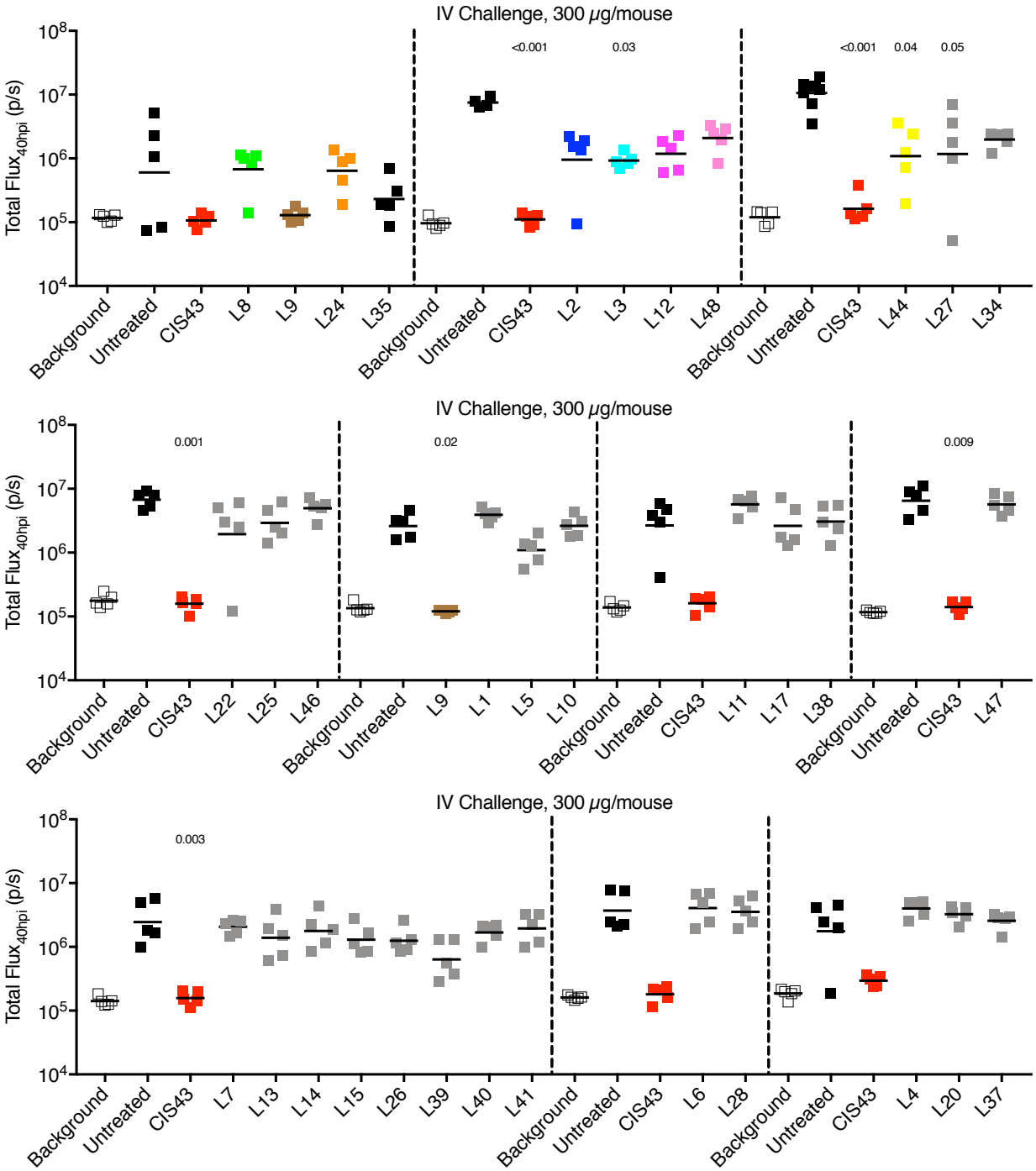

Figure 3.9: Screen for *in vivo* functional activity of L-series mAbs. Reduction of parasite liver burden in mice 40 h post-infection (hpi; n = 5/group; lines represent geometric mean) treated with 300 µg of mAbs L1-L48 or CIS43 2 hours before IV challenge with 2,000 Pb-PfCSP-SPZ. Significant differences (*P*-values) between each mAb and the untreated control (black) were determined using the Kruskal-Wallis test with Dunn's post-hoc correction. Dotted lines separate independent experiment.

3.6 Potency and binding specificity of mAb L9

Having identified L9 as the only mAb in the L-series panel that demonstrated comparable *in vivo* functional activity to CIS43 at 300 µg/mouse, I next set out to compare the potency of L9 more thoroughly to CIS43 and determine the epitope(s) on PfCSP targeted by L9.

3.6.1 *In vivo* potency of L9 compared to CIS43

Since 300 µg/mouse CIS43 and L9 both reduced liver burden to background levels, the next experiment retested protection against IV challenge at 300, 200, and 100 µg/mouse with 5 mice/group (**Figure 3.10A**). Importantly, this experiment included the neutralizing PfCSP mAb 311 isolated from a RTS,S-immunized subject[79] and was not powered to demonstrate statistical differences in potency between the mAbs. 300 and 200 µg/mouse CIS43, L9, and 311 reduced liver burden to background levels comparable to the unchallenged control mice; however, L9-treated mice had lower liver burden than CIS43- and 311-treated mice at 100 µg/mouse. These data suggested that lower mAb doses and increased mice/group would be needed to resolve statistical differences between CIS43 and L9. Subsequently, a dose titration (200, 100, 50, and 25 µg/mouse; 10 mice/group) comparing CIS43 and L9 was performed (**Figure 3.10B**). At the lower doses of 100 and 50 µg/mouse, L9 reduced liver burden significantly more than CIS43 compared to untreated controls. Together, these data suggest that L9 is more protective than CIS43 against IV challenge.

The gold standard for assessing the *in vivo* functional activity of PfCSP mAbs are natural transmission studies wherein mice are challenged with infected mosquito bites and assessed for sterile protection from parasitemia[84,185,213,219]. Thus, sterile protection mediated by CIS43 and L9

against five infected mosquito bites was assessed across three doses with 7 mice/group (**Figure 3.10C**). This experiment was not powered to resolve statistical differences between the mAbs. At 150 μg/mouse, L9 protected 100% of mice compared to 71% for CIS43; at 75 μg/mouse, L9 protected 43% of mice compared to 0% for CIS43. These data suggested that L9 may be more protective than CIS43 against mosquito bite challenge.

To extend these analyses, the abilities of L9 and CIS43 to reduce parasitemia following ID SPZ challenge were compared in an experiment with 15 mice/group. By introducing SPZ directly into the skin, ID challenge more closely mimics natural transmission by mosquito bites than the IV challenge model. Furthermore, the ID challenge model bypasses the inherent variability in mosquito bite challenge doses[221,222] (as it is impossible to control/quantify the number of SPZ inoculated by a mosquito when it bites) by standardizing the SPZ inoculum (i.e., 5,000 Pb-PfCSP-SPZ inoculated into the skin of mice). At 100 μg/mouse, L9-treated mice had no detectable parasitemia and were significantly more protected than CIS43-treated mice (**Figure 3.10D**). Serum mAb titers in separate groups of mice were sampled at various timepoints after passive transfer of 200, 100, 50, and 25 μg CIS43 or L9 (**Figure 3.10E**). CIS43 and L9 serum titers were similar across all doses and timepoints except for the 50 and 25 μg/mouse 2 hour timepoints. Collectively, these data demonstrate that L9 is more potently protective than CIS43 against Pb-PfCSP-SPZ challenge in normal mice.

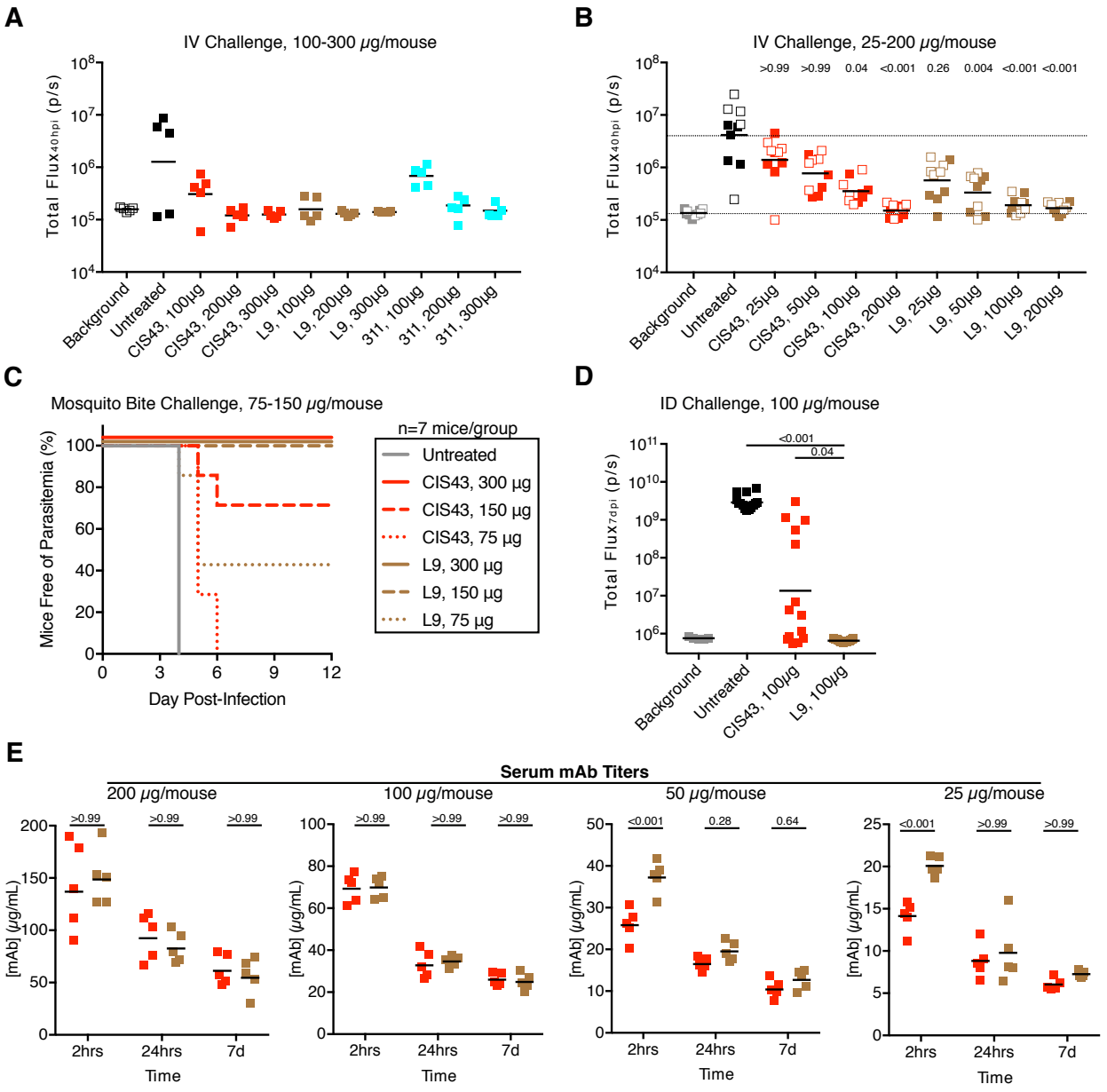

Figure 3.10: L9-mediated protection against Pb-PfCSP-SPZ challenge. (**A**) Liver burden reduction (bioluminescence; total flux, photons/sec) in mice 40 h post-infection (hpi; n=5/group) mediated by indicated doses of CIS43, L9, and 311 administered 2 hours before IV challenge with 2,000 Pb-PfCSP-SPZ. (**B**) Liver burden reduction in mice (n=10/group; data pooled from two independent experiments, solid vs. open squares) mediated by indicated doses of CIS43 and L9 against IV challenge. *P*-values were determined by comparing each mAb/dose to untreated control using the Kruskal-Wallis test with Dunn's post-hoc correction. Dotted lines were set at the geometric mean of the background (unchallenged) and untreated (challenged) control groups. (**C**) Survival curves of mice (n=7/group) challenged with five infected mosquito bites 2 hours after passive transfer of indicated mAb/doses. (**D**) Parasitemia reduction in mice 7 days post-infection (7dpi; n=15/group) mediated by 100 μg CIS43 or L9 administered 3 days before ID challenge with 5,000 Pb-PfCSP-SPZ. *P*-values were determined by comparing L9 to CIS43 and untreated control using the Kruskal-Wallis test with Dunn's post-hoc correction. (**E**) Serum mAb

titers 2 hours, 24 hours, and 7 days after administration of indicated doses of CIS43 or L9 in separate mice (n=5/group) determined through ELISA. Differences between CIS43 and L9 at each dose and timepoint were determined using a 2-way ANOVA with Bonferroni's post-hoc correction. In **A-B** and **D-E**, lines represent the geometric mean.

3.6.2 Neutralization of PfSPZ by L9

To extend the protection analysis of L9 against Pb-PfCSP-SPZ challenge, the extent to which L9 reduced liver burden in FRG-huHep human liver-chimeric mice challenged IV with wild-type PfSPZ was assessed[223]. Notably, FRG-huHep mice are marginally permissive to infection with PfSPZ and require a large IV challenge dose of 100,000 PfSPZ (i.e., 50-fold greater than Pb-PfCSP-SPZ challenge in normal mice). 50 or 10 µg of L9 (which resulted in serum concentrations as low as ~5 µg/mL) reduced liver burden to near-undetectable levels (**Figure 3.11A**). Moreover, in a separate study 25 µg/mouse of L9 reduced liver burden significantly more than 2A10 (**Figure. 3.11B**), an NANP-preferring mouse mAb commonly used as a benchmark in protection studies[77,79,84,106]. These data show that L9 is highly protective against PfSPZ challenge in human liver-chimeric mice.

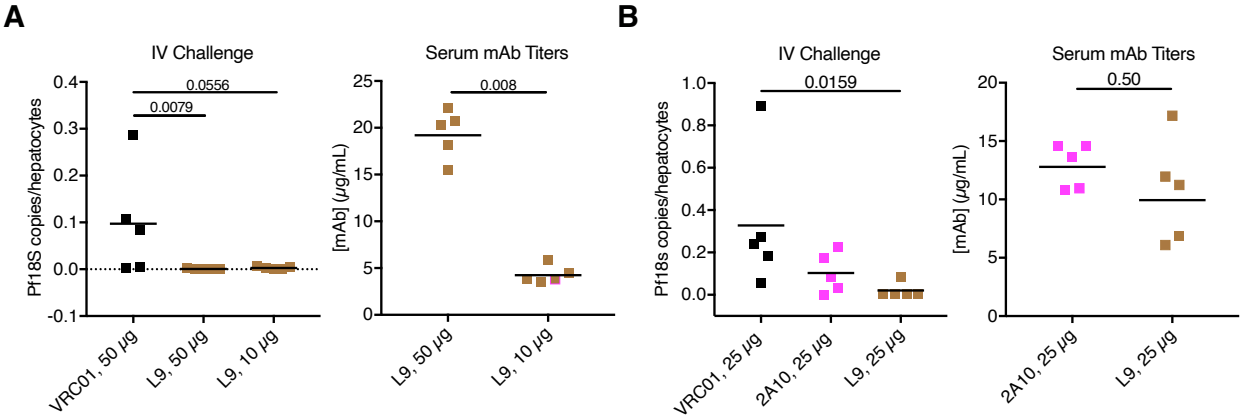

Figure 3.11: L9-mediated protection against PfSPZ challenge. (**A**) Left: liver burden reduction (Pf 18S rRNA normalized to number of human hepatocytes) in FRG-huHep mice (n=5/group) treated with 50 µg VRC01, 50 µg L9, or 10 µg L9 and challenged IV with 100,000 PfSPZ. Right: serum mAb titers in challenged mice. Differences between VRC01 and L9 were determined using the two-tailed Mann–Whitney test. (**B**) Left: liver burden reduction in FRG-huHep mice (n=5/group) treated with 25 µg VRC01, 2A10 (NANP-preferring mouse mAb), or L9 and challenged IV with 100,000 PfSPZ. Right: serum mAb titers in challenged mice.

3.6.3 Epitope mapping of L9 binding to PfCSP peptides

To define the specific epitope(s) in PfCSP recognized by L9 IgG, detailed mapping was performed using a series of 15mer peptides overlapping by four amino acids covering the repeat region of PfCSP (peptides 20–61; **Figure 3.12A**) and compared to CIS43 IgG as a benchmark (**Figure 3.12B**). Consistent with a previous report[84], CIS43 demonstrated preferential high-affinity binding to peptide 20 (PADGNPDPNANPNVD) and 21 (NPDPNANPNVDPNAN), which contain NPDP. Conversely, L9 preferentially bound peptide 22 (NANPNVDPNANPNVD) downstream of NPDP. Neither mAb bound peptide 29 (NANPNANPNANPNAN), which contains only NANP repeats. Alanine scanning mutagenesis of peptide 22 demonstrated that the two NPNV minor repeat motifs, created by the joining of NANP and NVDP repeats, were critical for L9 binding (**Figure 3.12C**). Importantly, peptide 22 is the only peptide that contains two NPNV motifs (**Figure 3.12A**), likely accounting for its strong recognition by L9. These data indicate that L9 recognizes an epitope distinct to CIS43 (i.e., the NPNV motif associated with NVDP minor repeats) and that both mAbs exhibit undetectable affinity for the ~4 NANP major repeats in peptide 29 in this assay.

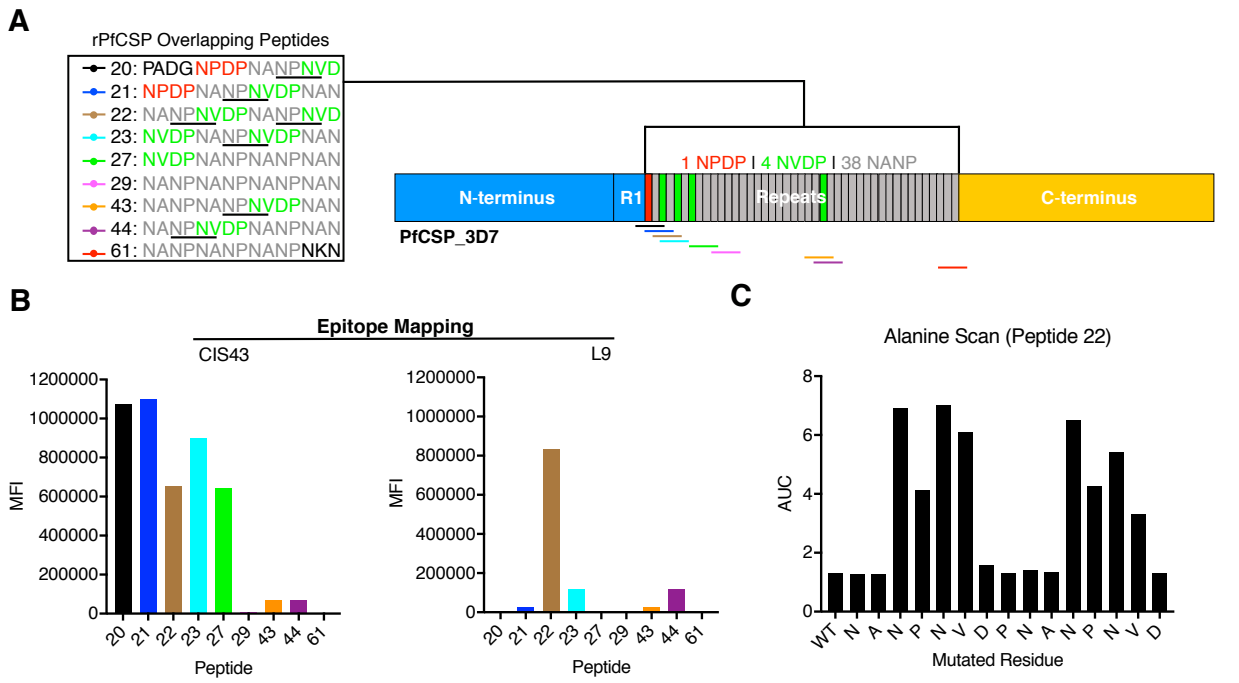

Figure 3.12: Mapping of the PfCSP peptide epitope(s) bound by L9. (A) Schematic of PfCSP in the 3D7 reference isolate depicting N-CSP, repeat region (with color-coded overlapping 15mer peptides 20-61), and C-CSP. Every NPNV motif in each peptide is underlined. **(B)** CIS43 and L9 binding to peptides 20-61 by ELISA, expressed as MFI. **(C)** Competition ELISA, expressed as AUC, of L9 binding to rPfCSP with varying concentrations of peptide 22 (wild-type, WT; leftmost bar) or variant peptides (subsequent bars) where the indicated residue was mutated to alanine or serine.

3.6.4 Epitope mapping of L9 binding to mutated rPfCSP constructs

Having demonstrated that L9 preferentially binds NPNV-containing peptide 22 over NANP-containing peptide 29, I next determined if the binding of L9 to FL rPfCSP was dependent on the presence of NVDP repeats. rPfCSP constructs were generated wherein the four NVDP repeats (denoted A, B, C, D) were mutated to NANP individually or in combination (**Figure 3.13** and **Appendix 1**). In total, fifteen rPfCSP "NVDP mutants" were generated: four single mutants (ΔA, ΔB, ΔC, ΔD), six double mutants (ΔAB, ΔAC, ΔAD, ΔBC, ΔBD, ΔCD), four triple mutants (ΔABC, ΔABD, ΔACD, ΔBCD), and one quadruple mutant (ΔABCD). The fifteen "NVDP mutant" sequences were cloned into the same vector which contained a C-terminal poly-histidine tag (**Figure 3.14A**). All plasmids were sequenced to double-check the

correct mutations were present before being expressed in 293F cells and affinity purified over a nickel nitrilotriacetic acid column followed by SEC (**Figure 3.14B**). To check whether the fifteen constructs had expressed and folded correctly, binding of the NANP-preferring mAb10 to these mutant constructs was compared to wild-type (WT) rPfCSP by ELISA (**Figure 3.14C**). mAb10 bound identically to all constructs, indicating that these mutant constructs had been generated successfully.

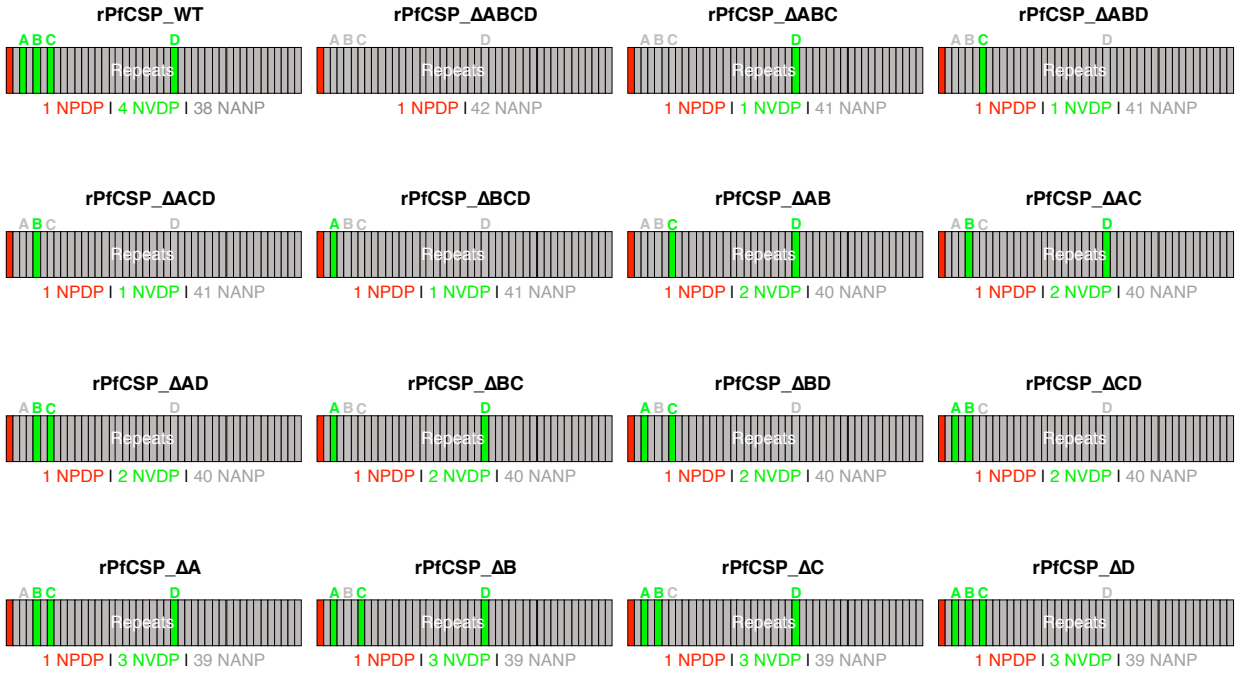

Figure 3.13: Schematics of rPfCSP NVDP repeat mutants. Repeat regions of wild-type rPfCSP (rPfCSP_WT; equivalent to rPfCSP_FL) and fifteen rPfCSP mutants with single, double, triple, or quadruple mutations changing NVDP to NANP. A, B, C, and D respectively refer to the first, second, third, and fourth NVDP repeat in the 3D7 reference isolate. N- and C-termini are identical for all constructs, but were omitted from the schematic for simplicity.

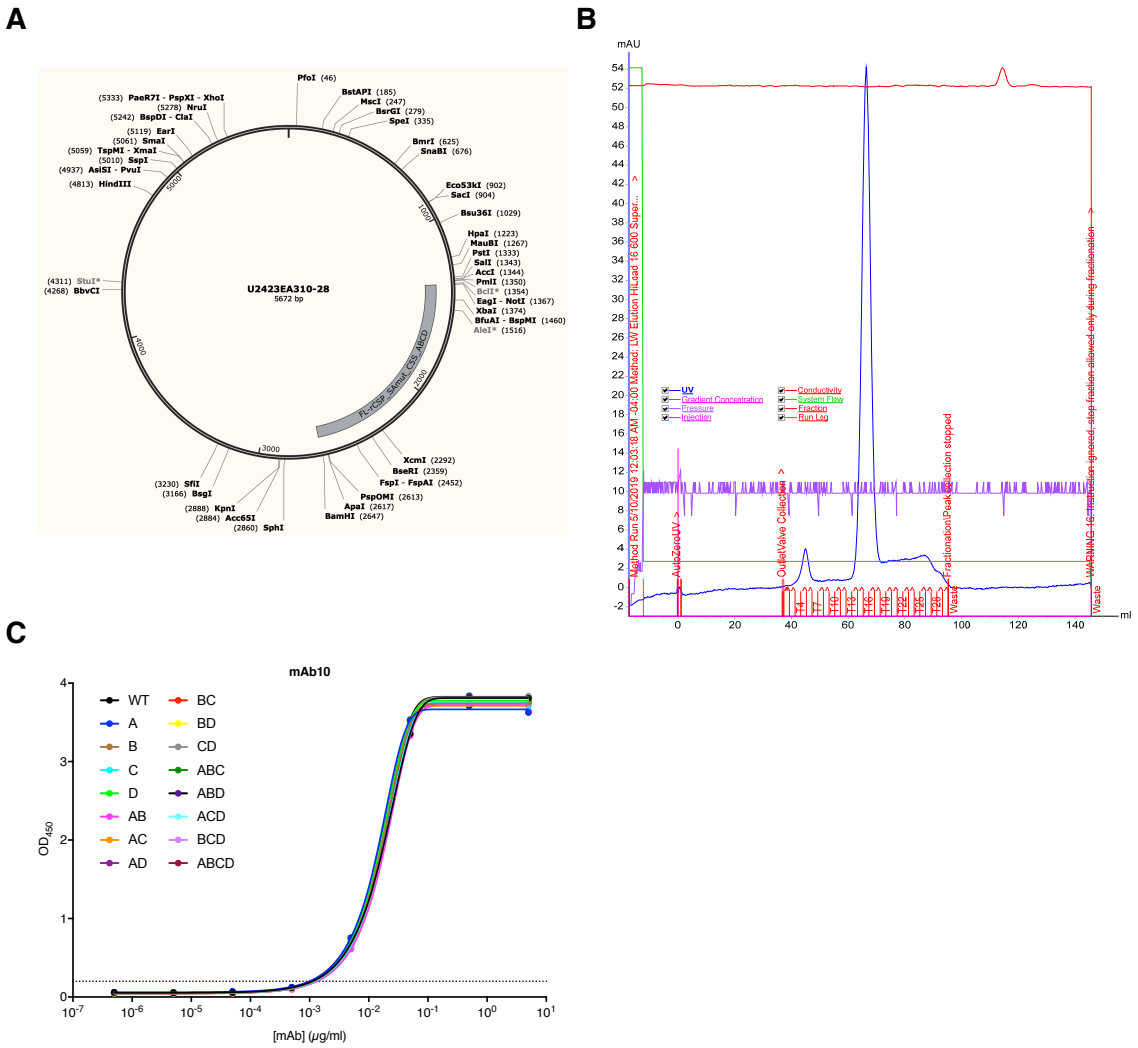

Figure 3.14: Generation and quality check of rPfCSP NVDP mutant constructs. (**A**) Example plasmid map of the plasmid vector with the rPfCSP_ΔABCD sequence. (**B**) Example SEC chromatogram of the purified rPfCSP_ΔABCD fraction. (**C**) Binding of varying concentrations of mAb10 to the WT and fifteen mutant NVDP rPfCSP constructs by ELISA.

The binding of L9 IgG to the fifteen rPfCSP NVDP mutant constructs was assessed by ITC and compared to rPfCSP_WT (**Figure 3.15A** and **Table 3.2**). L9 displayed two sequential binding events to rPfCSP_WT, with the first binding event involving ~2 antigen binding sites with an affinity of 22 nM and the second binding event involving ~9 antigen binding sites with an affinity of 47 nM. This distinctive "two-step binding" to rPfCSP was previously observed with CIS43 and was contingent upon a first high-affinity binding event with 1-2 antigen binding

sites at the junctional epitope that conformationally stabilized rPfCSP and enabled a second, lower affinity binding event. Mutating the NPDP to NANP abrogated two-step binding by CIS43 to rPfCSP and reduced its binding affinity by 18-fold and stoichiometry by 2-fold[84].

Interestingly, L9 binding was reduced to a single event only when all four NVDP were mutated to NANP (rPfCSP_ΔABCD), suggesting that the first high-affinity binding event targets NPNV motifs associated with NVDP minor repeats and requires at least one NPNV (**Figure 3.15A** and **Table 3.2**). Furthermore, the affinity of L9 for rPfCSP_ΔABCD decreased 3-fold compared to WT (ΔABCD K_{D1} = 73 nM vs. WT K_{D1} = 22 nM, respectively) while the total binding stoichiometry (N) was not appreciably perturbed ($N_{\Delta ABCD}$=12.7 vs. N_{WT}=11.2), indicating that L9 can bind NANP repeats if they are sufficiently concatenated like in rPfCSP_ΔABCD, which contains 42 NANP repeats.

L9 demonstrated two-step binding, as well as similar affinity and stoichiometry, for all other NVDP single, double, and triple mutants (**Figure 3.15A** and **Table 3.2**). As controls, the affinity of NANP-preferring mAb10 and 317 for rPfCSP_ΔABCD were found to be similar to rPfCSP_WT (**Figure 3.15B**), suggesting that mutating all NVDP to NANP repeats in rPfCSP did not significantly alter the binding of these NANP-preferring mAbs. Together, these data show that L9 requires at least one NVDP to bind rPfCSP in two steps and that the first high-affinity step targets NPNV motifs while the second lower-affinity step targets NPNA motifs.

A

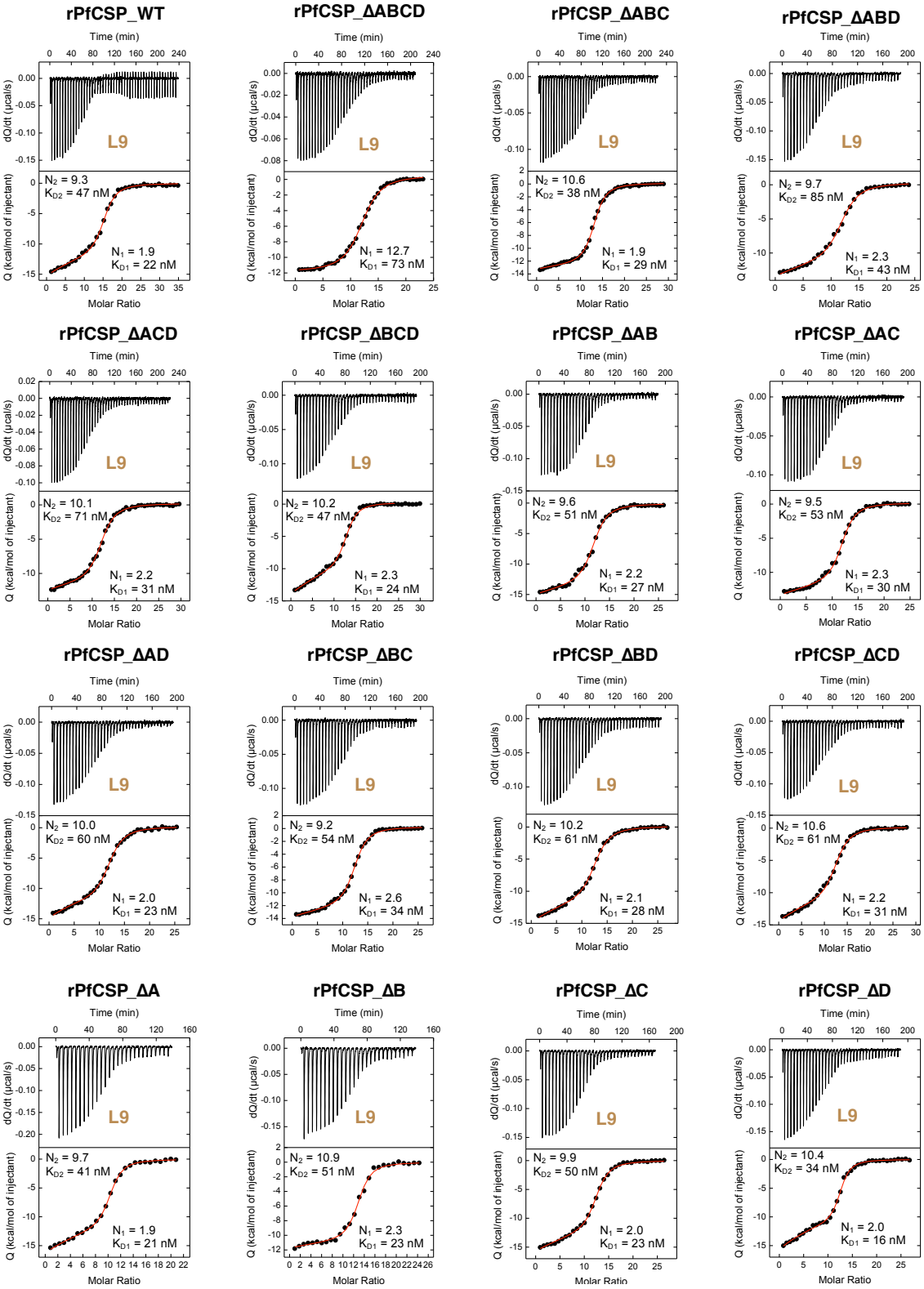
rPfCSP_WT
Time (min)
dQ/dt (µcal/s)
L9
N2 = 9.3
KD2 = 47 nM
N1 = 1.9
KD1 = 22 nM
Q (kcal/mol of injectant)
Molar Ratio
rPfCSP_ΔABCD
N2 = 10.6
KD2 = 38 nM
N1 = 12.7
KD1 = 73 nM
rPfCSP_ΔABC
N2 = 10.6
KD2 = 38 nM
N1 = 1.9
KD1 = 29 nM
rPfCSP_ΔABD
N2 = 9.7
KD2 = 85 nM
N1 = 2.3
KD1 = 43 nM
rPfCSP_ΔACD
N2 = 10.1
KD2 = 71 nM
N1 = 2.2
KD1 = 31 nM
rPfCSP_ΔBCD
N2 = 10.2
KD2 = 47 nM
N1 = 2.3
KD1 = 24 nM
rPfCSP_ΔAB
N2 = 9.6
KD2 = 51 nM
N1 = 2.2
KD1 = 27 nM
rPfCSP_ΔAC
N2 = 9.5
KD2 = 53 nM
N1 = 2.3
KD1 = 30 nM
rPfCSP_ΔAD
N2 = 10.0
KD2 = 60 nM
N1 = 2.0
KD1 = 23 nM
rPfCSP_ΔBC
N2 = 9.2
KD2 = 54 nM
N1 = 2.6
KD1 = 34 nM
rPfCSP_ΔBD
N2 = 10.2
KD2 = 61 nM
N1 = 2.1
KD1 = 28 nM
rPfCSP_ΔCD
N2 = 10.6
KD2 = 61 nM
N1 = 2.2
KD1 = 31 nM
rPfCSP_ΔA
N2 = 9.7
KD2 = 41 nM
N1 = 1.9
KD1 = 21 nM
rPfCSP_ΔB
N2 = 10.9
KD2 = 51 nM
N1 = 2.3
KD1 = 23 nM
rPfCSP_ΔC
N2 = 9.9
KD2 = 50 nM
N1 = 2.0
KD1 = 23 nM
rPfCSP_ΔD
N2 = 10.4
KD2 = 34 nM
N1 = 2.0
KD1 = 16 nM

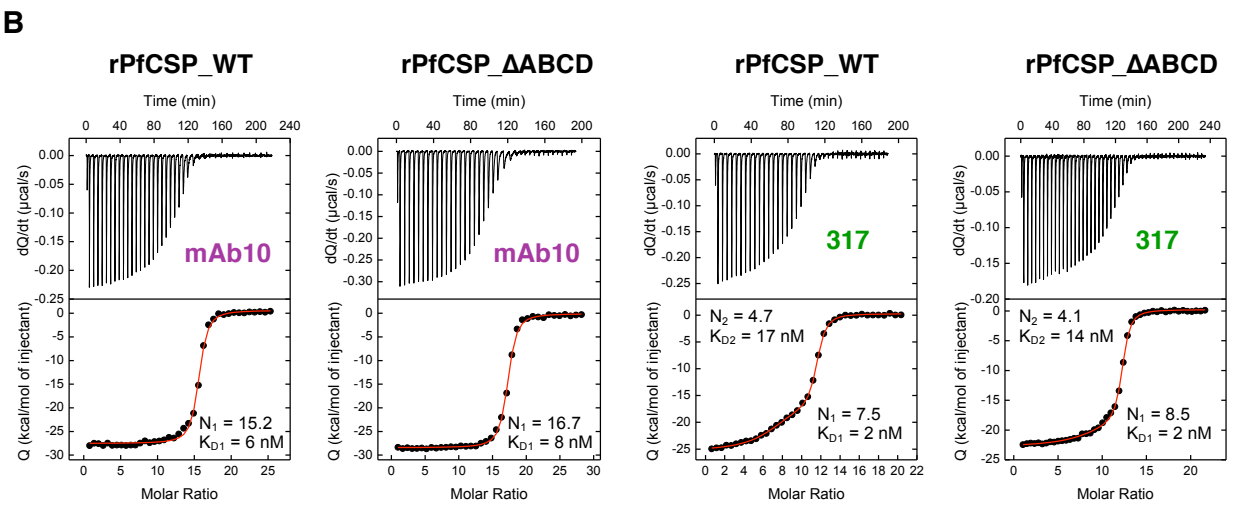

Figure 3.15: ITC of L9, mAb10, and 317 binding to rPfCSP NVDP mutants. (**A**) ITC plots of L9 IgG binding to the sixteen rPfCSP constructs depicted in Figure 3.13. (**B**) ITC plots of mAb10 and 317 IgG binding to rPfCSP_WT and rPfCSP_ΔABCD. ITC plots are representative of 2-3 independent experiments.

rPfCSP Construct	Binding Event 1					Binding Event 2				
	N_1	K_{D1} (nM)	ΔG_1 (kcal/mol)	ΔH_1 (kcal/mol)	$-T\Delta S_1$ (kcal/mol)	N_2	K_{D2} (nM)	ΔG_2 (kcal/mol)	ΔH_2 (kcal/mol)	$-T\Delta S_2$ (kcal/mol)
WT	1.9	22	-10.4	-30.0	+19.6	9.3	47	-10.0	-9.1	-0.9
ΔABCD	12.7	73	-9.7	-12.4	+2.7	-	-	-	-	-
ΔABC	1.9	29	-10.3	-17.4	+7.1	10.6	38	-10.1	-11.1	+1.0
ΔABD	2.3	43	-10.1	-19.6	+9.5	9.7	85	-9.6	-11.1	+1.5
ΔACD	2.2	31	-10.2	-17.7	+7.5	10.1	71	-9.8	-11.0	+1.2
ΔBCD	2.3	24	-10.4	-27.1	+16.7	10.2	47	-10.0	-8.7	-1.3
ΔAB	2.2	27	-10.3	-24.4	+14.1	9.6	51	-10.0	-10.4	+0.4
ΔAC	2.3	30	-10.3	-20.5	+10.2	9.5	53	-9.9	-10.9	+1.0
ΔAD	2.0	23	-10.4	-22.6	+12.2	10.0	60	-9.9	-10.8	+0.9
ΔBC	2.6	34	-10.2	-20.6	+10.4	9.2	54	-9.9	-11.2	+1.3
ΔBD	2.1	28	-10.3	-22.6	+12.3	10.2	61	-9.8	-10.5	+0.7
ΔCD	2.2	31	-10.2	-25.0	+14.8	10.6	61	-9.8	-9.8	+0.0
ΔA	1.9	21	-10.5	-28.6	+18.1	9.7	41	-10.1	-9.4	-0.7
ΔB	2.3	23	-10.4	-26.5	+16.1	10.9	51	-10.0	-9.6	-0.4
ΔC	2.0	23	-10.5	-25.7	+15.2	9.9	50	-10.0	-11.2	+1.2
ΔD	2.0	16	-10.6	-29.2	+18.6	10.4	34	-10.2	-9.1	-1.1

Table 3.2: ITC values of L9 binding to rPfCSP NVDP mutants. Raw values of the stoichiometry (N), dissociation constant (K_D), change in Gibbs energy of binding (ΔG), enthalpy (ΔH), and entropy contribution to Gibbs energy ($-T\Delta S$) of L9 IgG binding to wild-type rPfCSP (WT) and rPfCSP with various combinations of NVDP mutated to NANP. Binding events 1 and 2 (yellow and blue, respectively) are depicted. -, undetectable. All depicted values are averages of 2-3 independent experiments.

3.6.5 NVDP minor repeat conservation in Pf field isolates

Since two-step binding to rPfCSP by L9 requires at least one NVDP repeat, I next assessed the conservation of NVDP in PfCSP sequences from a large number of Pf field isolates (**Table 3.3**). While there was considerable variation in both the number and position of NVDP repeats, 100% of the 143 distinct Pf isolates collected around the world contained at least one NVDP and every NVDP was preceded by an NANP or ANP sequence that would give rise to NPNV. Furthermore, most (34 of 39, 87%) African isolates contained 4 NVDP repeats, similar to the 3D7 reference isolate. These data show that the NPNV epitope recognized by L9 is highly conserved, suggesting that L9 could react broadly with circulating Pf field isolates.

Central Repeat Region Sequence (0 = NPDP, 1 = NANP, 2 = NVDP)	No. of Repeats		Region Isolated				
	NANP	NVDP	Africa	Asia	Europe	Oceania	South America
0121212121111111111111112111111111111111111	37	5					
012121212111111111111111211111111111111111	37	4					
01212121211111111111111211111111111111111	38	4					
012121212111111111111112111111111111111111111	43	4					
0121212121111111111111111111111111111111111	40	4					
012121212111111111111111111111111111111111111	41	4					
01212121211111111111112111111111111111	36	4					
012121212111111111111112111111111111111	35	4					
0121212121111111111112111111111111111111	40	4					
012121212111111111111112111111111111111	36	4					
0121212121111111111111111111111111111111111	42	4					
012121212111111111111111112111111111111111	39	4					
01212121211111111111112111111111111111	36	4					
012121212111111111111111112111111111111111	40	4					
012121212111111111111111112111111111111111	38	4					
01212121211111111111112111111111111111	35	4					
0121212121111111111111111111111111111111	39	4					
012121212111111111111112111111111111111	37	4					
01212121211111111111112111111111111111111	39	4					
0121212121111111111111111111111111111111	38	4					
012121212111111111111111111112111111111111111	44	4					
01212121211111111112111111111111111111	37	4					
0121212121111111111211111111111111111	36	4					
012121212111111111111111112111111111111111	39	4					
01212121211111111112111111111111111111	39	4					
012121212111111111111111112111111111111111	37	4					
01212121211111111112111111111111111	34	4					
012121212111111111112111111111111111	33	4					
0121212121111111111112111111111111111111	38	4					
012121212111111111112111111111111111	35	4					
012121212111111111112111111111111111	33	4					
01212121211111111112111111111111111	32	4					
0121212121111111111111112111111111111111111111	44	4					
012121212111111111111112111111111111111111	43	4					
0121212121111111111111111111111111111111111111	43	4					
012121212111111111111111112111111111111111	41	4					
0121212121111111111111111112111111111111111	40	4					
012121212111111111111111112111111111111111	39	4					
0121212121111111111111112111111111111111111	39	4					
012121212111111111111112111111111111111111	38	4					
012121212111111111111112111111111111111111	38	4					
012121212111111111111112111111111111111111	38	4					
012111111212121111111121111111111111111111	37	4					
012111111212121111111121111111111111111111	36	4					
012121212111111111111112111111111111111111	36	4					
012121212111111111111112111111111111111111	36	4					
012121212111111111112111111111111111111111	35	4					
012121212111111111111112111111111111111111	35	4					
012121212111111111111112111111111111111111	34	4					
012121212111111111111112111111111111111111	34	4					
012121212111111111212111111111111111111111	31	4					
0121212121111111111111111111111111111111111111111	43	3					
012121212111111111111111111111111111111111111111	42	3					
01212121211111111111111111111111111111111111111	41	3					
012121212111111111111111111111111111111111111111	39	3					
0121212121111111111111111111111111111111111111111	40	3					
012121212111111111111111111111111111111111111111111	44	3					
012121212111111111111112111111111111111111111111111	44	3					
0121212121111111111111111111111111111111111111111111	45	3					
012121212111111111111111111111111111111111111111111111NAKP1	43	3					
01212121111111111111112111111111111111111111111	43	3					
012121211111111111111121111111111111111111111111	43	3					
01212KANP2111111111111111NGKPQCKPQCKPPMQILNAKP11NGNP11111111111111111	36	3					
012121212MQTKCRFQMQPNVDSKCNPIANP1111111111111111111111111111111111111111	40	3					
012121212111SANP1111111111111111111KGNP111111111111111	40	3					
0121212121111111111111111111111111111111111111111111111	48	3					
012121212111111111111NTNP1111111111111111111111111111	43	3					
012121211111111111111121111111111111111111111111111	45	3					
012121212NANS11111111111111111111111111111111111	39	3					
012121212111111111111NVNP1111111111111111111111	36	3					
0121212121111111111111111111111111111111111	38	3					
012121212111111111111111111111111111	30	3					
012121212NADP1YANP1111111111111111111111111111111111	39	3					
012121212111111111111111111111111111111111111111NAKP1111	42	3					
012121111111111111112111111111111111111111111	42	3					
012121111111111111112111111111111111111	38	3					
012121212111111111111111111111111111111111	37	3					
012121212111111111111111111111111111111111	36	3					
01212121111111111112111111111111111111	33	3					
012121212111111111111111111111111111111111	33	3					

Central Repeat Region Sequence (0 = NPDP, 1 = NANP, 2 = NVDP)	No. of Repeats		Region Isolated				
	NANP	NVDP	Africa	Asia	Europe	Oceania	South America
012121211111111111	14	3					
01212121111111111	13	3					
012111111111111211111111111111111111111111111111	45	2					
012121111111111111111111111111111111111111111111111	47	2					
NRDP121111111111111211111111111111111111111111111	45	2					
012111NAKP1111111211111NVNP1111111111111111111111111111111	47	2					
012121NVNP1111111111111111111111111111111111111111111111	50	2					
012111111111NQTQ121111111111111111111111111111	43	2					
012111111111111211111111111111111111111111111	46	2					
01211111111111211111111111111111111111111	44	2					
01NVVP121211111111111111111111111111111111111	39	2					
012121111111111111111111111111111111111111	42	2					
01211111111121111111111111111111111111111	42	2					
012111111111112111111NAANP1111111111111111	36	2					
01211111111121111111111111111111111111111	41	2					
012111111111121111111111111111111111111	39	2					
01211111121111111111111111	26	2					
012111NVNP1111111121111111111111111111111111111111111111	57	2					
012121111111111111111111111111111111111111111111111	49	2					
01211111111111211111NAKP1111111111111111111111111	45	2					
012111NVNP1111111121111111111111111111111111111111	44	2					
01211111111111112111111111111111111111111111	47	2					
0121NVDANPNP211111111111111111111111111111111111111	39	2					
012111111NAGA111121111111111111111111111111111	43	2					
012121111111111111111111111111111111111111111	45	2					
012121IVDP1111111111111111111111111111111111111	40	2					
01211111111111111NVNP11111112111111111111111	40	2					
012121111111111111111111111111111111111111	43	2					
01211111111211111NANH1111111111111111111111	39	2					
012111111111121111111111111111111111111	43	2					
012111111111111211111111111111111XXNP111	37	2					
01211111111111211111111111111111111111	41	2					
012111111111111211111111111111111	37	2					
01211111111111121111111111111111	33	2					
0121111111111112111111111111111	31	2					
012111111111111211111111111111	29	2					
0121NP1P11112111111111111111111	26	2					
012111111111111211111111111	26	2					
01211111111111121111111111	25	2					
012NASPSVNP1111111111111111NANL1111111111111111111111111	44	1					
0121111111111111111KANPKVDP1111111111111111111111111111	49	1					
0HANP21111111111111111111SANP11111111111111111	40	1					
012111111111111NASP1111111111111111111111111111111	44	1					
012NDPNP11111NVDS1111111111111111111111111111	37	1					
01211111111111NVNP11111111111111111111111111	41	1					
NPVL121111111111111111111111111111111111111111111	42	1					
012111111111111111111111111111111111111111111	42	1					
01211111111111NVNP111111111111111	28	1					
NADP1NAEPKANPNAEPNATPNADP11111211111111111111111111111111111	37	1					
0121NVNP1NVNP11111111KANP1NADP11111NAYP1111111111111111	37	1					
01211111111111NVNP11111111111111111111111111111111	50	1					
011111211111111111NANL1NANLYANPYANP1111111111111111111	38	1					
0PANP211111111111111NVNP111NAIP11111111111111111111	39	1					
012111111111111NVNP11111111111111111111111111111	44	1					
01211111111111MANP1111111111111111111111111	41	1					
012111111111111NVNP11111111111111111111111111	41	1					
012111111111111111111111111111111111111111111	45	1					
012111111111111111111111111111111111	35	1					
01111112111111111111111111111111	32	1					
012111111111111NVNP1111111111111	28	1					
01211111111111NVNP111111111111	25	1					
012111111111111111111111111111	29	1					
0121111111111111111111111111111	28	1					

Table 3.3: NVDP repeat conservation in Pf field isolates. The sequence of the central repeat region is depicted (0 = NPDP, 1 = NANP, and 2 = NVDP), along with the number of NANP and NVDP repeats and the region where the isolate was found. Isolates are ordered by number of NVDP repeats. A NPNV motif is formed by "12" (NANPNVDP). PfCSP from the 3D7 reference isolate is highlighted in yellow. Sequences were retrieved from GenBank.

3.7 Generation of L9 with a LS mutation to increase serum half-life

Having identified L9 as a PfCSP human mAb that is more potent than CIS43 at protecting mice from experimental SPZ challenge and shown that it binds a new site of

vulnerability (i.e., the NVDP minor repeats) on PfCSP, the VRC initiated preclinical development of L9 with a LS mutation to increase serum half-life (L9LS).

3.7.1 Generation and quality check of L9LS

The LS mutation refers to a methionine to leucine and asparagine to serine (M432L/N434S) mutations in the IgG Fc region that improves binding affinity to FcRn and improves recycling of IgG back into circulation, resulting in the extension of IgG serum half-life[224]. L9LS was generated via restriction digest of the L9 V_H plasmid ($L9_H$) and a plasmid (CMVR_VRC01LS) containing a IgG_1 Fc with a LS mutation, followed by ligation of the variable regions of $L9_H$ to CMVR_VRC01LS (**Figure 3.16A**). The resultant L9LS plasmid was sequenced and compared to wild-type L9, which confirmed that the V_H regions were identical and that the LS mutation in the Fc was present (**Figure 3.16B**).

A

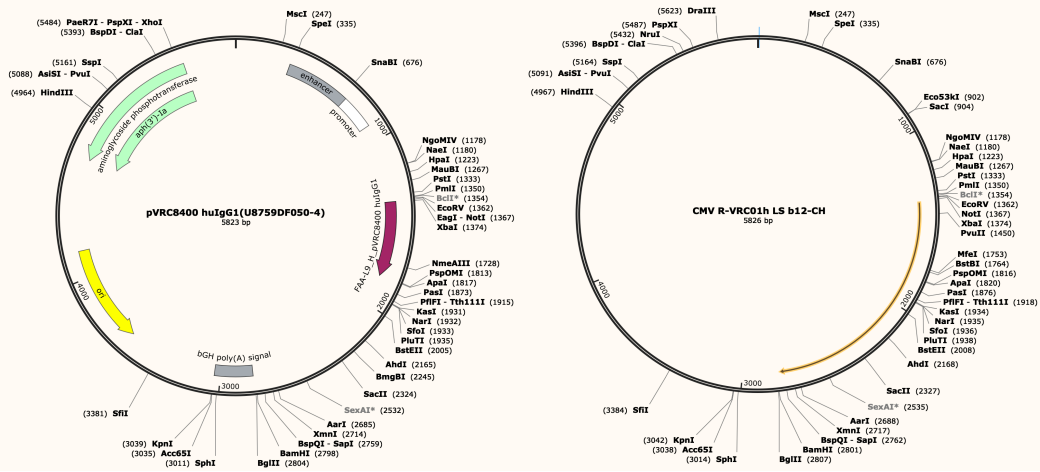

B

```
Consensus MGWSCIILFLVATATGVHSQVKLVESGGGVVQPGRSLRLSCEASGFIFSTYGMHWVRQAP   60
L9        ............................................................   60
L9-LS     ............................................................   60

Consensus GKGLEWVAVIWFDGSNIYYADSVKGRFTISRDNSKNTVFMQMDSLRAEDTAVYYCHRNFY  120
L9        ............................................................  120
L9-LS     ............................................................  120

Consensus DGSGPFDYWGQGTLVTVSSASTKGPSVFPLAPSSKSTSGGTAALGCLVKDYFPEPVTVSW  180
L9        ............................................................  180
L9-LS     ............................................................  180

Consensus NSGALTSGVHTFPAVLQSSGLYSLSSVVTVPSSSLGTQTYICNVNHKPSNTKVDKKVEPK  240
L9        ............................................................  240
L9-LS     ............................................................  240

Consensus SCDKTHTCPPCPAPELLGGPSVFLFPPKPKDTLMISRTPEVTCVVVDVSHEDPEVKFNWY  300
L9        ............................................................  300
L9-LS     ............................................................  300

Consensus VDGVEVHNAKTKPREEQYNSTYRVVSVLTVLHQDWLNGKEYKCKVSNKALPAPIEKTISK  360
L9        ............................................................  360
L9-LS     ............................................................  360

Consensus AKGQPREPQVYTLPPSRDELTKNQVSLTCLVKGFYPSDIAVEWESNGQPENNYKTTPPVL  420
L9        ............................................................  420
L9-LS     ............................................................  420

Consensus DSDGSFFLYSKLTVDKSRWQQGNVFSCSVXHEALHXHYTQKSLSLSPGK            469
L9        ........................M.....N.............                  469
L9-LS     ........................L.....S.............                  469
```

Figure 3.16: Generation of L9LS. (**A**) Plasmid maps of the V_H plasmid of L9 (left) and CMVR_Fc_LS_pVRC2077 (right), an empty plasmid vector that contained the V_H sequence of VRC01. **(B)** Protein alignment of L9 and L9LS; the LS mutation is highlighted in red.

To prepare for NHP PK studies, ~250 milligrams of L9 and L9LS were produced in four batches and each batch was quality checked by ELISA. L9 and L9LS bound similarly to rPfCSP_FL and peptide 22; furthermore, binding was identical between batches (**Figure 3.17A**). Interestingly, L9LS consistently bound peptide 22 slightly better than L9. Aliquots from all four batches were pooled and assessed for their ability to protect against IV challenge at 200 and 50 µg/mouse (**Figure 3.17B**). Both L9 and L9LS significantly and comparably reduced liver burden and subsequent parasitemia at both doses. These data confirm that L9LS displays identical

binding properties and *in vivo* SPZ neutralization to L9, indicating that the LS mutation has not perturbed the effectiveness of L9LS compared to its wild-type parent.

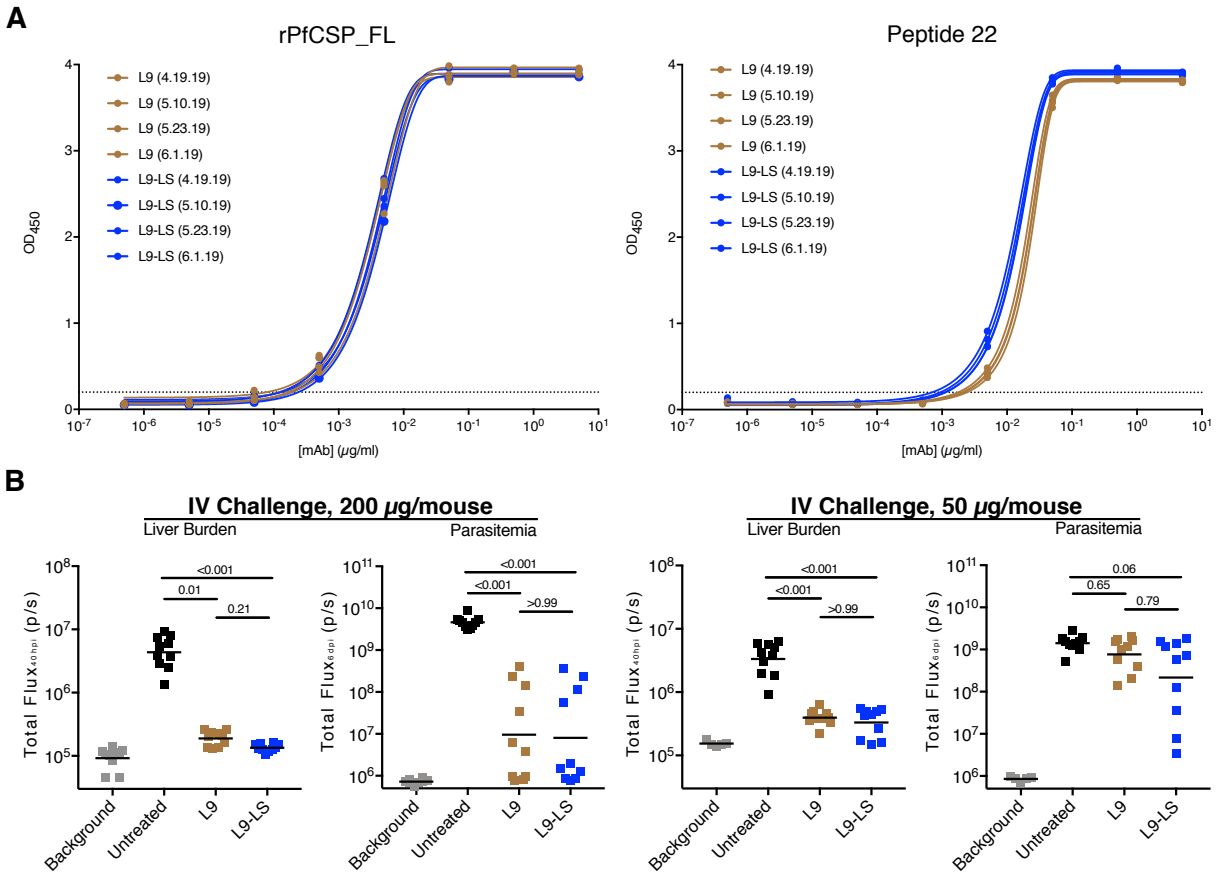

Figure 3.17: Quality check of L9LS. (**A**) Binding of varying concentrations of L9 and L9LS to rPfCSP_FL (left) and peptide 22 (right) measured by ELISA. Four batches of each mAb, denoted by the date (month.day.year), are shown. **(B)** Liver burden and parasitemia reduction (bioluminescence; total flux, photons/sec) in mice 40 h and 6 days post-infection (hpi/dpi; n=5/group) mediated by indicated doses of L9 and L9LS administered 2 hours before IV challenge with 2,000 Pb-PfCSP-SPZ. *P*-values were determined by comparing L9 and L9LS to each other and to untreated control using the Kruskal-Wallis test with Dunn's post-hoc correction.

To ensure that the antimalarial effect of L9LS is due to its specific recognition of PfCSP on PfSPZ and that this mAb has no cross-reactive neutralization of PfMZ, the ability of L9LS to inhibit MZ invasion of human erythrocytes was assessed in the GIA assay. L9LS and CIS43LS exhibited minimal inhibition comparable to the isotype negative control VRC01LS, confirming that neither PfCSP mAb has functional activity against PfMZ (**Figure 3.18**).

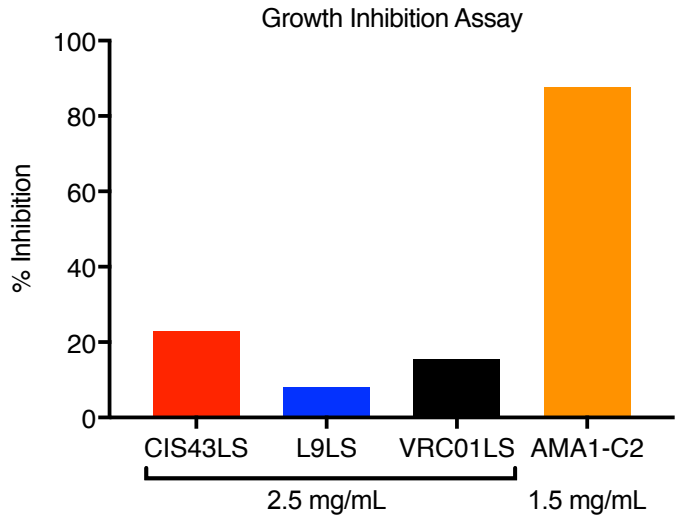

Figure 3.18: *In vitro* GIA of L9LS. Effect of 2.5 mg/mL CIS43LS and L9LS on the growth of merozoites from the Pf 3D7 isolate. 1.5 mg/mL AMA1-C2, neutralizing polyclonal serum directed against AMA1 on the surface of PfMZ, was included as a positive control. 2.5 mg/mL VRC01LS was included as a negative control.

3.7.2 PK of L9LS in NHPs

To determine whether the LS mutation extended the half-life of L9 *in vivo*, one male and two female rhesus macaques per group were IV administered a dose of 10 mg/kg CIS43LS, L9LS, and L9. mAb titers in serum collected at various timepoints throughout the ~4-month study were assessed by ELISA (**Figure 3.19**). L9LS had significantly higher serum concentrations than L9 throughout the study, confirming that the LS mutation extended the serum half-life of L9LS compared to its wild-type parent.

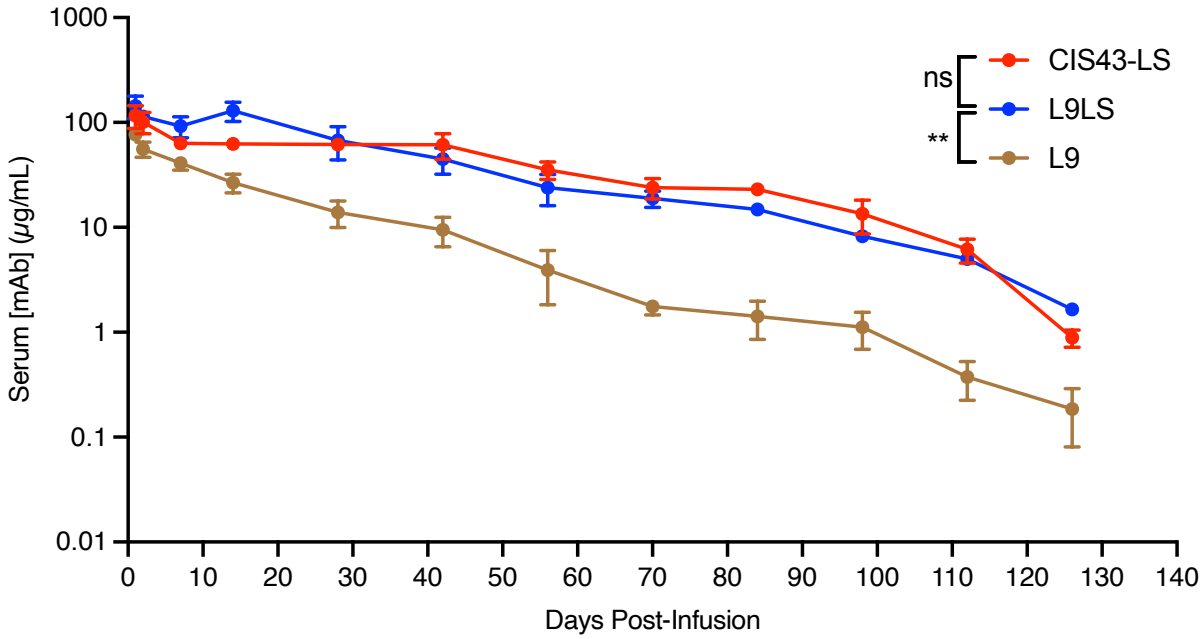

Figure 3.19: PK of CIS43LS, L9LS, and L9 in NHPs. Rhesus macaques were passively infused with mAbs at a dose of 10 mg IgG per kg of animal body weight (n=3/group). Error bars show standard deviation (SD). Statistics were performed using a two-way ANOVA with Geisser-Greenhouse correction to analyze the variance in serum concentrations between L9 vs. L9LS and CIS43LS vs. L9LS over time. ns, not significant, $p>0.05$; **, $p=0.0011$.

3.8 Generation of L9 anti-idiotypic mAbs

In addition to L9LS, anti-idiotypic antibodies against L9 were generated for use as reagents to study anti-drug antibody responses in humans and measure L9LS serum concentrations.

3.8.1 V_H/V_L gene amplification and cloning

Mice were immunized with L9 Fab to generate hybridomas. ELISA was used to screen hybridoma supernatants for reactivity against L9, but not CIS43. Four L9-specific IgG_1 clones (Id1, Id3, Id4, and Id5) were identified and the Ig genes were amplified using PCR with several primer sets and conditions optimized at the VRC (**Figure 3.20**). PCR amplicons were sequenced,

and high-quality Ig sequences were recovered for Id3-5; importantly, two Vκ sequences were obtained for Id3-5. V_H and Vκ sequences were respectively cloned into the pSBSmIgG1H and pSBSmK vectors banked at Gene Synthesis. Plasmids were expressed as recombinant mouse IgG_1, purified, and tested for binding to L9 or CIS43 by ELISA (**Figure 3.21**). All mouse mAbs demonstrated high bind to L9 and undetectable binding to CIS43. These data indicate that the six candidate anti-idiotypic mouse mAbs demonstrated high specificity for L9.

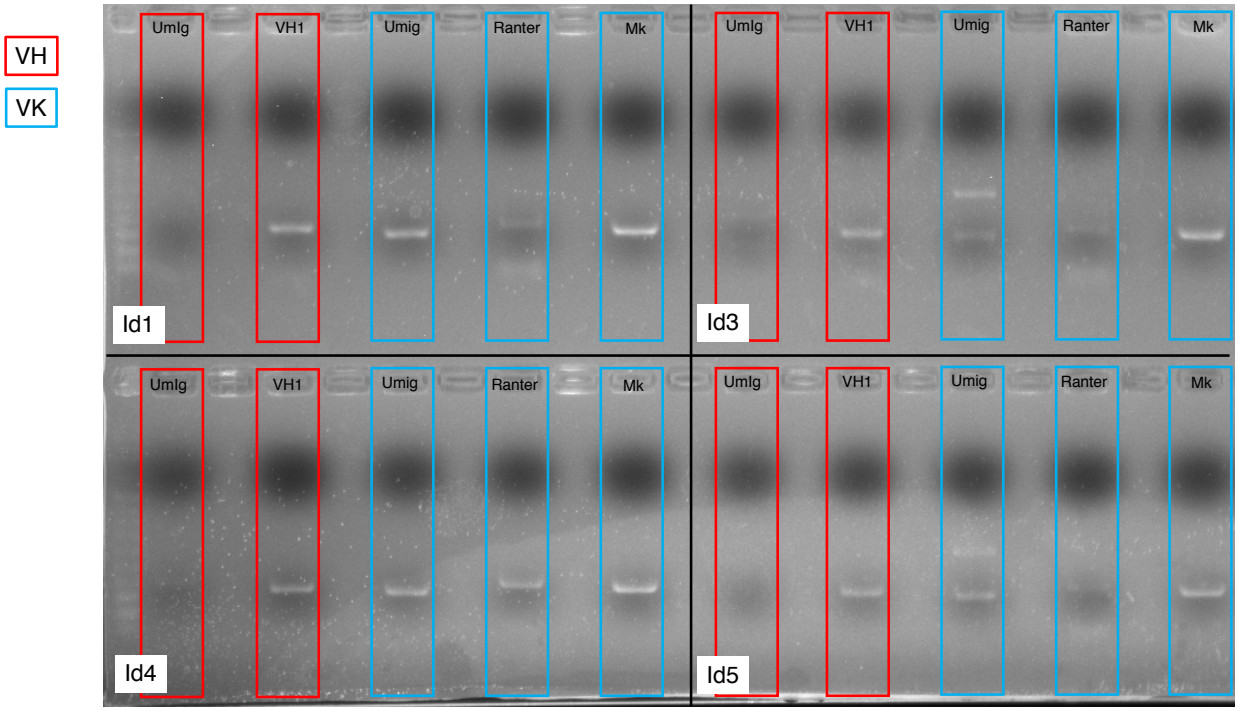

Figure 3.20: PCR of V_H and Vκ genes from four L9 anti-idiotypic hybridoma clones. Each lane represents a PCR amplicon run on a 1% agarose gel. Each lane is denoted by the specific primer used; red lanes are V_H (expected size ~500bp) and blue lanes are Vκ (expected size ~500bp). Each anti-idiotypic clone is numbered 1-5.

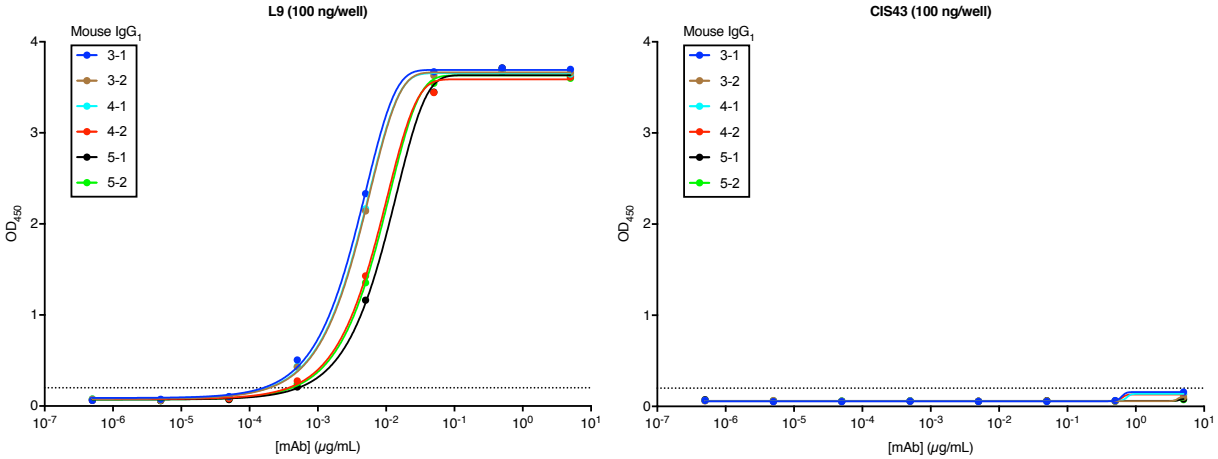

Figure 3.21: Specificity of mouse IgG1 for the idiotope of L9. Binding of varying concentrations of L9 anti-idiotypic mAbs (id3-1, id3-2, id4-1, id4-2, id5-1, id5-2; 1 and 2 indicates the first or second Vκ chain) to L9 and CIS43.

3.9 Discussion

This Chapter presents the isolation of L9, the first highly potent human mAb that preferentially binds the NPNV motif associated with NVDP minor repeats of PfCSP. The only mAbs previously reported to react against NVDP repeats are 2B6, a mouse mAb described as a reagent recognizing NVDPNANP that was never functionally assessed[225], and 311, which was reported to bind DPNANPNVDPNA and NPNVDPNANPNV in the µM range but had five-fold greater affinity for NANP[53,79]. Notably, the minimal peptide recognized by 2B6 does not contain NPNV and, compared to 311, L9 had very high binding to peptide 22 (NANPNVDPNANPNVD), which contains NPNV, but undetectable binding to peptide 29 (NANPNANPNANPNAN), which only contains NPNA, by ELISA.

The unique preference of L9 for NPNV motifs was further underscored by the demonstration that every NVDP had to be mutated to NANP to disrupt two-step binding of L9 to rPfCSP by ITC. These data suggest that L9 should bind all circulating strains, as 100% of known Pf field isolates have ≥1 NVDP and L9 maintained high-affinity binding to rPfCSP with ≥1

NVDP. Given its superior potency compared to CIS43 and the high conservation of its primary PfCSP epitope, L9 is a promising clinical candidate for malaria prophylaxis in travelers and aid workers, as well as seasonal control and elimination campaigns. Moreover, the NPNV minor repeat motif of PfCSP presents a neutralizing epitope not included in RTS,S that might improve next-generation malaria vaccines.

Clinical-grade L9LS was successfully manufactured by the VRC, and an investigational new drug (IND) application was submitted to the United States Food and Drug Administration (FDA) on 9 August 2021. I was fortunate enough to help draft the pre-clinical report contained within this IND application. The FDA issued a safe-to-proceed letter with some non-hold comments on 9 September 2021. VRC 614, a phase 1, dose escalation, open-label clinical trial with experimental CHMI to evaluate safety and protective efficacy of an anti-malaria human mAb, VRCMALMAB0114- 00-AB (L9LS), in healthy, malaria-naïve adults (https://clinicaltrials.gov/ct2/show/NCT05019729) began soliciting volunteers in September 2021. The first volunteer was infused with L9LS on 13 September 2021 and CHMI was performed on 26 October 2021. The results of this trial are on schedule to be submitted for peer review in early 2022.

Chapter IV: Binding and neutralization mechanisms of potent human PfCSP mAbs

4.1 Authorship statement

Sections of this Chapter were published in Wang et al., *Immunity* 2020 (10.1016/j.immuni.2020.08.014). Joe Francica fluorescently labeled PfCSP mAbs; Barbara Flynn performed competition ELISAs and measured serum and skin mAb titers in mice; Arne Schön performed ITC; Alvaro Molina-Cruz provided infected mosquitoes for SPZ isolation; Lais Pereira and Marlon Dillon dissected SPZ and performed IV/ID challenges; Yevel Flores-Garcia performed mosquito bite challenges; Bryan Mayer, Monica Gerber, and Raphael Gottardo assisted with statistical analyses of mosquito bite challenge data; Amanda Fabra-García performed *in vitro* HC-04 hepatocyte invasion assays; Azza Idris and Meghan Marquette performed SPZ invasion assays in primary human hepatocytes; James O'Connor performed intravital liver imaging.

4.2 Introduction

Shortly before I began my DPhil studies in 2018, four high-profile publications were published describing seven highly protective human PfCSP repeat mAbs (CIS43[84], mAb10[84], MGG4[213], MGU12[213], 1210[219], 311[79], and 317[79]) that were the most potent reported to date. While mAb10, 1210, 311 and 317 specifically bound NANP major repeats, CIS43, MGG4 and MGU12 were the first mAbs reported to exhibit dual-specificity for the junctional tetrapeptide NPDP and NANP repeats. Despite these key advances, the binding properties and mechanisms

that potent PfCSP mAbs use to neutralize SPZ *in vivo* remained unclear. In particular, while several studies had used multiphoton microscopy to visualize SPZ being neutralized by CSP antibodies in the skin of mice[98,102,103], no studies had investigated how CSP antibodies neutralize SPZ in the liver *in vivo*.

As these seven PfCSP mAbs were isolated and characterized in different labs with distinct methodologies, their binding properties and *in vivo* potency relative to each other remained unknown. Furthermore, the specific mechanism(s) these protective mAbs employ to neutralize SPZ are largely unclear. Only Kisalu et al. demonstrated that CIS43 inhibits cleavage of PfCSP *in vitro* and thereby blocks SPZ from invading hepatocytes[84]; every other study did not elucidate the mechanisms these mAbs used to neutralize SPZ and instead focused on characterizing the epitopes recognized by each mAb in atomic-level detail.

This Chapter compares the binding properties and SPZ neutralization mechanisms of these seven neutralizing human PfCSP mAbs along with L9, which was isolated concurrent with the initiation of this PfCSP mAb comparison study. Specifically, this Chapter characterizes the mAb panel's binding to PfCSP peptides and recombinant full-length proteins, potency across several complementary *in vivo* protection and PK studies in mice, and functional effects on SPZ *in vitro* and *in vivo* in the livers of mice.

4.3 Binding properties of a panel of eight neutralizing PfCSP human mAbs

4.3.1 Binding of the mAb panel to rPfCSP and SPZ

To facilitate consistent analyses in these studies, all eight mAbs in the panel were expressed in the same IgG_1 vector with identical constant regions (**Figure 3.4**). All mAbs in the panel were first tested for their binding to rPfCSP and Pb-PfCSP-SPZ. All mAbs showed

comparable dose-dependent binding to rPfCSP by ELISA (**Figure 4.1A**), with EC_{50} values ranging from 0.003 – 0.007 µg/mL, though 311 and 317 had higher EC_{50} values (0.02 and 0.04 µg/mL, respectively). All mAbs showed similar binding to native PfCSP on the surface of Pb-PfCSP-SPZ by flow cytometry (**Figure 4.1B**). mAb binding to rPfCSP was also compared by BLI (**Figure 4.1C**). Notably, every mAb in the panel bound rPfCSP with $K_{D(app.)}$ <0.001 nM except for CIS43 and L9, which had higher $K_{D(app.)}$ values (1.32 and 0.294 nM, respectively).

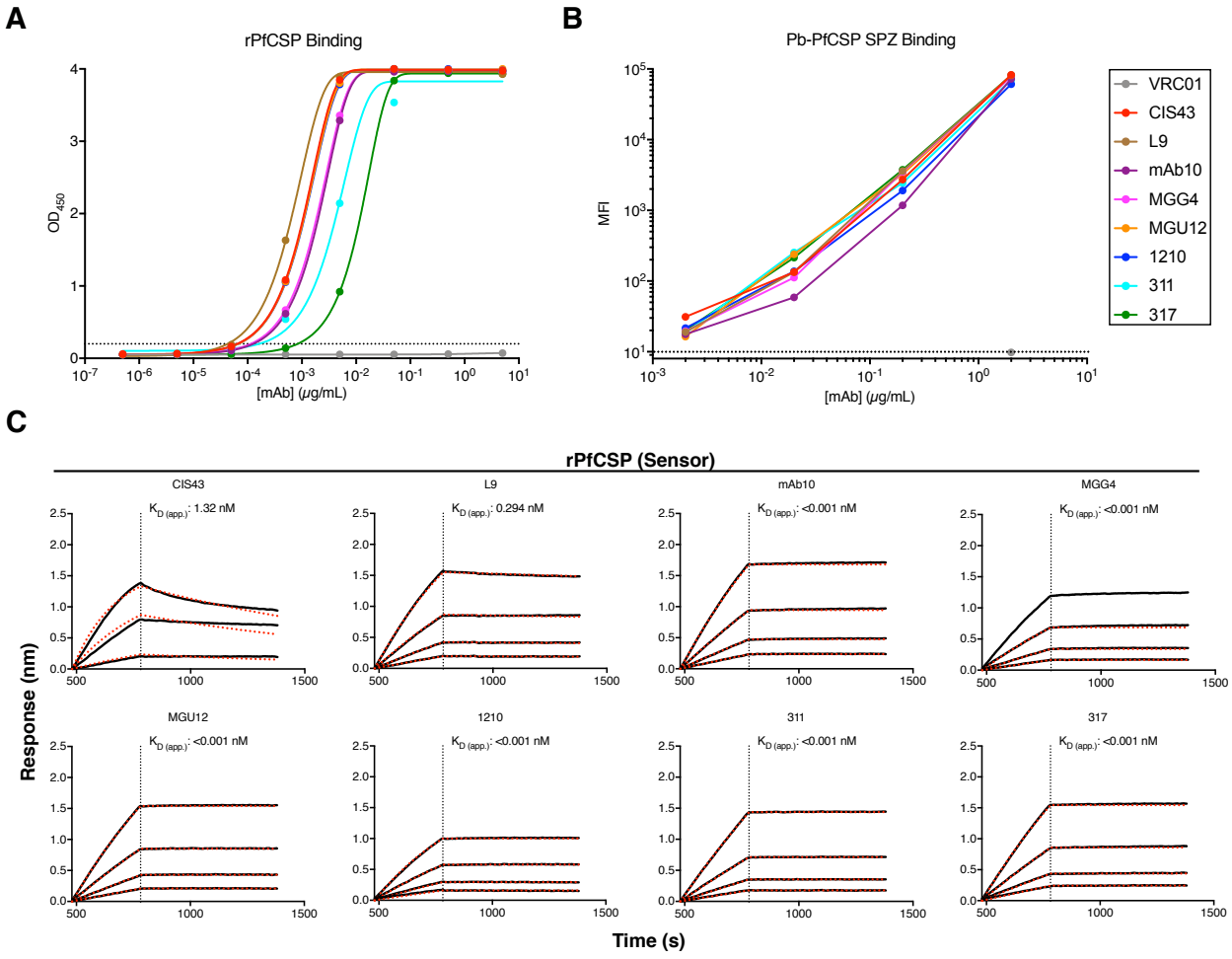

Figure 4.1: Comparison of mAb binding to rPfCSP and Pb-PfCSP-SPZ. (A) Binding of varying concentrations of mAbs to rPfCSP determined by ELISA; OD_{450} is plotted. (**B**) Binding of varying concentrations of mAbs to Pb-PfCSP-SPZ determined by flow cytometry. MFI of the mAb-bound SPZ is plotted. **(C)** Measurement of IgG binding to rPfCSP by BLI. Antibody binding curves are shown in black (raw data). Data were fitted (dotted red lines) with the binding

equations describing a 1:1 analyte-ligand binding model. Serial concentrations of antibodies used are as follow: 1.25, 0.625, 0.3125, and 0.15625 μg/mL. $K_{D(app.)}$ is shown.

4.3.2 mAb binding to PfCSP peptides

The preferred peptide(s) and epitope(s) for each mAb on rPfCSP were determined by competition ELISA with peptides 20-61 (**Figure 4.2A**). Competition ELISA uses a range of peptide concentrations to compete mAb binding to rPfCSP and is thus more sensitive than measuring mAb binding to peptides at a single peptide concentration. All mAbs except CIS43 and L9 were preferentially competed by peptide 29, which contains only NANP repeats. Conversely, rPfCSP binding by CIS43 and L9 was preferentially competed by peptides 21 (half maximal inhibitory concentration, IC_{50}=0.06 μg/mL) and 22 (IC_{50}=0.0004 μg/mL), respectively, and exhibited negligible competition by peptide 29 (IC_{50}=817.5 μg/mL and IC_{50}>1,000 μg/mL, respectively). The peptide preferences of these eight mAbs were substantiated using BLI to directly measure their apparent binding avidity to peptides 21, 22, and 29 (**Figure 4.3**).

Since the mAb panel showed different binding affinities for peptide 29 (which only contains NANP repeats), I determined the minimal number of NPNA repeats required for binding using $(NANP)_1$ to $(NANP)_9$ peptides (**Figure 4.2B**). None of the mAbs bound $(NANP)_1$ or $(NANP)_2$, consistent with previous reports that the minimum epitope of PfCSP repeat mAbs is 2 NPNA repeats[53,79,219]. mAb10, MGG4, MGU12, 1210, 311, and 317 bound peptides with ≥2 NPNA repeats (i.e., $(NANP)_3$ or higher) with greater affinity than CIS43 and L9. Interestingly, L9 binding increased from nearly undetectable for $(NANP)_3$ to $(NANP)_9$ binding that was comparable to CIS43, though still ~12-48% less than the other mAbs. These data show that, although CIS43 and L9 respectively prefer DPNA and NPNV motifs, they can bind NPNA when

these motifs are sufficiently concatenated on long peptides and presumably rPfCSP and native PfCSP on SPZ.

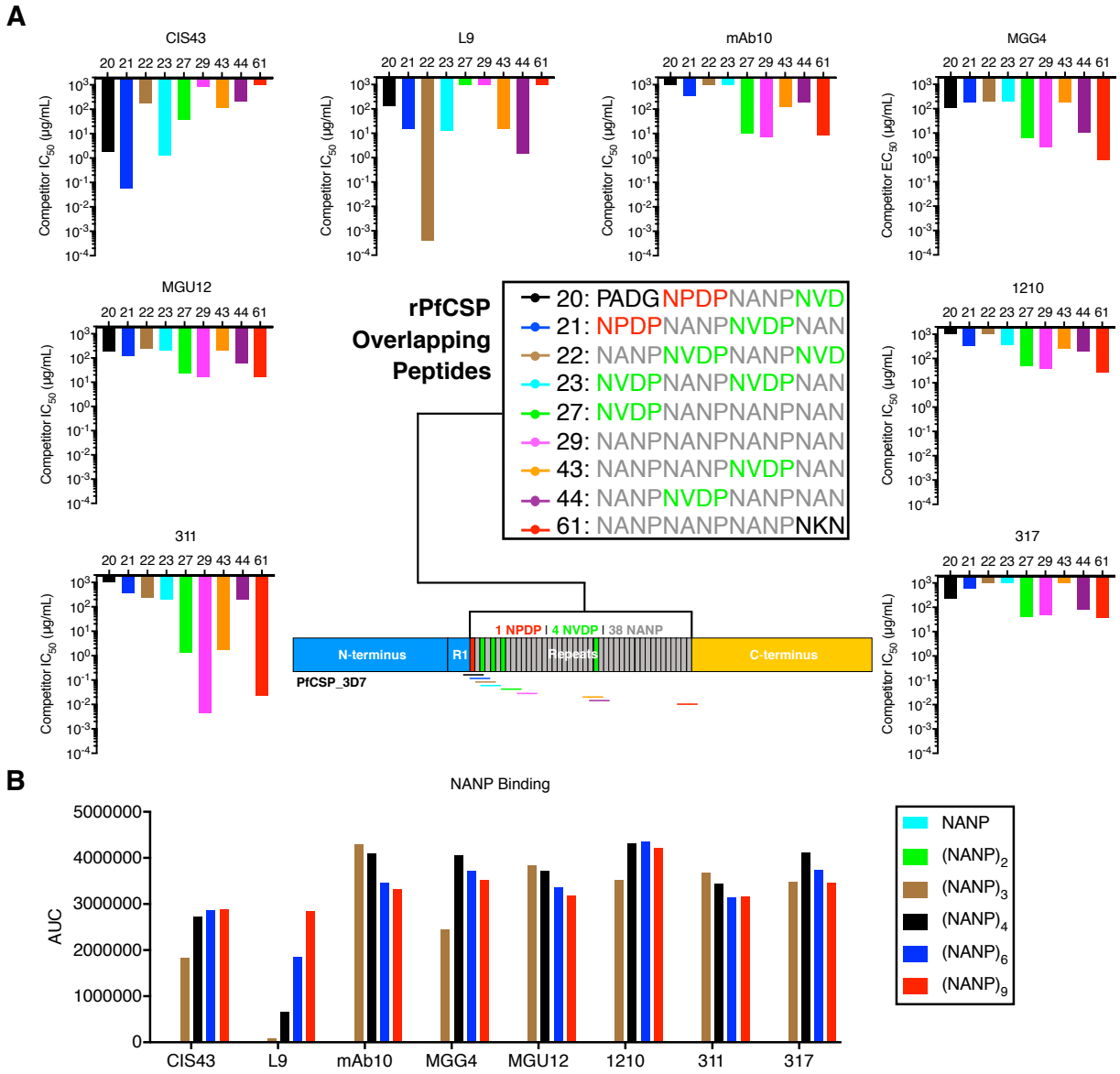

Figure 4.2: Peptide mapping of eight neutralizing human PfCSP mAbs. (A) Competition ELISA of mAbs binding to rPfCSP in the presence of varying concentrations of peptides 20-61 (shown in schematic of rPfCSP). The IC_{50} for competition by each peptide is depicted. (**B**) Binding of varying concentrations of mAbs to NANP-containing peptides of increasing length determined by ELISA and expressed as AUC. $(NANP)_1$ is composed of one NANP, $(NANP)_9$ is composed of 9 NANP repeats.

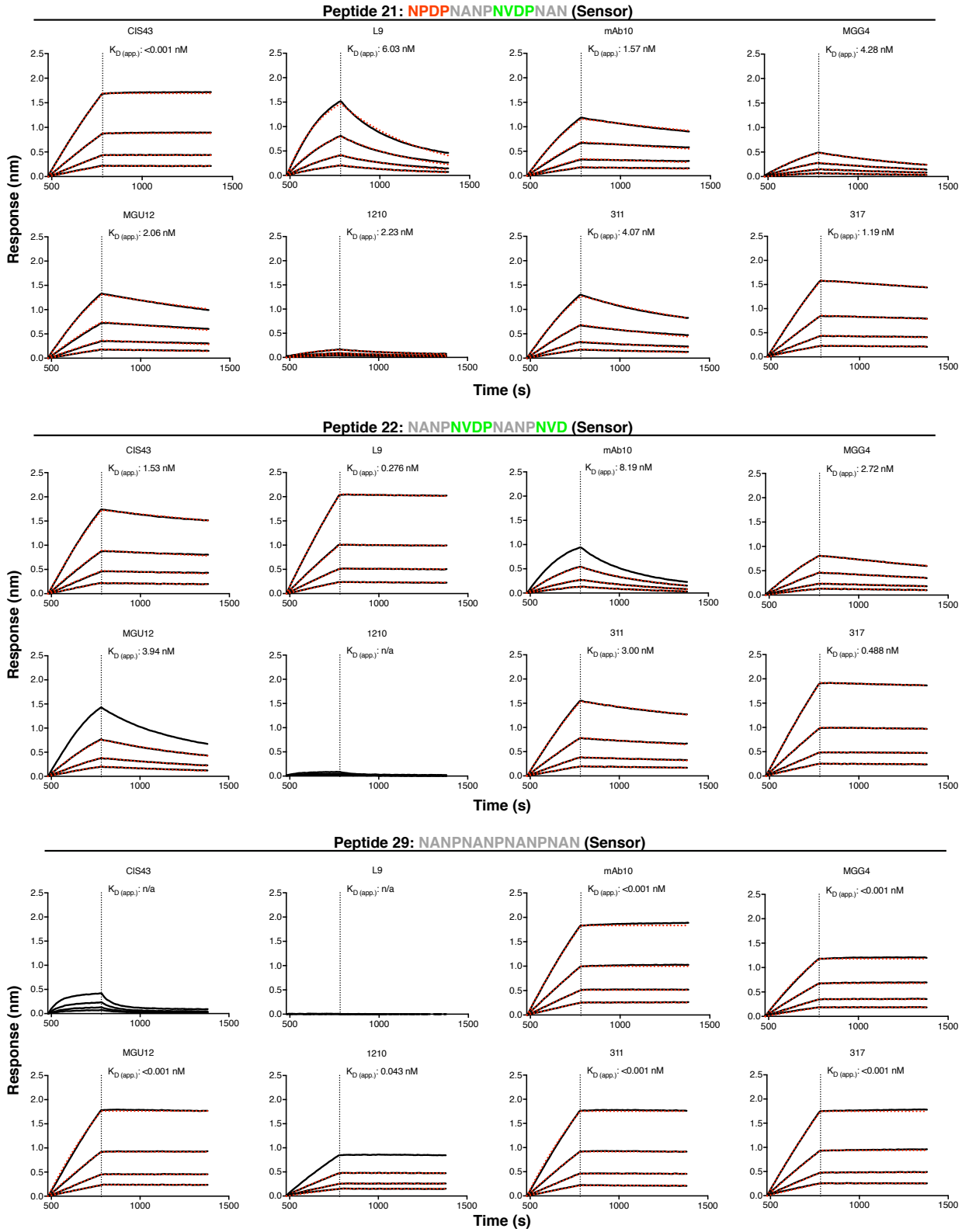

Figure 4.3: BLI of mAb binding to peptides 21, 22, and 29. Antibody binding curves are shown in black (raw data). Data were fitted (dotted red lines) with the binding equations describing a 1:1 analyte-ligand binding model. Serial concentrations of antibodies used are as

follow: 1.25, 0.625, 0.3125, and 0.15625 µg/mL. $K_{D(app.)}$ is shown. Data is representative of two independent experiments.

4.3.3 mAb binding to wild-type and truncated rPfCSP

To correlate the peptide binding characteristics of the mAb panel to their recognition of full-length recombinant protein, ITC was used to characterize the affinity and stoichiometry of their binding to rPfCSP. All mAbs bound rPfCSP with high affinity (K_{D1}= 2-29 nM) and stoichiometry (~7-16 binding sites) (**Figure 4.4A**). A unique feature of CIS43 that distinguished it from less potent mAbs was its ability to bind rPfCSP with two sequential events by ITC (termed "two-step binding"): the first binding event involved ~1 high-affinity binding site at NPDP and the second involves ~5 lower-affinity binding sites at NANP repeats[84]. Remarkably, L9, 311, and 317 also exhibited two-step binding to rPfCSP while 1210, mAb10, and MGU12 bound in a single step.

To further define the exact stoichiometry and affinity of the mAb panel for particular portions of the PfCSP repeat region, ITC was performed using three rPfCSP constructs with identical N- and C-termini but truncated repeat regions containing 23/4, 19/3, and 5/3 NANP/NVDP repeats (rPfCSP_23/4, rPfCSP_19/3, rPfCSP_5/3; **Figure 4.4B, Table 4.1,** and **Figure 4.5**). The increase in stoichiometry for all mAbs was approximately linear as the number of repeats was increased except for CIS43, which showed no appreciable binding to the last 15 NANP repeats (**Figure 4.4C**), consistent with its lower total stoichiometry compared to the other mAbs (N=7.2 for FL; **Figure 4.4A**). This suggests that, apart from CIS43, the binding of every mAb in the panel is evenly distributed across the repeat region.

Notably, the stoichiometry of binding event 1 (N_1) for CIS43, L9, and 311 was relatively unchanged as the repeat region was truncated (**Table 4.1**), suggesting that the epitopes

recognized by these mAbs in binding event 1 are located within rPfCSP_5/3. As the repeats were truncated down to 5/3, the affinity (K_{D1}, dissociation constant for binding event 1) of two-step binding mAbs (CIS43, L9, 311, 317) improved or was unchanged, while the K_{D1} of single-step binding mAbs (mAb10, MGG4, MGU12, 1210) worsened (**Figure 4.4D**). Interestingly, only 317 maintained two-step binding to rPfCSP_5/3 and had a measurable K_{D2}. Overall, these data suggest that the epitope(s) bound by the two-step binding mAbs in binding event 1 are located in the junctional region encompassed by rPfCSP_5/3 and that two-step binding is associated with high-affinity binding to rPfCSP_5/3.

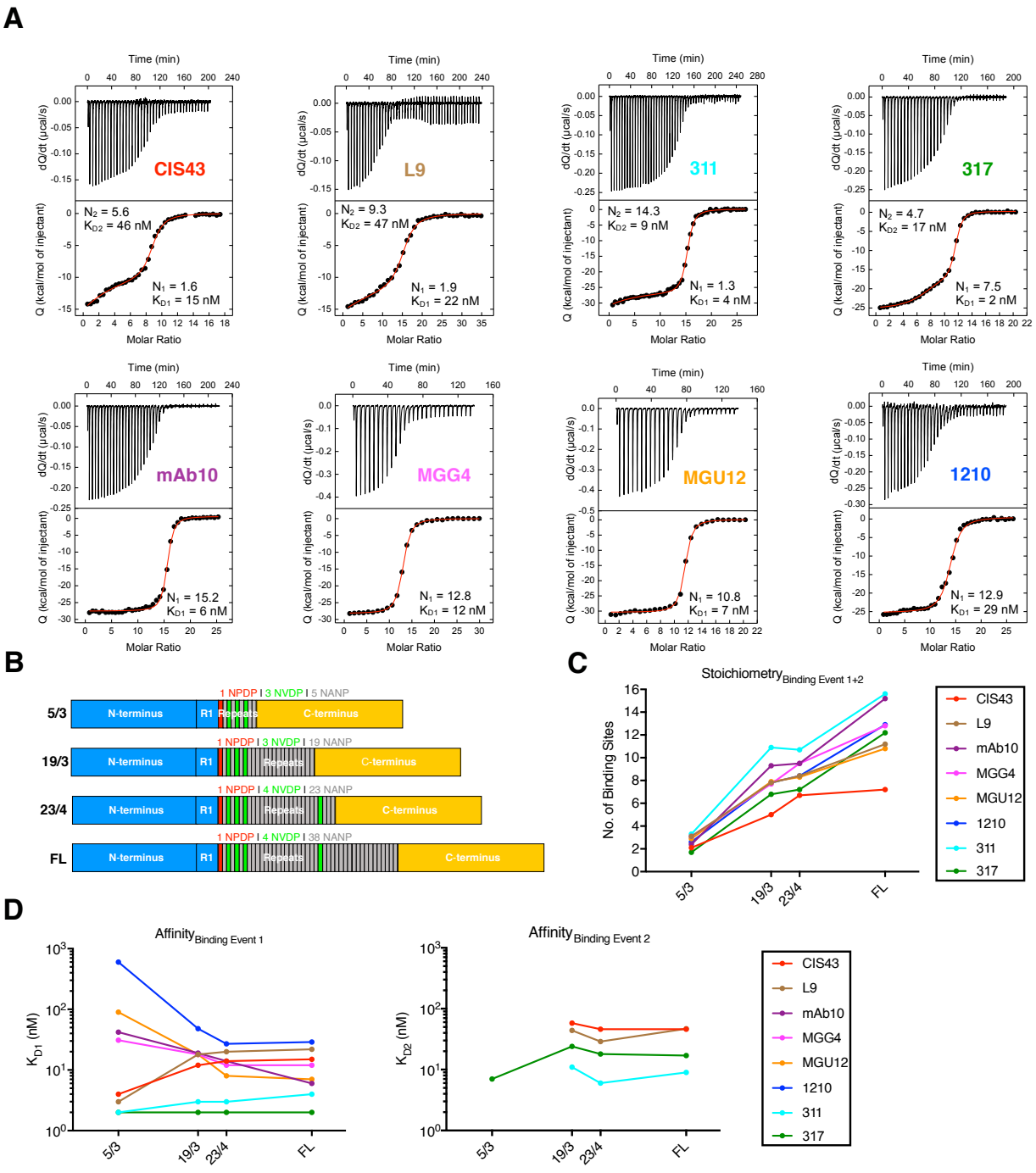

Figure 4.4: ITC analyses of mAb binding to rPfCSP. (**A**) ITC plots depicting the binding of CIS43, L9, 311, 317, mAb10, MGG4, MGU12, and 1210 IgG to rPfCSP_FL. ITC data was fit to a two-step binding model if the IgG titrant bound to two sets of sites with different affinity values. (**B**) Schematics of rPfCSP_FL and rPfCSP mutants with truncated repeat regions (23/4, 19/3, 5/3 NANP/NVDP repeats) and identical N- and C-termini. (**C**) Aggregate stoichiometry (binding events 1+2; no. of antigen binding sites) of mAb binding to 5/3, 19/3, 23/4, and FL rPfCSP determined through ITC. (**D**) Affinity (binding events 1 vs. 2; K_D, nM) of mAb binding to 5/3, 19/3, 23/4, and FL rPfCSP determined through ITC. All ITC plots are representative of 2-3 independent experiments; **C-D** reflect an average of these experiments.

mAb	CSP Construct	Binding Event 1					Binding Event 2				
		N_1	K_{D1} (nM)	ΔG_1 (kcal/mol)	ΔH_1 (kcal/mol)	$-T\Delta S_1$ (kcal/mol)	N_2	K_{D2} (nM)	ΔG_2 (kcal/mol)	ΔH_2 (kcal/mol)	$-T\Delta S_2$ (kcal/mol)
CIS43	FL	1.6	15	-10.6	-24.5	+13.8	5.6	46	-10.0	-9.6	-0.4
	23/4	2.1	14	-10.7	-20.6	+9.9	4.6	46	-10.0	-8.2	-1.8
	19/3	1.6	12	-10.8	-19.1	+8.3	3.4	58	-9.9	-7.0	-2.9
	5/3	2.1	4	-11.5	-16.4	+4.9	-	-	-	-	-
L9	FL	1.9	22	-10.4	-30.0	+19.6	9.3	47	-10.0	-9.1	-0.9
	23/4	2.0	20	-10.5	-32.1	+21.6	6.4	29	-10.3	-8.4	-1.9
	19/3	2.6	18	-10.6	-25.4	+14.1	5.2	44	-10.0	-7.6	-2.4
	5/3	3.1	3	-11.6	-17.0	+5.4	-	-	-	-	-
mAb10	FL	15.2	6	-11.2	-28.3	+17.1	-	-	-	-	-
	23/4	9.5	14	-10.7	-28.1	+17.4	-	-	-	-	-
	19/3	9.3	19	-10.5	-28.4	+17.9	-	-	-	-	-
	5/3	2.4	42	-10.1	-27.9	+17.8	-	-	-	-	-
MGG4	FL	12.8	12	-10.8	-27.6	+16.8	-	-	-	-	-
	23/4	9.5	12	-10.8	-26.7	+15.9	-	-	-	-	-
	19/3	7.7	18	-10.6	-25.1	+14.5	-	-	-	-	-
	5/3	3.1	31	-10.2	-27.5	+17.3	-	-	-	-	-
MGU12	FL	10.8	7	-11.1	-30.7	+19.6	-	-	-	-	-
	23/4	8.3	8	-11.0	-30.2	+19.2	-	-	-	-	-
	19/3	7.9	18	-10.6	-29.3	+18.7	-	-	-	-	-
	5/3	2.9	90	-9.6	-31.3	+21.7	-	-	-	-	-
1210	FL	12.9	29	-10.3	-26.8	+16.5	-	-	-	-	-
	23/4	8.4	27	-10.3	-26.3	+16.0	-	-	-	-	-
	19/3	7.8	48	-10.0	-27.3	+17.3	-	-	-	-	-
	5/3	2.6	600	-8.5	-31.4	+22.9	-	-	-	-	-
311	FL	1.3	4	-11.4	-44.7	+33.3	14.3	9	-11.0	-26.2	+15.2
	23/4	1.4	3	-11.7	-41.4	+29.7	9.3	6	-11.2	-25.3	+14.1
	19/3	1.3	3	-11.6	-40.9	+29.3	9.6	11	-10.9	-24.9	+14.0
	5/3	3.3	2	-11.8	-24.0	+12.2	-	-	-	-	-
317	FL	7.5	2	-11.9	-26.3	+14.4	4.7	17	-10.6	-16.7	+6.1
	23/4	4.2	2	-11.8	-25.8	+14.0	3.0	18	-10.6	-16.7	+6.1
	19/3	3.5	2	-11.9	-24.8	+12.9	3.3	24	-10.4	-16.7	+6.3
	5/3	0.5	2	-11.9	-28.0	+16.1	1.2	7	-11.1	-16.7	+5.6

Table 4.1: ITC values of mAb binding to FL and truncated rPfCSP. Raw values of the stoichiometry (N), dissociation constant (K_D), change in Gibbs energy of binding (ΔG), enthalpy (ΔH), and entropy contribution to Gibbs energy ($-T\Delta S$) of indicated mAb binding to FL rPfCSP and rPfCSP constructs with truncated repeat regions (23/4, 19/3, and 5/3 NANP/NVDP repeats). Binding events 1 and 2 (yellow and blue, respectively) are depicted. -, undetectable. All values are averages of 2-3 independent experiments.

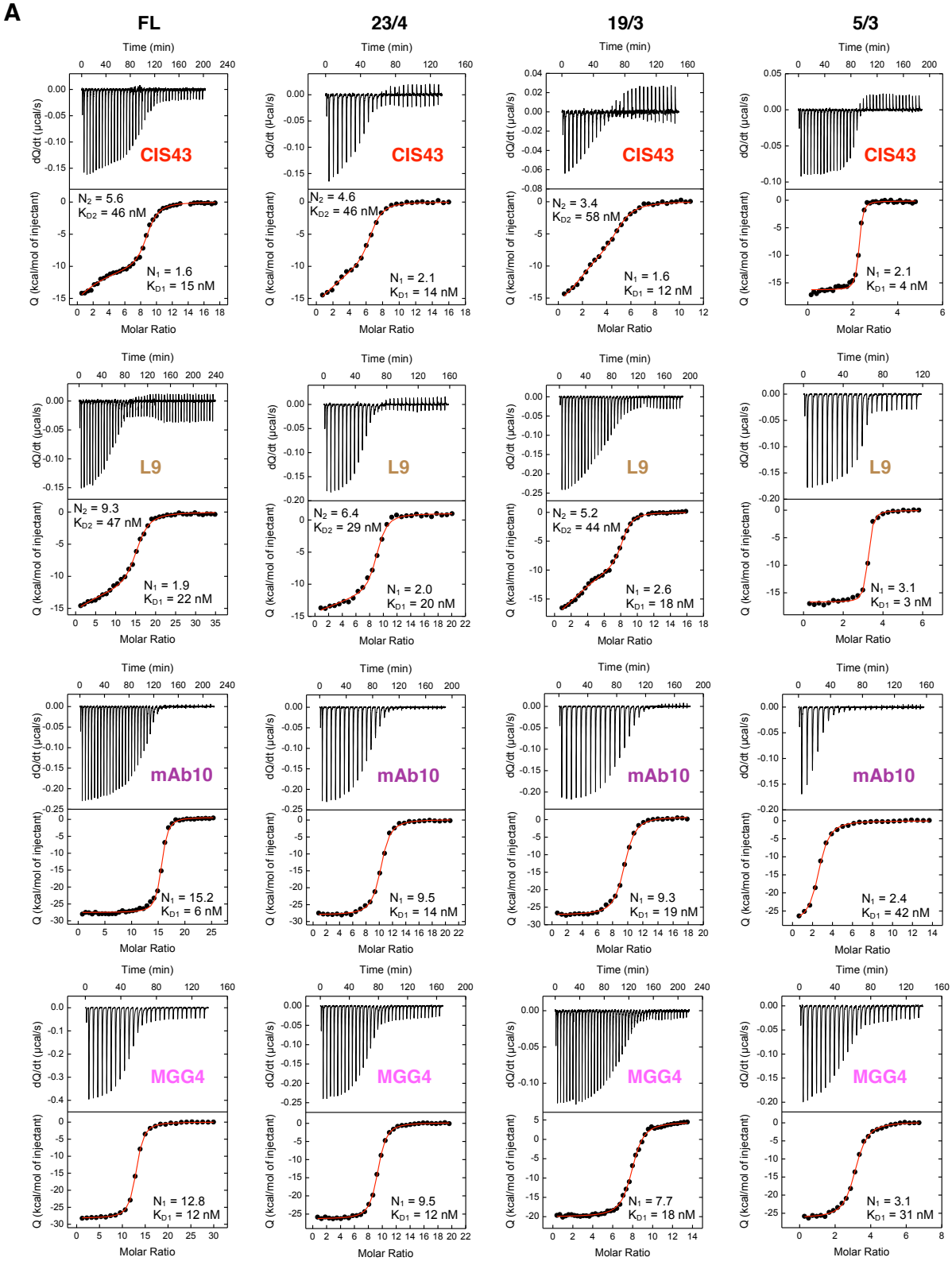
A
FL
23/4
19/3
5/3
Time (min)
dQ/dt (µcal/s)
Q (kcal/mol of injectant)
Molar Ratio
CIS43
N2 = 5.6
KD2 = 46 nM
N1 = 1.6
KD1 = 15 nM
N2 = 4.6
KD2 = 46 nM
N1 = 2.1
KD1 = 14 nM
N2 = 3.4
KD2 = 58 nM
N1 = 1.6
KD1 = 12 nM
N1 = 2.1
KD1 = 4 nM
L9
N2 = 9.3
KD2 = 47 nM
N1 = 1.9
KD1 = 22 nM
N2 = 6.4
KD2 = 29 nM
N1 = 2.0
KD1 = 20 nM
N2 = 5.2
KD2 = 44 nM
N1 = 2.6
KD1 = 18 nM
N1 = 3.1
KD1 = 3 nM
mAb10
N1 = 15.2
KD1 = 6 nM
N1 = 9.5
KD1 = 14 nM
N1 = 9.3
KD1 = 19 nM
N1 = 2.4
KD1 = 42 nM
MGG4
N1 = 12.8
KD1 = 12 nM
N1 = 9.5
KD1 = 12 nM
N1 = 7.7
KD1 = 18 nM
N1 = 3.1
KD1 = 31 nM

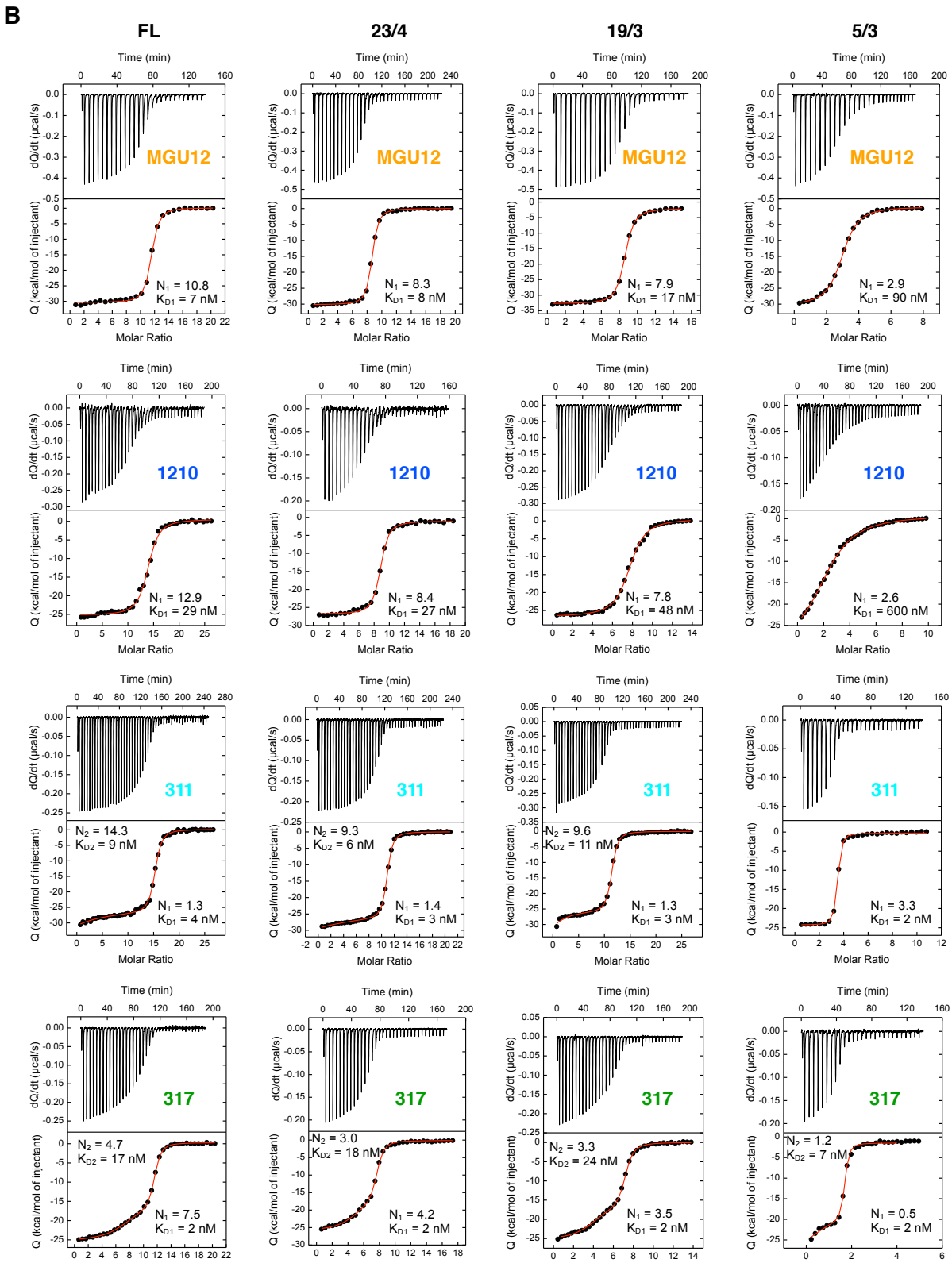

Figure 4.5: ITC plots of mAb binding to FL and truncated rPfCSP. (**A**) CIS43, L9, mAb10, MGG4 IgG and (**B**) MGU12, 1210, 311, and 317 IgG binding to FL, 23/4, 19/3, and 5/3 rPfCSP.

ITC plots are representative of 2-3 independent experiments; data is summarized in Figure 4.4 and Table 4.1.

4.4 *In vivo* functional activity of eight neutralizing PfCSP mAbs

4.4.1 Protection against SPZ challenge 2 hours after mAb administration

Multiple *in vivo* protection assays were used to compare the mAb panel's protective potency. First, mAb-mediated reduction of parasite liver burden following IV challenge with Pb-PfCSP-SPZ 2 hours after mAb passive transfer in mice was assessed (**Figure 4.6A**). The IV challenge model is a direct assessment of SPZ neutralization in the liver because IV-administered SPZ invade hepatocytes within 2 minutes[90]. Based on the IV challenge titration comparing CIS43 and L9 (**Figure 3.10B**), 75 and 25 μg/mouse were selected as the limiting doses that could differentiate protection between mAbs in the panel. At 75 μg/mouse, CIS43, L9, 311, and 317 significantly reduced liver burden compared to untreated control; reduction by mAb10, MGU12, and 1210 did not reach statistical significance. At 25 μg/mouse, only CIS43, L9, and 317 significantly reduced liver burden. Together, these data show that CIS43, L9, 311, and 317 mediated the greatest liver burden reduction following IV challenge.

To extend this analysis, mice were challenged with five infected mosquito bites 2 hours after passive transfer (**Figure 4.6B**). At 300 μg/mouse, CIS43, L9, 311, and 317 sterilely protected >80% of mice and were not significantly different. Conversely, 1210 (42%), mAb10 (33%), MGU12 (8%), and MGG4 (0%) were significantly less protective. At 100 μg/mouse, protection by CIS43, L9, 311, and 317 sterilely protected >60% of mice and were not significantly different, while 1210, MGG4, and MGU12 mediated only 0-17% protection.

mAb titers in the serum and skin 2 hours after passive transfer of 300 μg mAb were assessed in separate groups of mice (**Figure 4.6C**). Serum titers were similar between all mAbs

except for MGG4, which had undetectable titers near 0 μg/mL. Skin mAb titers were similar between all mAbs except for mAb10 (~13 μg/g), which was significantly greater than MGU12 and 317 (~2 μg/g for both). Interestingly, MGG4 was present in skin but barely detectable in serum, demonstrating that this mAb had distributed into the skin despite being rapidly cleared from the serum. Together, these data show that CIS43, L9, 311, and 317 are significantly more protective than 1210, mAb10, MGG4, and MGU12 against both IV and mosquito bite challenge 2 hours after mAb administration.

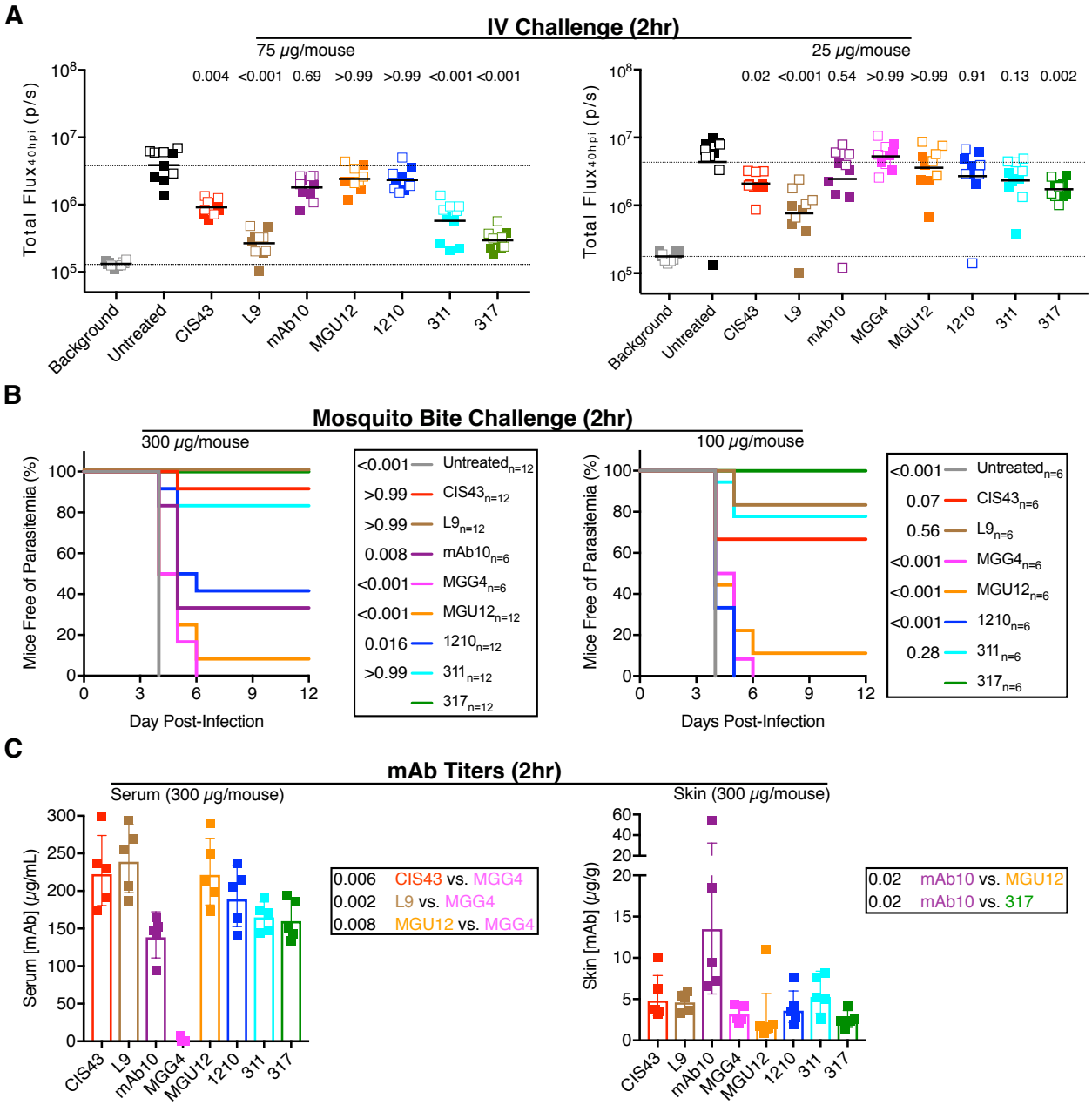

Figure 4.6: *In vivo* protection and PK of PfCSP mAbs 2 hours after passive transfer. (**A**) Liver burden reduction in mice 40 h post-infection (hpi; n=10/group; data pooled from two independent experiments, solid vs. open squares; lines represent geometric mean) mediated by 75 or 25 μg mAb administered 2 hours before IV challenge with 2,000 Pb-PfCSP-SPZ. Dotted lines were set at the geometric mean of the background (unchallenged) and untreated (challenged) control groups. *P*-values were determined by comparing each mAb to untreated control using the Kruskal-Wallis test with Dunn's post-hoc correction. (**B**) Survival curves of mice challenged with five infected mosquito bites 2 hours after passive transfer of 300 or 100 μg mAb (n indicates number of mice for each group; data were respectively combined from three independent blinded experiments). *P*-values were determined by comparing 317 to every other mAb and untreated control using the log-rank test. (**C**) Serum and skin mAb titers 2 hours after passive transfer of 300 μg mAbs in separate mice (n=5/group; bars set at geometric mean with

geometric SD) determined through ELISA. *P*-values were determined by comparing all mAbs to each other using the Kruskal-Wallis test with Dunn's post-hoc correction. Only significant *P*-values are shown.

4.4.2 Protection against SPZ challenge 3 days after mAb administration

It was possible that the initial *in vivo* potency hierarchy defined by challenging 2 hours after passive transfer largely reflected SPZ neutralization in the vasculature and liver, as the mAbs may not have had time to fully distribute into the skin, which is thought to be a major physiological site for antibody-mediated SPZ neutralization[98,102,103]. Thus, a kinetic analysis of L9 titers in skin and serum was performed over 7 days to define an optimal timepoint for ID or mosquito bite challenge in which mAbs have equilibrated in both the skin and serum (**Figure 4.7A**). While L9 was detectable in the skin at 2 hours (~10 μg mAb/g tissue), it peaked at 24 hours (~35 μg/g) and reached steady state by 3 days (~15 μg/g). Conversely, L9 serum titers peaked at 2 hours (~250 μg/mL) and also reached steady state by 3 days (~150 μg/mL).

Subsequently, serum and skin titers were measured for the entire mAb panel 3 days after passive transfer (**Figure 4.7B**). Serum titers (~150 μg/mL) were similar for all mAbs except MGG4, which was again undetectable. Skin titers were similar for all mAbs except for 311 (~3 μg/g); furthermore, skin titers trended higher at 3 days versus 2 hours (**Figure 4.6C**) for most mAbs except mAb10 and 311. These data suggested that 3 days after passive transfer allowed mAbs to equilibrate in the mice and was thus the optimal challenge timepoint. Finally, a dose titration of L9 was performed in the ID challenge model to define an optimal mAb dose for 3 day challenge (**Figure 4.7C**). All mice were sterilely protected at all doses except 50 μg/mouse; thus, this limiting dose was selected to compare all the mAbs in the panel.

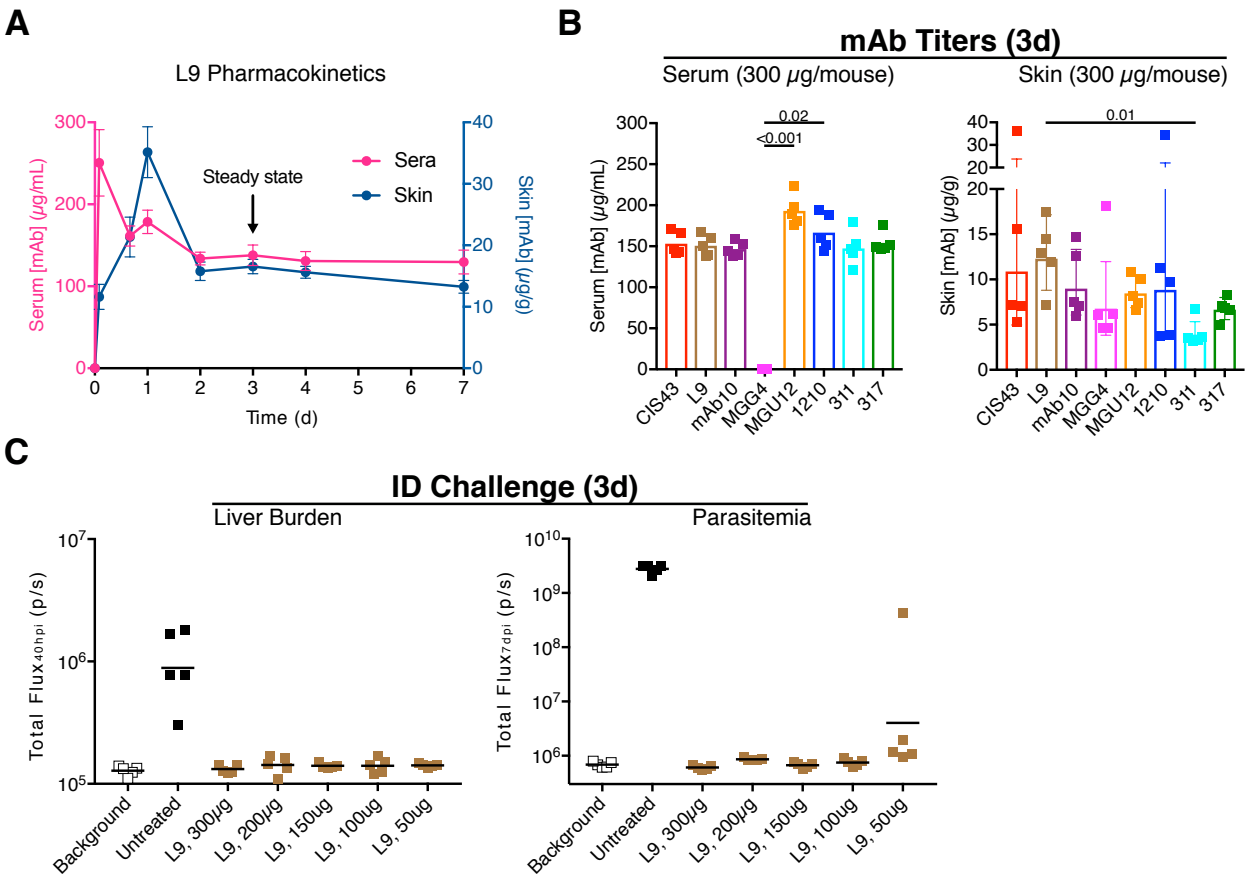

Figure 4.7: Optimization of the 3 day challenge timepoint. (**A**) Serum and skin titers in mice (n = 5/timepoint) over time following administration of 300 μg L9 (mean and SEM depicted). **(B)** Serum and skin mAb titers 3 days after passive transfer of 300 μg mAbs in mice (n=5/group; bars set at geometric mean with geometric SD) determined through ELISA. *P*-values were determined by comparing all mAbs to each other using the Kruskal-Wallis test with Dunn's post-hoc correction. (**C**) Liver burden (left) and parasitemia (right) reduction in mice 40 hours and 7 days post-infection (n=5/group) mediated by indicated doses or L9 administered 3 days before ID challenge with 5,000 Pb-PfCSP-SPZ.

Protection mediated by 50 μg/mouse of each mAb in the panel against 3 day ID challenge were assessed. Similar to the 2 hour challenge data (**Figure 4.6**), CIS43, L9, 311, and 317 mediated the greatest liver burden reduction against 3 day ID challenge (**Figure 4.8A**). When early-stage (Day 4 post-challenge) parasitemia was assessed, these same four mAbs again mediated the greatest parasitemia reduction, though CIS43 was less protective than L9, 311, and 317 (**Figure 4.8B**). When late-stage (Day 7 post-challenge) parasitemia was assessed, only L9

and 317 mediated a statistically significant reduction in parasitemia (**Figure 4.8C**). Together, these data suggest that L9 and 317 are the most protective mAbs against ID challenge.

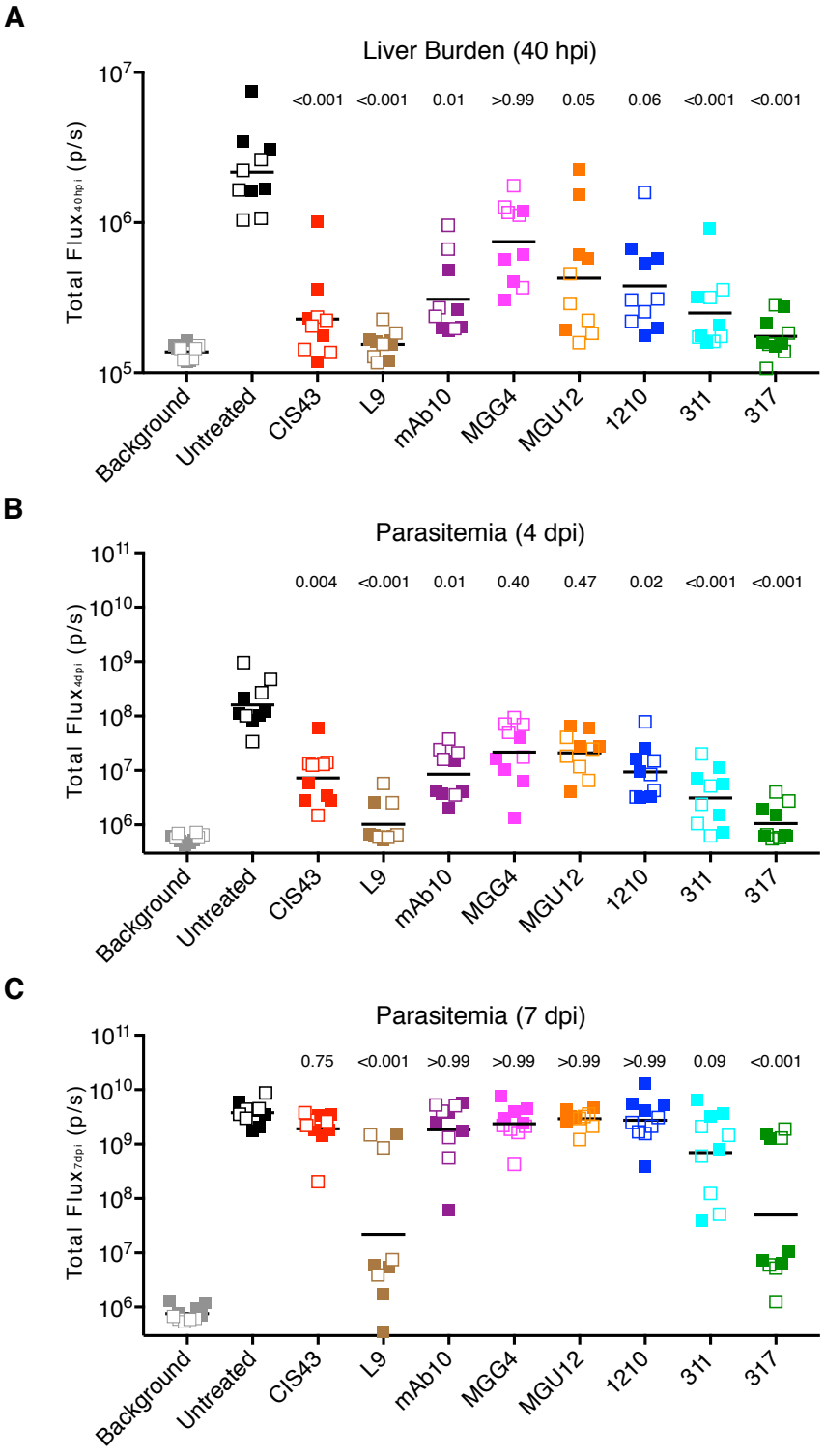

Figure 4.8: Protection against ID challenge mediated by eight neutralizing human PfCSP mAbs. (**A**) Liver burden 40 hours post-infection, (**B**) early-stage parasitemia 4 days post-infection, and (**C**) late-stage parasitemia 7 days post-infection in mice (n=10/group; data pooled from two independent experiments, solid vs. open squares; lines represent geometric mean) administered 50 μg of indicated mAbs 3 days before ID challenge with 5,000 Pb-PfCSP-SPZ. *P*-values were determined by comparing each mAb to untreated control using the Kruskal-Wallis test with Dunn's post-hoc correction.

To complete the analysis, sterile prevention of malaria mediated by the mAbs in the panel was assessed in seven independent studies wherein mice were challenged with five infected mosquito bites 3 days after mAb administration. Importantly, all studies were performed in a blinded manner across several mAb doses to establish a fully protective dose and then determine potency at more limiting doses; furthermore, MGG4 was excluded from these studies due to its poor serum PK. Results from each of the seven independent experiments are shown (**Figure 4.9**) to highlight the inherent variability of this assay and the need for large numbers of mice.

Within each dose, L9 was compared to the other mAbs for sterile protection against parasitemia (**Figure 4.10A**). At 600 μg/mouse, 94% of L9-treated mice were sterilely protected, which was comparable to 317 (100%) and CIS43 (94%), trended higher than mAb10 (67%) and 311 (50%), and was significantly greater than 1210 (18%) and MGU12 (0%). At 300 μg/mouse, sterile protection by L9 (64%) trended higher than 317 (44%) and was significantly greater than CIS43, mAb10, 1210 (~20%), 311 (13%), and MGU12 (0%). At 100 μg/mouse, L9 (40%) was significantly more protective than CIS43 (10%) and 317 (0%).

To determine whether differences in mAb titers prior to challenge may have contributed to differences in sterile protection, serum mAb titers were measured one day prior to challenge in all mice that underwent mosquito bite challenge (**Figure 4.10B**). Notably, L9 titers were similar to 317 at the lower doses of 300 and 100 μg/mouse despite providing improved protection.

Furthermore, mAb10 titers (~85 μg/mL) were significantly lower than the other mAbs at the 300 μg/mouse dose.

Based on the protection against mosquito bite challenge and mAb titers data, dose-response curves were generated using 2-parameter logistic (2PL) regression models (**Figure 4.10C**). From these models, protection elicited by each mAb can be summarized across all doses by the ED_{50} (effective dose required for 50% inhibition) and EC_{50} (effective serum concentration required for 50% inhibition). The ED_{50} and EC_{50} for MGU12, 1210, and 311 were not estimated from the 2PL model as MGU12 did not elicit protection and 311 and 1210 elicited <50% protection at the maximum dose of 600 μg/mouse. Additionally, superiority of L9 was assessed using this model by testing for a significantly greater odds of protection among mice receiving L9 compared to mice receiving other mAbs, adjusting for either dose or pre-challenge serum mAb titers.

The superior protective potency of L9 compared to the other mAbs in the panel was substantiated by its lowest ED_{50} and EC_{50} values (181.6 μg and 80.3 μg/mL, respectively) (**Figure 4.10D**; **Table 4.2**). mAb10 had a higher ED_{50} but lower EC_{50} than CIS43 due to its poorer serum PK (**Figure 4.10B**), suggesting that mAb10 might be more directly potent than CIS43 but requires higher dosing. Among the three mAbs that elicited at least 80% protection in the challenge studies (L9, 317, and CIS43), L9 had the lowest ED_{80} and EC_{80} values (325.7 μg and 145.1 μg/mL, respectively). Furthermore, the odds of L9-treated mice being protected from mosquito bite challenge were significantly higher than all other mAbs, adjusted across dose or pre-challenge titers (**Table 4.2**). Collectively, these data demonstrate that L9, followed by 317, are the two most potently protective mAbs in the panel against mosquito bite challenge.

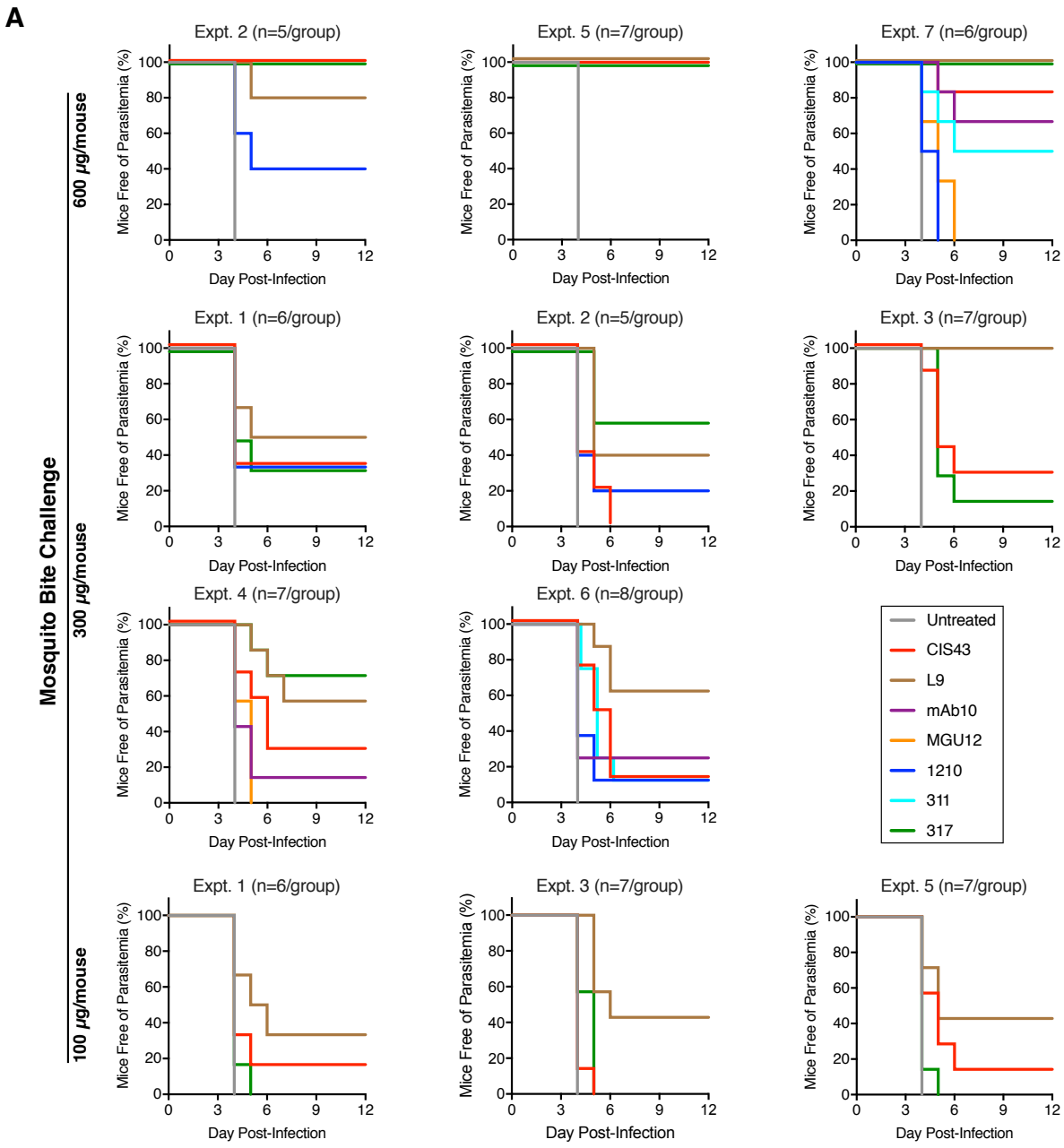
A
Mosquito Bite Challenge
600 μg/mouse
300 μg/mouse
100 μg/mouse
Expt. 2 (n=5/group)
Expt. 5 (n=7/group)
Expt. 7 (n=6/group)
Expt. 1 (n=6/group)
Expt. 2 (n=5/group)
Expt. 3 (n=7/group)
Expt. 4 (n=7/group)
Expt. 6 (n=8/group)
Expt. 1 (n=6/group)
Expt. 3 (n=7/group)
Expt. 5 (n=7/group)
Mice Free of Parasitemia (%)
Day Post-Infection
Untreated
CIS43
L9
mAb10
MGU12
1210
311
317

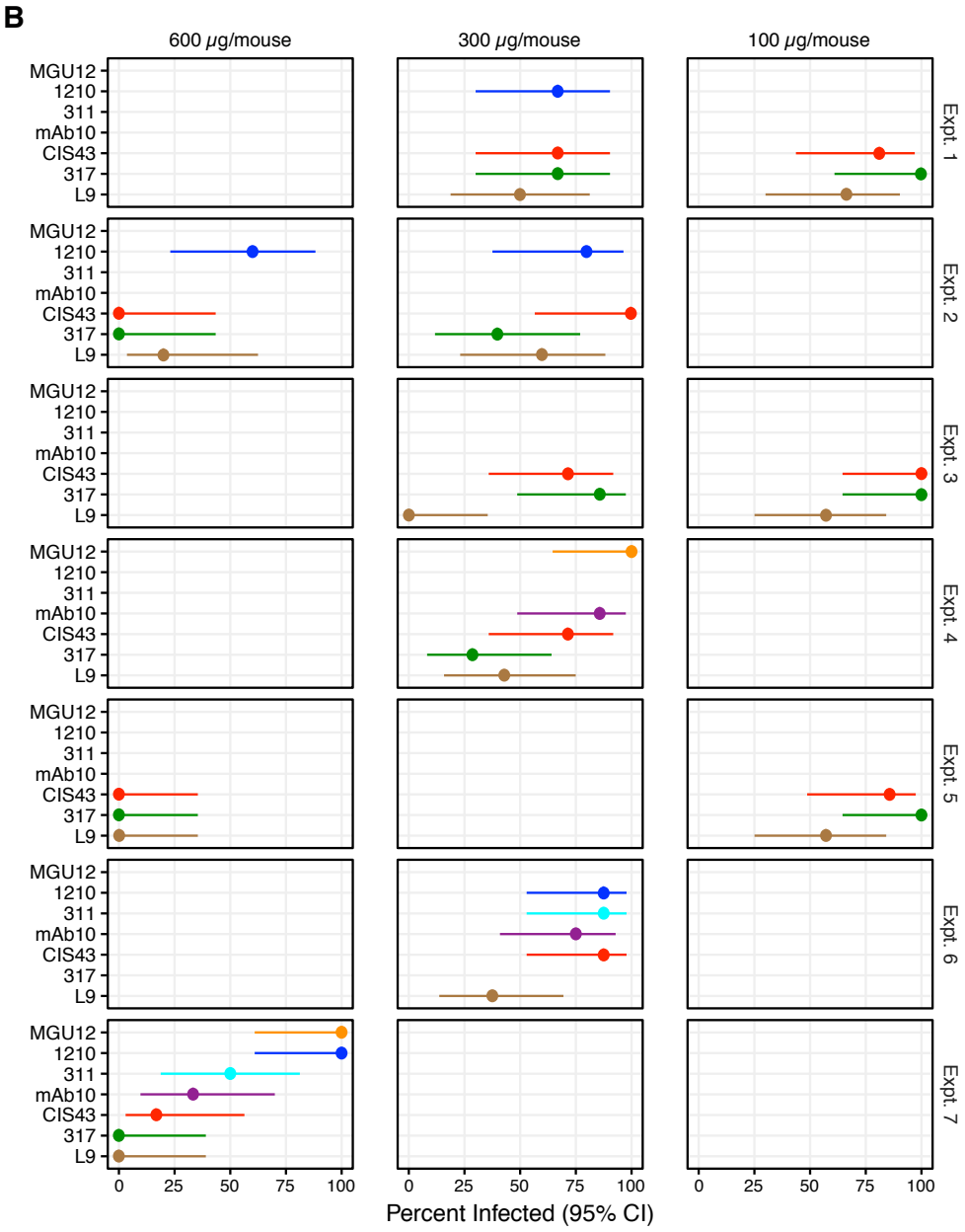

Figure 4.9: Individual mosquito bite challenge experiments comparing the functional activity of seven neutralizing human PfCSP mAbs. (**A**) Survival curves in mice treated with 600, 300, or 100 μg PfCSP mAbs 3 days prior to challenge with five infected mosquito bites. PfCSP mAb-mediated sterile protection against parasitemia was respectively assessed across seven independent experiments (n indicates number of mice/group, equivalent across mAbs within an experiment and dose). Different doses were used in the same experiment, but are presented in separate graphs subdivided by dose to facilitate comparison across experiments. All experiments were performed in a blinded manner with differing orders of coded mAbs. Combined data are shown in Figure 4.10A. (**B**) Mean and Wilson 95% confidence interval (CI) of the percentage of mice infected from **A** ordered by mean protection across doses.

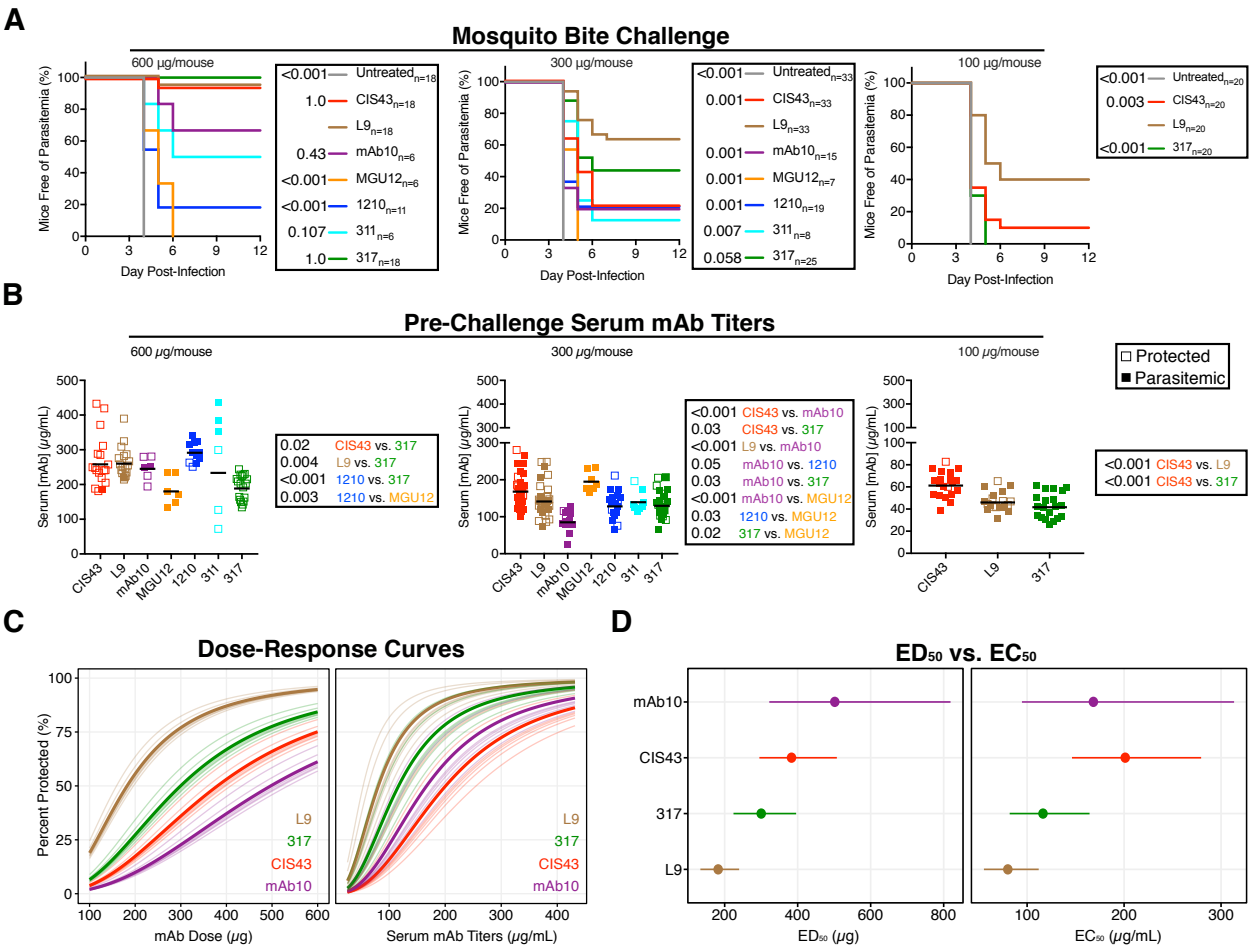

Figure 4.10: Protection against mosquito bite challenge mediated by seven neutralizing human PfCSP mAbs. (**A**) Survival curves of mice challenged with five infected mosquito bites 3 days after passive transfer of 600, 300, or 100 µg mAb (n indicates number of mice for each group; data were respectively combined from seven independent blinded experiments). *P*-values were determined by comparing L9 to every other mAb and untreated control using the log-rank test. (**B**) Serum mAb titers one day prior to challenge in mice from **A**. *P*-values were determined by comparing mAb titers to each other using the Kruskal-Wallis test with Dunn's post-hoc comparison. (**C**) Dose-response relationship of infection probability (percent protected) versus mAb dose (µg) and pre-challenge serum mAb titers (µg/mL) for L9, 317, CIS43, and mAb10 estimated by a 2PL regression model. Thick line denotes average relationship across all experiments; lighter lines denote individual experiment relationships predicted from the model. (**D**) ED_{50} and EC_{50} with 95% CI of L9, 317, CIS43, and mAb10 estimated from the 2PL model in **C**. Dose-response relationships were not estimated for MGU12, 1210, and 311 as they did not elicit enough protection for ED_{50} estimation within the experimental dose range.

		Dose (μg)			Serum mAb Titers (μg/mL)	
	mAb	Estimate (95% CI)	*P*-value		Estimate (95% CI)	*P*-value
ED_{50}				**EC_{50}**		
	L9	181.6 (133.5, 239.7)			80.3 (55.5, 112.0)	
	317	299.3 (224.2, 395.8)			116.5 (82.0, 164.4)	
	CIS43	382.5 (295.4, 507.3)			201.4 (146.3, 279.5)	
	mAb10	500.9 (322.3, 818.8)			168.5 (94.7, 313.4)	
ED_{80}				**EC_{80}**		
	L9	325.68 (246.2, 449.8)			145.10 (103.42, 212.73)	
	317	536.76 (399.5, 776.6)			210.52 (148.27, 324.34)	
	CIS43	685.92 (508.2, 1019.5)			363.93 (256.14, 568.05)	
OR						
	L9 vs. 317	3.33 (1.57, --)	0.014		2.43 (1.16, --)	0.025
	L9 vs. CIS43	5.95 (2.87, --)	<0.001		8.90 (4.18, --)	<0.001
	L9 vs. mAb10	11.39 (4.11, --)	<0.001		5.71 (1.76, --)	0.018
	L9 vs. 311	8.90 (2.79, --)	0.007		7.06 (2.26, --)	0.009
	L9 vs. 1210	12.18 (4.75, --)	<0.001		11.36 (4.45, --)	<0.001
	L9 vs. MGU12	107.47 (8.32, --)	0.008		96.43 (7.66, --)	0.008

Table 4.2: Numerical ED_{50}, EC_{50}, ED_{80}, EC_{80}, and OR values for mAb-mediated protection against mosquito bite challenge. Values were determined using 2PL regression mixed effects models of the protection and pre-challenge serum mAb titers data pooled across the seven independent blinded experiments and three doses shown in Figure 4.9. ED_{50}, ED_{80}, EC_{50}, and EC_{80} values were only estimated for mAbs that elicited that much protection in the experimental data. OR values for these mAbs vs. L9 were estimated from separate models. The one-sided 95% CI of the OR tests superiority of L9 over the comparison mAb. One-sided *P*-values were adjusted within column using Holm's stepwise adjustment.

4.5 Mechanisms of SPZ neutralization by PfCSP mAbs

To dissect the mechanisms contributing to the different *in vivo* potencies of the eight human PfCSP mAbs in the panel, several assays were used to examine mAb-mediated SPZ neutralization *in vitro* and in the liver.

4.5.1 mAb-mediated SPZ neutralization *in vitro*

The eight mAbs in the panel were first assessed for their abilities to inhibit PfSPZ invasion of HC-04 hepatocytes, an *in vitro* assay commonly used as a screen for mAb-mediated SPZ neutralization[220,226] (**Figure 4.11A**). PfSPZ were pre-incubated with varying concentrations of mAbs before application to cultured hepatocytes. All mAbs comparably and significantly reduced invasion relative to isotype control VRC01, except for 311 at 0.1 µg/mL. In a separate *in vitro* invasion assay that utilized primary human hepatocytes, all mAbs (except 311 at 0.1 µg/mL) again comparably and significantly reduced invasion relative to isotype control (**Figure 4.11B**). These data show that all mAbs in the panel except 311 comparably prevent SPZ hepatocyte invasion *in vitro.* Notably, these *in vitro* hepatocyte invasion assays did not predict *in vivo* protection against IV challenge (**Figure 4.6A**), substantiating that *in vitro* assays do not predict *in vivo* protection against SPZ challenge[84].

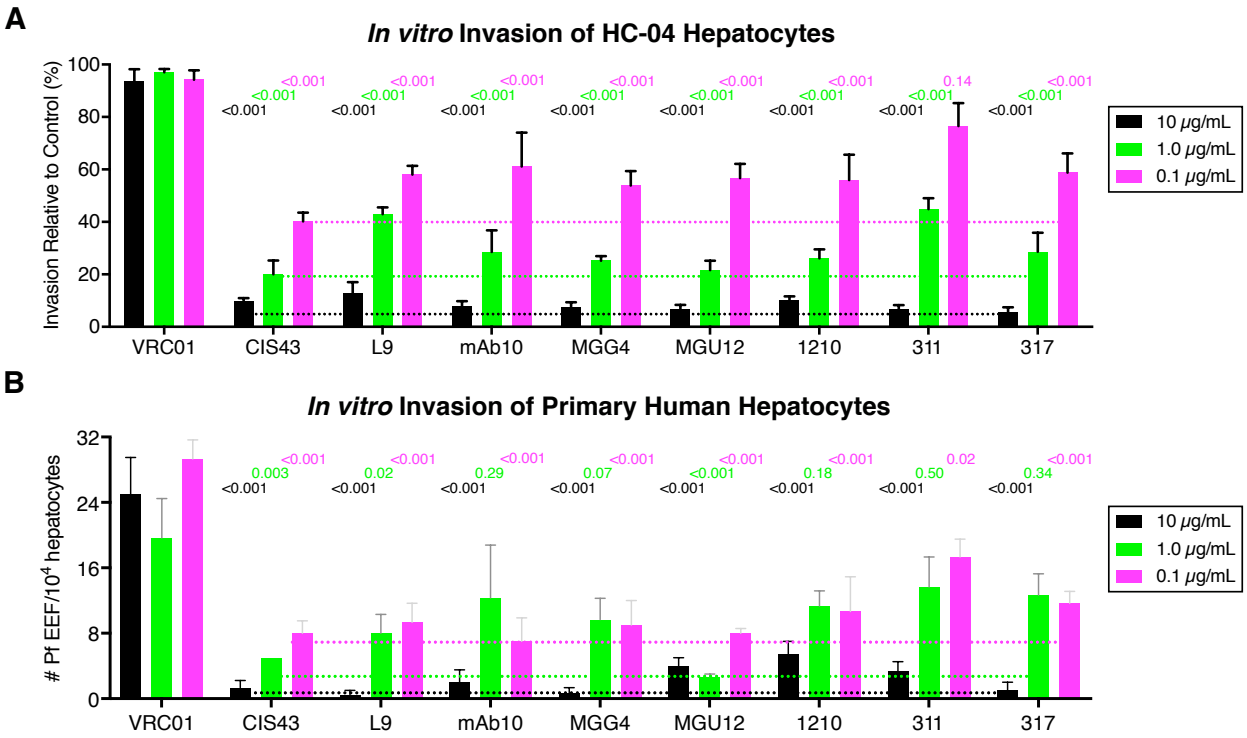

Figure 4.11: PfCSP mAb-mediated inhibition of PfSPZ hepatocyte invasion *in vitro.* (**A**) Inhibition of Pf invasion of HC-04 hepatocytes (50,000 cells per well; triplicate wells per mAb) by 10, 1.0, and 0.1 µg/mL PfCSP mAbs expressed as the percentage of hepatocytes invaded relative to no mAb controls. Data were combined from two independent experiments. (**B**)

Inhibition of Pf invasion of primary human hepatocytes (10,000 cells per well; triplicate wells per mAb) by 10, 1.0, and 0.1 μg/mL PfCSP mAbs expressed as the number of Pf exoerythrocytic forms (EEFs) per well. In **A** and **B**, bars represent the mean and SEM. For each concentration, inhibition mediated by each mAb was compared to VRC01 using a two-way ANOVA with Bonferroni's correction. Dotted line was set at the highest mAb-mediated invasion inhibition at each concentration.

4.5.2 mAb-mediated SPZ neutralization in the liver *in vivo*

To determine the potential *in vivo* mechanisms contributing to the clear differences in liver burden reduction meditated by the mAbs in the panel against IV challenge (**Figure 4.6A**), a new intravital imaging assay was developed to interrogate mAb-mediated SPZ neutralization in the liver. Importantly, complete prevention of hepatocyte infection is not expected in these studies due to the high SPZ inoculum required for imaging. Immediately following IV inoculation of AF405-labeled mAbs, Pb-PfCSP-SPZ expressing GFP, and rhodamine-labeled dextran into mice, Pb-PfCSP-SPZ were visualized by multiphoton microscopy as they exited liver sinusoids and traversed hepatocytes before invading a hepatocyte (**Figure 4.12A**). Traversal of hepatocytes was detected by the uptake of rhodamine-labeled dextran from sinusoids into hepatocytes with compromised membranes[96,227]; hepatocytes were classified as infected if they contained an intracellular SPZ but were dextran$^-$. mAb-induced CSPR and cytotoxicity (dotty death[98]) against SPZ were also observed in the liver (**Figure 4.12B**). Notably, CIS43 induced a unique "rounded" morphology in SPZ *in vivo* (**Figure 4.12B**) that was dissimilar to the morphologies induced by the other mAbs in the panel. Additional images and subjective descriptions of mAb-induced SPZ morphologies in the liver are shown in **Appendix 2**.

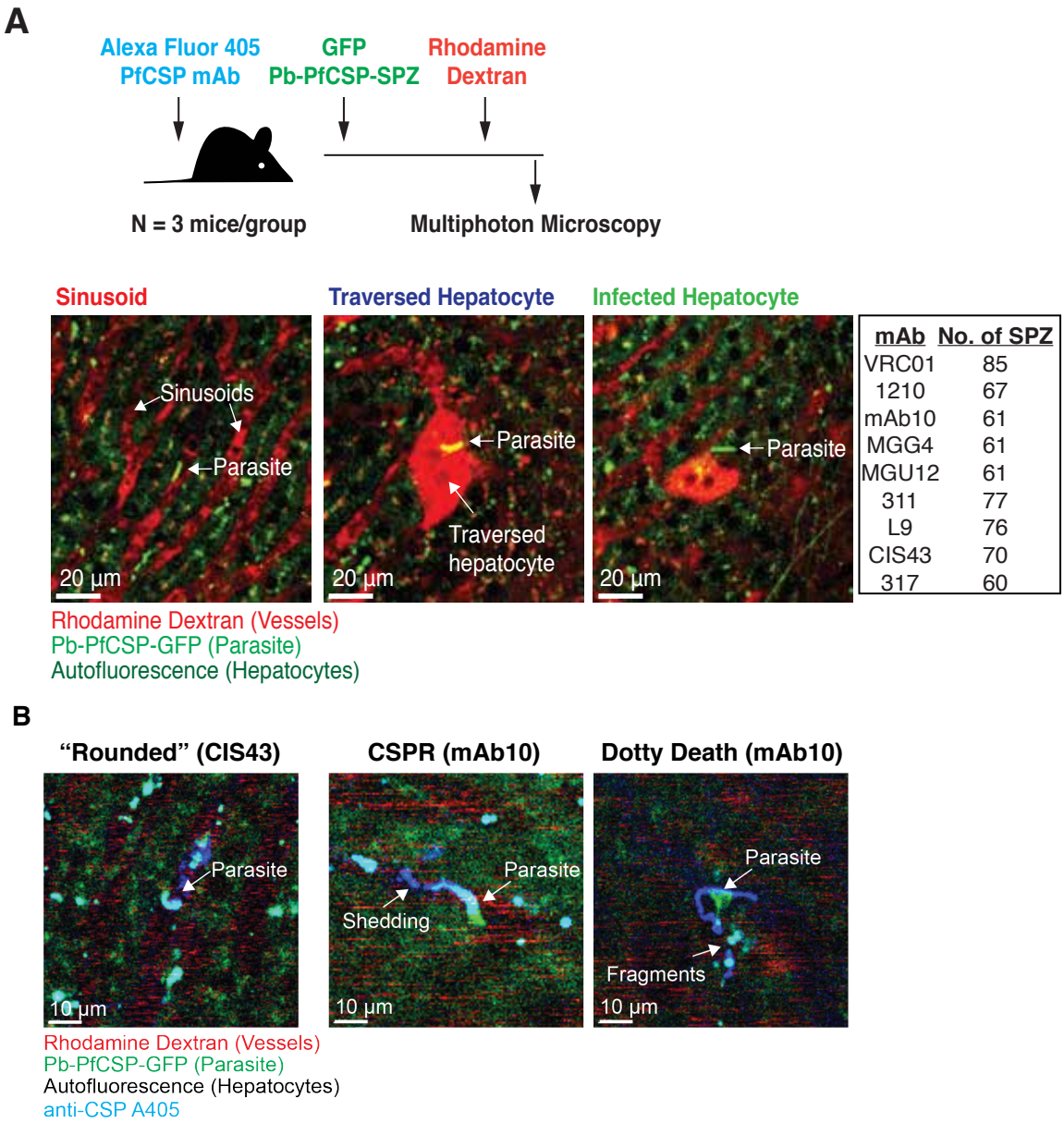

Figure 4.12: Intravital imaging of SPZ in the liver. (**A**) Schema for intravital imaging of Pb-PfCSP-SPZ in the livers of mice (N=3/group) sequentially administered 30 µg AF405-labeled mAb (blinded), 1 µg rhodamine-labeled dextran, and 100,000 Pb-PfCSP-SPZ expressing GFP. Observations across the 3 independent experiments/group were combined for analysis (total no. of SPZ observed across all 3 experiments for each mAb group are indicated). The locations and morphologies of individual Pb-PfCSP-SPZ were measured; traversal was detected by uptake of dextran into wounded hepatocytes. Representative images depict Pb-PfCSP-SPZ in the sinusoid, traversing a dextran^{+} hepatocyte, or invading a dextran^{-} hepatocyte. (**B**) Representative images depicting the unique "rounded" phenotype of SPZ bound by CIS43 and the CSPR and dotty death of SPZ bound by mAb10.

Consistent with the differences in protection mediated by the mAbs against IV challenge (**Figure 4.6A**), mice that received 311, L9, CIS43, and 317 had the highest percentages (47-67%) of Pb-PfCSP-SPZ trapped in the sinusoids and the lowest percentage (5-8%) of Pb-PfCSP-SPZ infecting hepatocytes (**Figure 4.13A**). Furthermore, only L9, CIS43, and 317 significantly prevented Pb-PfCSP-SPZ from initiating traversal (35-45% SPZ traversing ≥1 hepatocyte versus 73% in control) (**Figure 4.13B**). L9, mAb10, and CIS43 also significantly decreased the total number of hepatocytes traversed by the proportion of SPZ that did initiate traversal (**Figure 4.13C**), indicating that mAb10 did not prevent traversal but did decrease the overall number of hepatocytes traversed per SPZ. These data show that the four most protective mAbs against IV challenge (CIS43, L9, 311, and 317) limit hepatocyte infection by preventing Pb-PfCSP-SPZ egress from sinusoids and subsequent traversal of hepatocytes.

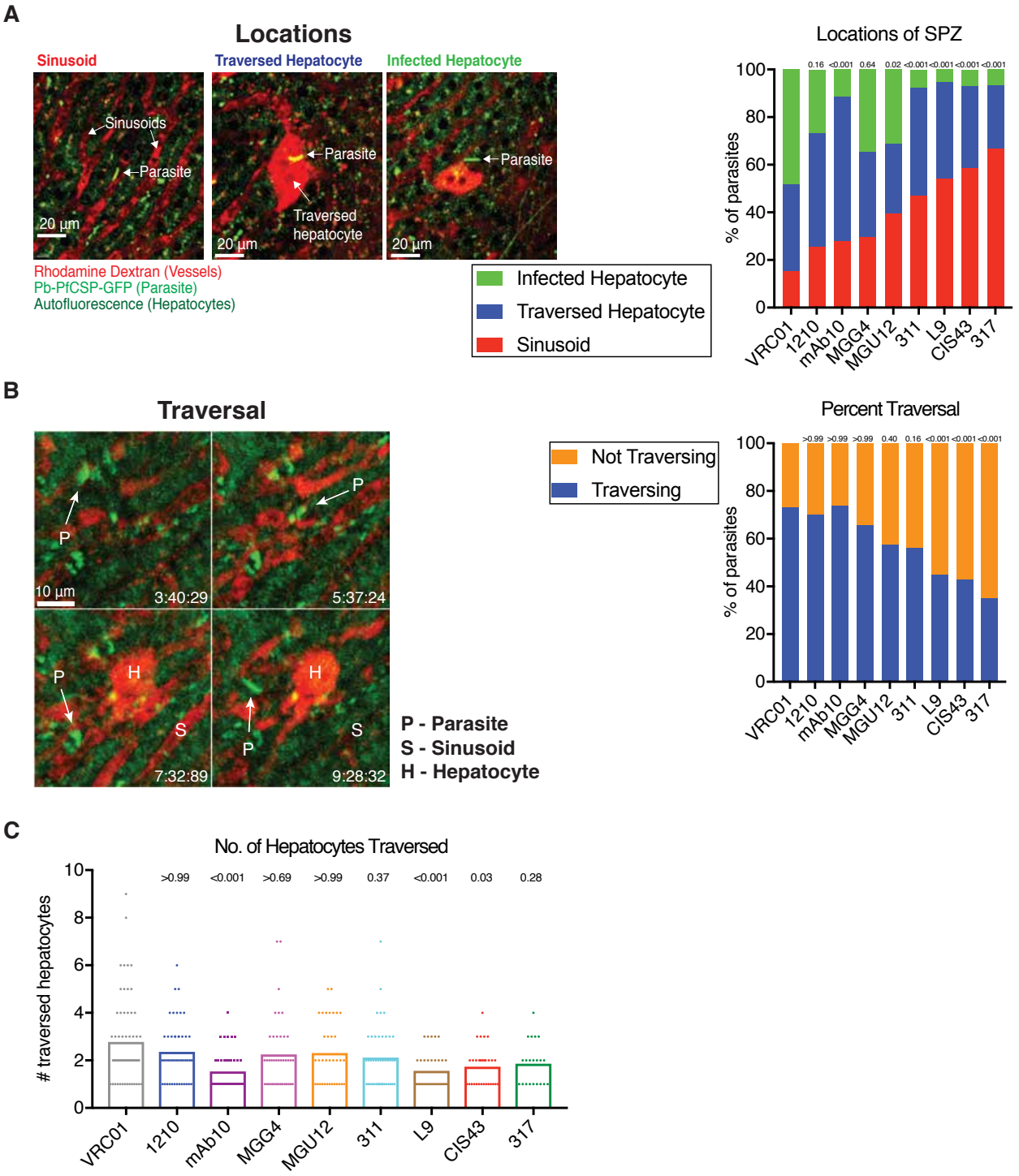

Figure 4.13: PfCSP mAb-mediated inhibition of SPZ egress from sinusoids and traversal of hepatocytes. (**A**) Left: the three locations SPZ are found in the liver. Right: percentage of SPZ observed in each of these three locations. (**B**) Left: time-lapse images (min:s:ms) of a SPZ exiting a sinusoid and traversing a hepatocyte; arrows and stars respectively indicate anterior and posterior ends of SPZ. Right: percentage of SPZ that initiated traversal and traversed ≥1 hepatocyte. (**C**) Number of hepatocytes traversed by the proportion of SPZ that initiated traversal. Bars represent the mean; each dot is an individual SPZ. *P*-values were determined by

comparing each mAb to VRC01 using the Kruskal-Wallis test with Dunn's post-hoc correction. **A-B**: *P*-values were determined by comparing each mAb to VRC01 using the chi-squared test with Bonferroni's correction.

Since no studies have assessed whether PfCSP mAbs induce the CSPR and dotty death of SPZ in the liver, the relative abilities of the mAbs in the panel to induce these linked cytotoxic processes was examined. *In vivo* CSPR was quantified by measuring the percentage of shedding SPZ and the lengths of their shed PfCSP tails (**Figure 4.14A**). L9 induced 70% of SPZ to shed, which was significantly higher than all mAbs except 311 (51%) and mAb10 (48%) (**Figure 4.14B**). Consistent with the morphology data wherein CIS43-treated SPZ had a characteristic "rounded" phenotype (**Figure 4.12**), CIS43 induced the shortest tails (~2 μm) while MGU12 generated the longest tails (~7.5 μm) (**Figure 4.14C**). SPZ underwent the CSPR primarily while migrating through sinusoids or traversing hepatocytes (57% and 36%, respectively) and rarely after infecting hepatocytes (7%) (**Figure 4.14D**).

Dotty death was quantified by counting the percentage and number of fragments arising from immobilized, mAb-bound SPZ undergoing CSPR (**Figure 4.14E**). 317 induced dotty death in ~43% of SPZ, which was significantly higher than all mAbs except mAb10 (38%), L9 (30%), and 311 (25%) (**Figure 4.14F**). Only 317, L9, mAb10, and 311 significantly fragmented SPZ in the liver (**Figure 4.14G**). Similar to CSPR, SPZ mostly underwent dotty death while migrating through sinusoids and traversing hepatocytes (47.5% for both) and rarely after infecting hepatocytes (5%) (**Figure 4.14H**).

Furthermore, I observed a cytotoxic phenomenon distinct from dotty death wherein immobilized, mAb-bound SPZ rapidly lost membrane integrity and burst, releasing GFP into the surrounding tissue and disappearing (**Figure 4.14I**). This "bursting" was a rare event and only observed with L9 and 317. Collectively, these data demonstrate that PfCSP mAbs directly induce

the cytotoxic death of SPZ in the liver and substantiate that most mAb-mediated neutralization of SPZ occurs prior to hepatocyte invasion.

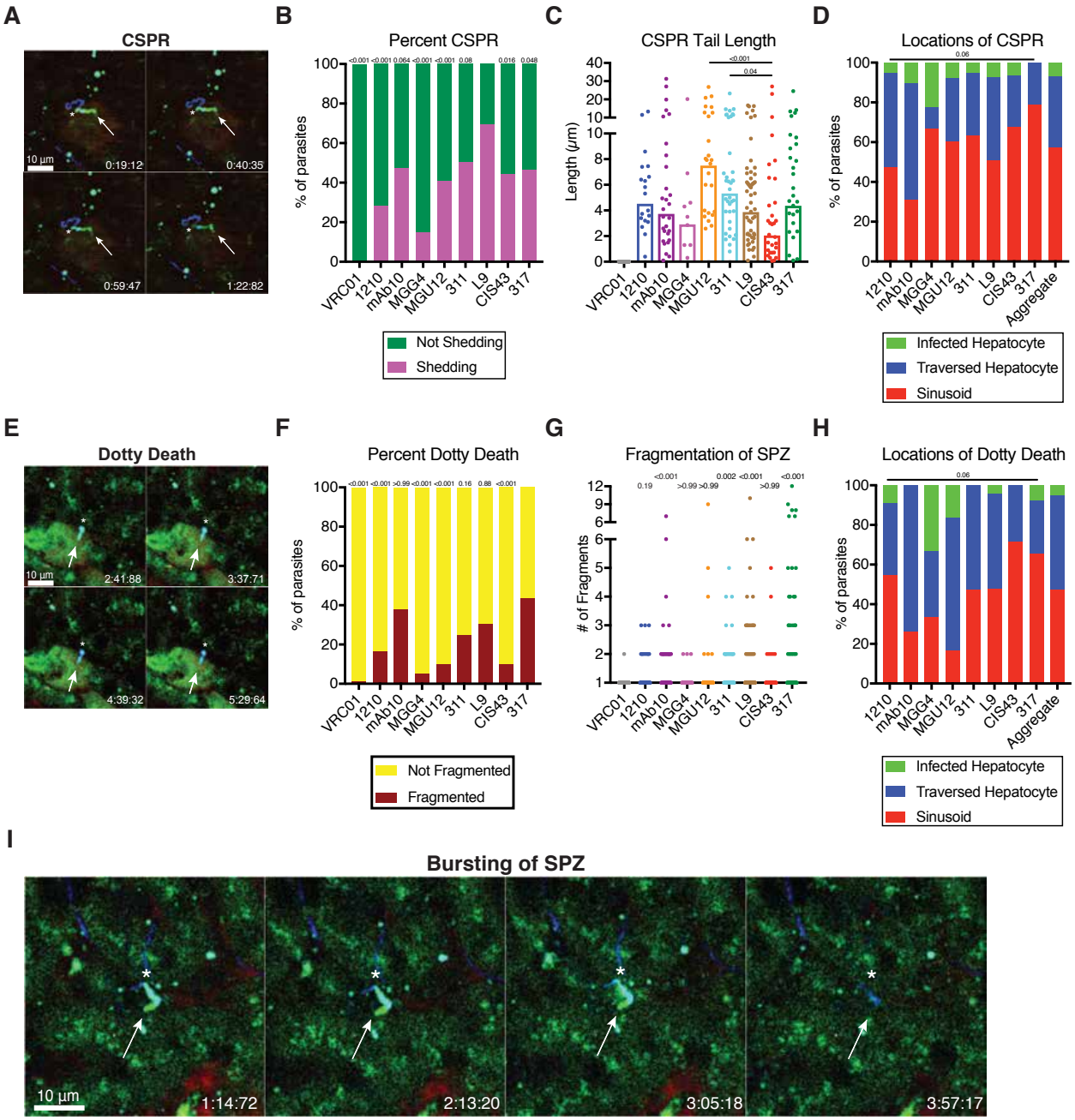

Figure 4.14: PfCSP mAb-induced CSPR and cytotoxic death of SPZ in the liver. (A) Time-lapse images (min:s:ms) of a SPZ that underwent a CSPR and shed a mAb-bound PfCSP tail in the liver. **(B)** Percentage of SPZ that underwent a CSPR. **(C)** Length of shed PfCSP tails in SPZ that underwent a CSPR. Bars represent the geometric mean; each dot is a SPZ. **(D)** Locations where SPZ underwent the CSPR. **(E)** Time-lapse images of a SPZ that underwent dotty death. **(F)** Percent of SPZ that underwent dotty death. **(G)** Number of fragments arising from SPZ undergoing dotty death; each dot is an individual SPZ. **(H)** Locations where SPZ underwent

dotty death. **(I)** Time-lapse images of an immobilized, mAb-bound SPZ bursting, leaking GFP, and rapidly disappearing. **A,E**: arrows and stars respectively indicate anterior and posterior ends of SPZ. **B,F**: *P*-values were determined by comparing each mAb to L9 (B) or 317 (F) using the chi-squared test with Bonferroni's post-hoc correction. **C,G**: *P*-values were determined by comparing each mAb to each other (C) or to VRC01 (G) using the Kruskal-Wallis test with Dunn's post-hoc correction. **D,H**: aggregate represents all SPZ combined from every mAb group. Location distribution did not vary significantly across the mAbs (omnibus chi-squared test).

Given their differences in SPZ neutralization, the degree to which the mAbs in the panel bound SPZ in the liver was assessed (**Figure 4.15**). Despite their near-identical SPZ binding *in vitro* (**Figure 4.1B**), there were marked differences between the mAbs' SPZ binding *in vivo* in the liver. Nearly all SPZ were bound by CIS43 (97%) and L9 (96%), which was significantly greater than all mAbs except 317 (85%). The lower *in vivo* SPZ binding of 1210, MGG4, and MGU12 (~50-60%) may contribute to their consistently poorer neutralization *in vivo* in the liver.

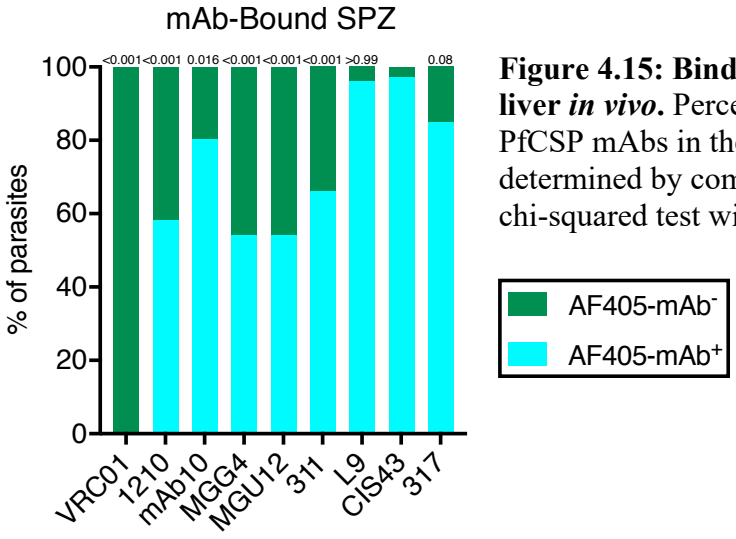

Figure 4.15: Binding of PfCSP mAbs to SPZ in the liver *in vivo*. Percentage of SPZ bound by AF405-labeled PfCSP mAbs in the livers of mice. *P*-values were determined by comparing each mAb to CIS43 using the chi-squared test with Bonferroni's post-hoc correction.

4.6 Discussion

This Chapter presents a thorough comparison of the binding properties, potency, and neutralization mechanisms of eight protective PfCSP human mAbs. Portions of Chapter III-IV were published as a Report in *Immunity*, with a scanning electron micrograph image of a L9-

treated PfSPZ undergoing a CSPR being selected as the cover of the October 2020 issue (**Figure 4.16A**). The *Immunity* Graphical Abstract summarizing the data presented in Chapter IV is shown in **Figure 4.16B**.

While PfCSP repeat mAbs preferentially target either DPNA/NPNV/NPNA, they can promiscuously bind peptides composed of all three tetrapeptides due to paratopes that accommodate the subtle differences between these motifs[79,84,219,228]. For example, while MGG4 and MGU12 has been reported to have dual specificity for the junctional epitope and NPNA repeats[213], this study's peptide mapping show that MGG4 and MGU12 should be classified as NPNA-preferring mAbs due to their minimal junctional affinity. Similarly, another study described two dual-specific mAbs (667 and 668) with some affinity for a junctional peptide KQPADGNPDPNANPNV (12 μM and 206 nM, respectively) but far greater affinity for a peptide containing only NPNA (176 nM and 55.6 nM, respectively)[215]. Consistent with these and other reports[79,84,219], these data classified mAb10, 1210, 311, and 317 as NPNA-preferring mAbs that can bind DPNA- and NPNV-containing peptides, albeit with much lower affinity. In contrast, CIS43 and L9 respectively exhibited ~1.4E4-fold and ~2.5E6-fold greater preference for DPNA-containing peptide 21 and NPNV-containing peptide 22 compared to peptide 29, which contains only NPNA. Given their binding promiscuity, PfCSP repeat mAbs are more accurately classified based on their preferred peptides, which is stringently determined by competition ELISAs with short peptides across a range of concentrations. Finally, the observation that the three most protective mAbs in this study (CIS43, L9, and 317) are respectively DPNA-, NPNV-, and NPNA-preferring mAbs demonstrates that peptide preference may not predict *in vivo* protection but is useful for classification.

Despite their different peptide preferences, these three mAbs and 311 demonstrated two-step binding to rPfCSP_FL and high-affinity binding to rPfCSP_5/3 by ITC. While CIS43 and L9 were cloned from subjects immunized with radiation-attenuated PfSPZ presenting PfCSP_FL, 311 and 317 were cloned from subjects immunized with RTS,S/AS01[79], which does not include the junctional region in rPfCSP_5/3. These data suggest that two-step binding is exhibited by promiscuous repeat mAbs that preferentially bind a specific epitope (e.g., DPNA or NPNV) but have achieved significant cross-reactivity to other epitopes (e.g., NPNA), resulting in two binding events to rPfCSP_FL with distinct affinities. Of note, previous ITC analyses of 311 and 317 using peptides did not report two-step binding[79], highlighting the importance of additionally classifying repeat mAbs based on their binding to FL rPfCSP proteins by ITC.

The most protective mAbs against IV challenge (CIS43, L9, 311, and 317) demonstrated two-step binding to rPfCSP_FL and high affinity for rPfCPS_5/3. In contrast, mAbs with high-affinity, multivalent binding to rPfCSP_FL (mAb10, MGU12, and 1210) showed no protection at limiting doses. These data suggest that high-affinity, multivalent binding to rPfCSP_FL may be necessary, but is not sufficient, for potent *in vivo* SPZ neutralization in the liver. Notably, a recent analysis also finds that high PfCSP affinity is a prerequisite for SPZ neutralization and that NANP-preferring mAbs with cross-reactivity to junctional peptides are more potent[229]. Though further studies are needed to understand the relationship between two-step binding, junctional and NANP region cross-reactivity, and SPZ neutralization, these data suggests that ITC might be useful for down-selecting two-step binding PfCSP mAbs for functional testing *in vivo.* Importantly, these data establishes the potency hierarchy of eight protective mAbs isolated by various labs around the world, with L9 followed by 317 being significantly more potent than all other mAbs in the panel. These data show that mAb L9 is currently the most promising

clinical candidate for malaria prophylaxis and further justify the decision to clinically develop L9.

In terms of elucidating how antibodies neutralize SPZ *in vivo*, this study built upon prior mechanistic studies in the skin (i.e., the initial physiological site for CSP antibodies to neutralize SPZ)[98,102,103] by providing the first *in vivo* evidence that PfCSP mAbs neutralize SPZ in the liver by direct cytotoxic killing and by preventing SPZ egress from sinusoids to traverse and invade hepatocytes. CSP antibodies are known to prevent SPZ traversal and invasion of HC-04 hepatocytes, a commonly used *in vitro* neutralization assay[213,220,230]. However, this *in vitro* assay did not predict *in vivo* protection against IV challenge likely due to its lack of liver sinusoids, which are a major barrier that SPZ must cross to access hepatocytes[96,231]. Effective SPZ neutralization in the vasculature and liver may be critical to prevent malaria, as a low number of SPZ are directly inoculated into the vasculature following mosquito bites[232,233] and even a single SPZ that invades a hepatocyte can initiate a blood-stage infection[234].

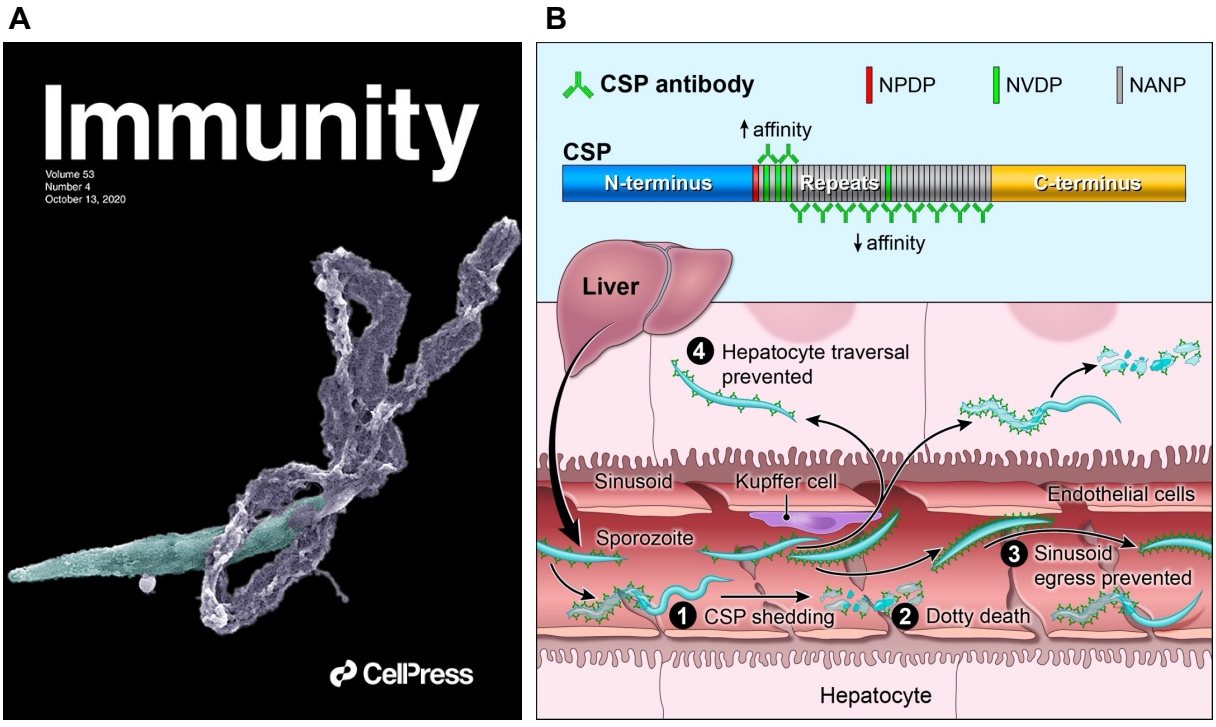

Figure 4.16: *Immunity* cover image and graphical abstract. (A) Pseudo-colored scanning electron micrograph image of a PfSPZ incubated with L9 (10 μg/mL) undergoing a CSPR, which was selected as the October 2020 *Immunity* cover. **(B)** Graphical abstract depicting L9 IgG binding to PfCSP and the mechanisms employed by PfCSP mAbs to neutralize SPZ in the liver.

Chapter V: Isolation and characterization of PfCSP minor repeat mAbs

5.1 Authorship statement

Sections of this Chapter were posted on *bioRxiv* as Wang, Hurlburt et al. (https://doi.org/10.1101/2021.08.11.455919) and are currently in press at *Cell Reports*. Azza Idris and Barbara Flynn sorted the PBs and performed competition ELISAs and alanine scans; Nicholas Hurlburt performed SEC and structural studies; Arne Schön performed ITC; Yevel Flores-Garcia performed CSPR/motility assays and mosquito bite challenge; Patience Kiyuka, Lais Pereira, Marlon Dillon, and Brian Bonilla provided SPZ for flow cytometry and performed IV challenges.

5.2 Introduction

Chapter IV compared the binding and potency of eight protective human PfCSP mAbs to determine which epitopes might improve immunogen design and select the most potent mAb for clinical development. mAb L9, which preferentially binds NVDP repeats and cross-reacts with NANP repeats, was shown to be the most protective mAb in the panel and consequently the most potent PfCSP mAb isolated to date. Notably, L9 and other potent mAbs bound rPfCSP in two binding events with distinct affinities by ITC, suggesting that this *in vitro* signature of "two-step binding" may be correlated with *in vivo* SPZ neutralization[85].

Similar to most human PfCSP repeat mAbs, L9 is encoded by Ig V_H3-33 and Vκ1-5 (heavy and kappa chain variable domains) (**Table 3.1**)[235]. Most V_H3-33/Vκ1-5 mAbs

preferentially bind NANP repeats and express an 8–amino-acid–long Vκ complementarity-determining region 3 (KCDR3:8) and a tryptophan at position 52 in HCDR2 (H.W52)[219,236,237]. Furthermore, these NANP-preferring mAbs require a minimal epitope of three NANP[79] and rPfCSP binding is abrogated when V_H3-33 is paired with Vκ1-5 with KCDR3:9[219]. Conversely, L9 expresses KCDR3:9 but binds rPfCSP with high affinity, preferentially binds NVDP repeats, and can only bind NANP repeats if they are sufficiently concatenated[85]. These data suggest that V_H3-33/Vκ1-5 mAbs can also target NVDP repeats; however, it is unclear whether the L9 B cell lineage originated as a NANP binder that mutated to acquire NVDP affinity, as has been suggested for NPDP-reactive mAbs[213,238], or vice versa.

The specific aim of this Chapter was to elucidate how the L9 B cell lineage developed by isolating and characterizing mAbs clonally related to L9. Specifically, this Chapter compares the binding properties of L9 lineage mAbs to rPfCSP peptides and full-length protein using techniques like ELISA, BLI, ITC, and X-ray crystallography and correlates these parameters to recognition of native PfCSP on SPZ *in vitro* by flow cytometry and ultimate neutralization of SPZ *in vitro* and *in vivo*.

5.3 Isolation of a panel of mAbs clonally related to L9

L9 was isolated from a volunteer immunized with radiation-attenuated PfSPZ[85,169]. To isolate clonally-related mAbs, $CD3^-CD20^-CD19^+CD27^+CD38^+$ plasmablasts (PBs) were sorted from the same volunteer 7 days after the second and third immunizations. A total of 480 PBs were isolated, from which 194 high-quality IgG V_H sequences were cloned. These sequences were compared to the L9 V_H ($L9_H$) to identify clonally-related sequences. Two V_H ($D2_H$ and $F10_H$) from PBs collected after the second immunization were clonally related to $L9_H$ (**Figure**

5.1). Specifically, all three V_H were encoded by V_H3-33*01/06, J_H4*02, and had a 13-amino-acid-long HCDR3; furthermore, the HCDR3 of $D2_H$ and $F10_H$ were 85% identical to $L9_H$ (**Table 5.1**).

Regarding light chains, only F10κ was cloned. F10κ and L9κ were Vκ1-5*03, Jκ1*01, and had a 9-amino-acid-long KCDR3; furthermore, the KCDR3 of F10κ was 89% identical to L9κ (**Table 5.1**). The V_H/Vκ sequences of D2, F10, and L9 were used to infer their most recent common ancestor ($L9_{MRCA}$) V_H/Vκ, which were respectively 0.35% and 0% diverged from germline. Notably, the V_H/Vκ of L9 were more somatically mutated than those of D2 and F10 (**Table 5.1** and **Figure 5.2A**) and all V_H genes encoded H.W52 in HCDR2, which has been shown to be critical for binding NANP repeats[219]. An alignment of the amino acid sequences for the V_H/Vκ (**Figure 5.2B-C**) demonstrates the exact mismatches between the mAbs in the panel.

Figure 5.1: Isolation of mAbs clonally related to L9. (A) Phylogenetic tree of 194 V_H genes cloned from PBs isolated from the same volunteer that yielded L9. L9 is highlighted in red, along with the two V_H sequences (D2 and F10) most closely related to $L9_H$. 4C and 5G refer to PBs respectively isolated at weeks 9 and 17 (i.e., one week after the second and third PfSPZ immunization); the number indicates the plate into which each PB was sorted.

A

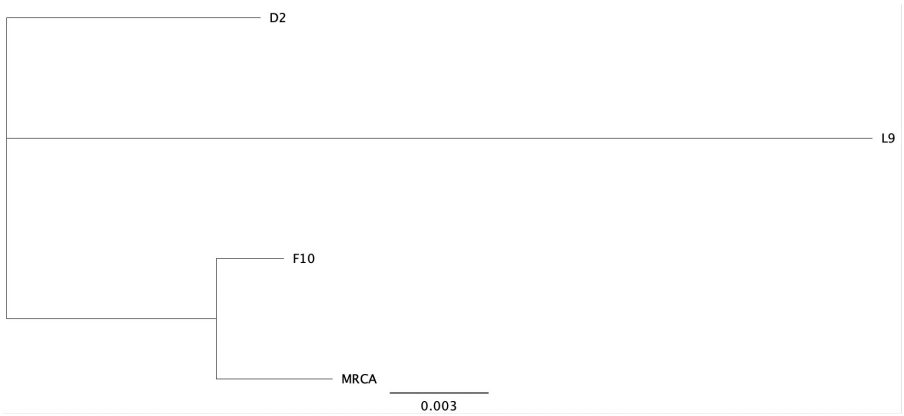

B

```
Consensus QVQLVESGGGVVQPGRSLRLSCAASGFTFSXYGMHWVRQAPGKGLEWVAVIWYDGSNKYY
D2        ........................S..T.................A.........
MRCA      ............................S.............................
F10       ............................S.........................R..
L9        ..K..................E....I..T.....................F....I..

Consensus ADSVKGRFTISRDNSKNTLFLQMNSLRAEDTAVYYCHRNYYDSSGPFDYWGQGTLVTVSS
D2        ............................................................
MRCA      ...................Y........................................
F10       ............................................................
L9        .................V.M..D..............F..G.................
```

C

```
Consensus DIQMTQSPSTLSASVGDRVTITCRASQSISRWLAWYQQKPGKAPKLLIYKASSLESGVPS
L9        ........................F...............................
MRCA      ............................S...........................
F10       ..............................V......A...................

Consensus RFSGSGSETXFTLTISSLQPDDVATYYCQQYTSYGRTFGQGTKVEIK
L9        .........H..................E.................
MRCA      .......G.E............F........N..............
F10       .........D.....................................
```

Figure 5.2: Relatedness of L9 lineage mAbs. (A) Phylogenetic tree of the V_H genes of mAbs in the L9 lineage and their MRCA. **(B-C)** Amino acid alignment of the V_H of L9, D2, F10, and MRCA (B) and the Vκ of L9, F10, and MRCA (C). Consensus sequence and mismatched amino acids are indicated.

Designation	Isotype	VH	V_H divergence (nt, %)	J_H	J_H divergence (nt, %)	HCDR1.2.3 Lengths	HCDR3 AA Sequence
$D2_H$	IgG		2.43	4*02	10.64	8.8.13	HRNYYDSSGPFDY
$F10_H$	IgG	3-33*01	1.39		10.64	8.8.13	HRNYYDSSGPFDY
$L9_H$	IgG	3-33*06	4.17		10.64	8.8.13	HRNFYDGSGPFDY
$MRCA_H$	IgG		0.35		8.51	8.8.13	HRNYYDSSGPFDY

Designation	Isotype	VK	VK divergence (nt, %)	JK	JK divergence (nt, %)	KCDR1.2.3 Lengths	KCDR3 AA Sequence
F10κ	IgG	1-5*03	3.23	1*01	5.41	6.3.9	QEYTSYGRT

L9κ	IgG	3.94	5.41	6.3.9	QQYTSYGRT
MRCAκ	IgG	0.00	5.41	6.3.9	QQYNSYGRT

Table 5.1: Immunoglobulin V/J-gene family usage of L9 lineage mAbs. mAb designation, isotype, V_H/Vκ and percent divergence from germline, J_H/Jκ gene families percent divergence from germline, V_H/Vκ CDR1.2.3 lengths, and HCDR3/KCDR3 amino acid sequences of the L9 clonal relatives isolated in this study. nt = nucleotide, H = heavy, κ = kappa, J = joining, AA = amino acid.

5.4 Binding of L9 lineage mAbs to PfCSP peptides

To elucidate the contribution of Igκ to mAb recognition of PfCSP and resultant SPZ neutralization, chimeric mAbs were created wherein $L9_H$ was paired with F10κ ($L9_HF10κ$) and $F10_H$ was paired with L9κ ($F10_HL9κ$). As D2κ was not recovered, L9κ and F10κ were paired with $D2_H$ to respectively create the chimeric mAbs $D2_HL9κ$ and $D2_HF10κ$ (**Figure 5.3A**).

All mAbs in the panel were assessed for their binding to full-length rPfCSP ($rPfCSP_{FL}$); the NANP-preferring PfCSP mAb 317[79] and the anti-HIV-1 mAb VRC01[239] were respectively included as positive and negative controls. All mAbs bound $rPfCSP_{FL}$, confirming that mismatching Igκ with Ig_H did not interfere with antigen recognition by the chimeric mAbs (**Figure 5.3B**). Notably, L9κ-containing mAbs (L9, $F10_HL9κ$, $D2_HL9κ$) had higher $rPfCSP_{FL}$ binding compared to F10κ-containing mAbs (F10, $L9_HF10κ$, $D2_HF10κ$). $L9_{MRCA}$ had the lowest $rPfCSP_{FL}$ binding, likely due to its low divergence from germline (**Table 5.1**).

L9 was reported to preferentially bind the two adjacent NPNV motifs associated with the NVDP repeats in the 15mer peptide 22 (NANPNVDPNANPNVD) and weakly cross-react with the eight concatenated NPNA motifs in the 36mer peptide $(NANP)_9$[85]. To determine if the mAbs in the panel had similar binding properties, I measured their peptide 22 and $(NANP)_9$ binding by ELISA (**Figure 5.3B**). Similar to L9, all mAbs demonstrated higher binding to peptide 22 than to $(NANP)_9$. As with $rPfCSP_{FL}$, L9κ-containing mAbs had higher peptide 22 binding than F10κ-

containing mAbs and $L9_{MRCA}$ had lower, but detectable, peptide 22 binding. The only mAbs with weak, though detectable, $(NANP)_9$ binding were L9 and $D2_HL9\kappa$.

To quantify the mAb panel's avidity for peptide 22, BLI was used to measure their $K_{D(app.)}$ for peptide 22 (**Figure 5.3C**). Consistent with the ELISA data, L9κ-containing mAbs had $K_{D(app.)}$ 100-700-fold lower than F10κ-containing mAbs, suggesting that L9κ improves mAb avidity for peptide 22. Together, these data show that the mAbs in the panel preferentially bind the NVDP-containing peptide 22 over the NANP-containing $(NANP)_9$ and that, compared to F10κ, L9κ improves binding to $rPfCSP_{FL}$, peptide 22, and $(NANP)_9$.

To further characterize the mAb panel's interactions with peptide 22, alanine scanning mutagenesis was used to define the critical residues within the peptide 22 sequence bound by each mAb (**Figure 5.3D**). Unlike L9 IgG, which clearly bound both NPNV motifs, F10 IgG mostly bound the first NPNV motif in peptide 22 and did not appear to bind the second NPNV. Remarkably, L9κ-containing IgG clearly bound both NPNV motifs while F10κ-containing IgG had more equivocal NPNV binding, with binding being targeted more towards the first NPNV. Furthermore, SEC of Fabs bound to peptide 22 showed that L9κ-containing Fab-peptide 22 complexes eluted earlier (i.e., were larger) than F10κ-containing Fab-peptide 22 complexes, suggesting that peptide 22 is bound by two L9κ-containing Fabs but only one F10κ-containing Fab (**Figure 5.3E**). These data show that the higher peptide 22 avidity of L9κ-containing mAbs compared to F10κ-containing mAbs is because L9κ enables high-affinity binding to two adjacent NPNV motifs instead of one.

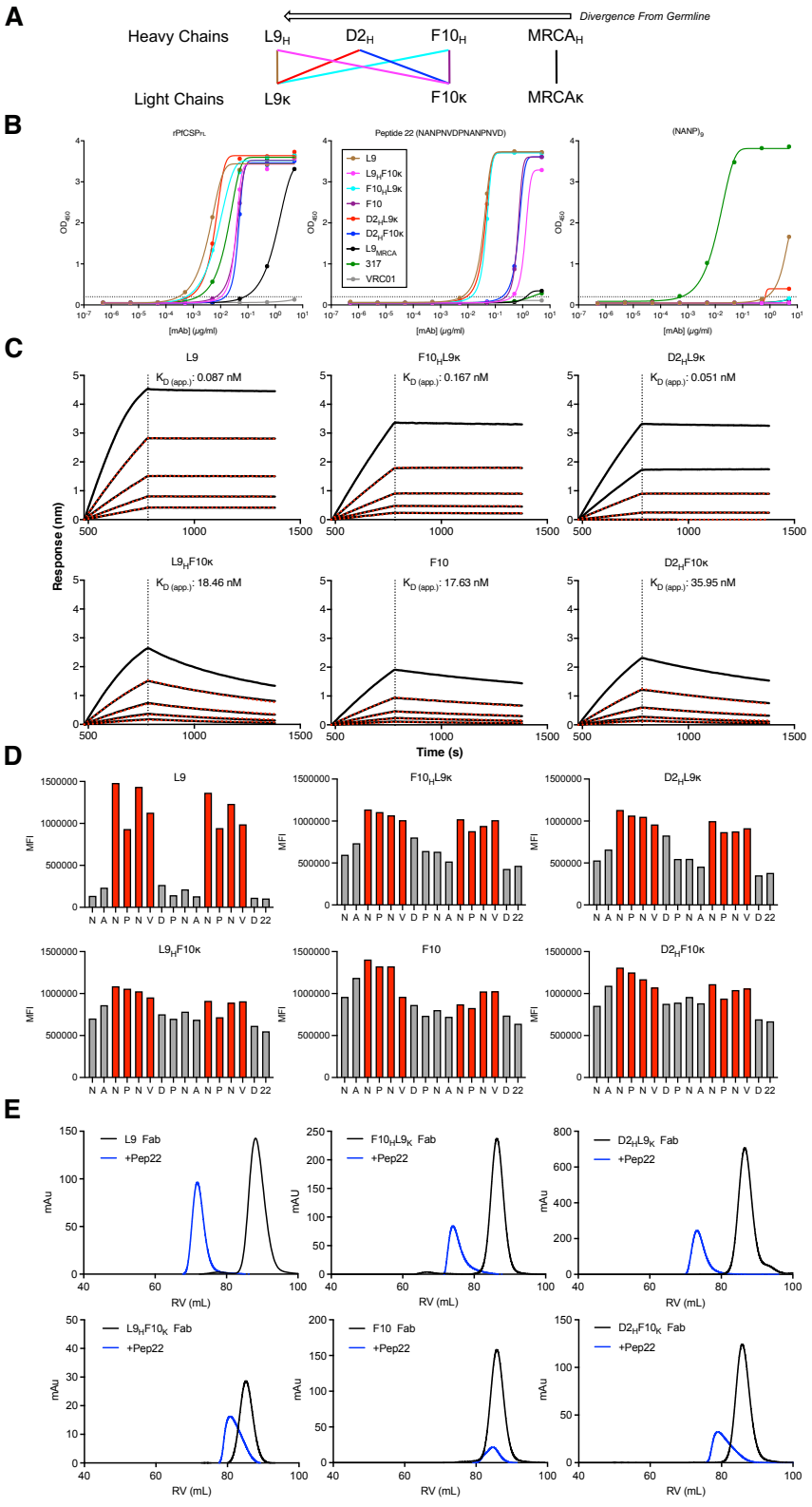

Figure 5.3: Binding of L9 lineage mAbs to peptide 22 and $(NANP)_9$. (A) Ig heavy and light chain pairings matched to create normal mAbs (L9, F10, $L9_{MRCA}$) and chimeric mAbs ($L9_HF10\kappa$, $F10_HL9\kappa$, $D2_HL9\kappa$, $D2_HF10\kappa$) used in this study. Each heavy and light chain's divergence from

germline is depicted. **(B)** Binding of various concentrations of indicated mAbs to $rPfCSP_{FL}$ (left), peptide 22 (NANPNVDPNANPNVD, middle), and $(NANP)_9$ (right) measured by ELISA; OD_{450} is plotted. The NANP-preferring PfCSP mAb 317 and the anti-HIV-1 mAb VRC01 were included as positive and negative controls, respectively. **(C)** Binding response (nm) and apparent avidity (KD_{app}, nM) of indicated mAbs binding to peptide 22 determined through BLI. **(D)** Competition ELISA of indicated mAbs binding to $rPfCSP_{FL}$ and various concentrations of peptide 22 (rightmost bar) or variant peptides (other bars) where the indicated amino acid was mutated to alanine or serine. AUC is plotted. **(E)** SEC plots of indicated Fabs incubated with peptide 22 (Fabs alone, black peak; Fabs+pep22, blue peak). All data are representative of two independent experiments.

To extend the analysis for L9, ITC was used to measure the affinity and stoichiometry of L9 Fabs binding to 15mer peptides 22, 25 (NVDPNANPNVDPNAN), and 29 (NANPNANPNANPNAN), as well as a minimal 8mer peptide (NANPNVDP) (**Table 5.2**). L9 bound ~2 binding sites with an affinity of 13 nM on peptide 22 (two NPNV) and ~1 binding site with an affinity of 1,000 and 1,900 nM on peptide 25 and NANPNVDP, respectively (one NPNV). L9 had no detectable binding to peptide 29, which contains 3 NPNA motifs. Collectively, these data confirm that L9 lineage mAbs recognize NPNV instead of NPNA, that L9 IgG requires two adjacent NPNV motifs for high-affinity binding to NVDP-containing peptides, and that pairing L9κ with closely-related Ig_H is sufficient to enable cross-linking of two NPNV motifs.

mAb	Antigen	Binding Event 1					Binding Event 2				
		N_1	K_{D1} (nM)	ΔG_1 (kcal/mol)	ΔH_1 (kcal/mol)	$-T\Delta S_1$ (kcal/mol)	N_2	K_{D2} (nM)	ΔG_2 (kcal/mol)	ΔH_2 (kcal/mol)	$-T\Delta S_2$ (kcal/mol)
L9 Fab	Pep 22	1.6	13	-10.8	-15.8	+5.0	-	-	-	-	-
	Pep 25	1.0	1000	-8.2	-13.8	+5.6	-	-	-	-	-
	Pep 29	-	-	-	-	-	-	-	-	-	-
	NANPNVDP	0.7	1900	-7.8	-6.4	-1.4	-	-	-	-	-

Table 5.2: ITC of L9 Fab binding to various peptides. ITC measurements of the stoichiometry (N), dissociation constant (K_D), change in Gibbs free energy (ΔG), change in enthalpy (ΔH), and change in entropy contribution to Gibbs free energy (−TΔS) of L9 Fab binding to peptides (pep 22, NANPNVDPNANPNVD; pep 25, NVDPNANPNVDPNAN; pep 29, NANPNANPNANPNAN; minimal peptide, NANPNVDP). "-" indicate undetectable parameters. Tabulated values were averaged from 2-3 independent experiments.

5.5 Structural studies of L9 lineage mAbs in complex with NANPNVDP

Next, X-ray crystallography was used to investigate the binding mechanism of L9 at the atomic scale, but diffracting crystals could only be generated in the absence of peptides and a structure of L9 Fab alone (apo-L9) was solved to 2.93 Å (**Figure 5.4A**). To gain structural insight into the NPNV binding mechanism of L9, Fabs of $F10_HL9\kappa$ and $L9_HF10\kappa$ in complex with the NANPNVDP peptide were crystallized and their structures were solved to 1.89 Å and 2.23 Å, respectively (**Figure 5.5A,C**). The data collection and refinement statistics are summarized in Appendix 3. $F10_HL9\kappa$ Fab binds NANPNVDP with the NPNV motif adopting a type-1 β-turn (**Figure 5.4B**) that the NPNA motif was shown to adopt[240] and is commonly found in NPNA-preferring repeat mAbs (**Figure 5.5B**)[79,219,241]. All three HCDRs and the KCDR1 and KCDR3 bind NANPNVDP with a total buried surface area (BSA) of ~373 $Å^2$, ~203 $Å^2$ from the Ig_H and ~170 $Å^2$ from Igκ (**Figure 5.5E**). The two Asn residues form a network of hydrogen bonds with both Ig_H/Igκ, with the Val sitting in a hydrophobic pocket formed by three aromatic residues on the KCDR1, KCDR3, and HCDR3 (**Figure 5.5B**). Surprisingly, the structure of $L9_HF10\kappa$ Fab-NANPNVDP showed an almost identical binding mechanism to $F10_HL9\kappa$ Fab-NANPNVDP (**Figure 5.5D,F**). The NPNV adopts the type-1 β-turn structure and is bound with a total BSA of ~364 $Å^2$, ~196 $Å^2$ from Ig_H and ~168 $Å^2$ from Igκ (**Figure 5.5E**).

To further investigate the differences between $L9_HF10\kappa$ and $F10_HL9\kappa$, both structures were aligned by their shared cognate NANPNVDP peptide. The two peptides align with a root mean square deviation (RMSD) of 0.189 $Å^2$ over six carbon atoms (**Figure 5.5F**). The only two residues that differ in the binding site, positions 96 (L9:Phe and F10:Tyr) and 99 (L9:Gly and F10:Ser) in Ig_H by Kabat numbering, are both main chain interactions and are unlikely to contribute to differences between the two chimeric mAbs. The interacting residues in both Igκ are identical. There are three differences in Igκ that may contribute to the increased binding

potential of L9κ. In the KCDR3, Glu_{90} in L9κ is charge swapped to a Gln in F10κ and is the only difference near the binding site. Two other differences occur in KCDR1 and framework region three where Ser_{28} and Asp_{70} in F10κ are mutated to aromatic residues in L9κ, Phe_{28} and His_{70}, both of which are solvent exposed. All three of these residues in L9κ are unusual mutations, occurring in less than 1% of kappa chain sequences (abYsis)[242]. These structures likely represent the binding mechanism of L9 to NPNV, but further structural information is needed to determine why L9κ enables binding to two adjacent NPNV motifs, as in peptide 22.

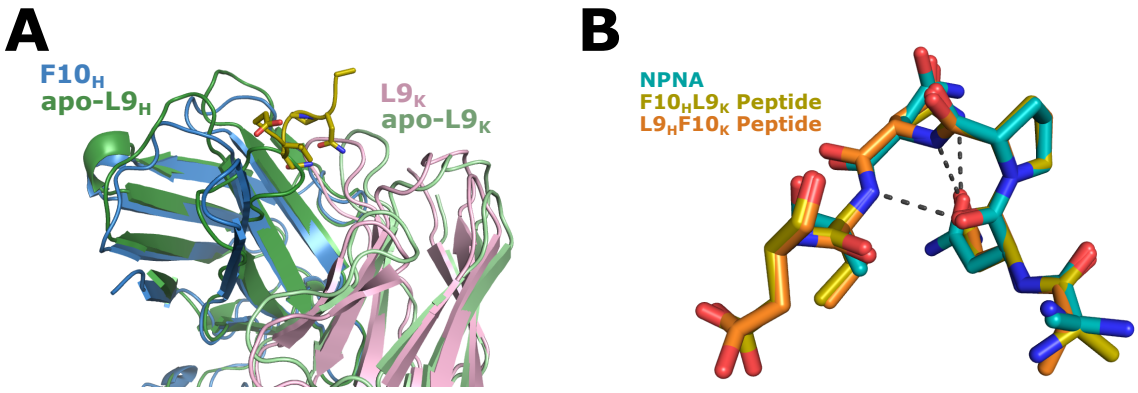

Figure 5.4: Structure of apo-L9 Fab and comparison of NANPNVDP peptide to NPNA type-1 β-turn. (A) The structure of apo-L9 Fab aligned to $F10_HL9_K$ Fab. (B) Alignment of NANPNVDP peptide to crystal structure of NPNA, overall RMSD of 0.089 $Å^2$ over four carbon atoms, showing the near-identical type-1 β-turn.

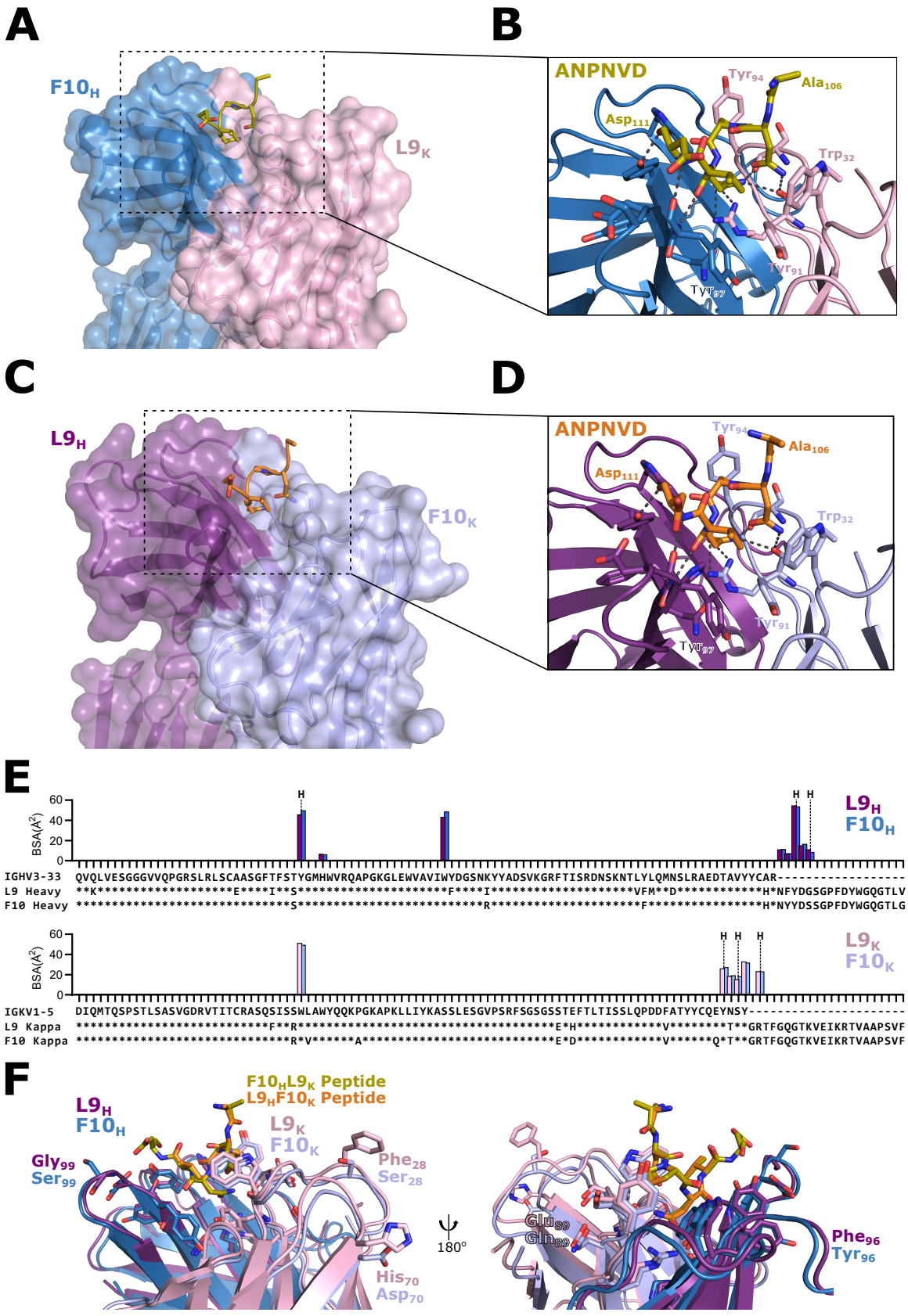
A
B
C
D
E
F
F10H
L9K
L9H
F10K
ANPNVD
Tyr94
Ala106
Asp111
Trp32
Tyr91
Tyr97
BSA(Å2)
60
40
20
0
IGHV3-33 QVQLVESGGGVVQPGRSLRLSCAASGFTFSTYGMHWVRQAPGKGLEWVAVIWYDGSNKYYADSVKGRFTISRDNSKNTLYLQMNSLRAEDTAVYYCAR----------
L9 Heavy **K**********E****I**S**********F****I**********VFM**D**********H*NFYDGSGPFDYWGQGTLV
F10 Heavy **********S**********R**********F**********H*NYYDSSGPFDYWGQGTLG
IGKV1-5 DIQMTQSPSTLSASVGDRVTITCRASQSISSWLAWYQQKPGKAPKLLIYKASSLESGVPSRFSGSGSSTEFTLTISSLQPDDFATYYCQEYNSY----------
L9 Kappa **********F**R**********E*H**********V********T**GRTFGQGTKVEIKRTVAAPSVF
F10 Kappa **********R*V******A**********E*D**********V******Q*T**GRTFGQGTKVEIKRTVAAPSVF
F10HL9K Peptide
L9HF10K Peptide
Gly99
Ser99
Phe28
Ser28
His70
Asp70
180°
Glu89
Gln89
Phe96
Tyr96

Figure 5.5: Crystal structures of $F10_HL9\kappa$ and $L9_HF10\kappa$ in complex with the NANPNVDP peptide. (A) Structures of $F10_HL9\kappa$ Fab and **(C)** $L9_HF10\kappa$ Fab bound to NANPNVDP. The structures are shown in a cartoon representation with a transparent surface representation. The sidechains of the peptides are shown. **(B)** and **(D)** respectively show zoomed-in images of the binding sites in A and C. Peptide interacting residues are shown in stick representations, with hydrogen bonds represented by dashed lines. Named residues are depicted to orient structure to location of CDRs. **(E)** BSA plots of each Fab residue interacting with the peptide and a sequence alignment with the germline V-genes. Residues involved in hydrogen bonding are marked with a "H". **(F)** Structural alignment of the $F10_HL9\kappa$ and $L9_HF10\kappa$ Fab structures using the NANPNVDP peptide. Residues that differ between the two structures are labeled.

5.6 Elucidation of the evolution of L9 lineage mAbs

To further define the evolution of epitope reactivities in L9 lineage mAbs, the binding of $L9_{MRCA}$, F10, and L9 to three rPfCSP constructs (FL, 5/3, $\Delta(NVDP)_4$; **Figure 5.6A**) were measured by ELISA; 317 was included as a NANP-preferring control mAb. $rPfCSP_{5/3}$ is a truncated construct containing only the junctional region (i.e., NPDP followed by 5 NANP interspersed with 3 NVDP repeats); $rPfCSP_{\Delta(NVDP)4}$ has 1 NPDP and 42 NANP repeats, as all four NVDP were changed to NANP.

F10 and L9 had high $rPfCSP_{FL}$ and $rPfCSP_{5/3}$ binding but only L9 had detectable $rPfCSP_{\Delta(NVDP)4}$ binding (**Figure 5.6B**). Notably, $L9_{MRCA}$ only bound $rPfCSP_{FL}$ and $rPfCSP_{5/3}$ and had no measurable $rPfCSP_{\Delta(NVDP)4}$ binding. Given these three mAbs' relative degrees of somatic mutation (L9 > F10 > $L9_{MRCA}$, with $L9_{MRCA}$ being near-germline; **Table 5.1**), these data suggest that the L9 lineage has baseline affinity for the junctional region and mutates to gain NANP cross-reactivity.

The binding preferences of the L9 lineage were corroborated by competition ELISA showing that a junctional peptide more potently competed mAb binding to $rPfCSP_{FL}$ and $rPfCSP_{5/3}$ than $(NANP)_9$, with the degree of competition correlating to the mAbs' somatic

mutations (**Figure 5.6C**). Notably, L9 was the only mAb that detectably bound $rPfCSP_{\Delta(NVDP)4}$ and the junctional peptide more potently competed L9 binding than $(NANP)_9$.

To extend the epitope mapping analysis, peptides 20-61 spanning the repeat domain were used to compete $L9_{MRCA}$, F10, and L9 binding to $rPfCSP_{FL}$ (**Figure 5.6D**). These data confirmed the markedly high affinity of L9 for peptide 22, the relatively high binding of F10 and $L9_{MRCA}$ to peptides 21/22/23/43 (all contain ≥1 NPNV), and all three mAbs' low/undetectable binding to peptides 27/29/61 (all lack NPNV). Furthermore, all three mAbs preferentially bound $(NPNV)_4$ compared to $(NPNA)_4$, confirming that the core motif recognized by these mAbs is NPNV. Collectively, these data show that the L9 V_H3-33/Vκ1-5 B cell lineage originated as subdominant NPNV binders that somatically mutated to acquire affinity for immunodominant NPNA motifs.

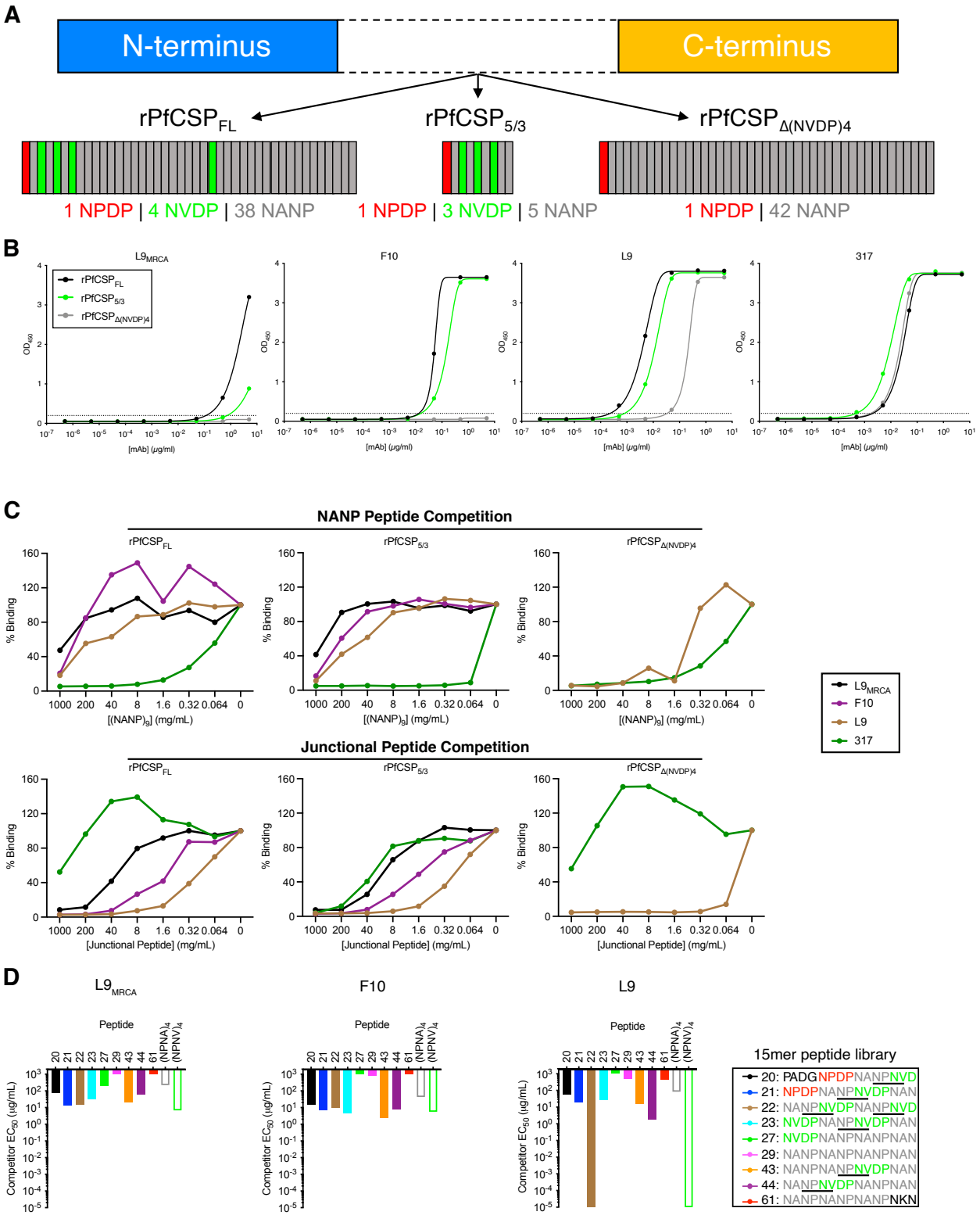

Figures 5.6: Mapping the evolution of epitope reactivities of L9 lineage mAbs. (A) Schematics of rPfCSP constructs with identical N- and C-termini but different repeat regions (rPfCSP$_{FL}$: 1 NPDP, 4 NVDP, 38 NANP; rPfCSP$_{5/3}$: 1 NPDP, 5 NANP, 3 NVDP;

rPfCSP$_{\Delta(NVDP)4}$: 1 NPDP, 42 NANP). **(B)** Binding of various concentrations of indicated mAbs to rPfCSP$_{FL,}$ rPfCSP$_{5/3}$, and rPfCSP$_{\Delta(NVDP)4}$ determined through ELISA; OD$_{450}$ is plotted. **(C)** Competition ELISA of indicated mAbs binding to rPfCSP$_{FL,}$ rPfCSP$_{5/3}$, and rPfCSP$_{\Delta(NVDP)4}$ in the presence of varying concentrations of junctional peptide 21-25 (NPDPNANPNVDPNANPNVDPNANPNVDPNAN) and (NANP)$_9$ peptide; OD$_{450}$ is plotted. **(D)** Competition ELISA of indicated mAbs binding to rPfCSP$_{FL}$ in the presence of varying concentrations of 15mer color-coded peptides numbered 20-61 and 16mer peptides (NPNA)$_4$ and (NPNV)$_4$. EC$_{50}$ for competition by each peptide is depicted.

5.7 Binding of L9 lineage mAbs to full-length PfCSP proteins

To elucidate how the mAb panel's relative affinities for NPNV and NPNA motifs impacted their binding to full-length protein, ITC was used to measure their binding stoichiometry and affinity to rPfCSP$_{FL}$, rPfCSP$_{5/3}$, and rPfCSP$_{\Delta(NVDP)4}$. I previously reported that the most potent mAbs for protecting against *in vivo* SPZ challenge, including L9, bound rPfCSP$_{FL}$ in two binding events with distinct affinities (termed "two-step binding") and displayed high-affinity binding to the junctional region in rPfCSP$_{5/3}$. Furthermore, I showed that L9 binds rPfCSP$_{\Delta(NVDP)4}$ in a single step with lower affinity, confirming that L9 requires NPNV to two-step bind rPfCSP but can cross-react with NPNA motifs[85].

Remarkably, L9κ-containing mAbs (L9, F10$_H$L9κ, D2$_H$L9κ) bound rPfCSP$_{FL}$ in two steps while F10κ-containing mAbs (F10, L9$_H$F10κ, D2$_H$F10κ) bound in a single step, resulting in the higher stoichiometry of L9κ-containing mAbs for rPfCSP$_{FL}$ (**Table 5.3**). The mAbs' stoichiometry in binding event 1 (N_1) for rPfCSP$_{FL}$ and rPfCSP$_{5/3}$ were similar (~2-3 binding sites), suggesting that the epitopes bound by these mAbs in binding event 1 are contained in rPfCSP$_{5/3}$ (**Table 5.3**). Furthermore, only L9κ-containing mAbs had detectable binding to rPfCSP$_{\Delta(NVDP)4}$ with L9 having the highest stoichiometry (~13 binding sites).

The mAb panel's affinity in binding event 1 (K_{D1}) was better for rPfCSP$_{5/3}$ (1.2-6.5 nM) compared to rPfCSP$_{FL}$ (5-58 nM), further indicating that binding event 1 is directed toward

rPfCSP$_{5/3}$ (**Table 5.3**). Consistent with the (NANP)$_9$ ELISA data (**Figure 5.3B**), only L9κ-containing mAbs had detectable affinity for rPfCSP$_{\Delta(NVDP)4}$ with L9 having the best affinity, though significantly less than the NANP-preferring mAb 317 (73 vs. 2 nM; **Table 5.3**). Collectively, the ITC data confirm that all mAbs in the panel have high-affinity binding to NPNV motifs in the junctional region (i.e., rPfCSP$_{5/3}$), that L9κ imparts lower-affinity binding to concatenated NPNA motifs (i.e., rPfCSP$_{\Delta(NVDP)4}$), and that two-step binding to rPfCSP$_{FL}$ seen in L9κ-containing mAbs is due to their respective high- and low-affinity binding to NPNV and NPNA motifs.

mAb	Antigen	Binding Event 1					Binding Event 2				
		N_1	K_{D1} (nM)	ΔG_1 (kcal/mol)	ΔH_1 (kcal/mol)	$-T\Delta S_1$ (kcal/mol)	N_2	K_{D2} (nM)	ΔG_2 (kcal/mol)	ΔH_2 (kcal/mol)	$-T\Delta S_2$ (kcal/mol)
L9 IgG	FL	1.9	22	-10.4	-30.0	+19.6	9.3	47	-10.0	-9.1	-0.9
	5/3	3.1	3	-11.6	-17.0	+5.4	-	-	-	-	-
	$\Delta(NVDP)_4$	12.7	73	-9.7	-12.4	+2.7	-	-	-	-	-
$L9_HF10\kappa$ IgG	FL	2.5	58	-9.9	-11.7	+1.8	-	-	-	-	-
	5/3	2.2	2.1	-11.8	-18.2	+6.4	-	-	-	-	-
	$\Delta(NVDP)_4$	-	-	-	-	-	-	-	-	-	-
$F10_HL9\kappa$ IgG	FL	3.4	7	-11.1	-14.1	+3.0	6.8	400	-8.7	-10.3	+1.6
	5/3	2.4	1.2	-12.2	-15.8	+3.6	-	-	-	-	-
	$\Delta(NVDP)_4$	8.1	96	-9.6	-9.9	+0.3	-	-	-	-	-
F10 IgG	FL	3.4	14	-10.7	-13.4	+2.7	-	-	-	-	-
	5/3	2.1	4	-11.4	-17.5	+6.1	-	-	-	-	-
	$\Delta(NVDP)_4$	-	-	-	-	-	-	-	-	-	-
$D2_HL9\kappa$ IgG	FL	3.6	5	-11.3	-9.2	-2.1	7.7	270	-9.0	-6.5	-2.5
	5/3	2.2	1.6	-12.0	-13.0	+1.0	-	-	-	-	-
	$\Delta(NVDP)_4$	9.7	87	-9.6	-7.3	-2.3	-	-	-	-	-
$D2_HF10\kappa$ IgG	FL	2.7	32	-10.2	-11.5	+1.3	-	-	-	-	-
	5/3	2.3	6.5	-11.2	-15.6	-4.4	-	-	-	-	-
	$\Delta(NVDP)_4$	-	-	-	-	-	-	-	-	-	-
317 IgG	FL	7.5	2	-11.9	-26.3	+14.4	4.7	17	-10.6	-16.7	+6.1
	5/3	0.5	2	-11.9	-28.0	+16.1	1.2	7	-11.1	-16.7	+5.6
	$\Delta(NVDP)_4$	8.5	2	-11.8	-23.3	+11.5	4.1	14	-10.7	-17.6	+6.9

Table 5.3: ITC of L9 lineage mAbs binding to rPfCSP. ITC measurements of the stoichiometry (N), dissociation constant (K_D), change in Gibbs free energy (ΔG), change in enthalpy (ΔH), and change in entropy contribution to Gibbs free energy (−TΔS) of indicated IgG binding to rPfCSP constructs (FL, 1 NPDP, 4 NVDP, 38 NANP; 5/3, 1 NPDP, 3 NVDP, 5 NANP; $\Delta(NVDP)_4$, 1 NPDP, 42 NANP). "-" indicate undetectable parameters. Tabulated values were averaged from 2-3 independent experiments.

5.8 Binding and neutralization of SPZ by the mAb panel

To determine whether the mAb panel's stoichiometry and affinity for rPfCSP$_{FL}$ correlate with their recognition of native PfCSP$_{FL}$ on the surface of SPZ, flow cytometry was used to

quantify mAb binding to Pb-PfCSP-SPZ. All mAbs in the panel bound Pb-PfCSP-SPZ *in vitro* (**Figure 5.7A**). Consistent with the $rPfCSP_{FL}$ ELISA and ITC data (**Figures 5.3A, Table 5.3**), L9κ-containing mAbs (L9, $F10_HL9κ$, $D2_HL9κ$) had higher Pb-PfCSP-SPZ binding compared to their counterpart F10κ-containing mAbs (F10, $L9_HF10κ$, $D2_HF10κ$) while $L9_{MRCA}$ had the lowest $rPfCSP_{FL}$ binding.

Next, the functional ability of each mAb in the panel to induce the CSPR and immobilize Pb-PfCSP-SPZ *in vitro* was assessed as these two inhibitory phenotypes are associated with protection against SPZ challenge *in vivo*. L9κ-containing mAbs induced the CSPR in >80% and immobilized >90% of Pb-PfCSP-SPZ, which was significantly greater than the 48-64% and 52-68% respectively mediated by F10κ-containing mAbs (**Figure 5.7B-C**). These data suggest that L9κ-containing mAbs more potently neutralize Pb-PfCSP-SPZ *in vitro* than their counterpart F10κ-containing mAbs.

To extend the *in vitro* functional analysis, I next determined the mAb panel's relative abilities to lower parasite liver burden *in vivo* in C57/BL6 mice challenged IV with Pb-PfCSP-SPZ. Mice that received 100 μg of L9κ-containing mAbs had significantly lower liver burden than mice that received 100 μg of their F10κ-containing counterpart mAbs (**Figure 5.7D**). To extend these findings, I tested the mAb panel's abilities to prevent parasitemia in mice challenged with Pb-PfCSP-SPZ-infected mosquitoes, which mimics the natural route of malaria transmission. 300 μg L9κ-containing mAbs mediated 70-100% sterile protection in mice, which was greater than the 28-70% protection provided by F10κ-containing mAbs (**Figure 5.7E**). Collectively, these data show that L9κ improves the ability of NVDP-preferring mAbs to neutralize Pb-PfCSP-SPZ *in vitro* and *in vivo.*

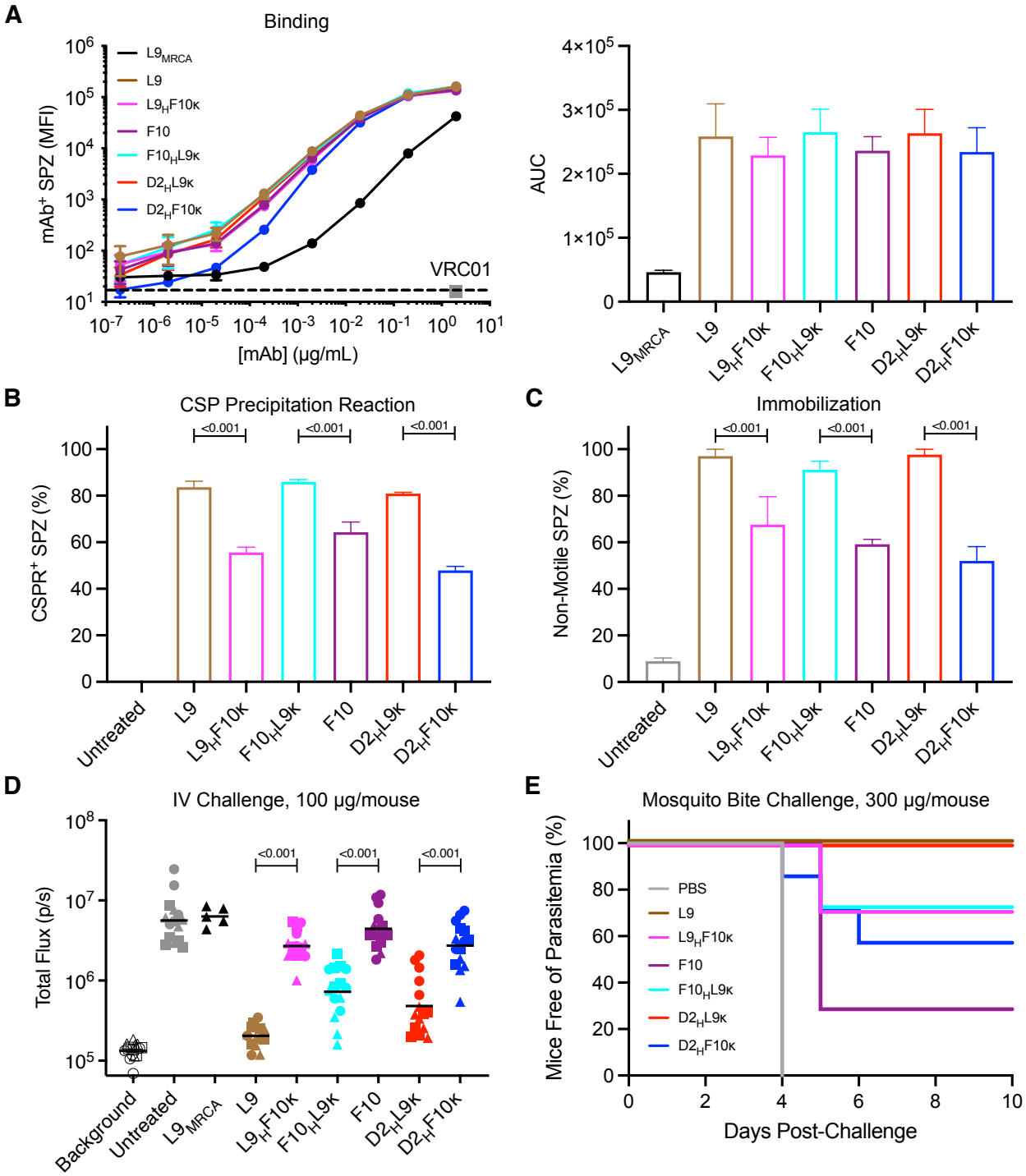

Figure 5.7: Binding and neutralization of Pb-PfCSP-SPZ by L9 lineage mAbs. (A) Left: binding of various concentrations of indicated mAbs to Pb-PfCSP-SPZ determined by flow cytometry; MFI of mAb-bound SPZ is plotted. Mean and SEM values from four independent experiments are shown except for $L9_{MRCA}$, which was from two experiments. Right: AUC and SEM values calculated from the MFI plots. **(B)** Percentage of SPZ undergoing the CSPR after incubation with 50 μg/mL of indicated mAb for 15 min. Bar graphs show the mean and SEM from six independent experiments. **(C)** Percentage of non-motile SPZ after incubation with 25

μg/mL of indicated mAb for 15 min. Bar graphs show the mean and SEM from two independent experiments. (B-C): *P*-values reflect comparisons between L9κ-containing mAbs and their F10κ-containing counterparts using Fisher's exact test. **(D)** Reduction in parasite bioluminescence (total flux, photons/sec) in the livers of mice (n=15/group; data pooled from three independent experiments indicated by squares, circles, and triangles) mediated by 100 μg of indicated mAbs administered 2 h before IV challenge with 2,000 Pb-PfCSP-SPZ. *P*-values reflect comparisons between L9κ-containing mAbs and their F10κ-containing counterparts using the two-tailed Mann–Whitney test. **(E)** Survival curves of mice (n=7/group) challenged with five infected mosquito bites 24 h after passive transfer of 300 μg of indicated mAb.

5.9 Discussion

This study showed that the Igκ light chain of L9, a highly potent human PfCSP mAb that preferentially binds the subdominant NVDP minor repeats[85], is critical for this antibody's unique binding properties and potent neutralization of SPZ. This finding was shown by pairing mAbs clonally related to L9 with different Ig_H/Igκ to create L9κ-containing chimeric mAbs that recapitulated the binding properties of L9 (i.e., binds two adjacent NPNV motifs, cross-reacts with concatenated NPNA motifs, and two-step binds $rPfCSP_{FL}$). Conversely, pairing $L9_H$ and other V_H with the Igκ of a closely related mAb, F10κ, resulted in chimeric mAbs that bound only one NPNV motif and lacked NPNA affinity and two-step binding. Furthermore, these data confirm that two-step binding is detected by ITC when a mAb exhibits two distinct affinities for the junctional region and NANP repeats on $rPfCSP_{FL}$, as has been previously suggested[85].

These data also show that cross-linking two adjacent NVDP repeats, cross-reacting with NANP repeats, and two-step binding rPfCSP are binding properties correlated with higher binding to native PfCSP on Pb-PfCSP-SPZ, enhanced neutralization of Pb-PfCSP-SPZ *in vitro*, and improved protection against *in vivo* Pb-PfCSP-SPZ challenge. Furthermore, a recently published study used transgenic SPZ lines expressing CSP with knocked-out and knocked-in NANP/NVDP repeats to show that the preferred epitope of L9 (i.e., NANPNVDPNANPNVDP) is necessary and sufficient for L9 to bind and neutralize SPZ *in vivo*[209]. Thus, it is likely that the

improved SPZ neutralization mediated by L9κ-containing mAbs is due to their preferential high-affinity divalent binding of adjacent NVDP repeats in the first binding step, rather than their lower affinity multivalent cross-reactivity with NANP repeats in the second binding step. Collectively, this study identifies discrete binding properties associated with potent SPZ neutralization by NVDP-preferring mAbs.

In terms of assessing the evolution of human NVDP-preferring repeat antibodies, this study showed that the L9 V_H3-33/Vκ1-5 B cell lineage has baseline affinity for NVDP repeats in the junctional region and somatically mutated to acquire NANP cross-reactivity. Specifically, the L9 lineage germline binds one NPNV and evolves to bind two adjacent NPNV motifs and concatenated NPNA motifs. This evolutionary pathway differs from a previous study showing that a large panel of V_H3-33/Vκ1-5 PfCSP human mAbs had baseline NANP affinity centered on the conserved (N/D)PNANPN(A/V) core motif and evolved to acquire NPDP/NVDP cross-reactivity[237]. Having shown that the core motif bound by L9 lineage mAbs is NPNV, the present study suggests that some rare V_H3-33/Vκ1-5 lineages initially target subdominant NVDP repeats and evolve later to cross-react with immunodominant NANP repeats. These key findings are summarized in the Graphical Abstract below (**Figure 5.8**).

Overall, these data have implications for improving the design of PfCSP-based vaccine immunogens. RTS,S notably lacks NPNV motifs and only presents NPNA motifs along with the C-terminus. As L9 is the most potent human PfCSP mAb isolated to date[85], future PfCSP-based immunogens should include the L9 preferred epitope of ≥2 adjacent NPNV repeats (NANPNVDPNANPNVDP) to induce L9-like antibodies by expanding naïve V_H3-33/Vκ1-5 B cells with low baseline affinity for NPNV motifs.

Lastly, structural studies showed that $F10_HL9\kappa$ and $L9_HF10\kappa$ both bound NPNV in the minimal peptide NANPNVDP in a type-1 β-turn that was near-identical to the NPNA type-1 β-turn commonly observed for NANP-preferring mAbs[79,219,241], suggesting that recognition of single NPNV motifs does not differ between these mAbs. The convergent conformations adopted by these subtly different tetrapeptides is in line with a previous study which also observed that cross-reactive PfCSP mAbs bind different repeat epitopes in near-identical conformations[237]. Further structural studies on longer peptides containing ≥2 NPNV motifs and $rPfCSP_{FL}$ are needed to elucidate how L9κ contributes to binding adjacent NPNV motifs with high affinity and cross-reacting with NPNA motifs, as well as how these binding properties contribute to SPZ neutralization.

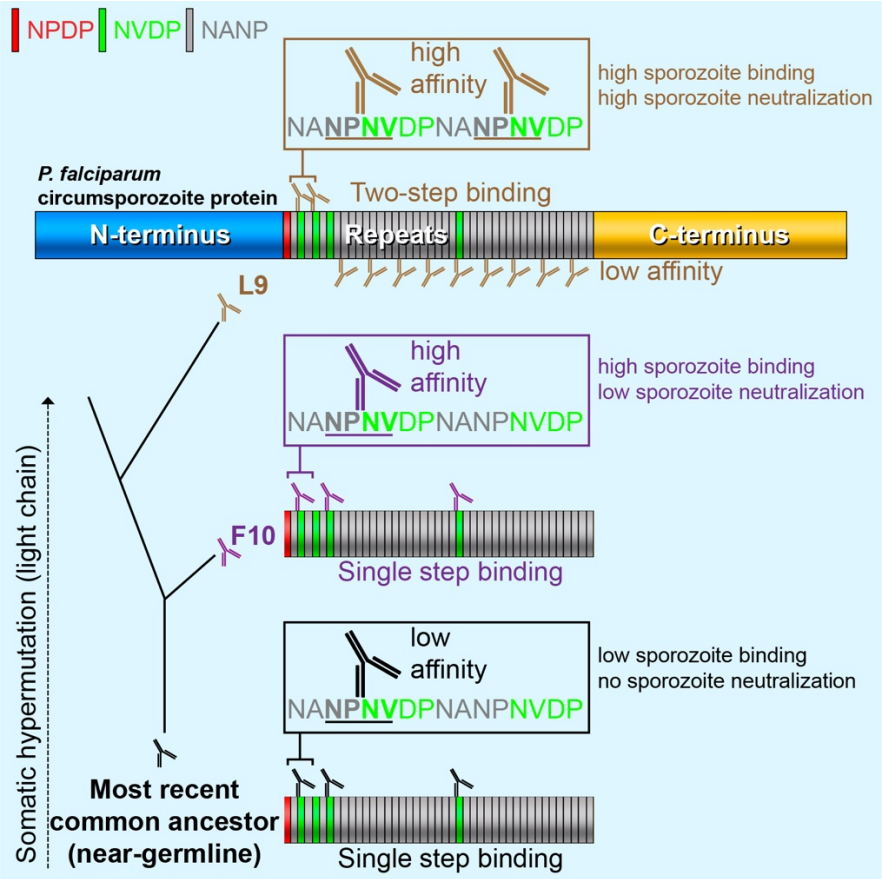

Figure 5.8: *Cell Reports* graphical abstract. Graphical abstract depicting the evolution of the L9 antibody lineage's epitope recognition patterns and how L9 binds PfCSP in two steps with distinct affinities.

Chapter VI: Binding and protection of PfCSP mAb and vaccine combinations

6.1 Authorship statement

Sections of this Chapter were published in Wang et al., *PLOS Pathogens* 2021 (https://doi.org/10.1371/journal.ppat.1010133). Lais Pereira and Alvaro Molina-Cruz provided SPZ; Arne Schön performed circular dichroism and ITC experiments; Joshua Tan helped with surface plasmon resonance experiments; Lais Pereira, Patience Kiyuka, Marlon Dillon, and Brian Bonilla performed mouse protection studies; Vladimir Vigdorovich, Nicholas Dambrauskas, and Noah Sather provided the recombinant C-CSP protein; Alexander Anderson and Gary Matyas provided the ALF-Q adjuvant; Alexandra Spencer and Adrian Hill provided the R21 vaccine; Shanping Li and Peter Crompton provided serum from Malians living in malaria-endemic regions.

6.2 Introduction

It is well-established that PfCSP mAbs against the immunodominant repeat region potently neutralize SPZ *in vivo* and prevent malaria infection. Indeed, most neutralizing PfCSP mAbs isolated to date are NANP-specific[235], and anti-NANP antibodies correlate with RTS,S-mediated protection in Phase III trials[155]. The RTS,S immunogen is comprised of 19 NANP repeats and C-CSP, and notably lacks N-CSP. Thus, there is much debate about whether N-CSP is targeted by protective antibodies and if its presence might improve the efficacy of CSP-based

vaccines. Another outstanding question is whether antibodies against C-CSP contribute to RTS,S-mediated protection and if the removal of C-CSP from RTS,S will improve its efficacy.

N-CSP is an attractive target for antibodies, as it is an essential SPZ adhesive ligand and contains the five amino acid motif RI that is highly conserved across CSP of all *Plasmodium* species (**Figure 6.1**). Various post-translational modifications of N-CSP are critical for its function. Specifically, proteolytic cleavage of N-CSP at each of two PEXEL sites facilitate export of CSP from the endoplasmic reticulum to the plasma membrane[69–72] while cleavage of N-CSP at RI is required for CSP to bind HSPGs on hepatocytes[65,66,68].

Studies of polyclonal serum suggest that N-CSP is targeted by protective antibodies. For instance, serum from naturally infected humans display high N-CSP reactivity[243–247], N-CSP-specific polyclonal antibodies were shown to mediate more *in vitro* opsonophagocytosis than repeat- or C-CSP-specific antibodies[112], and reactivity against a RI-containing N-CSP peptide was associated with protection in children from endemic regions[247]. Furthermore, serum from mice immunized with N-CSP peptides inhibited SPZ invasion of hepatocytes *in vitro*[247,248]. Importantly, one study reported that N-CSP (particularly RI) contains immunologically cryptic epitopes and suggested that SPZ may hide functional moieties critical to adhesion[248]. These data suggest that neutralization by N-CSP-specific antibodies may be limited by the masking of this domain from antibody recognition.

Despite these promising polyclonal serum data, only one weakly protective human mAb called MAD2-6 (whose epitope encompasses part of RI and the upstream lysines) has been isolated from a naturally-infected volunteer. Importantly, MAD2-6 neutralized SPZ *in vivo* despite weakly binding SPZ *in vitro*[171]. Conversely, several N-CSP mAbs have been isolated from mice immunized with N-CSP peptides[67,106]. One of these mouse mAbs, 5D5, binds further

upstream of the MAD2-6 epitope[171] and was initially reported to bind PfSPZ by immunofluorescence microscopy and protect mice from challenge with transgenic Pb expressing N-CSP[106]. However, a more recent study showed that, despite binding rPfCSP with high-affinity, 5D5 had low PfSPZ binding by imaging flow cytometry and did not mediate protection against PfSPZ invasion of hepatocytes *in vitro* or Pb-PfCSP-SPZ challenge in mice *in vivo*[249]. Overall, these data show that native N-CSP on the surface of SPZ is poorly accessible to antibodies and suggest that the neutralization of N-CSP-specific antibodies might benefit from increasing the availability of their target epitopes in native CSP.

In terms of antibodies against C-CSP, there is some evidence that C-CSP-specific antibodies contribute to SPZ neutralization. Specifically, serum from mice immunized with C-CSP peptides inhibits SPZ hepatocyte invasion *in vitro*[68,250]. In the context of RTS,S-immunized adults and/or children, C-CSP antibodies in polyclonal serum mediate phagocytosis and complement fixation *in vitro*[108,251] and C-CSP-specific IgG avidity and breadth correlate with RTS,S efficacy[252,253]. C-CSP IgG_2/IgA_2[254] and C-CSP IgG_4[255] have been associated with protection; however another report showed that C-CSP $IgG_{2/4}$ were associated with increased malaria risk whereas C-CSP $IgG_{1/3}$ were associated with protection[256]. Moreover, genetic analyses of Pf field isolates showed that C-CSP is highly polymorphic and that RTS,S is less effective against non-3D7 strains, suggesting that C-CSP is under substantial immune pressure[257,258]. Together, these data suggest that C-CSP antibodies neutralize SPZ *in vitro* and may be associated with RTS-S-mediated protection *in vivo* when accompanied by repeat antibodies.

Based on these data, efforts have been made to isolate and characterize C-CSP mAbs from PfSPZ-immunized adult volunteers, resulting in the publication of three C-CSP human

mAbs to date[84,226]. Despite displaying high-affinity binding to rPfCSP, these three C-CSP mAbs had minimal SPZ binding and neutralization *in vitro* and *in vivo*[84,226]. These data suggest that, like N-CSP, C-CSP is also inaccessible on the surface of SPZ. Indeed, native PfCSP on SPZ has been shown to undergo reversible conformational changes to mask C-CSP[67,68], with the repeat region acting as a flexible spring between N- and C-CSP[75,76]. These data indicate that PfCSP is structurally labile and may adopt different conformations to mask C-CSP from antibody recognition.

Conformational masking has been described for viral glycoproteins like envelope glycoprotein 120 (gp120) on HIV-1; furthermore, the binding of certain antibodies has been shown to trigger additional conformational changes in gp120[259]. Similarly, binding of the human PfCSP mAb CIS43 to the unique tetrapeptide NPDP at the junction of N-CSP and the repeat region has been proposed to induce conformational changes in full-length recombinant CSP (FL-rCSP)[84]. These data suggest that combining a repeat mAb that changes the conformation of PfCSP with a conformation-dependent C-CSP mAb may improve the binding and neutralization of the C-CSP mAb. Indeed, combining mAbs that bind different epitopes on gp120 has been shown to synergistically block HIV-1 infection[260,261].

This Chapter defines the accessibility of epitopes in native N- and C-CSP on SPZ to recognition by PfCSP mAbs and the potential role of N- and C-CSP-specific mAbs in preventing malaria infection when combined with PfCSP repeat mAbs. Specifically, I investigated the ability of the N-CSP mAb 5D5 to bind Pb-PfCSP-SPZ and PfSPZ *in vitro* by flow cytometry and protect mice from *in vivo* Pb-PfCSP-SPZ challenge when combined with neutralizing PfCSP repeat mAbs. I also assembled the largest known panel of human C-CSP mAbs and characterized their *in vitro* SPZ binding and *in vivo* SPZ neutralization alone or in combination with

neutralizing repeat mAbs. I extended this analysis by assessing whether combinations of potent NPDP/NVDP/NANP-specific repeat mAbs provided increased protection *in vivo* compared to single repeat mAbs. Finally, I evaluated whether passive administration of repeat- or C-CSP-specific mAbs in mice immunized with a next-generation RTS,S-like vaccine[210] provided improved protection compared to each intervention alone. Collectively, these data provide insight into how PfCSP mAbs can be optimally used to prevent malaria alongside PfCSP-based vaccines.

6.3 Assembly of a mAb panel against N-CSP, repeat region, and C-CSP

A panel of published and unpublished mAbs targeting each domain of PfCSP was assembled (**Figure 6.1 and Table 6.1**). The only N-CSP mAb in the panel is the humanized mouse mAb 5D5, which was reported to bind a linear epitope in N-CSP directly upstream of the cleavage site in RI[106,249]. Twelve human mAbs that preferentially bind the three tetrapeptides (NPDP, NVDP, and NANP) in the repeat region were also assembled. BLI was used to confirm the preference of these mAbs for NPDP-containing peptide 21, NVDP-containing peptide 22, and NANP-containing peptide 29. Importantly, all repeat mAbs had high binding to SPZ but varying (none – high) levels of protection *in vivo*. Lastly, thirteen human mAbs that bind C-CSP were assembled. Two C-CSP mAbs in the panel, 1710 and mAb15, have been previously reported[84,226]. The panel's eleven other C-CSP mAbs were isolated from a PfSPZ-immunized subject, as described in Chapter III (L-series and R-series mAbs).

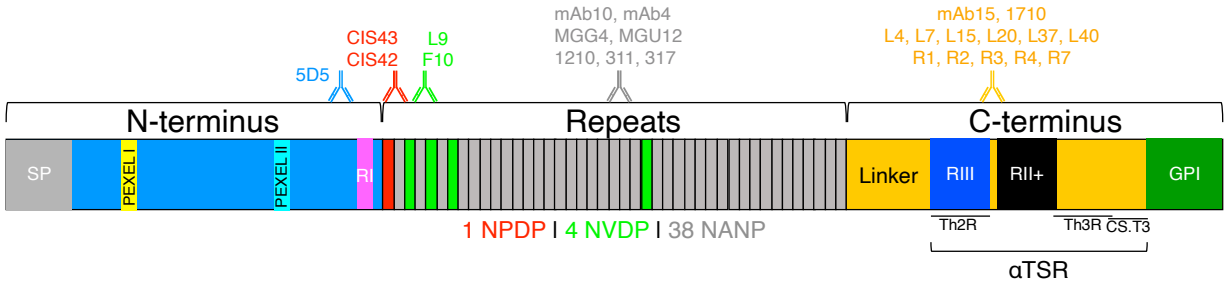

Figure 6.1: Approximate PfCSP epitopes bound by mAbs used in this Chapter.

mAb	Isotype	Species	Antigen	BLI Apparent Avidity (nM) Pep21	Pep22	Pep29	SPZ Binding	SPZ Neutralization	Reference
VRC01	IgG	Human	HIV-1 gp120	n/a	n/a	n/a	None	None	[262]
5D5	IgG	Mouse	N-CSP	n/a	n/a	n/a	Low	None	[106,249]
CIS43	IgG	Human	CSP Repeats NPDP	<0.001	1.5	undet.	High	High	[84,178]
CIS42	IgG	Human		0.26	0.90	2.29	High	Very Low	[84] This Study
L9	IgG	Human	CSP Repeats NVDP	6.0	0.28	undet.	High	High	[178]
F10	IgG	Human		1.50	11.32	undet.	High	Very Low	This Study
mAb10	IgG	Human		1.6	8.2	<0.001	High	Moderate	[84,178]
MGG4	IgG	Human		4.28	2.72	<0.001	High	Low	[213] This Study
MGU12	IgG	Human		2.1	3.9	<0.001	High	Low	[178,213]
1210	IgG	Human	CSP Repeats NANP	2.2	100	0.043	High	Low	[178,219]
311	IgG	Human		4.1	3.0	<0.001	High	Moderate	[79,178]
317	IgG	Human		1.2	0.49	<0.001	High	High	[79,178]
mAb4	IgG	Human		undet.	7.24	0.39	High	Very Low	[84] This Study
mAb26	IgG	Human		undet	undet	5.07	High	None	[50] This Study
L4	IgG	Human		n/a	n/a	n/a	Low	None	This Study
L7	IgG	Human		n/a	n/a	n/a	Low	None	This Study
L15	IgM	Human		n/a	n/a	n/a	Low	None	This Study
L20	IgM	Human		n/a	n/a	n/a	Low	None	This Study
L37	IgM	Human		n/a	n/a	n/a	Low	None	This Study
L40	IgM	Human		n/a	n/a	n/a	Low	None	This Study
R1	IgG	Human	C-CSP	n/a	n/a	n/a	Low	None	This Study
R2	IgG	Human		n/a	n/a	n/a	Low	None	This Study
R3	IgG	Human		n/a	n/a	n/a	Low	None	This Study
R4	IgG	Human		n/a	n/a	n/a	Low	None	This Study
R7	IgM	Human		n/a	n/a	n/a	Low	None	This Study
mAb15	IgG	Human		n/a	n/a	n/a	Low	None	[84]
1710	IgG	Human		n/a	n/a	n/a	Low	None	[226]

Table 6.1: Classification of mAbs against N-CSP, repeat region, and C-CSP. mAb designation, original isotype (IgG vs. IgM; all mAbs used in this study were expressed as IgG_1), species (human vs. mouse), target antigen, BLI apparent avidity for select PfCSP 15mer repeat peptides (peptide 21 NPDPNANPNVDPNAN, peptide 22 NANPNVDPNANPNVD, peptide 29 NANPNANPNANPNAN), SPZ binding (none, low, high), SPZ neutralization (none, very low, low, moderate, high), and references used to classify mAbs. Undet., undetectable; n/a, not applicable.

6.4 Combinations of N-CSP and repeat mAbs

A previous study showed that 5D5 binds rPfCSP with high affinity but does not bind or neutralize SPZ, suggesting that the 5D5 epitope is inaccessible on native PfCSP[249]. Furthermore,

5D5 binds upstream of the proteolytic cleavage site in N-CSP[106,249] and the protease inhibitor E-64 has been shown to inhibit PfCSP cleavage[65]. Thus, I hypothesized that proteolytic cleavage of N-CSP limits the ability of 5D5 to bind SPZ by removing its target epitope on native PfCSP and that 5D5 SPZ binding might be enhanced by inhibiting cleavage using E-64 (**Figure 6.2A**).

To determine if 5D5 SPZ binding could be improved *in vitro*, flow cytometry was used to measure the binding of 5D5 to Pb-PfCSP-SPZ with or without E-64 (**Figure 6.2B**). Only ~19% of Pb-PfCSP-SPZ were bound by 5D5 at baseline, which increased to ~85% with the addition of E-64; furthermore, the MFI increased 7-fold from 241 to 1717. 5D5 Pb-PfCSP-SPZ binding without or with E-64 was measured across four independent experiments, which confirmed that E-64 significantly improved the binding of 5D5 to Pb-PfCSP-SPZ (**Figure 6.2C**), likely by inhibiting the cysteine protease responsible for cleaving PfCSP on the surface of SPZ[65].

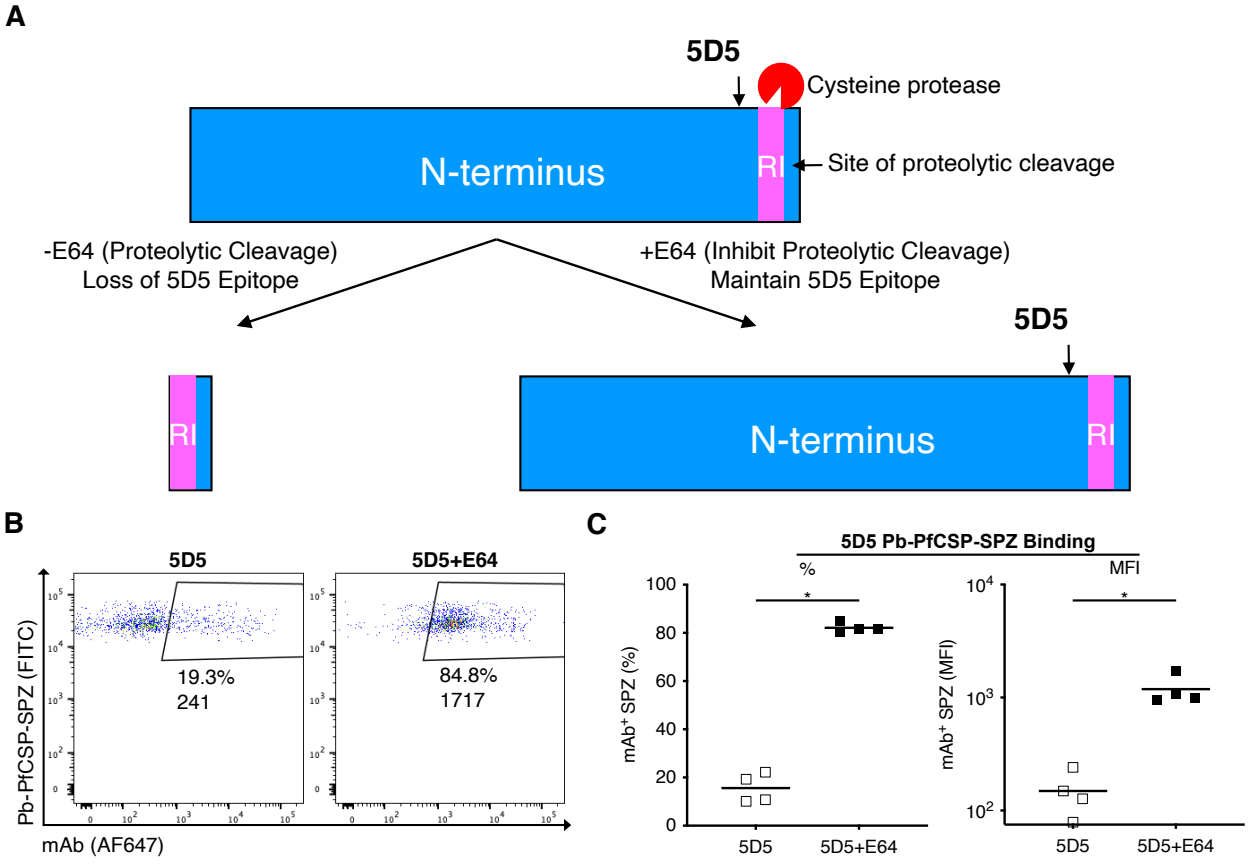

Figure 6.2: 5D5 binding to Pb-PfCSP-SPZ is improved by E-64-mediated inhibition of PfCSP proteolytic cleavage. (A) Schematic of the PfCSP N-terminus depicting the approximate epitope of 5D5 upstream of the proteolytic cleavage site in RI and the effect of E-64 on the availability of the 5D5 epitope for mAb binding. **(B)** Representative flow cytometry plots of Pb-PfCSP-SPZ incubated with 20 μg/mL 5D5, without or with 10 μM E-64. The percentage and MFI of mAb-bound Pb-PfCSP-SPZ is shown. **(C)** Effect of E-64 on the percentage and MFI of Pb-PfCSP-SPZ bound by 5D5 measured across four independent experiments. *P*-values were calculated using the two-tailed Mann Whitney test (*: $p<0.05$).

6.4.1 Development of an assay to measure mAb inhibition of N-CSP cleavage

The junctional mAb CIS43 has been shown to inhibit the proteolytic cleavage of PfCSP on PfSPZ likely due to steric hindrance, as the unique tetrapeptide NPDP bound by CIS43 is only three amino acids downstream of the RI cleavage site in N-CSP[84] (**Figure 6.1**). CIS43-mediated inhibition of PfCSP was determined by a previously reported pulse-chase assay that involves the metabolic labeling and immunoprecipitation of CSP from SPZ, which requires radioactive labeling and large amounts of SPZ (0.5-1.0 x 10^6 SPZ/condition)[65]. Having demonstrated that 5D5 binding to Pb-PfCSP-SPZ is improved by E-64-mediated inhibition of proteolytic cleavage, I next wanted to determine if repeat mAbs could also improve the Pb-PfCSP-SPZ binding of 5D5.

To measure repeat mAb-mediated inhibition of native PfCSP proteolytic cleavage on SPZ, a flow cytometry-based assay based on 5D5 binding was developed that required no radioactive labeling and only a few thousand SPZ/condition. Specifically, freshly dissected Pb-PfCSP-SPZ were incubated with unlabeled repeat mAb or E-64 for 1 hour, then with AF647-labeled 5D5 for 10 min (**Figure 6.3A**). As a control, 5D5-AF647 bound ~19% of Pb-PfCSP-SPZ without E-64 and ~83% with E-64 (**Figure 6.3B**), which was similar to Figure 6.2B-C. CIS43 exerted a dose-dependent potentiation of 5D5-AF647 binding (**Figure 6.3C**), with the lowest and

highest CIS43 concentrations mediating 5D5-AF647 binding that were respectively similar to the -E-64 and +E-64 baselines in Figure 6.3B.

To extend the analysis, the effect of a dose titration of CIS43 and eight other repeat mAbs on 5D5-AF647 Pb-PfCSP-SPZ binding was performed (**Figure 6.3D**). All mAbs except mAb26 exerted a dose-dependent potentiation of 5D5-AF647 binding, with the highest repeat mAb concentrations mediating 5D5-AF647 binding comparable to the +E-64 control and mAbs L9, mAb10, and MGU12 most potently improving 5D5-AF647 binding (EC_{50} = 1.09 – 1.23 µg/mL). mAb26 is a NANP-specific repeat mAb that was previously shown to be completely ineffective at preventing SPZ hepatocyte invasion *in vitro*[84], which likely contributes to its minimal effect in this 5D5-based binding assay. Importantly, the C-CSP-specific mAb15 and VRC01 had no effect on 5D5-AF647 binding above the -E-64 baseline. Together, these data demonstrate that 5D5 binding to Pb-PfCSP-SPZ is potently potentiated by co-incubation with most repeat mAbs *in vitro.*

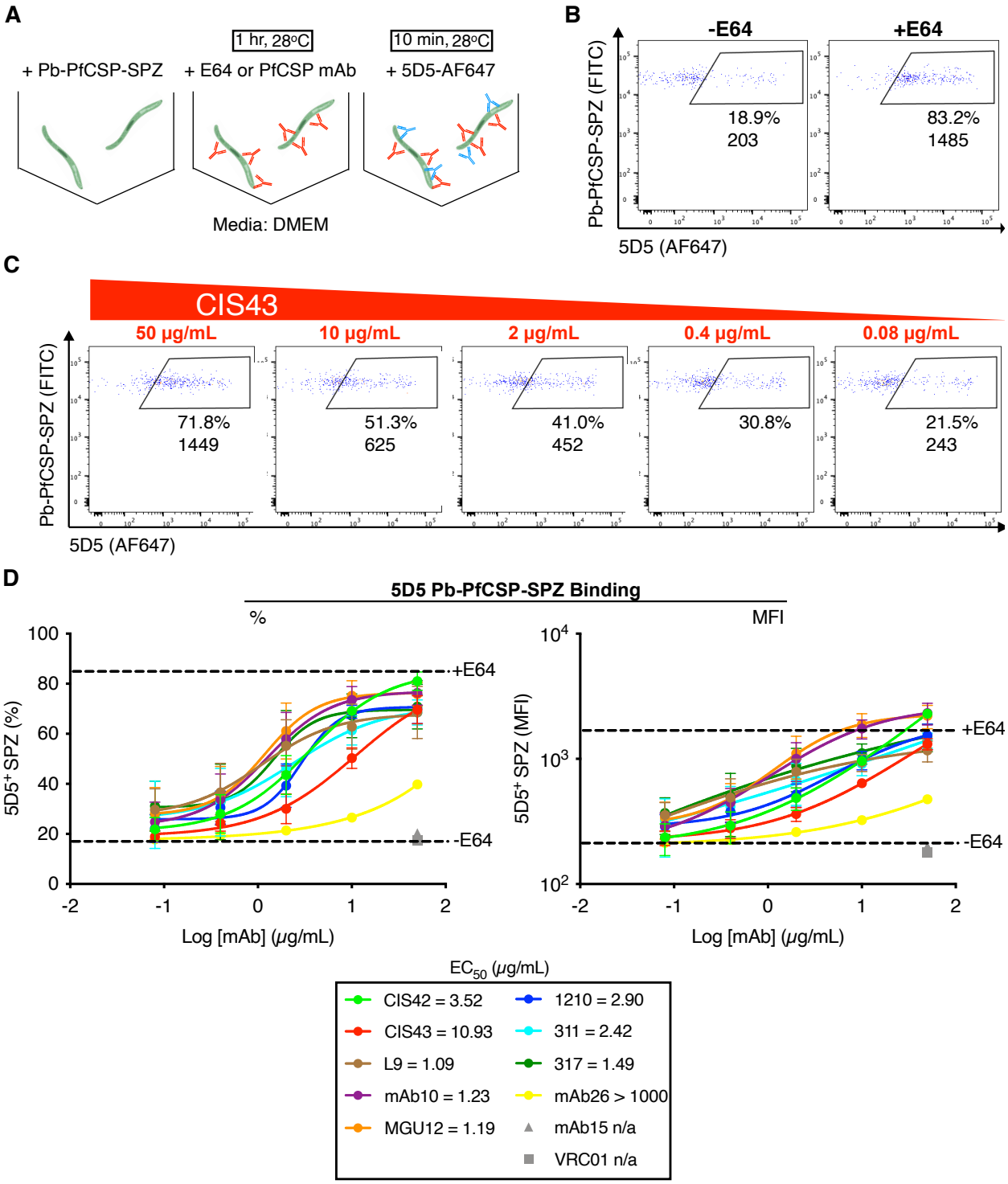

Figure 6.3: PfCSP repeat mAbs improve the binding of 5D5 to Pb-PfCSP-SPZ. (A) Experimental setup to measure 5D5-AF647 Pb-PfCSP-SPZ binding. Freshly dissected Pb-PfCSP-SPZ (8,000/well) are incubated for 1 hour at 28°C in media (DMEM) containing either 10 µM E-64 or varying concentrations of unlabeled PfCSP mAb; subsequently, Pb-PfCSP-SPZ are stained with 20 µg/mL 5D5-AF647 for 10 min at 28°C prior to fixation and flow cytometric

analysis. **(B)** Representative flow cytometry plots of Pb-PfCSP-SPZ incubated with 20 μg/mL 5D5-AF647 ± 10 μM E-64. The percentage and MFI of 5D5-bound Pb-PfCSP-SPZ is shown. **(C)** Representative flow cytometry plots of Pb-PfCSP-SPZ incubated with varying concentrations of unlabeled CIS43 (50-0.08 μg/mL) prior to staining with 20 μg/mL 5D5-AF647. The percentage and MFI of 5D5-bound Pb-PfCSP-SPZ is shown. **(D)** Improvement in 5D5-AF647 Pb-PfCSP-SPZ binding, measured as increasing percentages (left) or MFI (right) of $5D5^+$ SPZ, mediated by varying concentrations of unlabeled PfCSP mAbs. Data were combined from three independent experiments and are represented as mean and SEM. EC_{50} values for each unlabeled mAb is shown and were calculated using the $5D5^+$ SPZ percentage values; dotted lines were set at the geometric mean of the 5D5-AF647 ± E-64 controls from the three independent experiments.

It was previously shown that incubating SPZ with CSP repeat-specific mAbs triggers the CSPR, wherein repeat mAbs cross-link CSP on the surface of SPZ and cause the SPZ to shed their existing outer CSP coats and expose underlying new and uncleaved CSP molecules[98]. This phenomenon might confound the 5D5-AF647 flow cytometry assay detailed in Figure 6.3, as the repeat mAb-mediated improvement in 5D5-AF647 binding could be due to the repeat mAbs stripping off existing PfCSP molecules to reveal uncleaved PfCSP molecules that are then bound by 5D5-AF647. To determine if the CSPR affected 5D5 Pb-PfCSP-SPZ binding, the 5D5-AF647-based flow cytometry assay was repeated in the presence of the actin polymerization inhibitor cytochalasin D (CD), which was previously shown to inhibit the CSPR[98,263] (**Figure 6.4A**).

The addition of CD did not affect 5D5-AF647 Pb-PfCSP-SPZ binding, as 5D5-AF647 bound ~21% of Pb-PfCSP-SPZ without E-64 and ~76% with E-64 (**Figure 6.4B**) which was comparable to Figure 6.3B and Figure 6.2B-C. Similar to Figure 6.3C, CIS43 exerted a dose-dependent potentiation of 5D5-AF647 Pb-PfCSP-SPZ binding (**Figure 6.4C**), with the lowest and highest CIS43 concentrations mediating 5D5-AF647 binding that were respectively similar to the -E-64 and +E-64 baselines in Figure 6.4B.

Of the nine repeat mAbs in the panel, CIS42 and CIS43 most potently improved 5D5-AF647 binding to Pb-PfCSP-SPZ (**Figure 6.4D**). The other mAbs improved 5D5-AF647 binding only at the highest concentration (100 μg/mL), though still to a lesser degree than CIS42 and CIS43. These results are concordant with a previous report showing that CIS43 inhibits PfCSP cleavage on PfSPZ and that CIS42 binds the same junctional epitope NPDP as CIS43, albeit at a different angle[84]. Together, these data show that mAbs CIS42 and CIS43 (which preferentially target the junctional epitope adjacent to the PfCSP cleavage site in RI) potently improve 5D5-AF647 Pb-PfCSP-SPZ binding by preventing PfCSP cleavage and suggest that the 5D5-AF647 flow cytometry-based assay could be used as a simple, high-throughput assay for measuring PfCSP cleavage on SPZ.

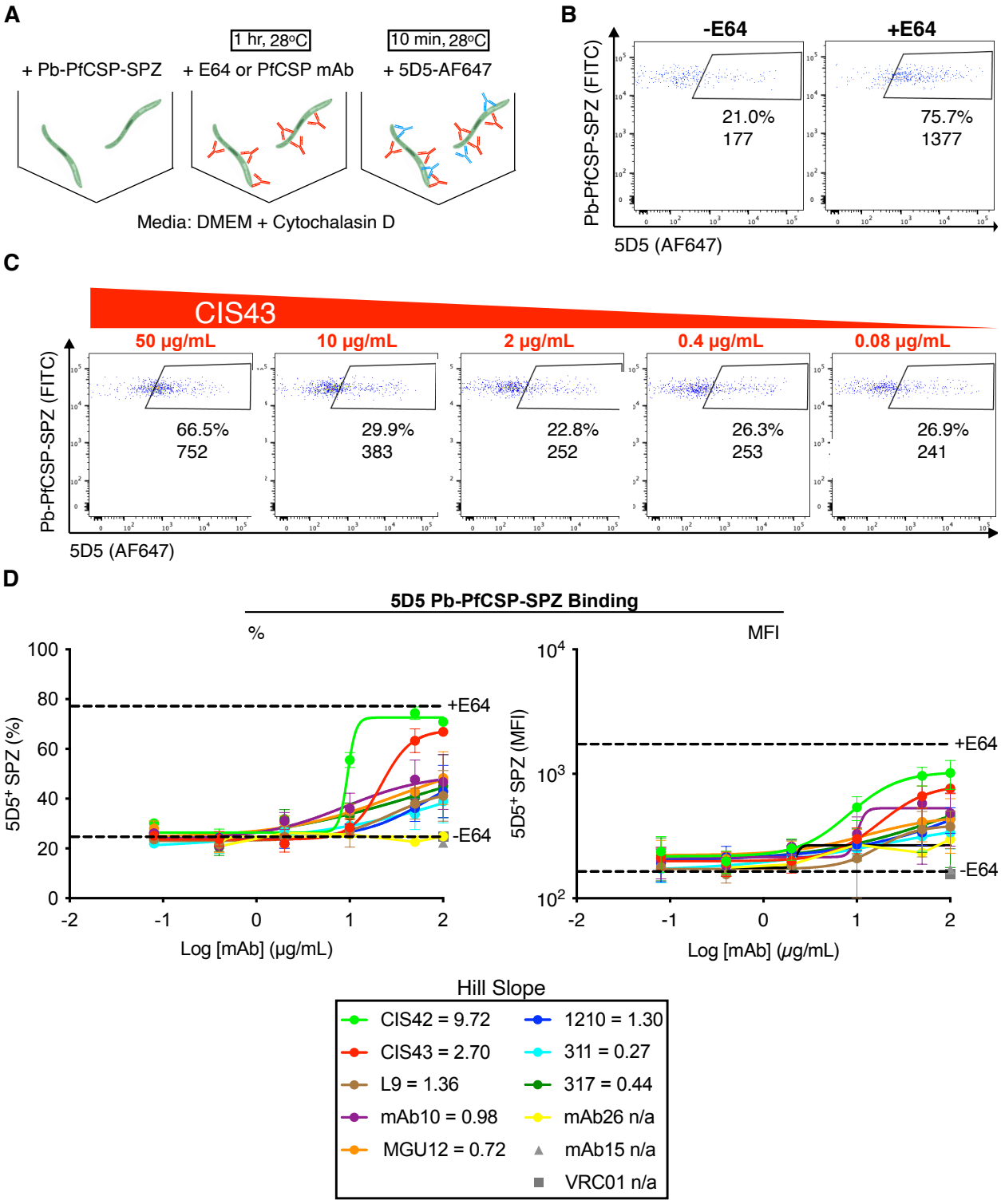

Figure 6.4: The PfCSP junctional mAbs CIS42 and CIS43 potently inhibit PfCSP cleavage on Pb-PfCSP-SPZ. (A) Experimental setup to measure PfCSP cleavage on SPZ. Freshly dissected Pb-PfCSP-SPZ (8,000/well) are incubated for 1 hour at 28ºC in media (DMEM + 0.5 µM cytochalasin D) containing either 10 µM E-64 or varying concentrations of unlabeled PfCSP

mAb; subsequently, Pb-PfCSP-SPZ are stained with 20 μg/mL 5D5-AF647 for 10 min at 28°C prior to fixation and flow cytometric analysis. **(B)** Representative flow cytometry plots of Pb-PfCSP-SPZ incubated with 20 μg/mL 5D5-AF647 ± 10 μM E-64. The percentage and MFI of 5D5-bound Pb-PfCSP-SPZ is shown. **(C)** Representative flow cytometry plots of Pb-PfCSP-SPZ incubated with varying concentrations of unlabeled CIS43 (50-0.08 μg/mL) prior to staining with 20 μg/mL 5D5-AF647. The percentage and MFI of 5D5-bound Pb-PfCSP-SPZ is shown. **(D)** Inhibition of PfCSP proteolytic cleavage on Pb-PfCSP-SPZ, measured as increasing percentages (left) or MFI (right) of $5D5^+$ SPZ, mediated by varying concentrations of unlabeled PfCSP mAbs. Data were combined from four independent experiments and are represented as mean and SEM. The hill slope for each unlabeled mAb is shown and were calculated using the $5D5^+$ SPZ percentage values; dotted lines were set at the geometric mean of the 5D5-AF647 ± E-64 controls from the four independent experiments.

6.4.2 *In vivo* protection of N-CSP and repeat mAb combinations

Having demonstrated that E-64 or PfCSP repeat mAbs improve the binding of 5D5 to Pb-PfCSP-SPZ, I next investigated whether combining E-64 or repeat mAbs with 5D5 would lead to improved protection against Pb-PfCSP-SPZ challenge in mice. Consistent with previous reports[171,249], passive transfer of 300 μg/mouse of humanized 5D5 and the original murine 5D5 both elicited no liver burden reduction in mice challenged IV with Pb-PfCSP-SPZ (**Figure 6.5A**). Furthermore, pre-incubating Pb-PfCSP-SPZ with 10 μM E-64 prior to IV challenge did not significantly improve 5D5 neutralization of E-64-treated Pb-PfCSP-SPZ (**Figure 6.5B**). These data show that treating Pb-PfCSP-SPZ with E-64 prior to IV challenge did not improve 5D5 neutralization *in vivo* despite improving 5D5 Pb-PfCSP-SPZ binding *in vitro*.

CIS42 and CIS43 were identified as the two repeat mAbs that most potently inhibited PfCSP cleavage and improved 5D5 Pb-PfCSP-SPZ binding (**Figure 6.4D**). To determine if these mAbs improved 5D5 neutralization *in vivo*, combinations of CIS42+5D5 or CIS43+5D5 were passively transferred into mice before IV challenge. Liver burdens in mice treated with CIS42+5D5 and CIS43+5D5 were not significantly different from mice treated with CIS42 and CIS43 alone (**Figure 6.5C**). To extend this analysis, I also tested two other repeat mAbs (mAb10

and MGU12) that most potently improved 5D5-AF647 Pb-PfCSP-SPZ binding without CD (**Figure 6.3D**). Similar to the CIS42+5D5 and CIS43+5D5 data, liver burdens in mice treated with mAb10+5D5 and MGU12+5D5 were not significantly different from mice treated with mAb10 and MGU12 alone (**Figure 6.5D**). Together, these data show that combining 5D5 with neutralizing repeat mAbs that target the junctional epitope or NANP repeat region does not enhance 5D5 neutralization against Pb-PfCSP-SPZ *in vivo* despite improving 5D5 binding to Pb-PfCSP-SPZ *in vitro*.

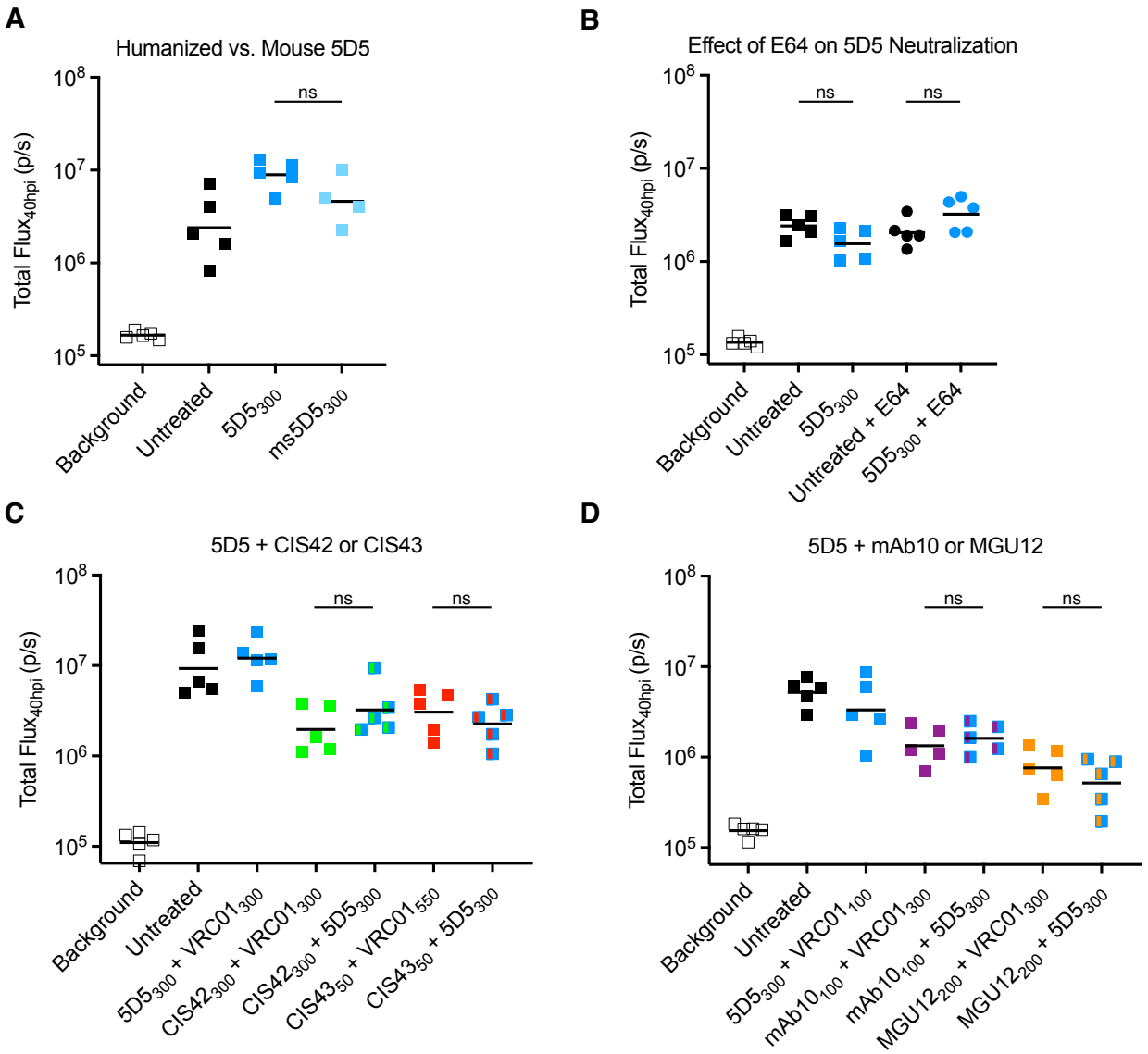

Figure 6.5: 5D5 neutralization is not improved by combination with E-64 or repeat mAbs *in vivo.* (A-C) Liver burden (bioluminescence; total flux, photons/sec) 40 hours post-infection (hpi; n=5/group, line indicates geometric mean) in mice challenged IV with 2,000 Pb-PfCSP-SPZ. Indicated mAb doses (μg) are written in subscripts under the mAb names; the anti-HIV-1 mAb VRC01 was used as an isotype control to normalize mAb doses. *P*-values were determined using the two-tailed Mann-Whitney test. ns (not significant), p>0.05. **(A)** Effect of humanized and original mouse 5D5 on Pb-PfCSP-SPZ. **(B)** Effect of 5D5 on E-64-treated Pb-PfCSP-SPZ. **(C)** Effect of combining CIS42 and CIS43 with 5D5. **(D)** Effect of combining 5D5 with mAb10 and MGU12.

6.4.3 Comparison of N-CSP mAb binding to PfSPZ and Pb-PfCSP-SPZ

To further validate the 5D5-AF647 flow cytometry assay's ability to report on PfCSP cleavage on the surface of SPZ, the ability of the mAb panel to improve 5D5 binding to wild-type PfSPZ was assessed. 5D5-AF647 demonstrated high (~90% and MFI of 1099) binding to PfSPZ without E-64; the addition of E-64 mediated only a modest increase to ~95% and MFI of 2020 (**Figure 6.6A**). 5D5 binding was virtually unperturbed by increasing amounts of the repeat mAbs in the panel across two independent experiments (**Figure 6.6B**), which was unsurprising given the marginal effect of E-64. 5D5 Pb-PfCSP-SPZ and PfSPZ binding without or with E-64 were compared across several different experiments, which confirmed that E-64 significantly improves 5D5 binding to Pb-PfCSP-SPZ but not PfSPZ (**Figure 6.6C**). Collectively, these data show that 5D5-AF647 has discrepantly high PfSPZ binding but low Pb-PfCSP-SPZ binding, suggesting that the flow cytometry-based 5D5-AF647 assay is not applicable to PfSPZ.

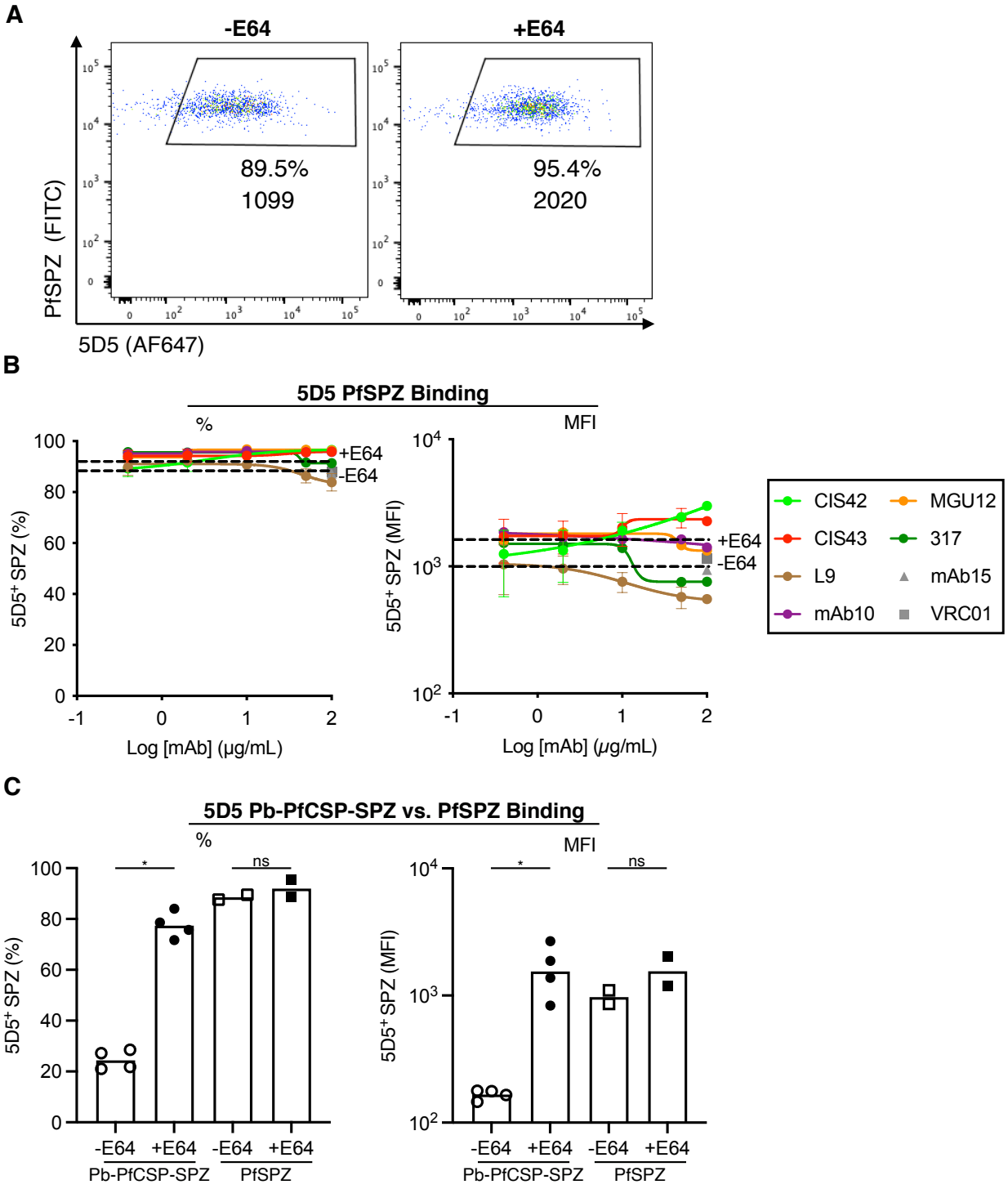

Figure 6.6: Comparison of 5D5-AF647 binding to PfSPZ and Pb-PfCSP-SPZ. (A) Representative flow cytometry plots of PfSPZ incubated with 20 µg/mL 5D5-AF647 ± 10 µM E-64 in DMEM + 0.5 µM CD. The percentage and MFI of 5D5-bound Pb-PfCSP-SPZ is shown. **(B)** Effect of varying concentrations of unlabeled repeat mAbs on the PfSPZ binding of 5D5-AF647, measured as percentages (left) and MFI (right) of $5D5^+$ SPZ. Data were combined from two independent experiments. **(C)** Comparison of the effect of E-64 on the percentage (left) and

MFI (right) of Pb-PfCSP-SPZ and PfSPZ bound by 5D5 measured across multiple independent experiments. *P*-values were calculated using the two-tailed Mann Whitney test (*: $p<0.05$; ns, $p>0.05$).

5 µg/mL soluble heparin, glycosaminoglycans that are more highly sulfated than HSPGs, have been shown to induce proteolytic cleavage of CSP on SPZ *in vitro*[66]. Hypothesizing that heparin could be used to induce cleavage of PfCSP on PfSPZ *in vitro* and thus decrease 5D5 binding, I measured the PfSPZ binding of 5D5 and several control PfCSP mAbs when co-incubated with heparin. Heparin did not alter the PfSPZ binding of 5D5, L9, and the C-CSP-specific mAb15 (**Figure 6.7A**). As a control, the binding of 5D5 to rPfCSP was unperturbed by heparin as measured by ELISA (**Figure 6.7B**). These data further substantiate that the N-CSP epitope recognized by 5D5 is available in PfSPZ but not in Pb-PfCSP-SPZ.

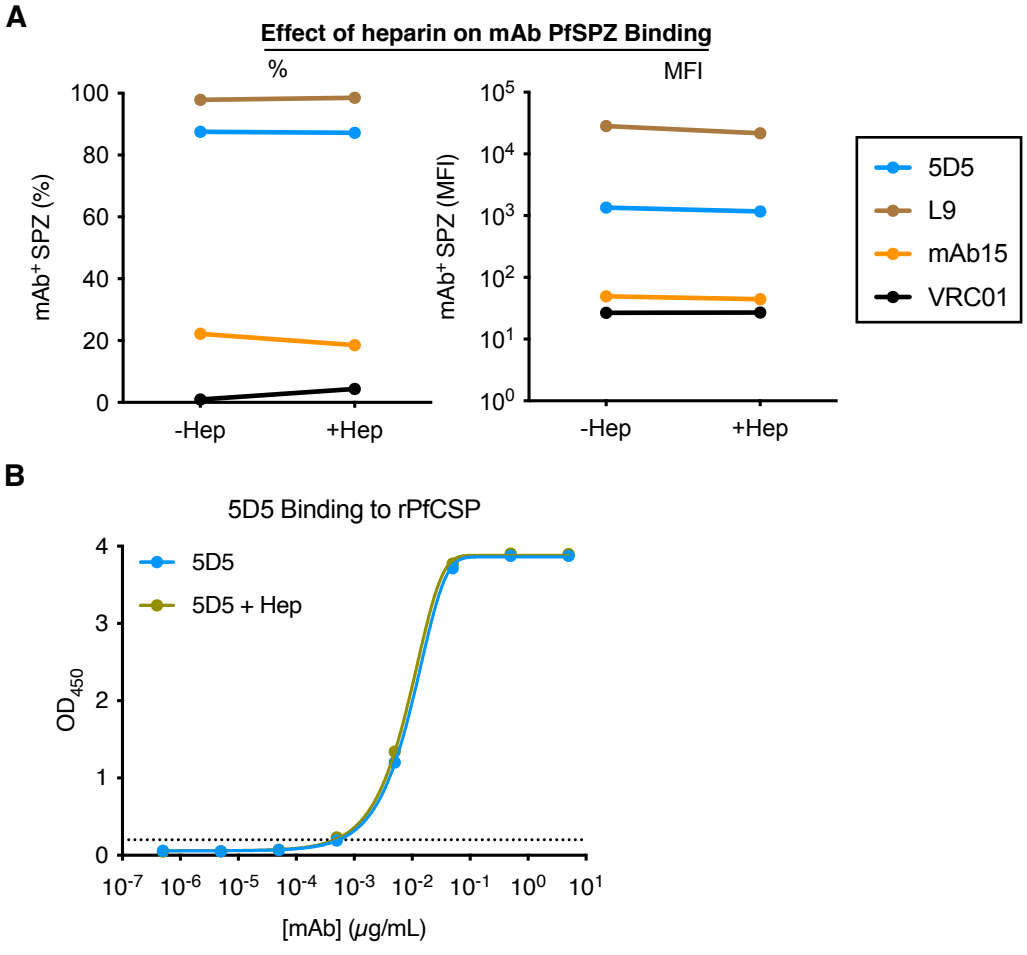

Figure 6.7: Effect of heparin on 5D5 binding to PfSPZ and rPfCSP. (A) Binding of indicated mAb (20 μg/mL) to PfSPZ without or with 5 μg/mL heparin, measured by flow cytometry and expressed as the percentage (left) and MFI (right) of mAb^+ PfSPZ. **(B)** Binding of varying concentrations of 5D5 to rPfCSP without or with 5 μg/mL heparin, determined by ELISA. OD_{450} is plotted.

6.5 Combinations of C-CSP mAbs and repeat mAbs

All C-CSP mAbs in the panel bound FL-rCSP and C-CSP, but not N-CSP or the 36mer repeat peptide $(NANP)_9$, by ELISA (**Figure 6.8A**). Notably, C-CSP was expressed in mammalian cells and only includes part of the linker sequence and the entire αTSR subdomain (**Figure 6.1**). To determine the fine epitopes recognized by these mAbs, mapping was performed using overlapping 15mer linear peptides spanning C-CSP. None of the C-CSP mAbs had detectable peptide binding by ELISA (**Figure 6.9**), corroborating that C-CSP mAbs recognize conformational C-CSP epitopes[226]. To extend this analysis, surface plasmon resonance (SPR) was used to perform epitope binning of the 13 C-CSP mAbs binding to FL-rCSP, with the N-CSP mAb 5D5 and the NANP-specific mAb10 included as controls (**Figure 6.8B**). The C-CSP mAbs fell broadly into three bins. Most mapped to the same bin as 1710, which binds an epitope overlapping the Th2R/Th3R T cell epitopes in the αTSR and is the only C-CSP mAb whose structure has been solved[226]. Notably, R2/R7 and L4 mapped to different bins. Together, these data indicate that most of the C-CSP mAbs compete for the same C-CSP epitope in the αTSR.

However, all C-CSP mAbs showed low *in vitro* binding to Pb-PfCSP-SPZ harvested from the salivary glands of mosquitoes (**Figure 6.8C**). Moreover, passive transfer of 300 μg of each C-CSP mAb into mice did not lower parasite liver burden following IV challenge with Pb-PfCSP-SPZ (**Figure 6.8D**). As a positive control, 300 μg/mouse of CIS43 lowered liver burden to background levels and completely protected mice from SPZ challenge. These data show that,

despite binding FL-rCSP, C-CSP-specific mAbs do not bind native PfCSP on salivary gland SPZ and are non-neutralizing *in vivo*.

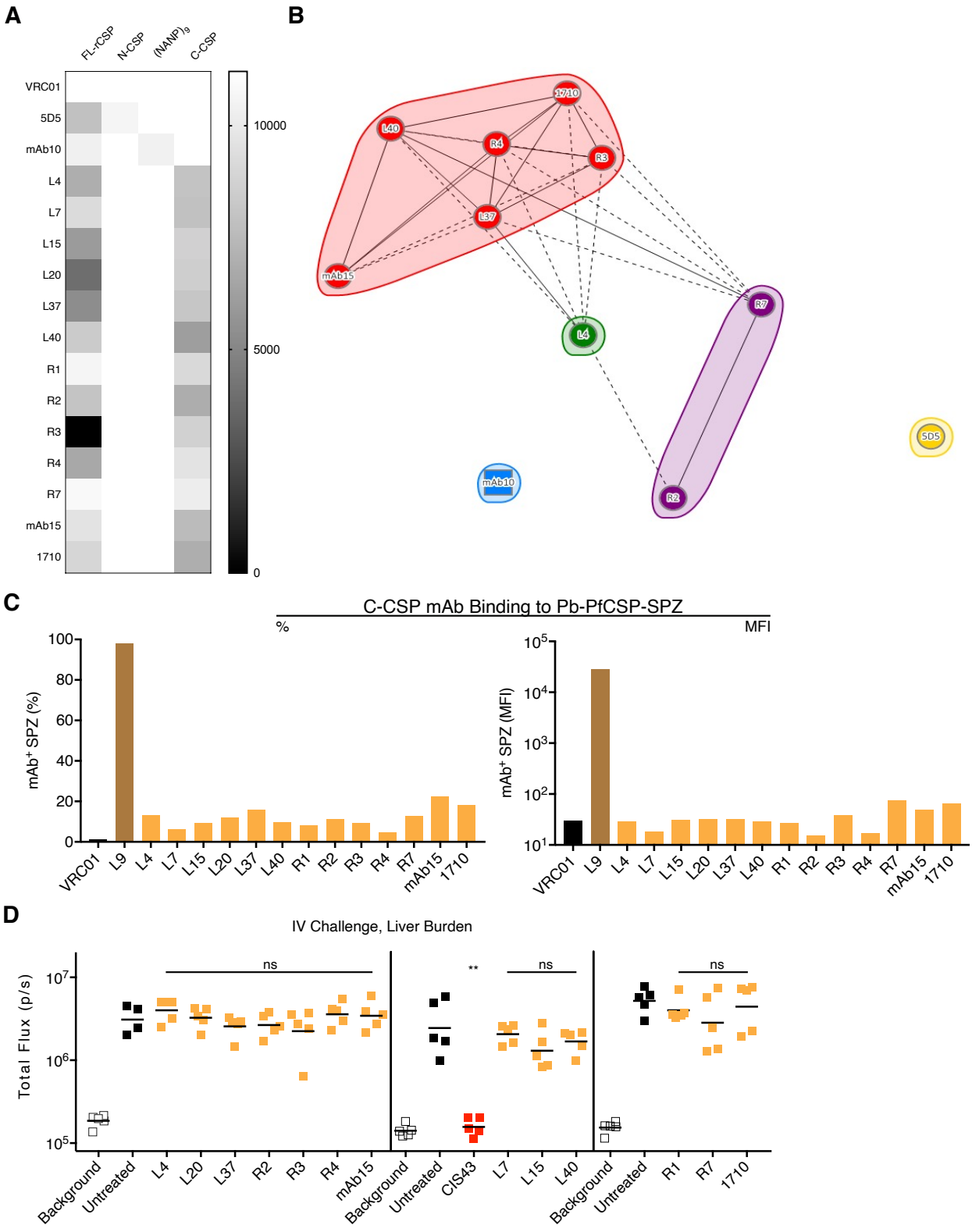

Figure 6.8: Binding and *in vivo* protection mediated by C-CSP-specific mAbs. (A) Heat map of AUC values of thirteen C-CSP mAbs binding to FL-rCSP, N-CSP, 36mer peptide $(NANP)_9$, and C-CSP by ELISA. VRC01 (anti-gp120 mAb), 5D5 (N-CSP mAb), and mAb10 (NANP-preferring repeat mAb) were respectively included as a negative isotype control, positive control N-CSP mAb, and positive control repeat mAb. Data were averaged from 2-3 independent experiments. **(B)** Epitope binning of C-CSP mAbs binding to FL-rCSP measured by SPR. All mAbs were tested as both ligands and analytes; several mAbs (L7, L15, L20, R1, mAb10) were excluded due to poor ligand and/or analyte binding to FL-rCSP. Solid lines indicate two-way competition; dotted lines indicate one-way competition. **(C)** Percentage and MFI of Pb-PfCSP-SPZ bound by 20 µg/mL of indicated mAb, measured by flow cytometry. VRC01 and L9 (NVDP-preferring repeat mAb) were included as negative and positive controls. **(D)** Liver burden (bioluminescence; total flux, photons/sec) in mice 40 hours post-challenge (n=5/group; line indicates geometric mean) mediated by 300 µg of indicated mAbs administered 2 hours before IV challenge with 2,000 Pb-PfCSP-SPZ. CIS43 (NPDP-preferring repeat mAb) was included as a positive control. Vertical lines separate independent experiments. *P*-values were determined by comparing mAbs to untreated control using the Kruskal-Wallis test with Dunn's post-hoc correction. **, $p<0.01$; ns (not significant), $p>0.05$.

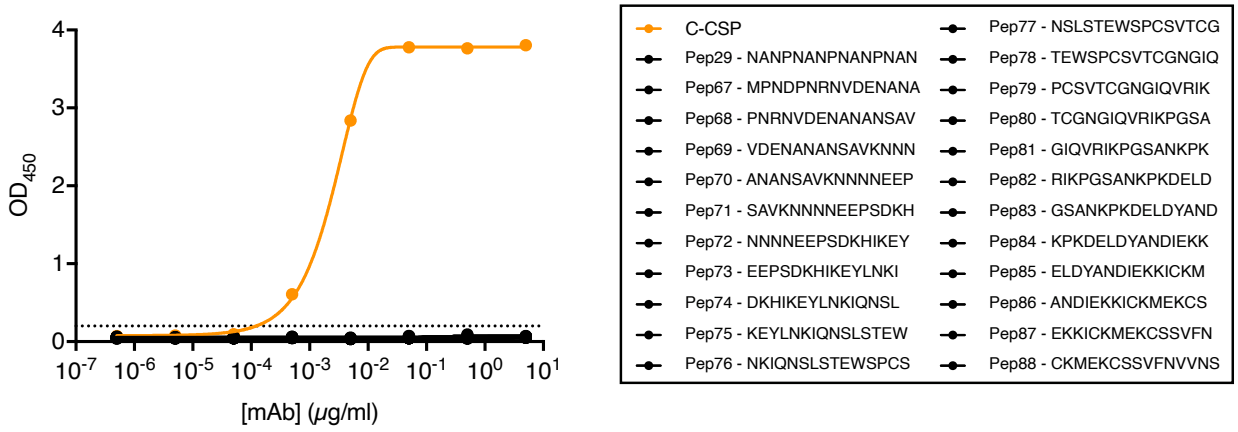

Figure 6.9: Peptide mapping of C-CSP mAbs. Binding of varying concentrations of thirteen pooled C-CSP-specific mAbs (L4 – 1710) to 15mer overlapping peptides numbered 67-88 as determined by ELISA. OD_{450} is plotted; peptide sequences are depicted. C-CSP and the NANP-containing peptide 29 were included as positive and negative controls, respectively.

6.5.1 Conformational changes in rPfCSP

It was previously reported that CIS43 binds to FL-rCSP in two steps with two affinities in a sequential fashion. Furthermore, it was hypothesized that the first high-affinity binding event caused conformational changes in FL-rCSP that enabled a second, lower affinity binding event to several other sites on FL-rCSP[84]. A subsequent study reported that mAbs L9, 311, and 317 also

exhibited a similar "two-step binding" phenotype to FL-rCSP[178]. Conformational changes should be accompanied by significant changes in enthalpy (ΔH) due to burial of hydrophobic amino acid residues away from water, which manifest as large and negative changes in heat capacity (ΔC_p)[264,265]. Thus, to assess if the binding of these four two-step binding mAbs induce conformational changes in FL-rCSP, ΔC_p for the binding of each mAb was determined by measuring ΔH at different temperatures (**Figure 6.10A**).

For the first binding step, large negative ΔC_p values were observed for 311 and CIS43 (ΔC_{p1} = -1.75 and -0.89 kcal/K/mol, respectively) while the values for L9 and 317 (ΔC_{p1} = -0.27 and -0.35 kcal/K/mol, respectively) were considerably smaller and closer to the magnitudes expected for binding events where only residues in the interacting surfaces contribute to the binding energetics (**Figure 6.10B**). The heat capacity changes associated with the second binding events (ΔC_{p2}) were modest for all four mAbs (ΔC_{p2} range = -0.02 to -0.25 kcal/K/mol). Taken together, these results suggest that, of the four two-step binding mAbs, only 311 and CIS43 induced significant conformational changes in FL-rCSP and only during the first binding step. These data are consistent with previous reports showing that 311, but not 317, Fabs induce a conformational change in the NANP repeats that cause rCSP to adopt an extended spiral conformation[53,79].

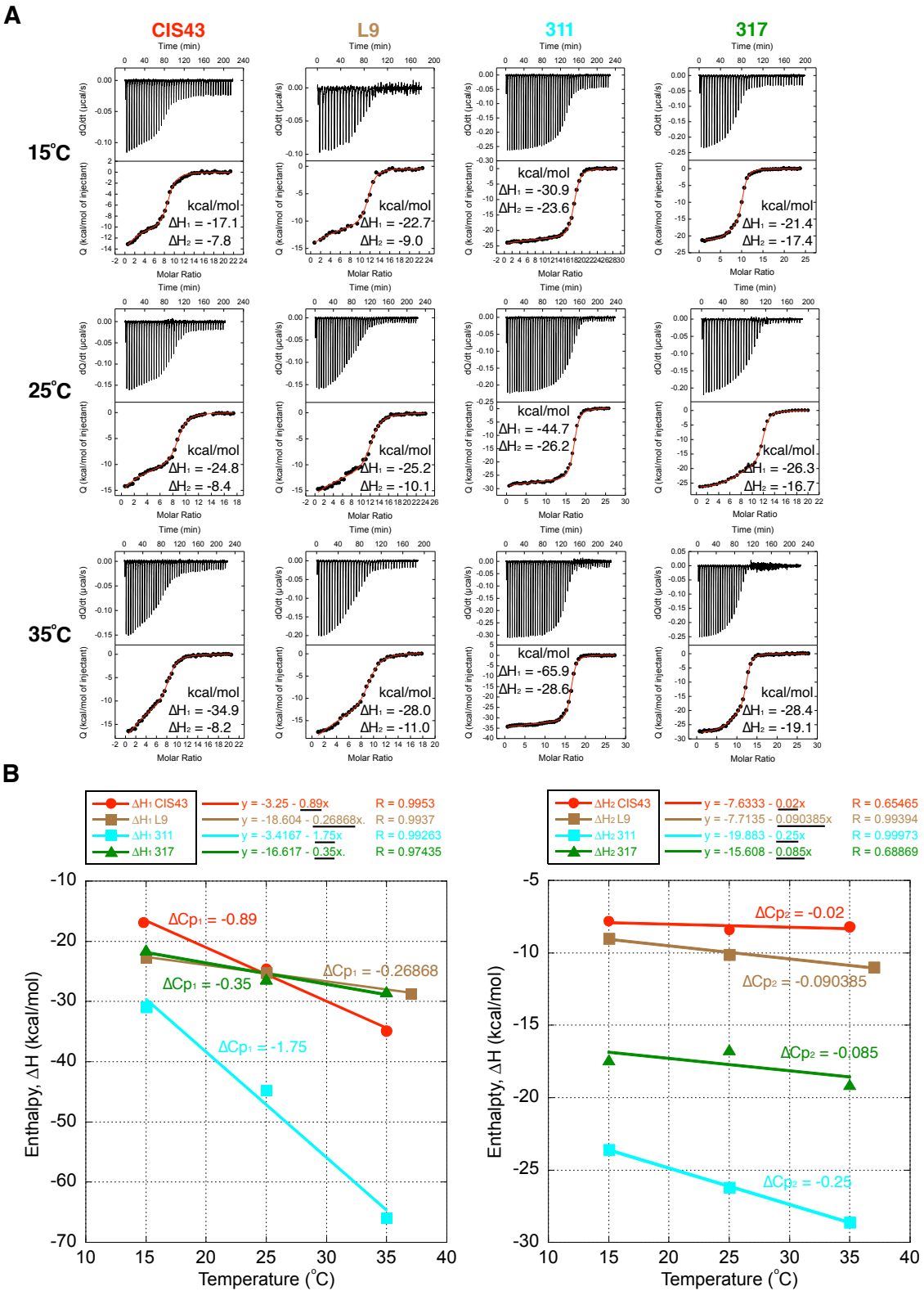

Figure 6.10: Conformational changes in FL-rCSP induced by CIS43, L9, 311, and 317. (**A**) ITC plots of CIS43, L9, 311, and 317 IgG binding to FL-rCSP at indicated temperatures (15-35°C).

Top, dQ/dt (change in heat flow, Q, as a function of time, t). Bottom, the integrated heat associated with each IgG injection shown as a function of the molar ratio between IgG antigen binding sites and FL-rCSP in the calorimetric cell. The red line represents the result from best nonlinear least squares fit of the data. Enthalpy values of the first and second binding events (ΔH_1 and ΔH_2, respectively) are shown. (**B**) Plots of the enthalpy changes ΔH as a function of temperature (15-35^{o}C) for the binding of each mAb to the first (ΔH_1, left panel) and second (ΔH_2, right panel) sets of sites, respectively. The equation of each line (y = mx + b) and correlation coefficient (R) are depicted. ΔCp associated with each binding event is equal to m (the slope of the line) and is underlined in the equation of the line and depicted in the plots for each mAb.

6.5.2 Conformational changes in native PfCSP on SPZ

Prior studies have suggested that CSP on SPZ isolated from mosquito salivary glands (SG) and midguts (MG) adopt two conformations, with C-CSP being masked ("closed" conformation) on SG SPZ and exposed ("open" conformation) on MG SPZ[67]. I hypothesized that C-CSP mAbs might differentiate between the "closed" and "open" conformations of PfCSP; thus, I compared the binding of several C-CSP mAbs to SG- and MG SPZ isolated from Pb-PfCSP-SPZ-infected mosquitoes. Consistent with Figure 6.8, all C-CSP mAbs showed low binding to "closed" PfCSP on SG SPZ (10-20% mAb^{+} SPZ) and increased binding to "open" PfCSP on MG SPZ (20-88% mAb^{+} SPZ), most notably mAb15 and L15 (**Figure 6.11A-B**). These data further substantiate the existence of distinct PfCSP conformations on MG versus SG SPZ[67] and suggest that C-CSP mAbs can be used to distinguish between native PfCSP conformations.

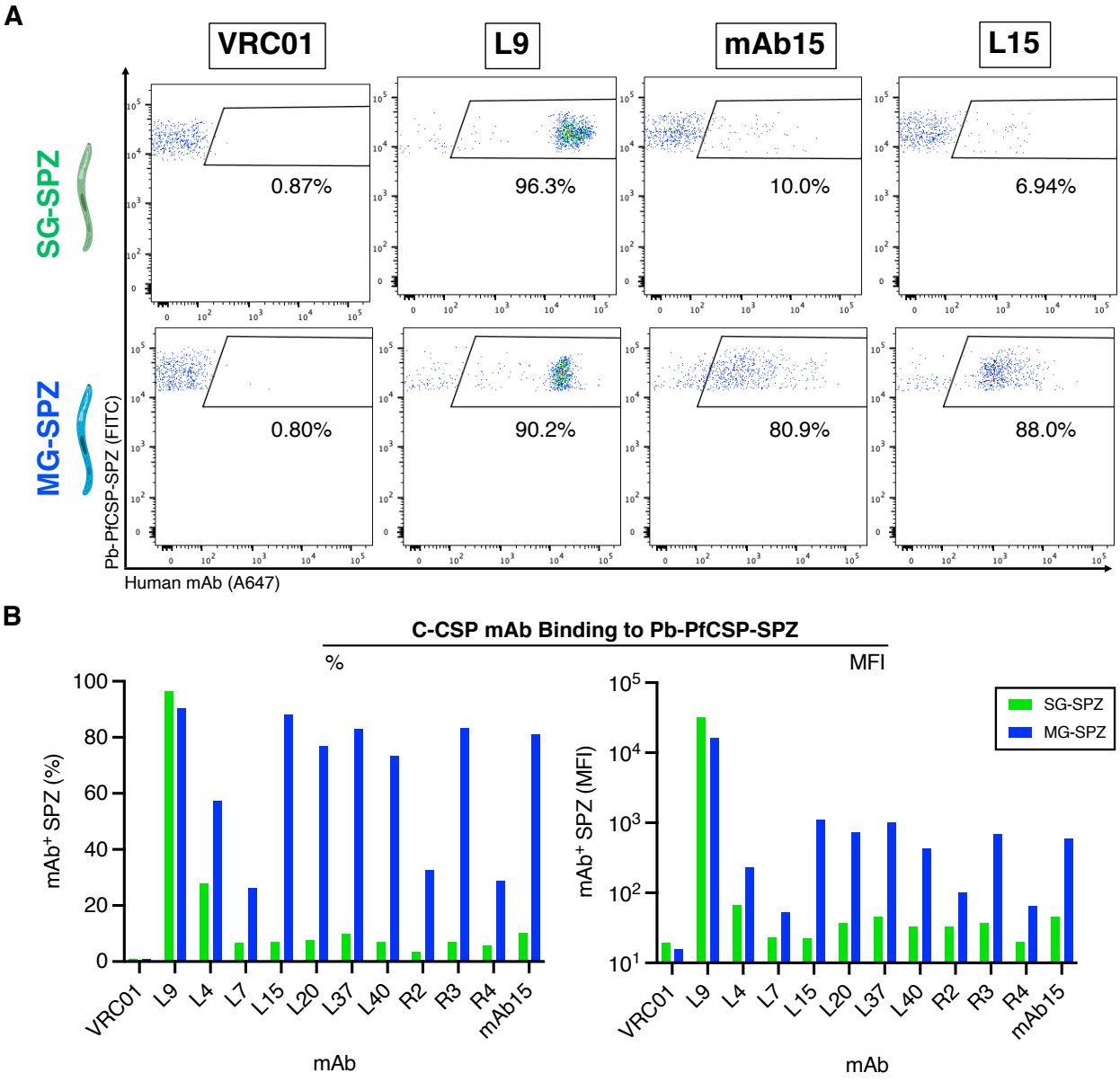

Figure 6.11: Binding of C-CSP mAbs to SG and MG Pb-PfCSP-SPZ. (A) Representative flow cytometry plots depicting 20 µg/mL of indicated mAb binding to Pb-PfCSP-SPZ harvested from the salivary glands (SG SPZ, green) or midguts (MG SPZ, blue) of mosquitoes. **(B)** Percentage and MFI of SG vs. MG Pb-PfCSP-SPZ bound by 20 µg/mL of indicated mAb, measured by flow cytometry. VRC01 and L9 (NVDP-specific repeat mAb) were included as negative and positive controls.

6.5.3 Development of an assay to measure changes in native PfCSP conformation

Having observed that certain repeat mAbs (311 and CIS43) can change the conformation of FL-rCSP, I hypothesized that the binding of repeat mAbs to SG SPZ might change the conformation of native PfCSP and improve C-CSP mAb binding. To test this, AF750-labeled mAb15 and L15, the two C-CSP mAbs that most clearly distinguished between the "open" vs. "closed" conformations of PfCSP on MG vs. SG SPZ (**Figure 6.11**), were used as reporters for the conformation of native PfCSP. SG Pb-PfCSP-SPZ or PfSPZ were co-incubated with unlabeled NPDP-, NVDP-, or NANP-preferring repeat mAbs of various potencies and either mAb15- or L15-AF750 before flow cytometry analysis (**Figure 6.12A-B**).

Remarkably, all nine repeat mAbs tested (including 311 and CIS43) comparably improved mAb15- and L15-AF750 SG SPZ binding from 10-20% to 80-90% mAb^+ SPZ, with a >100-fold increase in MFI (**Figure 6.12C**). The potentiation of C-CSP mAb binding was specific to repeat mAbs, as co-incubating mAb15- and L15-AF750 with the N-CSP mAb 5D5 did not alter their binding. Furthermore, mixing all the repeat mAbs in the panel (Repeat mAb Mix) to simulate a polyclonal response improved mAb15- and L15-AF750 binding comparably to each repeat mAb alone. PfCSP repeat mAb-mediated potentiation of C-CSP mAb SPZ binding was dose-dependent, as >4 μg/mL of the NANP-preferring mAb10 was required to maximally improve C-CSP mAb binding (**Figure 6.12D**).

It has been proposed that N-CSP masks C-CSP on SG SPZ and that proteolytic cleavage of N-CSP reveals C-CSP[68]. Thus, I tested whether the protease inhibitor E-64 affected C-CSP mAb SPZ binding. Adding E-64 did not significantly alter C-CSP mAb binding to either Pb-PfCSP-SPZ or PfSPZ when co-incubated with mAb10, suggesting that cleavage of N-CSP does not affect C-CSP accessibility to antibodies (**Figure 6.12E**). Collectively, these data show that

the binding of antibodies to the flexible repeat region potentiates the SG SPZ binding of C-CSP-specific mAbs, likely by changing the conformation of native PfCSP to unmask C-CSP.

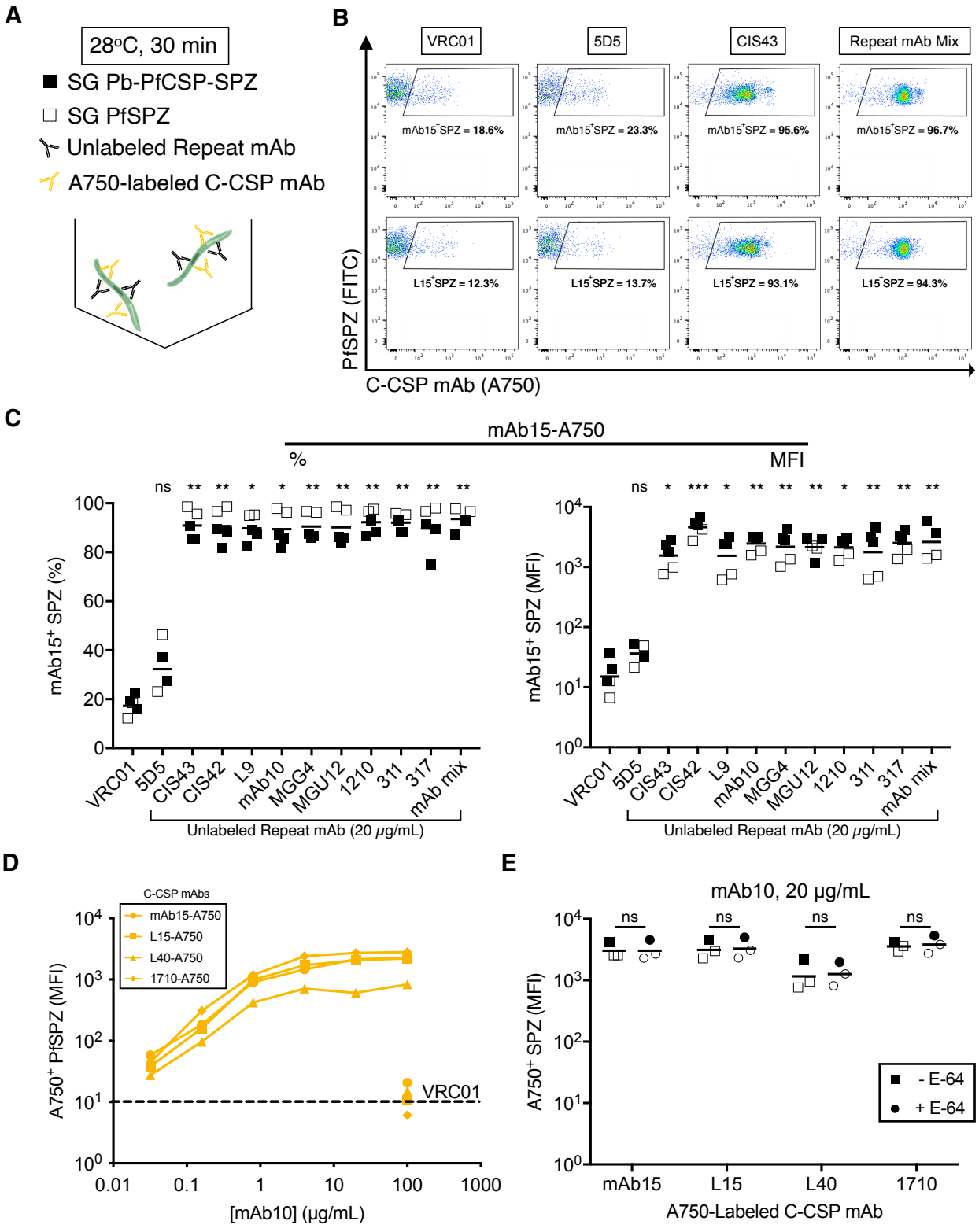

Figure 6.12: Effect of PfCSP repeat mAbs on C-CSP mAb SPZ binding. (A) Experimental schema for measuring the binding of AF750-labeled mAbs to SG Pb-PfCSP-SPZ or PfSPZ in the presence of unlabeled mAbs. **(B)** Representative flow cytometry plots depicting 20 μg/mL mAb15-AF750 (top panel) or L15-AF750 (bottom panel) binding to SG PfSPZ in the presence of 20 μg/mL unlabeled VRC01, 5D5, CIS43, and repeat mAb mix (mAb mix, CIS43-317 in C). Percentages of $mAb15^+$ or $L15^+$SPZ are shown. **(C)** Percentage and MFI of Pb-PfCSP-SPZ (filled squares) and PfSPZ (open squares) bound by 20 μg/mL mAb15-AF750 when co-incubated with 20 μg/mL of specified unlabeled mAb. *P*-values were determined by comparing PfCSP mAbs to VRC01 using the Kruskal-Wallis test. **(D)** Dose-dependent improvement in PfSPZ binding of four AF750-labeled C-CSP mAbs (20 μg/mL) mediated by increasing concentrations (0.032–100 μg/mL) of unlabeled NANP-preferring mAb10; 100 μg/mL unlabeled VRC01 was set as the baseline (dotted line). Data are representative of two independent experiments. **(E)** Binding of four AF750-labeled C-CSP mAbs (20 μg/mL) to Pb-PfCSP-SPZ (filled symbols) or PfSPZ (open symbols) when co-incubated with unlabeled mAb10 (20 μg/mL), with or without the protease inhibitor E-64 (squares, no E-64; circles, + E-64). *P*-values were determined by comparing -E-64 to +E-64 for each C-CSP mAb using a two-way ANOVA with Sidak's post-hoc correction. (C, E): ***, $p<0.001$; **, $p<0.01$; *, $p<0.05$; ns (not significant), $p>0.05$.

6.5.4 *In vivo* protection of C-CSP and repeat mAb combinations

The demonstration that repeat mAbs improve the SPZ binding of C-CSP mAbs *in vitro* (**Figure 6.12**) raised the possibility that repeat mAbs could act cooperatively with C-CSP mAbs to neutralize SPZ *in vivo*. To assess this, all C-CSP mAbs were combined with mAb10, a NANP-preferring repeat mAb that binds FL-rCSP in a single step[84] and improves C-CSP mAb SPZ binding comparably to all repeat mAbs tested (**Figure 6.12C**). Given the dose-dependent potentiation of C-CSP mAb SPZ binding by repeat mAbs (**Figure 6.12D**), I reasoned that selecting mAb10, which is not the most protective repeat mAb in the panel (**Table 6.1**), would allow for higher repeat mAb dosing in mice and thus might increase the chances of detecting *in vivo* cooperativity with C-CSP mAbs.

C-CSP mAb and mAb10 combinations were passively transferred into mice prior to IV challenge with Pb-PfCSP-SPZ. C-CSP mAbs were dosed at 300 μg/mouse while mAb10 was given at 100 μg/mouse, a dose that lowers liver burden to the midpoint of the assay's dynamic

range and thus enables detection of any additional protective effects attributable to each C-CSP mAb. VRC01 was included as an isotype control at 300 μg/mouse. None of the IV challenged mice treated with combinations of C-CSP mAbs and mAb10 had liver burdens that were significantly different from mice treated with mAb10+VRC01 (**Figure 6.13A**).

Since the skin is a major physiological site for CSP antibodies to neutralize SPZ[98,103], mice were then subjected to ID challenge. C-CSP mAbs were again dosed at 300 μg/mouse while the dose of mAb10 was lowered to 30-50 μg/mouse to account for the lower antibody threshold required to protect against ID challenge[178]. As in the IV challenge data, when compared to mAb10+VRC01 all C-CSP mAbs + mAb10 combinations did not significantly lower liver burden or subsequent parasitemia following ID challenge (**Figure 6.13B**).

Given the dependence of C-CSP mAbs on the conformation of PfCSP, I expanded the *in vivo* neutralization analysis to include the two-step binding mAbs CIS43 and 311, which both significantly changed the conformation of FL-rCSP by ITC (**Figure 6.10A**) and are more potent than mAb10 at lowering liver burden following IV challenge[178]. Combinations of CIS43 or 311 (50 μg/mouse) and mAb15 or L15 (300 μg/mouse) were passively transferred into mice prior to IV challenge. Liver burdens in mice treated with CIS43 or 311 + mAb15 or L15 combinations were similar to mice treated with CIS43 + VRC01 or 311 + VRC01 (**Figure 6.14A**). Collectively, these data show that the potentiation of C-CSP mAb SPZ binding by repeat mAbs *in vitro* did not translate into increased SPZ neutralization *in vivo*.

To determine if the SPZ binding of repeat mAbs was affected by the presence of mAbs targeting N- and C-CSP, Pb-PfCSP-SPZ or PfSPZ were co-incubated with 2 μg/mL AF750-labeled mAb10 or CIS43 and 100 μg/mL unlabeled C-CSP mAbs, 5D5, or VRC01. When compared to VRC01 + mAb10 or VRC01 + CIS43, none of the C-CSP mAbs in the panel or 5D5

significantly altered the SPZ binding of mAb10-AF750 (**Figure 6.13C**) or CIS43-AF750 (**Figure 6.14B**). These data suggest that the binding of mAbs to N- and C-CSP do not alter the SPZ binding of repeat mAbs *in vitro*.

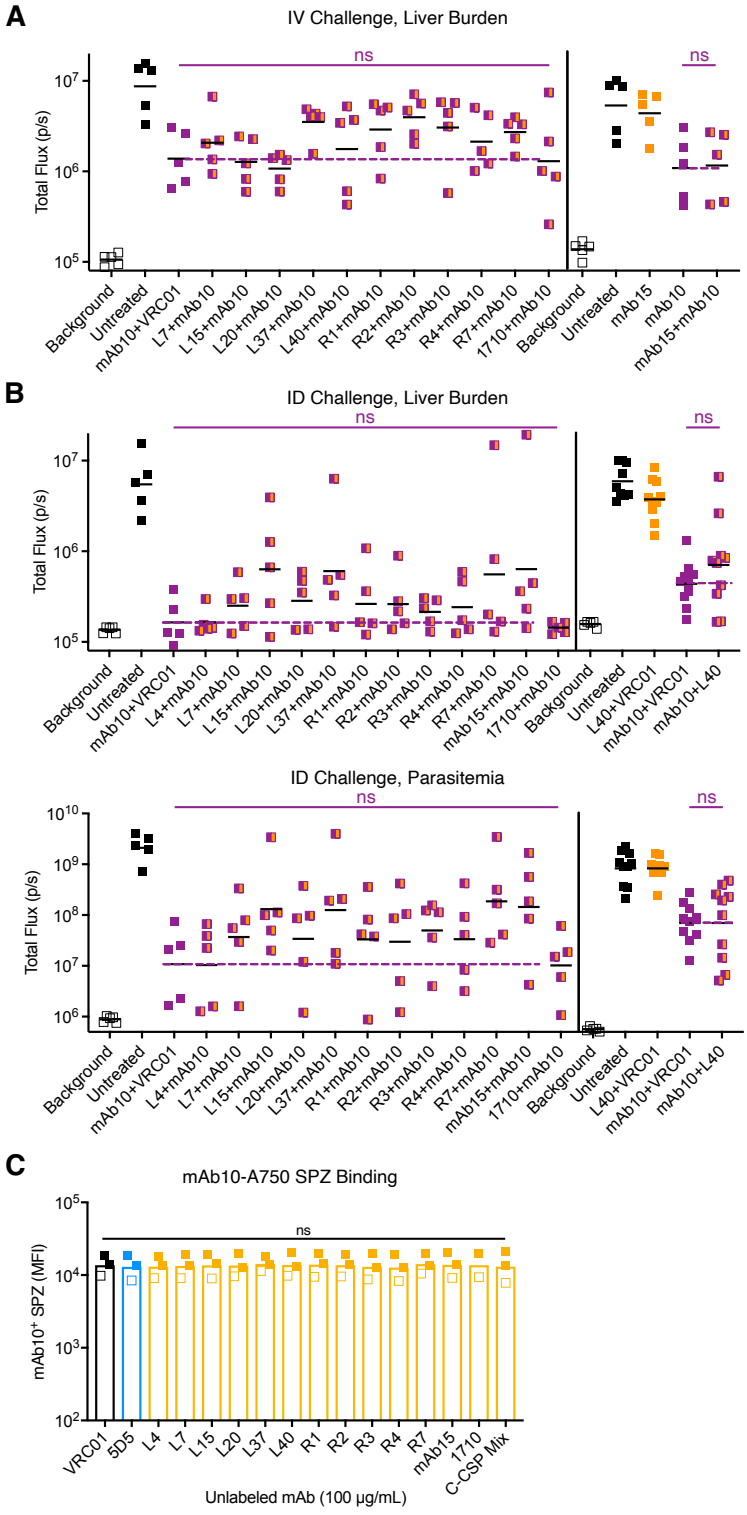

Figure 6.13: *In vivo* protection and binding mediated by mAb10 and C-CSP mAb combinations. (A) Liver burden in mice (n=5/group; line indicates geometric mean) 40 hours post-challenge mediated by indicated mAb combinations (mAb10, 100 µg; C-CSP mAbs or VRC01, 300 µg) administered 2 hours before IV challenge with 2,000 Pb-PfCSP-SPZ. **(B)** Liver burden (top) and parasitemia (bottom) in mice (n=5-10/group) respectively 40 hours and 5 days post-challenge mediated by indicated mAb combinations (mAb10, 50 µg in left experiment, 30 µg in right experiment; C-CSP mAbs or VRC01, 300 µg) administered 24 hours before ID challenge with 5,000 Pb-PfCSP-SPZ. (A-B): *P*-values were determined by comparing C-CSP mAb + mAb10 (orange/purple squares) to mAb10 + VRC01 (purple squares) using either the two-tailed Mann-Whitney test (2 comparisons) or the Kruskal-Wallis test with Dunn's post-hoc correction (>2 comparisons). Purple dotted lines were set at mAb10 + VRC01; vertical lines separate independent experiments. **(C)** MFI of Pb-PfCSP-SPZ (filled squares) and PfSPZ (open squares) bound by 2 µg/mL mAb10-AF750 when co-incubated with 100 µg/mL of specified unlabeled mAb. *P*-values were determined by comparing PfCSP mAbs to VRC01 using the Kruskal-Wallis test. (A-C): ***, p<0.001; **, p<0.01; *, p<0.05; ns (not significant), p>0.05.

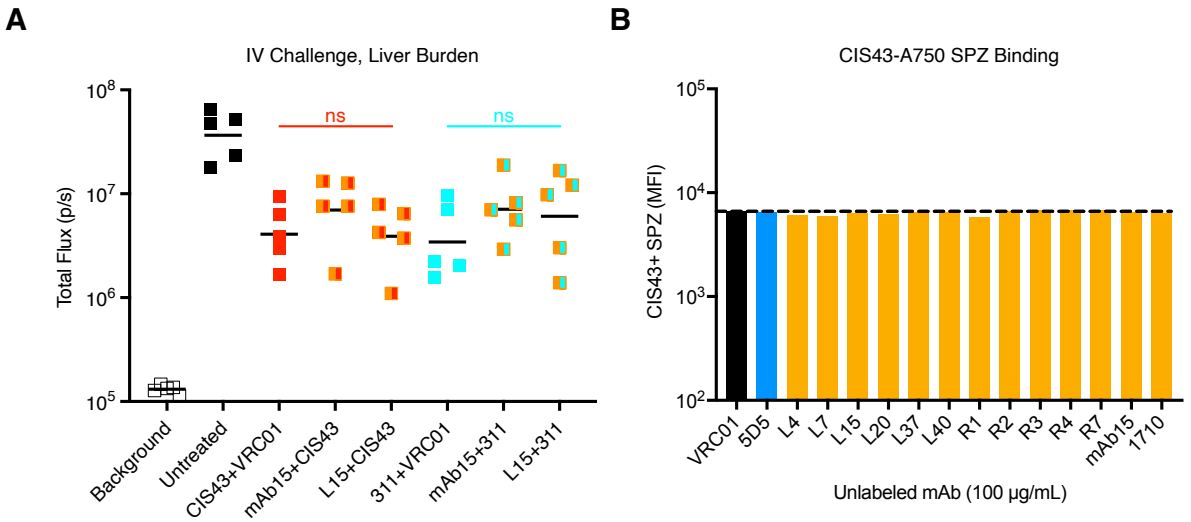

Figure 6.14: *In vivo* protection and binding mediated by CIS43/311 and C-CSP mAb combinations. (A) Liver burden in mice (n=5/group; line indicates geometric mean) 40 hours post-challenge mediated by indicated mAb combinations (CIS43 and 311, 50 µg; VRC01, mAb15, L15, 300 µg) administered 2 hours before IV challenge with 2,000 Pb-PfCSP-SPZ. *P*-values were determined by comparing repeat mAb + VRC01 to C-CSP mAb + repeat mAb using the Kruskal-Wallis test with Dunn's post-hoc correction. *, p<0.05; ns (not significant), p>0.05. **(B)** MFI of Pb-PfCSP-SPZ bound by 2 µg/mL CIS43-AF750 when co-incubated with 100 µg/mL of specified unlabeled mAb.

6.6 Combinations of mAbs against different tetrapeptides in the repeat region

Having determined that C-CSP mAbs do not neutralize Pb-PfCSP-SPZ *in vivo* alone or in combination with repeat mAbs, I next focused on assessing whether combining protective mAbs

targeting the three types of tetrapeptides in the PfCSP repeat region offered improved protection compared to each repeat mAb alone. CIS43, L9, and 317 are highly potent human PfCSP mAbs respectively classified as NPDP-, NVDP-, and NANP-preferring repeat mAbs (**Table 6.1**)[178]. Furthermore, CIS43 and L9 are currently in clinical trials for malaria prophylaxis.

To assess whether combining these potent mAbs cooperatively improved protection against IV challenge, CIS43, L9, and 317 were tested alone at doses of 50 μg/mouse (a dose that results in breakthrough infection) and in combination with VRC01 or each other (25+25 μg/mouse per mAb) (**Figure 6.15A**). Liver burdens in mice that received PfCSP mAb combinations were not significantly different than mice that received single mAbs or both respective PfCSP mAb + VRC01 controls. To extend this analysis, I tested CIS43, L9, and 317 combinations across a range of doses (100, 50, and 25 μg/mouse; **Figure 6.16A-C**). Concordant with Figure 6.15A, the mAb combinations largely provided protection that was comparable to single mAbs.

Given the proximity of the different tetrapeptides to each other in the PfCSP repeat region and the promiscuous binding of repeat mAbs to peptides composed of all three tetrapeptides[178,228], I hypothesized that CIS43, L9, and 317 might compete with each other to bind PfCSP repeat epitopes on SPZ. To test this hypothesis, AF750-labeled L9 binding to Pb-PfCSP-SPZ was measured in the presence of varying concentrations of unlabeled CIS43, L9, and 317. All three mAbs reduced L9-AF750 SPZ binding, with CIS43 showing the greatest degree of antagonism (**Figure 6.15B**). Together, these data show that combining highly potent NPDP-, NVDP-, and NANP-preferring repeat mAbs does not provide improved *in vivo* protection compared to each mAb alone and that even mAbs which preferentially recognize distinct tetrapeptides compete for PfCSP repeat epitopes on SPZ.

As combining protective and non-protective mAbs has been shown to synergistically neutralize PfMZ[266], I also assessed whether combining L9 with three poorly neutralizing NPDP-, NVDP-, and NANP-preferring mAbs (CIS42, F10, and mAb4 respectively; **Table 6.1**) would result in improved protection compared to L9 alone. L9 alone was significantly more protective than L9+CIS42 and L9+F10 and provided protection comparable to L9+mAb4 (**Figure 6.15C**). As in Figure 6.15B, CIS42, F10, and mAb4 all lowered L9-AF750 SPZ binding, with CIS42 mediating the greatest reduction (**Figure 6.15D**). As with mAb10-AF750 and CIS43-AF750 (**Figures 6.13C, 6.14B**), L9-AF750 SPZ binding was not significantly affected by 5D5 or all C-CSP mAbs tested (**Figure 6.15E**). Collectively, these data confirm that combining mAbs targeting different repeat epitopes does not offer improved protection *in vivo* and that mAbs directed against the repeat region, but not N- or C-CSP, antagonize the binding of other repeat mAbs.

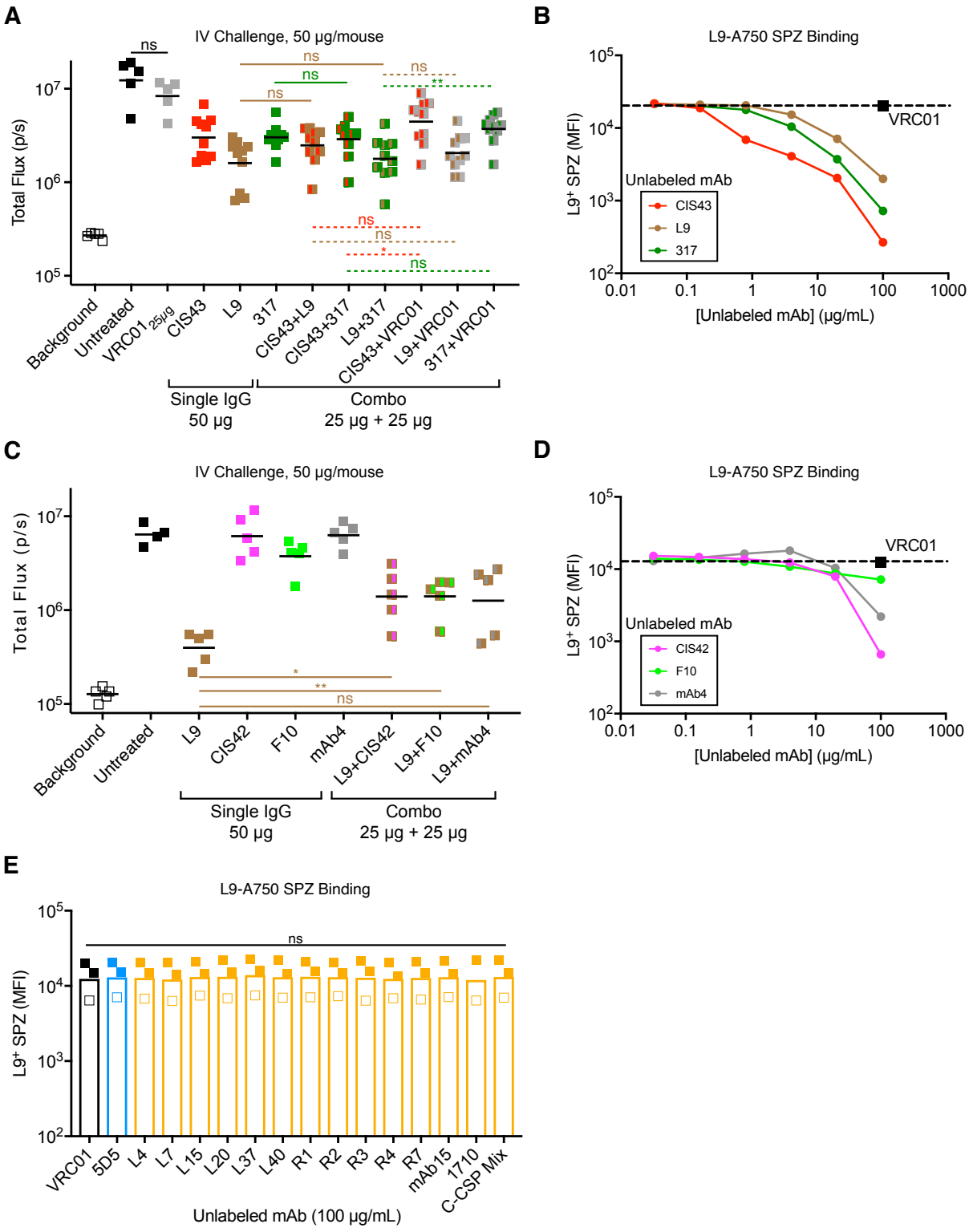

Figure 6.15: *In vivo* protection and binding of PfCSP repeat mAb combinations. (A) Liver burden in mice 40 hours post-challenge (n=10/group) mediated by CIS43, L9, and 317 alone (50 µg) and in combination with each other or isotype control VRC01 (25+25 µg) administered 2 hours before IV challenge with 2,000 Pb-PfCSP-SPZ. *P*-values were determined by comparing

PfCSP mAb combinations to L9 or 317 alone using the two-tailed Mann-Whitney test (solid lines) or PfCSP mAb combinations to their respective PfCSP mAb + VRC01 controls using the Kruskal-Wallis test (dotted lines). **(B)** MFI of Pb-PfCSP-SPZ bound by 2 µg/mL L9-AF750 when co-incubated with varying concentrations (0.032–100 µg/mL) of unlabeled CIS43, L9, or 317. **(C)** Liver burden in mice 40 hours post-challenge (n=5/group) mediated by L9, CIS42, F10, and mAb4 alone (50 µg) and in combination (25+25 µg) administered 2 hours before IV challenge with 2,000 Pb-PfCSP-SPZ. *P*-values were determined by comparing mAb combinations to L9 alone using the two-tailed Mann-Whitney test. **(D)** MFI of Pb-PfCSP-SPZ bound by 2 µg/mL L9-AF750 when co-incubated with varying concentrations (0.032–100 µg/mL) of unlabeled CIS42, F10, or mAb4. **(E)** MFI of Pb-PfCSP-SPZ (filled squares) and PfSPZ (open squares) bound by 2 µg/mL L9-AF750 when co-incubated with 100 µg/mL of specified unlabeled mAb. *P*-values were determined by comparing PfCSP mAbs to VRC01 using the Kruskal-Wallis test. (A, C): lines represent geometric mean. (B, D): dotted lines represent L9-AF750 co-incubated with 100 µg/mL unlabeled VRC01; data are representative of two independent experiments. (A, C, E): ***, p<0.001; **, p<0.01; *, p<0.05; ns (not significant), p>0.05.

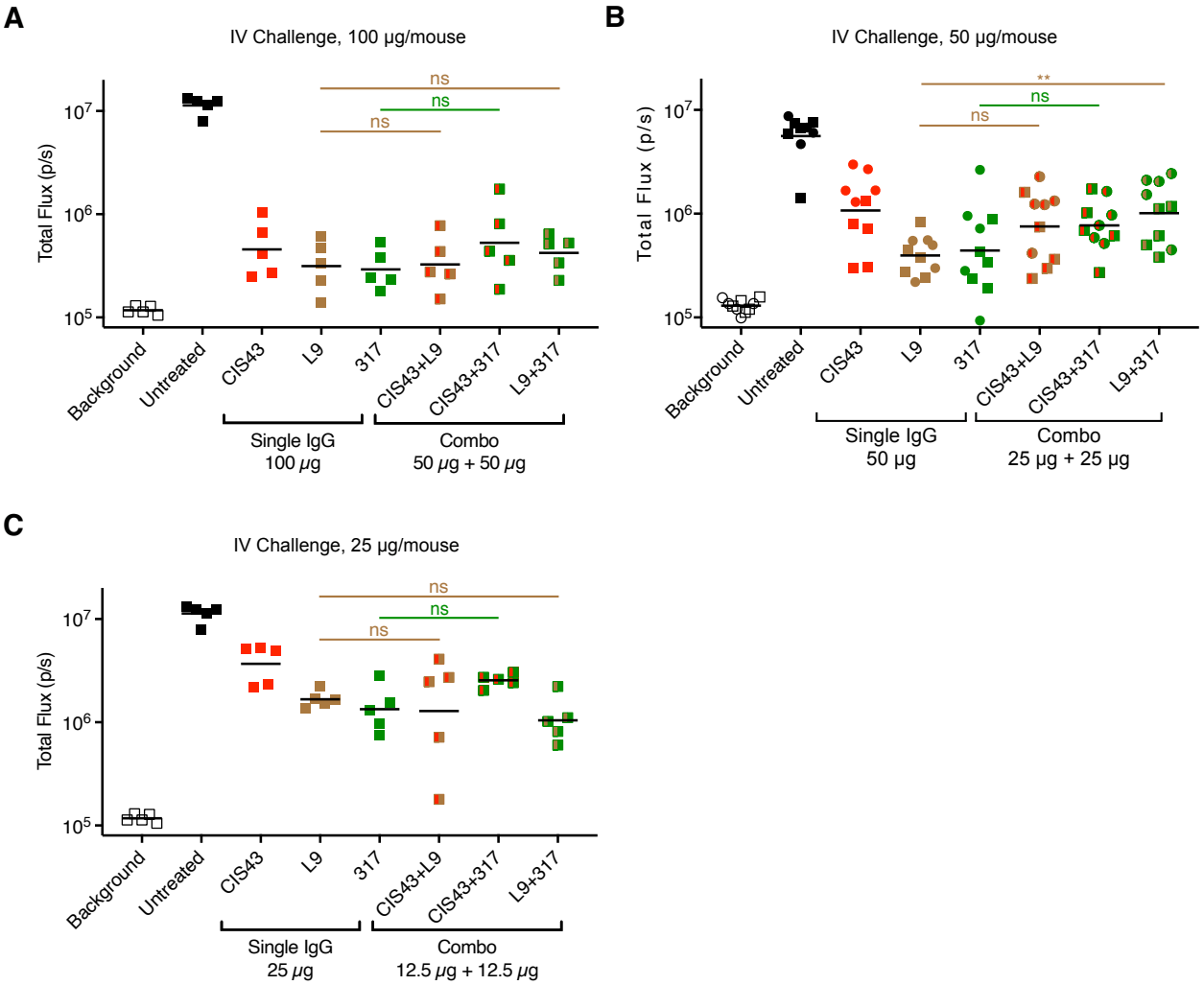

Figure 6.16: *In vivo* protection of CIS43, L9, and 317 mAb titration combinations. (A-C) Liver burden 40 hours after IV challenge with 2,000 Pb-PfCSP-SPZ in mice (n=5-10/group; 50μg data in B was combined from two experiments represented by circles and squares) that received CIS43, L9, and 317 alone (A, 100 μg; B, 50 μg; C, 25 μg) or in combination (A, 50+50 μg; B, 25+25 μg; C, 12.5+12.5 μg). Black lines represent geometric mean. *P*-values were determined by comparing mAb combinations to L9 or 317 alone using the two-tailed Mann-Whitney test. ***, $p<0.001$; **, $p<0.01$; *, $p<0.05$; ns (not significant), $p>0.05$.

6.7 Combining active-and-passive immunization with PfCSP vaccines and mAbs

Since the SPZ binding of repeat mAbs is antagonized by other repeat mAbs (**Figure 6.15B,D**) but not N- or C-CSP mAbs (**Figures 6.13C, 6.14B, 6.15E**), I next determined how a polyclonal PfCSP antibody response would affect the SPZ binding of repeat mAbs. The Pb-PfCSP-SPZ binding of AF750-labeled CIS43, L9, or 317 was assessed in the presence of serum pooled from ten naïve mice immunized three times with R21 (virus-like particles composed of 19 NANP repeats and C-CSP fused to a single hepatitis B surface antigen[210]), fifteen naïve US adults immunized three times with irradiated PfSPZ[267], and ten children or adults with the highest FL-rCSP titers from a cohort of 768 Malian volunteers naturally exposed to malaria[171]. Serum from a malaria-naïve US adult was included as a negative control.

While malaria-naïve serum had no effect on mAb binding compared to buffer alone, serum from vaccinated or malaria-exposed individuals significantly decreased mAb binding to SPZ. Serum from R21-vaccinated mice exerted the greatest antagonistic effect, with CIS43 showing the greatest binding reduction (**Figure 6.17A**). The antagonistic effect of R21 vaccine serum was likely due to its higher overall FL-rCSP titers compared to serum from the PfSPZ vaccine or natural exposure groups (**Figure 6.17B**). These data show that polyclonal PfCSP antibody responses compete with repeat mAbs for native PfCSP binding sites on SPZ *in vitro*.

To extend the analysis, I used a combined active-and-passive immunization approach to assess *in vivo* protection in mice vaccinated with R21 that also received CIS43, L9, or 317 prior to IV challenge (**Figure 6.17C**). Importantly, mice received a dose of R21 that lowered liver burden to the approximate midpoint of the assay's dynamic range. R21-vaccinated mice that received 150 μg/mouse of mAb had significantly lower liver burdens than mice that received R21 alone, but not mAb alone (**Figure 6.17D**). These data suggest that R21-induced polyclonal antibodies did not significantly perturb mAb-mediated protection *in vivo* despite competing for SPZ binding *in vitro* (**Figure 6.17A**).

Notably, when the mAb dose was lowered to 50 μg/mouse (**Figure 6.17E**) R21-vaccinated mice that received 50 μg of CIS43 or L9 had significantly lower liver burdens than naïve mice that only received 50 μg of each mAb while mice that received R21+317 trended towards lower liver burden than mice that received 317 only. When compared to mice that received R21 only, mice that received R21+L9 and R21+317 had significantly lower liver burden while mice that received R21+CIS43 trended towards lower liver burden. Furthermore, lowering the mAb dose to 25 μg/mouse (**Figure 6.17F**) largely confirmed the 50 μg/mouse data, with the R21+mAb combinations providing greater protection than mAb alone and trending towards greater protection than R21 alone. Together, these data show that potent repeat mAbs act cooperatively with vaccine-induced polyclonal PfCSP antibody responses against the repeat region and C-CSP to provide improved protection against SPZ challenge in mice despite competing for native PfCSP epitopes on SPZ.

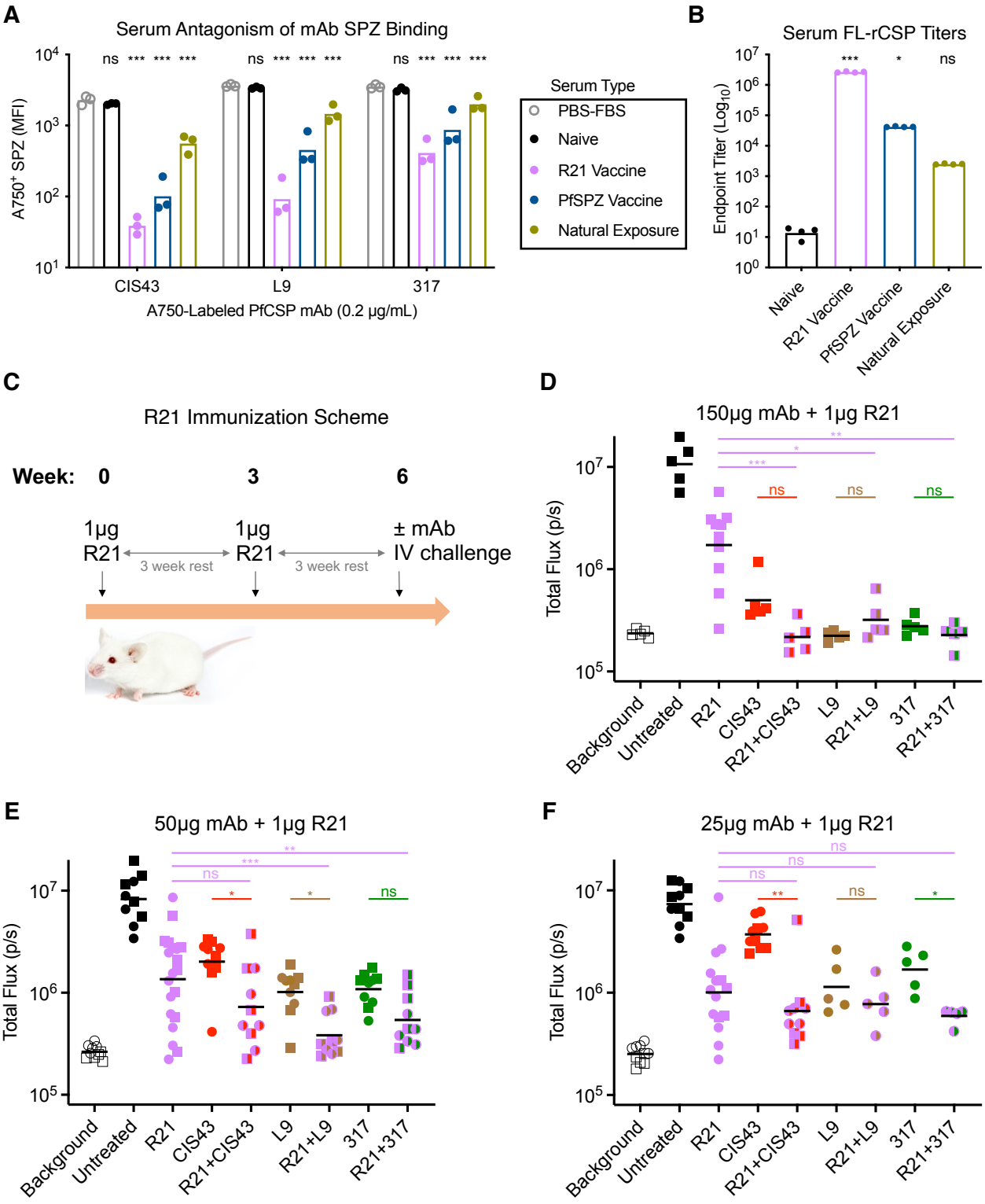

Figure 6.17: Binding and *in vivo* protection from combining PfCSP repeat mAbs and vaccines. (A) MFI of Pb-PfCSP-SPZ bound by 0.2 µg/mL CIS43-, L9-, or 317-AF750 when co-incubated with 10% PBS-FBS or 1:5 diluted serum pooled from either one naïve US adult volunteer, ten naïve mice immunized 3x with 1 µg R21 + adjuvant, fifteen naïve US adults immunized three times with $9x10^5$ irradiated PfSPZ, and ten Malian children/adults naturally

exposed to malaria. For each PfCSP repeat mAb, *P*-values were determined by comparing each serum type to the PBS-FBS control using a two-way ANOVA with Bonferroni's post-hoc correction. **(B)** Endpoint titers of pooled serum from A binding to FL-rCSP measured by ELISA. *P*-values were determined by comparing serum types to naïve serum using the Kruskal-Wallis test. **(C)** R21 immunization scheme in normal mice, which received two intramuscular injections of 1 μg R21 + adjuvant at three week intervals prior to passive transfer of PfCSP repeat mAbs 2 hours before IV challenge with 2,000 Pb-PfCSP-SPZ. **(D-F)** Liver burden 40 hours after IV challenge with 2,000 Pb-PfCSP-SPZ in mice (n=5-20/group; 50μg/25μg data in E/F were combined from two experiments represented by circles and squares) immunized with 1 μg R21 alone; mice administered CIS43, L9, and 317 alone (D, 150 μg; E, 50 μg; F, 25 μg); and mice immunized with 1 μg R21 and administered CIS43, L9, and 317 (D, 150 μg; E, 50 μg; F, 25 μg). *P*-values were determined by comparing each R21 + mAb combination to the R21 alone control using the Kruskal-Wallis test (pink lines) and R21 + mAb combination to each respective mAb alone control using the two-tailed Mann-Whitney test. (A-B, D-F): ***, $p<0.001$; **, $p<0.01$; *, $p<0.05$; ns (not significant), $p>0.05$.

Given the improved protection observed with combining R21 and repeat mAbs, I also wanted to determine the protective efficacy of combining R21 with C-CSP mAbs *in vivo*. mAb15 and R2 bound to distinct epitopes on FL-rCSP (**Figure 6.8B**), while various repeat mAbs were confirmed to potentiate the SPZ binding of mAb15 and L15 (**Figure 6.12**). Thus, R21 was combined with this subset of three C-CSP mAbs. Liver burdens in mice that received R21 and 300 μg/mouse of C-CSP mAbs were not significantly different than mice that received R21 alone (**Figure 6.18**). These data show that, even when combined with polyclonal antibody responses against the repeat region and C-CSP, relatively high doses (300 μg/mouse) of C-CSP mAbs do not neutralize SPZ *in vivo*.

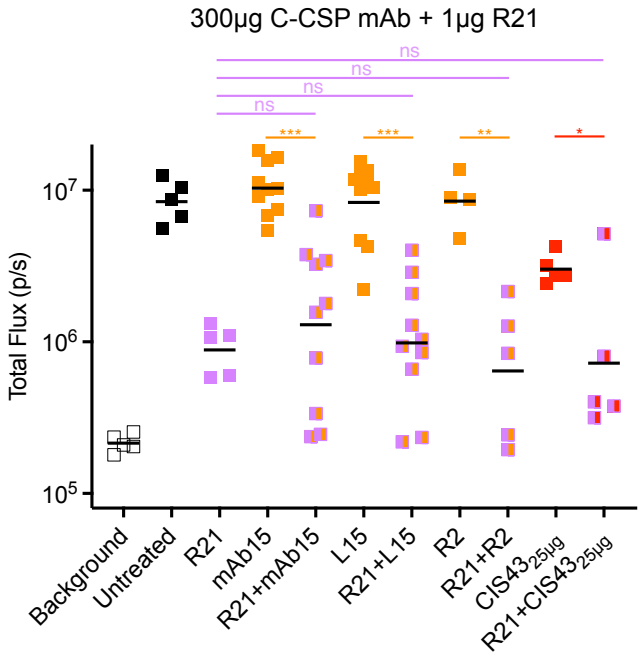

Figure 6.18: *In vivo* protection from combining C-CSP mAbs and PfCSP vaccine. Liver burden 40 hours after IV challenge with 2,000 Pb-PfCSP-SPZ in mice (n=5-10/group) immunized with 1 µg R21 alone; mice administered 300 µg of C-CSP mAbs (mAb15, L15, R2) or 25 µg of CIS43 alone as a control; and mice immunized with 1 µg R21 and administered 300 µg of C-CSP mAbs (mAb15, L15, R2) or 25 µg of CIS43. *P*-values were determined by comparing each R21 + mAb combination to the R21 alone control using the Kruskal-Wallis test (pink lines) and R21 + mAb combination to each respective mAb alone control using the two-tailed Mann-Whitney test. ***, $p<0.001$; **, $p<0.01$; *, $p<0.05$; ns (not significant), $p>0.05$.

6.8 Discussion

This Chapter provided the most comprehensive analysis to date of the binding and protective efficacy of combining mAbs and vaccines targeting all three domains of PfCSP. Section 6.4 investigated methods to improve the ability of the N-CSP-specific humanized mouse mAb 5D5 to bind native PfCSP on the surface of SPZ *in vitro* and whether improving this binding would result in enhanced SPZ neutralization *in vivo*. Via flow cytometry, I show that the binding of 5D5 to Pb-PfCSP-SPZ is improved by the presence of the cysteine protease inhibitor E-64, which inhibits the parasite protease responsible for cleaving CSP and thus preserves the 5D5 epitope upstream of the proteolytic cleavage site in RI[65].

Using fluorescently-labeled 5D5 and a panel of human PfCSP mAbs specific for the three types of tetrapeptides in the repeat region, I subsequently show that co-incubating 5D5 with most NPDP-, NVDP-, and NANP-specific repeat mAbs potently improves 5D5 Pb-PfCSP-SPZ binding likely due to the CSPR stripping off the existing PfCSP coat to reveal uncleaved PfCSP molecules with the intact 5D5 epitope in N-CSP[98]. When the CSPR was abrogated by the addition of CD[98,263], only the NPDP-specific junctional mAbs CIS42 and CIS43 potently improved 5D5 Pb-PfCSP-SPZ binding comparable to the E-64 control, consistent with a previous report showing that CIS43 inhibits proteolytic cleavage of PfCSP on PfSPZ by binding to the junctional epitope NPDP directly downstream of RI[84]. A notable limitation of this study was the lack of comparison of the 5D5-AF647 flow cytometry-based assay to the established pulse-chase metabolic labeling assay for measuring inhibition of PfCSP cleavage[65,106]; however, the finding that CIS43 inhibited cleavage in the 5D5-AF647 assay was consistent with results obtained using the pulse-chase assay. Together, these data show that the poor binding of 5D5 to Pb-PfCSP-SPZ is due to removal of its N-CSP epitope by proteolytic cleavage and that inhibition of proteolytic cleavage by either E-64 or junctional repeat mAbs can potentiate 5D5 Pb-PfCSP-SPZ binding *in vitro*.

However, the potentiation of 5D5 Pb-PfCSP-SPZ binding by co-incubation with E-64 or repeat mAbs *in vitro* did not translate into improved 5D5 neutralization *in vivo* against E-64-treated Pb-PfCSP-SPZ or when 5D5 was combined with repeat mAbs. This lack of cooperative neutralization is likely due to 5D5 binding an inherently non-neutralizing N-CSP epitope and is in agreement with a previous report showing that 5D5 is ineffective at preventing PfSPZ invasion of hepatocytes *in vitro* or lowering liver burden in mice challenged with Pb-PfCSP-SPZ[249]. The only study that reported a protective effect for 5D5 utilized a transgenic Pb that

expressed only N-CSP[106]; in contrast, all subsequent studies of 5D5 have shown that it is ineffective at neutralizing wild-type PfSPZ or Pb-PfCSP-SPZ which express FL PfCSP, which are more biologically relevant than Pb expressing only N-CSP[171,249]. Together, these data confirm that 5D5 is a non-neutralizing N-CSP-specific mAb.

Furthermore, I present discrepant data showing that 5D5 has low SG Pb-PfCSP-SPZ binding that is markedly improved by E-64 but high SG PfSPZ binding that is relatively unaffected by E-64. This discrepancy may limit the biological relevance of the improvement of 5D5 binding to Pb-PfCSP-SPZ, as this transgenic model is only used to test the functional activity of PfCSP mAbs in mice. One possible explanation for this discrepancy is that, unlike PfSPZ, Pb-PfCSP-SPZ may constitutively express the cysteine protease responsible for processing PfCSP and thus constantly cleave PfCSP on their surface resulting in low 5D5 binding. There is active debate as to when CSP is cleaved on the surface of SPZ. For instance, one study of wild-type PbSPZ proposed a model wherein N-CSP is only cleaved when SPZ encounter HSPGs on the surface of hepatocytes prior to invasion[68]. Another study of wild-type PfSPZ proposed a different model wherein N-CSP is uncleaved when SPZ are in the MG and is cleaved when SPZ enter the SG[268]. Overall, these data indicate that there may be differences between how PfCSP is proteolytically processed on wild-type PfSPZ compared to transgenic PbSPZ expressing PfCSP.

Another possible explanation for the discrepant 5D5 binding to PfSPZ versus Pb-PfCSP-SPZ could be conformational differences in native PfCSP. Specifically, the conformation of PfCSP on PfSPZ may make the 5D5 epitope more available for mAb binding. 5D5 has been shown to potently inhibit PfCSP proteolytic cleavage on PfSPZ[84]; thus, it is possible that 5D5 can inhibit PfCSP cleavage on PfSPZ and improve the availability of its own epitope. The 5D5

binding discrepancy reported in this study is further complicated by conflicting prior reports. The original paper reporting the discovery of 5D5 in 2015 showed that 5D5 robustly bound PfSPZ by immunofluorescence microscopy. A follow-up study in 2020 showed that 5D5 had low (~20-30% $5D5^{+}$) PfSPZ binding[249] while another study in 2021 reported high (MFI of 10^4-10^5) PfSPZ binding[171]. Collectively, these data highlight the inconsistent ability of 5D5 to bind SPZ and suggest that further N-CSP-specific mAbs should be isolated to determine the availability of epitopes in N-CSP.

Section 6.5 focused on the SPZ binding and neutralization of the largest known panel of thirteen human C-CSP-specific mAbs. Despite binding FL-rCSP, all C-CSP mAbs did not bind or neutralize SG Pb-PfCSP-SPZ. These data are consistent with prior studies which reported that two human C-CSP-specific mAbs neither bound nor neutralized SG Pb-PfCSP-SPZ *in vitro* and *in vivo*[226] and that native PfCSP on SPZ is conformationally labile[67,68], which likely results in the masking of C-CSP on SG SPZ from antibody recognition.

Additionally, I show that several repeat PfCSP mAbs with different target epitopes and *in vivo* protective potencies comparably potentiate the SG SPZ binding of C-CSP mAbs *in vitro*. These data clarify a previous report that PfSPZ immunization in humans preferentially induces antibody responses against the immunodominant repeat region and that subdominant C-CSP-specific responses are only expanded after subsequent boosts[269]. Specifically, repeat antibodies induced after the prime likely induce conformational changes in PfCSP that improve the accessibility of C-CSP to immune recognition, resulting in the expansion of C-CSP-specific responses upon subsequent PfSPZ immunizations. Notably, only a subset of repeat mAbs (i.e., 311 and CIS43) significantly changed the conformation of FL-rCSP, underscoring the discrepancies between recombinant versus native PfCSP and the need for new techniques to

interrogate the native structure of PfCSP on SPZ. Collectively, these data suggest that C-CSP antibodies require the presence of repeat antibodies to bind native PfCSP on SPZ.

The potentiation of C-CSP mAb SPZ binding by repeat mAbs *in vitro* did not translate into improved protection *in vivo*. This lack of cooperative neutralization could be due to all C-CSP mAbs in the panel recognizing non-neutralizing epitopes or to potential limitations in this study's assays and/or models. Specifically, the human IgG_1 vector used to express mAbs in this study may be inefficient at activating Fc receptors or fixing complement in normal B6 mice and the transgenic Pb-PfCSP-SPZ used for challenges in this study may not perfectly model wild-type PfSPZ. Several studies have reported that C-CSP antibodies induced by RTS,S immunization are correlated with vaccine efficacy in phase III trials[252–254] and such antibodies can mediate human complement fixation and phagocytosis by human monocyte cell lines *in vitro*[108,251]. Thus, C-CSP + repeat mAb combinations might prove more protective compared to each mAb class alone if tested via *in vitro* studies with human cell lines, *in vivo* studies in mice with humanized Fc receptors, or in CHMI studies.

It remains possible that polyclonal antibodies against the repeat region and C-CSP induced by vaccination may provide improved *in vivo* protection. The heterogeneous antibody response induced by RTS,S immunization might enable polyclonal C-CSP antibodies to functionally inhibit SPZ via a mechanism not observed in the passive transfer of limited numbers of mAbs shown here. While this study tested the largest panel of human C-CSP mAbs yet reported (i.e., thirteen C-CSP mAbs), this number is much lower than the hundreds of PfCSP repeat mAbs assessed for neutralization to date[235].

Section 6.6 focused on determining whether combining highly potent PfCSP human mAbs (CIS43, L9, and 317) that target the three different tetrapeptides in the repeat region would

provide improved protection compared to each mAb alone. This is an important issue for the clinical development of PfCSP mAbs for malaria prophylaxis, as targeting two distinct PfCSP epitopes could lead to improved protection against malaria as has been seen with viral infections like HIV-1, Ebola, and SARS-CoV-2[260,270,271]. A recent Phase I clinical trial showed that administration of CIS43 was safe and protected all nine CIS43-treated volunteers following CHMI[168]. A similar clinical trial for L9 has recently been initiated; thus, it is possible that CIS43, L9, and other protective PfCSP mAbs might be combined in the future.

Here, combining CIS43, L9, and 317 (i.e., the three of the most potent NPDP-, NVDP-, and NANP-preferring human mAbs described to date) did not result in improved protection compared to either mAb alone. Similarly, combining L9 with three poorly neutralizing NPDP-, NVDP-, and NANP-preferring human mAbs (CIS42, F10, and mAb4 respectively) conferred less protection than L9 alone. While it is possible that other combinations of repeat mAbs not tested in this study may provide superior protection compared to a single repeat mAb, the data demonstrating that the SPZ binding of a potent repeat mAb (i.e., L9) is antagonized by other repeat mAbs *in vitro* indicate that the efficacy of repeat mAb combinations may be limited by competition between mAbs that promiscuously cross-react with adjacent epitopes which share common residues[178,228]. Conversely, the observation that N- and C-CSP mAbs had no effect on repeat mAb SPZ binding even at a 50-fold excess suggests that mAbs targeting non-repeat domains may behave non-competitively when combined with repeat mAbs.

Interestingly, the SPZ binding of the NVDP-preferring mAb L9 was more potently antagonized by NPDP-preferring mAbs (CIS43, CIS42) and NANP-preferring mAbs (317, mAb4) than by NVDP-preferring mAbs (L9, F10). These data are somewhat counterintuitive, as one might expect L9 to antagonize itself most potently. A possible explanation is that the binding

of CIS43 and CIS42 to NPDP may induce conformational changes in the repeat region[84] that lower the binding of L9 to NVDP/NANP repeats. 317 and mAb4 have higher affinity for NANP repeats than L9 (**Table 6.1**) and there are more NANP than NVDP repeats in PfCSP (38 vs. 4, respectively); thus, 317 and mAb4 are likely outcompeting L9 for more epitopes in the 38 NANP repeats and thus have a greater effect on the SPZ binding of L9 than L9 and F10, which compete for fewer epitopes in the 4 NVDP repeats. These data highlight the limitations of extrapolating mAb recognition of native PfCSP epitopes based on peptides or recombinant protein and the importance of developing techniques to study mAb binding to SPZ at the atomic scale.

Section 6.7 focused on combining active-and-passive immunization against PfCSP. Remarkably, despite the lack of improved protection from combining repeat + C-CSP or repeat + repeat mAbs, combining R21 vaccination (which induces antibodies against the repeat region and C-CSP) with potent repeat mAbs provided improved *in vivo* protection compared to R21 or each mAb alone. However, combining R21 with non-neutralizing C-CSP mAbs did not provide any additional protection. These data highlight the limitations of predicting *in vivo* protection against SPZ challenge based on *in vitro* binding assays. RTS,S- and R21-mediated protection is thought to be mediated primarily by antibodies, though both have been shown to induce $CD4^+$ T cell responses[210,272]. Overall, these data suggest that vaccine-induced polyclonal repeat- and C-CSP-specific antibodies may interact cooperatively with (or at least do not lower the efficacy of) potent repeat mAbs to neutralize SPZ *in vivo* and that passive administration of protective PfCSP mAbs in RTS,S- or R21-vaccinated individuals will provide enhanced protection against malaria.

Overall, this Chapter has implications for the optimal implementation of PfCSP mAbs to prevent malaria. No protective advantage was observed from combining the neutralizing human PfCSP repeat mAbs used in this study, which are the most potent reported to date[178], indicating

that each mAb should be used as stand-alone interventions. However, the data showing that potent repeat mAbs can enhance protection in mice given sub-optimal doses of R21 suggest that passive transfer of PfCSP mAbs could be used to boost protection in vaccinated infants.

Chapter VII: Isolation of human mAbs against the RH5-CyRPA-Ripr complex

7.1 Authorship statement

Shanping Li and Peter Crompton provided plasma and PBMCs from the Mali cohort; Carolyn Nielsen and Simon Draper provided PBMCs from the VAC063 trial; Gavin Wright provided the RH5, CyRPA, and Ripr proteins; Simon Draper and Matthew Higgins provided the stabilized RCR complex; Joshua Tan screened plasma from the Malians; Ludmila Krymskaya and David Ambrozak sorted B cells; Lauren Purser screened a subset of mAbs for antigen reactivity; Kazutoyo Miura and Ababacar Diouf performed GIA assays.

7.2 Introduction

The three components of the RH5-CyRPA-Ripr trimeric complex, which MZ utilize to invade erythrocytes, are leading Pf malaria blood-stage vaccine targets[78,118]. Only one study has reported the isolation of seventeen anti-RH5 human mAbs from subjects immunized with a heterologous prime-boost of chimpanzee adenovirus 63 (ChAd63) and modified vaccinia Ankara (MVA) expressing RH5[145], while no anti-CyRPA and anti-Ripr human mAbs have been isolated to date[118]. Isolating neutralizing human RCR mAbs and identifying the epitopes targeted by these mAbs and how they evolved will facilitate improvement of RCR-based malaria vaccines and identification of potent mAbs for clinical development as malaria prophylactics.

This Chapter details the isolation of a large panel of human RCR mAbs from subjects living in an endemic area of Mali and human RH5 mAbs from subjects immunized with recombinant RH5.

7.3 Isolation of RH5-CyRPA-Ripr mAbs from naturally infected humans

A cohort of 1,187 subjects aged 1 month to 43 years from the rural village of Kalifabougou, Mali (where intense Pf transmission occurs in a clearly defined malaria season from June to December) were previously enrolled and followed longitudinally since 2011[273].

7.3.1 Isolation of RH5-CyRPA-Ripr mAbs using MBC culture

To select a promising subject from which to clone mAbs, I focused on 768 of these 1,187 naturally infected subjects who had available plasma and PBMCs. RH5-coated beads were used to measure the RH5 reactivity of plasma from the 768 subjects, which identified four subjects with the highest anti-RH5 IgG titers (**Figure 7.1A**). When mixed with MZ-infected and uninfected erythrocytes, plasma from these four subjects had the highest MZ neutralization (~100%) in the GIA assay (**Figure 7.1B**). Of these four subjects, Subject 2 had the most available PBMC timepoints and was thus selected for mAb cloning.

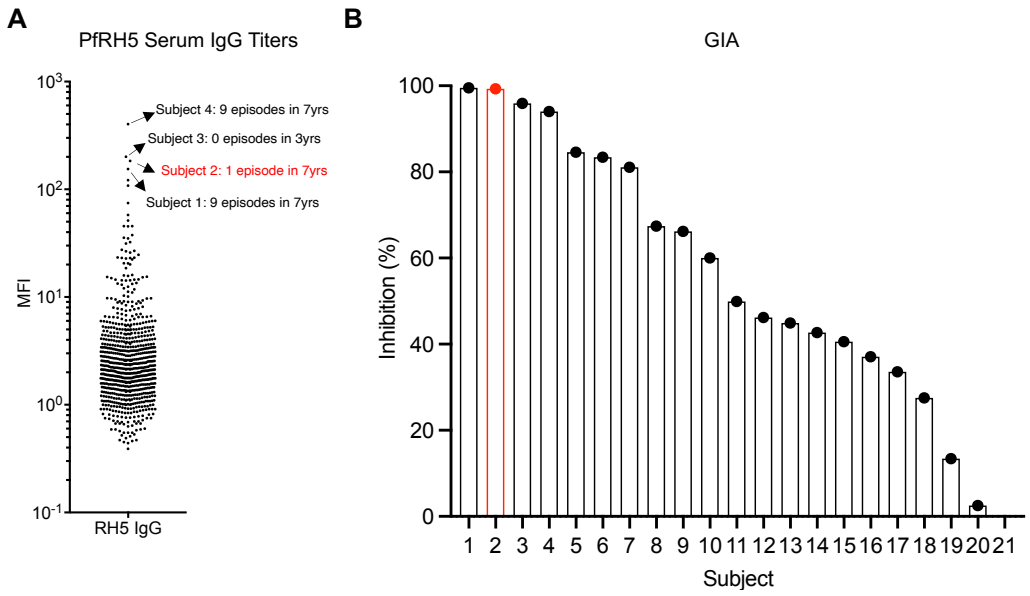

Figure 7.1: **Anti-RH5 titers and GIA of plasma from Malian subjects. (A)** Binding of plasma IgG to RH5-coated beads from 768 Malian individuals plotted as MFI. The subject ID and number of clinical malaria episodes since enrollment for four subjects with the highest RH5 plasma titers are noted. **(B)** GIA of Pf_3D7 mediated by plasma (10 mg/mL) from 21 subjects with the highest RH5 titers in A. Subject 2, the subject selected for mAb cloning, is highlighted in red.

A previously reported protocol for isolating antigen-specific MBCs via MBC culture[171] was used to clone mAbs from cryopreserved PBMCs collected from Subject 2, with the mAbs coded Mali2 (Mali subject 2) (**Figure 7.2**). 90,624 IgG^+ MBCs were bulk sorted, plated in 384-well plates (2 cells/well; 45,312 wells across 118 plates), and cultured for 2 weeks in activation media; subsequently, culture supernatants were harvested, and cells were frozen at -80ºC. Of the 45,312 wells, 151 wells (0.33%) bound beads coated with RH5, CyRPA, Ripr, or the stabilized RCR complex. 81 matched-pair Ig genes were cloned from the 151 wells and 61 were expressed as IgG_1.

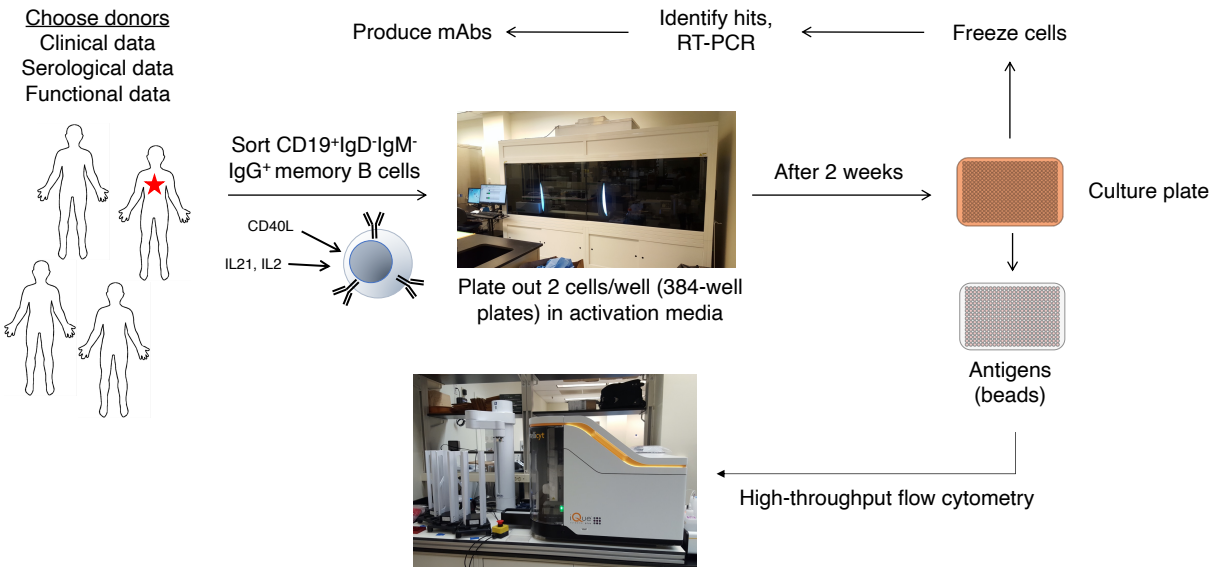

Figure 7.2: **Workflow for isolating antigen-specific B cells using MBC culture.**

Of these 61 IgG_1, 24 (39%) had detectable binding to RH5-CyRPA-Ripr/RCR (**Figure 7.3A**). 14 of 24 (58%) bound only the RCR complex, suggesting that mAbs may be non-specifically binding this large and potentially sticky complex. Furthermore, several mAbs (Mali2-21, -55, -115, -130, and -153) appeared to weakly cross-react with both RH5 and Ripr. Nearly all the mAbs had low binding to RH5-CyRPA-Ripr and did not bind RCR; the only mAb that demonstrated high CyRPA and RCR binding was Mali2-142.

All 24 mAbs in the panel had low (<40%) GIA at the relatively high concentration of 1 mg/mL (**Figure 7.3B**). Conversely, the most potent published RH5 human mAb (R5.016) has ~100% GIA at 1 mg/mL and an EC_{50} of ~10 µg/mL[145]. These data indicate that most mAbs cloned via the MBC culture system had low antigen binding and limited *in vitro* MZ neutralization.

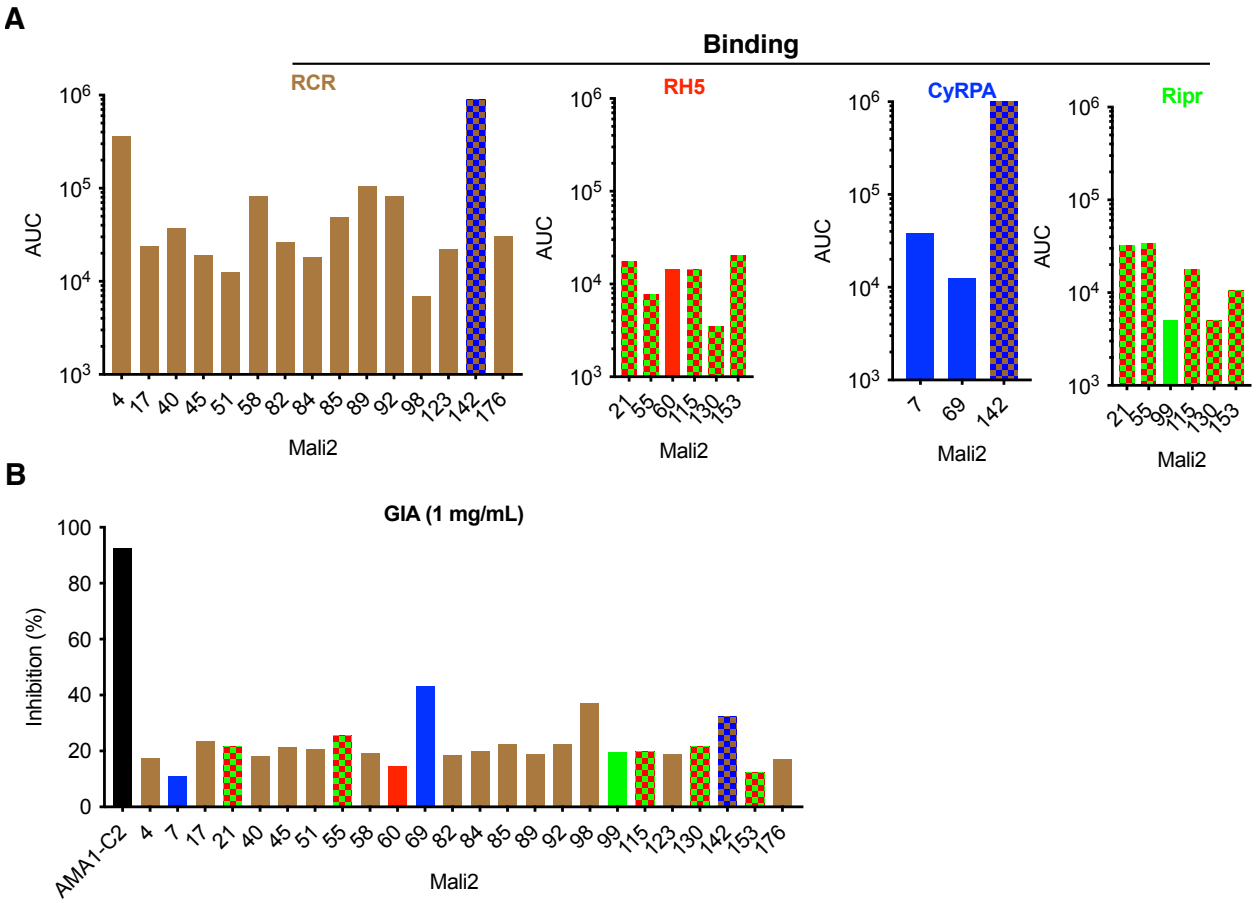

Figure 7.3: **Binding and neutralization of Mali2 mAbs cloned via MBC culture. (A)** AUC values calculated from varying concentrations (1–0.01 µg/mL) of indicated Mali2 mAb binding to RCR, RH5, CyRPA, and Ripr in the beads-based assay. Bars with two colors indicate that mAb bound to both types of antigens. **(B)** GIA of Pf_3D7 mediated by Mali2 mAbs (1 mg/mL). The anti-AMA1 polyclonal serum C2 was used as a positive control.

7.3.2 Isolation of RH5-CyRPA-Ripr mAbs using the Beacon Optofluidic System

Given the low percentage of positive supernatant hits (0.33%) and the low binding of most Mali2 mAbs isolated via the labor-intensive MBC culture system (which allows for screening only one subject at a time), I was concerned that the RH5-CyRPA-Ripr-specific mAbs were extremely rare and that the 2-week MBC activation produced high levels of antibodies that non-specifically bound the antigen-coated beads and were thus identified as false positives. To address these issues, I switched to the Beacon Optofluidic System to isolate additional mAbs

from multiple subjects. The Beacon enables real-time measurement of antibody secretion from live single B cells using fluorescence microscopy and thus should have a higher fidelity in identifying antigen-specific B cells. An added benefit is that the Beacon enables mAb isolation from PBs, which cannot be cultured.

I developed an optimized protocol to isolate antigen-specific PBs and MBCs using the Beacon (**Figure 7.4**). IgG^+ PBs were bulk sorted and immediately loaded onto the Beacon for analysis. IgG^+ MBCs were bulk sorted, plated in either 96- or 384-well plates (2,500 cells/well or 100 cells/well, respectively), and respectively incubated for 6 or 10 days in activation media. Subsequently, culture supernatants were screened for antigen specificity and MBCs from positive wells were loaded onto the Beacon for analysis.

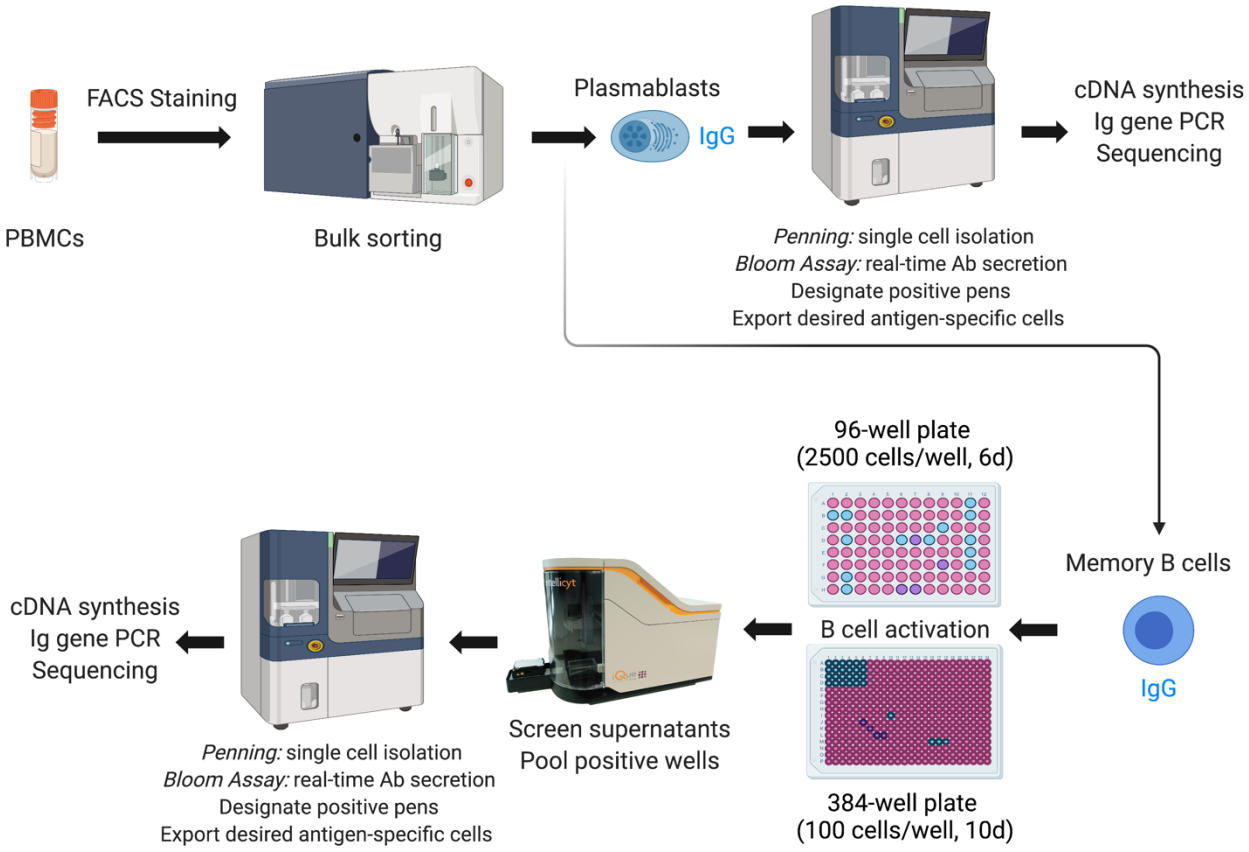

Figure 7.4: **Workflow for isolating antigen-specific B cells using the Beacon.**

To facilitate subject selection, I expanded my analysis of RH5 plasma reactivity to include reactivity against CyRPA, Ripr, MSP1, and PfCSP (**Figure 7.5A**). MSP1 and PfCSP are immunodominant antigens on MZ and SPZ, respectively[274,275], and were included as positive controls. Titers against RH5-CyRPA-Ripr were ~1,000-fold lower than MSP1 and ~10-fold lower than PfCSP. The discrepancy between MSP1 and PfCSP is likely due to the exponentially greater force of MZ infection compared to SPZ infection[33].

Of the 768 available subjects, 50 with the highest RH5-CyRPA-Ripr titers were selected for analysis in the Beacon workflow using the 96-well plate format. Of these 50 subjects, only 18 had detectable RH5-CyRPA-Ripr/RCR-specific MBCs in PBMCs. Of the 2,720 MBC wells screened (~6.80E6 MBCs), only 0.1–0.3% of wells were RH5-CyRPA-Ripr-specific, which was ~10- and 100-fold lower than PfCSP and MSP1, respectively (**Figure 7.5B**). Interestingly, 1.51% of wells bound only RCR, substantiating that this complex is sticky and is bound non-specifically by mAbs. These data are in agreement with the low antigen reactivity of MBCs from Mali2 and underscore the rarity of RH5-CyRPA-Ripr mAbs in humans naturally exposed to malaria.

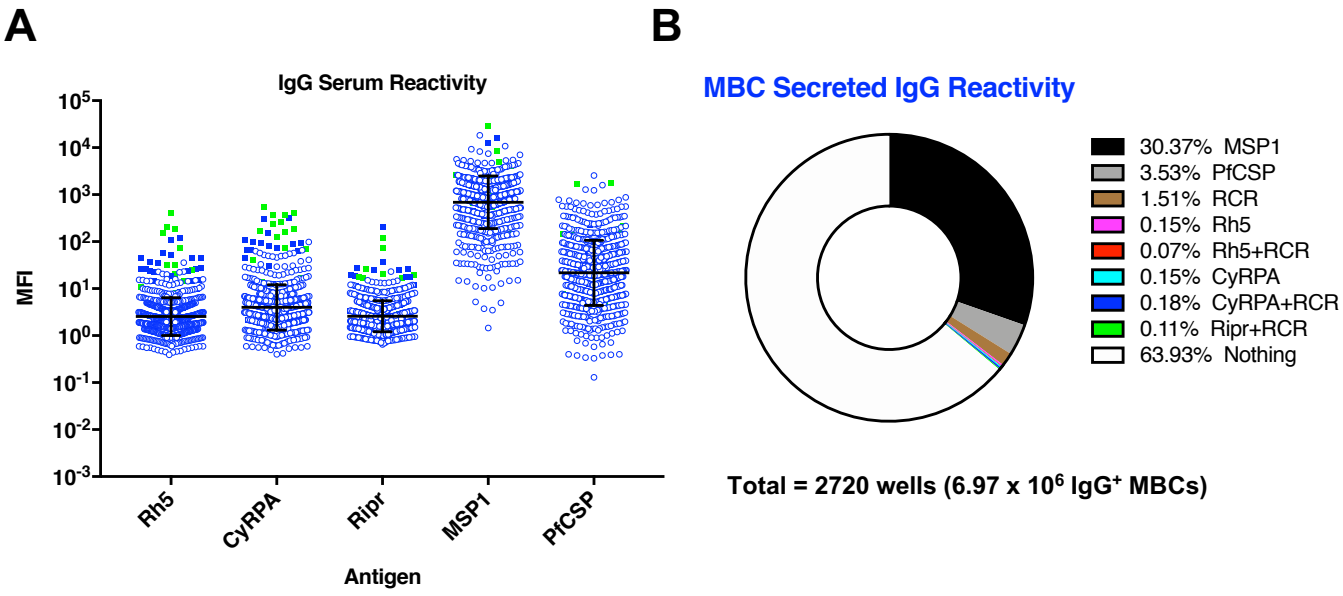

Figure 7.5: **IgG$^+$ plasma and MBC reactivity against various Pf antigens. (A)** Binding of plasma IgG to beads coated with RH5, CyRPA, Ripr, MSP1, and PfCSP from 768 Malian individuals. The 50 donors with the highest RH5-CyRPA-Ripr titers are indicated by filled squares; the 18 donors with detectable RH5-CyRPA-Ripr-specific MBCs are indicated in green. **(B)** Percentage of MBC wells (2,500 MBCs/well) with supernatants that bound the indicated antigens.

A total of 168 mAbs were isolated using the Beacon from these 18 Malian subjects and coded MMS (Mali multiple subjects). 86 of 168 mAbs (51%) were determined to be antigen-specific (i.e., 38 RH5, 36 CyRPA, and 12 Ripr) by measuring binding to antigen-coated beads across varying mAb concentrations (**Figure 7.6A**). Many MMS mAbs showed high binding comparable to the positive controls R5.016 (RH5/RCR) and Mali2-142 (CyRPA/RCR) (**Figure 7.6B**). Of the 37 CyRPA mAbs isolated (Mali2-142 and 36 MMS mAbs), 10 (27%) had demonstrated higher binding to CyRPA than to RCR, suggesting that these mAbs bound to epitopes that are less accessible in the stabilized RCR complex.

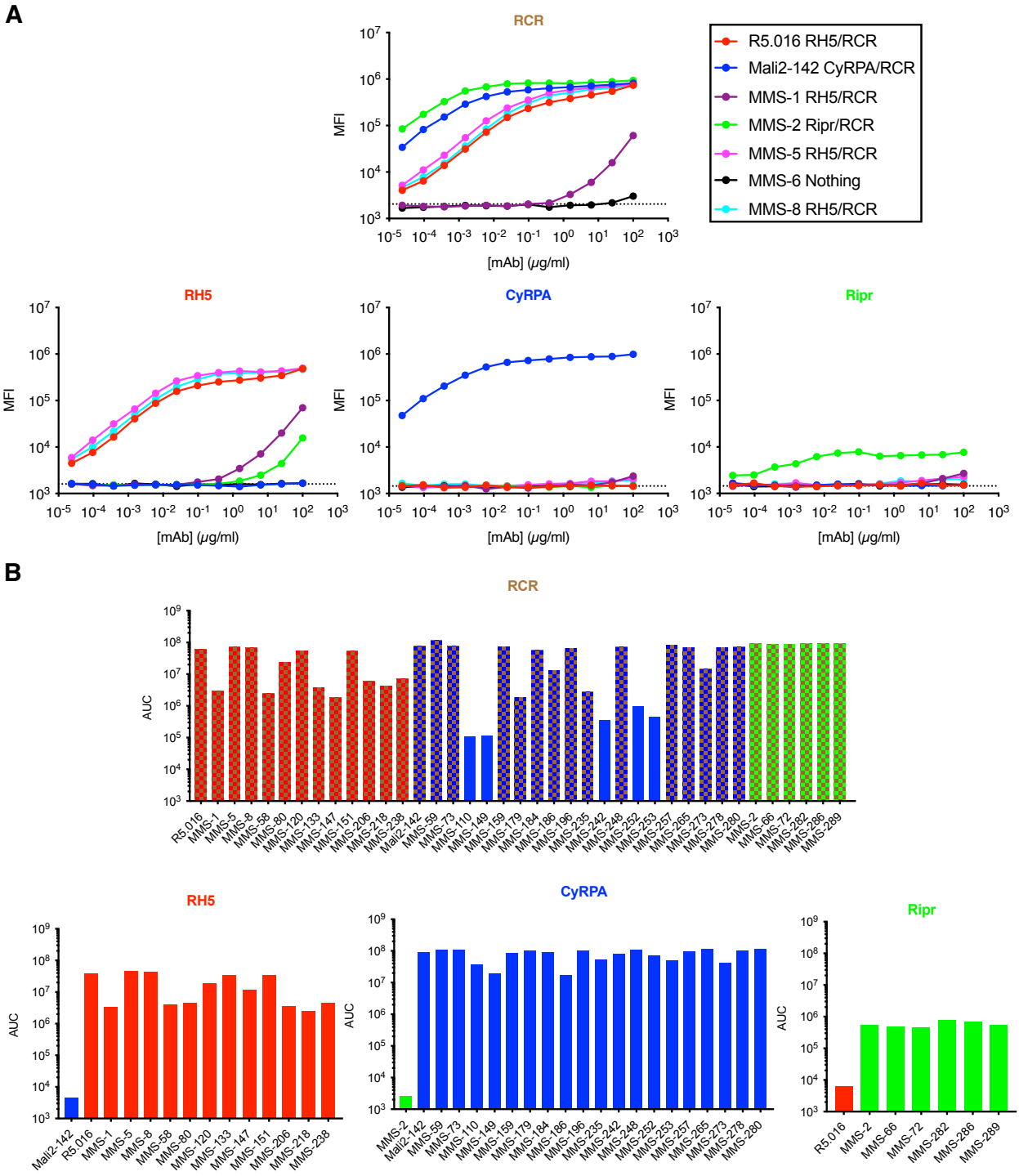

Figure 7.6: Binding of MMS mAbs cloned via the Beacon. (A) Binding of varying concentrations (100–2.4 x 10^{-5} µg/mL) of MMS mAbs (1-8) to RCR-, RH5-, CyRPA-, and Ripr-coated beads. R5.016 and Mali2-142 were respectively included as RH5- and CyRPA-specific mAb controls. **(B)** AUC values calculated from curves in A for 37 of 86 MMS mAbs. The binding data for the remaining 49 MMS mAbs were not shown as they were generated by a different person with a different set of mAb concentrations.

7.4 Isolation of RH5 mAbs from vaccinated humans

To compare the RH5-specific human mAbs isolated from naturally infected subjects to those cloned from vaccinated subjects, I obtained PBMCs from the VAC063 trial at Oxford. VAC063 was an open-label Phase I/IIa dose escalation blood-stage malaria CHMI trial to assess the safety, immunogenicity, and efficacy of recombinant RH5 with the adjuvant $AS01_B$ in healthy, malaria naïve adults aged 18-45 years. The only published human RH5 mAbs to date were isolated from the VAC057 trial at Oxford, where healthy adult subjects were immunized with a heterologous prime-boost of ChAd63-MVA expressing $RH5^{145}$. Thus, cloning mAbs from VAC063 would additionally enable comparison of antibodies generated by recombinant RH5 protein + adjuvant compared to RH5 delivered by viral vectors.

7.4.1 Isolation of RH5 mAbs using the Beacon Optofluidic System

I focused my attention on Groups 1 and 4 of VAC063, where subjects were respectively immunized with 2 and 50 μg of RH5 three times at 4-week intervals. PBMCs from four VAC063 subjects collected at day 140, 12 weeks after the last immunization, were obtained and processed in the 384-well plate format of the optimized Beacon protocol (**Figure 7.4**). As a control, PBMCs from the top four Malian subjects with the highest RH5-CyRPA-Ripr antigen responses (**Figure 7.5**) were also processed in the 384-well plate format. Screening MBC culture supernatants for RH5 binding showed that VAC063 subjects had significantly higher proportions of RH5-specific MBCs than Malian subjects (**Figure 7.7**). Specifically, there were 34-fold more $RH5^+$ wells in VAC063 (~1.7%) vs. Malian subjects (0.05%) and 230-fold more RH5/RCR^+ wells in VAC063 (~46%) vs. Malian subjects (0.2%). The difference in RCR^+ wells was not

significant (2.4% vs. 0.8%), further suggesting that RCR-only wells were due to non-specific antibody binding. These data show that vaccination with recombinant RH5 + adjuvant generates significantly higher levels of RH5-specific MBCs than natural infection.

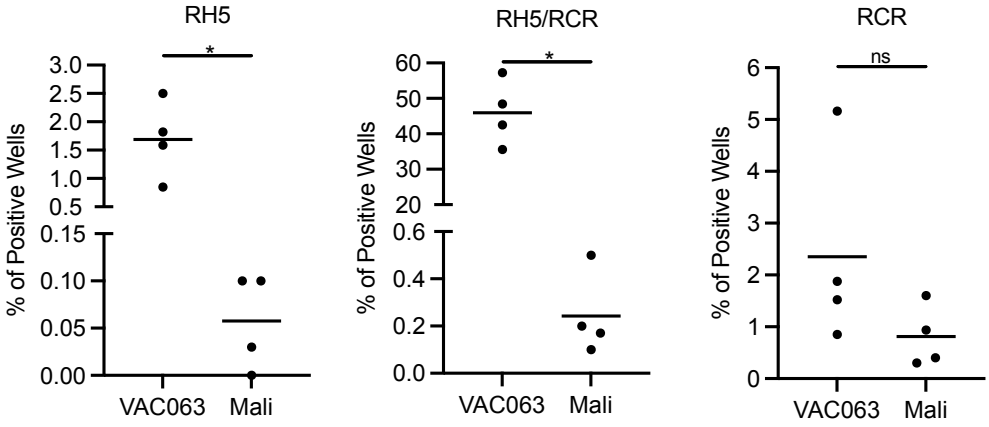

Figure 7.7: Comparison of RH5-specific MBC responses in VAC063 and Malian subjects. Percentage of wells positive for RH5 only, RH5/RCR, and RCR only in 384-well plates (100 cells/well) containing stimulated MBCs from four VAC063 and four Malian subjects. The Malian subjects were selected because they had the highest MBC responses in the 96-well plate format (data in Figure 7.5). *P*-values were determined using the two-tailed Mann-Whitney test (*, $p<0.05$; ns, $p>0.05$).

MBCs from positive VAC063 wells were pooled and loaded onto the Beacon for analysis. A total of 181 mAbs were isolated using the Beacon and coded VAC063. 124 of 181 mAbs (69%) were determined to be RH5-specific by measuring binding to antigen-coated beads across varying mAb concentrations with R5.016 as a control (data not shown). 13 of 124 (10%) VAC063 mAbs had higher binding to RH5 than RCR; the remaining 111 mAbs had comparable binding to RH5 and RCR.

Analysis of the rates of somatic hypermutation (SHM) in the V_H and V_L of mAbs from vaccinated versus naturally infected subjects was performed. The SHM rates for the 17 published RH5 mAbs isolated from VAC057[145] were retrieved and compared to the SHM rates for the 124 RH5 mAbs cloned from VAC063 and the 38 RH5 MMS mAbs cloned from Malians; the 37

CyRPA and 12 Ripr MMS mAbs were also included in this analysis. MMS RH5 mAbs were significantly more mutated than mAbs from VAC057 and VAC063 in both the V_H (7.4% vs. 1.7% and 2.6% divergence from germline; **Figure 7.8A**) and V_L (5.0% vs. 1.8% and 1.9% divergence from germline; **Figure 7.8B**). Interestingly, V_H for the Ripr mAbs trended towards being more mutated than the CyRPA and RH5 mAbs (10.5% vs. 7.4% and 7.4% divergence from germline). Overall, these data show that mAbs induced by natural infection are significantly more mutated than mAbs induced by RH5 vaccination with either viral vectors (VAC057) or protein + adjuvant (VAC063).

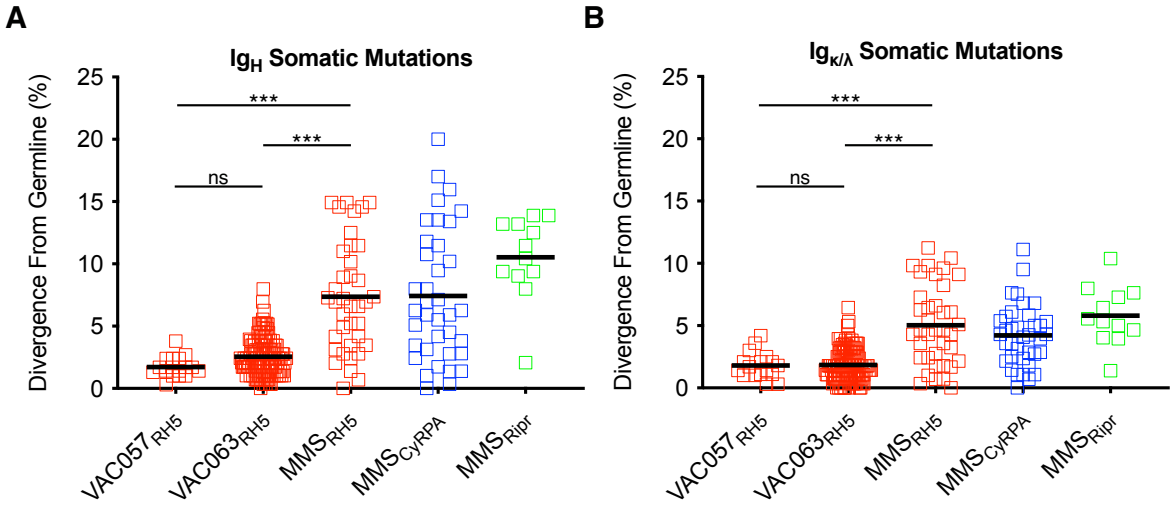

Figure 7.8: Comparison of somatic mutation rates in RH5-CyRPA-Ripr mAbs isolated from vaccinated and naturally infected humans. Percent divergence from germline in the **(A)** heavy chain and **(B)** light chain of mAbs against RH5 (red), CyRPA (blue), and Ripr (green) cloned from VAC057[145] (n=17), VAC063 (n=124), and naturally infected Malians (n=38 RH5, 37 CyRPA, 12 Ripr). *P*-values were determined using the Kruskal-Wallis test with Dunn's post-hoc correction for multiple comparisons (***, p<0.001; ns, p>0.05).

7.5 Discussion

The initial data presented in this Chapter indicate that B cell responses against the trimeric RH5-CyRPA-Ripr MZ invasion complex induced by natural infection are low,

especially when compared to vaccination. Consequently, RH5-CyRPA-Ripr-specific mAbs are rare and difficult to isolate. However, mAbs induced by natural infection were significantly more mutated than mAbs induced by vaccination, suggesting that constant malaria infections in the field over many years drove a significant amount of affinity maturation. To my knowledge, this panel of human RH5-CyRPA-Ripr is unique in that it is the first to compare RH5 mAbs generated by natural infection versus vaccination and also is the first known panel of human mAbs against CyRPA and Ripr. Ongoing studies are being performed to determine the mAb panel's gene usage, epitopes, affinity, and neutralization by GIA. If any potent neutralizing mAbs are identified, then X-ray crystallography or cryo-electron microscopy will be used to examine their binding to their respective antigens at atomic-level resolution.

Chapter VIII: Conclusions and future directions

8.1 Key Findings

The data presented in this Thesis provide many insights into protective mAbs against important Pf malaria vaccine antigens. A summary of the Key Findings of this Thesis are as follows:

- The subdominant NVDP minor repeats of PfCSP are neutralizing epitopes targeted by potently protective mAbs like L9, which is currently being tested in a Phase I clinical trial (Chapter III)
- Cytotoxic PfCSP mAbs can directly kill SPZ in the liver by cross-linking CSP on their surface, triggering the deleterious CSPR and causing the parasites to die in a characteristic "dotty death" phenotype (Chapter IV)
- PfCSP mAbs prevent SPZ from exiting liver sinusoids to infect hepatocytes (Chapter IV)
- Cross-reactivity with the junctional and NANP repeat region of PfCSP is a feature of potent PfCSP mAbs, which manifests as "two-step binding" via ITC (Chapters IV-V)
- The kappa light chain of L9 is required for this mAb's unique abilities to cross-link two adjacent NVDP minor repeats, cross-react with NANP major repeats, and potently neutralize SPZ *in vivo* (Chapter V)
- L9 lineage mAbs bind NPNV/NPNA minor/major repeat motifs in a similar type-1 β-turn (Chapter V)
- The L9 B cell lineage has baseline NVDP affinity and mutates to bind NANP repeats (Chapter V)

- The binding of repeat-specific mAbs causes conformational changes in both recombinant and native PfCSP (Chapter VI)
- C-CSP-specific mAbs require the presence of repeat-specific mAbs to conformationally unmask native PfCSP and enable their binding to SPZ (Chapter VI)
- Combinations of two mAbs against different epitopes on PfCSP (repeat + C-CSP or repeat + repeat) does not provide improved *in vivo* protection against SPZ challenge compared to single repeat mAbs (Chapter VI)
- Polyclonal anti-PfCSP serum or repeat-specific mAbs antagonize the SPZ binding of other repeat-specific mAbs by competing for PfCSP repeat epitopes; however, N- and C-CSP-specific mAbs do not antagonize the SPZ binding of repeat mAbs (Chapter VI)
- Combining potent repeat mAbs, but not C-CSP mAbs, with vaccine-induced polyclonal antibodies against the repeat region and C-CSP provides improved *in vivo* protection against SPZ challenge (Chapter VI)
- RH5, CyRPA, and Ripr are poorly immunogenic and the frequencies of circulating MBCs specific for these three antigens are extremely low in malaria-exposed subjects (Chapter VII)
- RH5 human mAbs induced by natural malaria exposure are significantly more mutated than RH5 human mAbs induced by vaccination (Chapter VII)

8.2 Future directions

8.2.1 Clinical testing of L9LS

The Phase I clinical trial of L9LS (NCT05019729) was initiated in September 2021 and subjects were challenged with infected mosquitoes in October 2021. The safety and protection analysis of this trial is complete, and the manuscript describing this data should hopefully be

submitted for peer review by February 2022. Depending on the interim results of NCT05019729, the NIH has plans to initiate Phase II testing of L9LS in both Mali and Kenya in 2022 prior to the start of the rainy season in summer 2022.

8.2.2 PfCSP-based vaccine design

The recent demonstration that the subdominant NPDP junctional epitope and the NVDP minor repeats are protective epitopes generated ongoing efforts in the Seder lab and other labs around the world to develop next-generation PfCSP-based vaccines including these epitopes. I am involved in this ongoing work, which has already resulted in my co-authorship on a publication entitled "Design of Alphavirus Virus-Like Particles Presenting Circumsporozoite Junctional Epitopes That Elicit Protection against Malaria," which was published in *Vaccines* (10.3390/vaccines9030272).

8.2.3 Development of more potent RCR-specific mAbs

The plan for the large panel of RH5-, CyRPA-, and Ripr-specific human mAbs I isolated is to split the data into two separate manuscripts. The first manuscript will compare the potency, evolution, and target epitopes of RH5 mAbs induced by natural infection (MMS mAbs) and vaccination (VAC063 mAbs). The second manuscript will define the potency, evolution, and target epitopes of the CyRPA- and Ripr-specific mAbs and determine whether combining them with RH5 mAbs (i.e., as mAb cocktails or as bispecific/trispecific mAbs) will result in improved MZ neutralization in the GIA assay. The ultimate goal of this entire project will be to identify a potent candidate (either single mAb, mAb cocktail, or bispecific/trispecific mAb) targeting the RCR complex to advance for clinical development and testing.

8.2.4 Combining mAbs against PfCSP and RCR

As stated in Chapter I, Aim 3 of my Thesis was to assess the protective efficacy of a multi-stage mAb cocktail against PfCSP and PfRH5 (or CyRPA or Ripr). If/when a potent best-in-class RCR-specific mAb is identified, it can be combined with L9LS and assessed in the liver- and blood-humanized FRG mouse model to determine if a multi-stage mAb cocktail targeting both PfSPZ and PfMZ can provide improved protection against malaria infection compared to each stage-specific mAb alone. This work will likely be carried out by the lab of Dr. Brandon Wilder at Oregon Health and Sciences University, who has an established collaboration with both the Seder and Draper labs and is funded by the Gates Foundation to test Pf-specific mAbs in the FRG mouse model.

8.3 Final remarks

Passive transfer of potent antimalarial monoclonal antibodies targeting sporozoites and merozoites is an emerging modality for protecting people from *Plasmodium falciparum* malaria. Alongside existing interventions (e.g., antimalarial drugs, insecticides, and bed nets) and the newly-approved RTS,S vaccine, antimalarial monoclonal antibodies should help significantly limit the morbidity and mortality of malaria and hopefully eradicate this ancient infectious disease for good. The data presented in this Thesis significantly advance our understanding of antimalarial monoclonal antibodies and will hopefully contribute towards the implementation of these antibodies as prophylactic or therapeutic biologics in the near future.

References

1. Murphy, K. & Weaver, C. *Janeway's Immunobiology*. (Garland Science, 2017).
2. Behring, E. & Kitasato, S. *Dtsch Med. Wochenschr.* **49**, 1113–1114 (1890).
3. Briney, B., Inderbitzin, A., Joyce, C. & Burton, D. R. Commonality despite exceptional diversity in the baseline human antibody repertoire. *Nature* **566**, 393–397 (2019).
4. Köhler, G. & Milstein, C. Continuous cultures of fused cells secreting antibody of predefined specificity. *Nature* **256**, 495–497 (1975).
5. Rajewsky, K. The advent and rise of monoclonal antibodies. *Nature* **575**, 47–49 (2019).
6. Ho, M. Inaugural Editorial: Searching for Magic Bullets. *Antib Ther* **1**, 1–5 (2018).
7. Crowell, T. A. *et al.* Safety and efficacy of VRC01 broadly neutralising antibodies in adults with acutely treated HIV (RV397): a phase 2, randomised, double-blind, placebo-controlled trial. *Lancet HIV* **6**, e297–e306 (2019).
8. Mulangu, S. *et al.* A Randomized, Controlled Trial of Ebola Virus Disease Therapeutics. *N Engl J Med* **381**, 2293–2303 (2019).
9. Dougan, M. *et al.* Bamlanivimab plus Etesevimab in Mild or Moderate Covid-19. *N Engl J Med* **385**, 1382–1392 (2021).
10. Nerlich, A. G., Schraut, B., Dittrich, S., Jelinek, T. & Zink, A. R. Plasmodium falciparum in ancient Egypt. *Emerg Infect Dis* **14**, 1317–1319 (2008).
11. Kwiatkowski, D. P. How Malaria Has Affected the Human Genome and What Human Genetics Can Teach Us about Malaria. *Am J Hum Genet* **77**, 171–192 (2005).
12. Whitfield, J. Portrait of a serial killer. *Nature* (2002) doi:10.1038/news021001-6.
13. Prevention, C.-C. for D. C. and. CDC - Malaria - About Malaria - Biology - Malaria Parasites. https://www.cdc.gov/malaria/about/biology/parasites.html (2018).

14. Fact sheet about malaria. https://www.who.int/news-room/fact-sheets/detail/malaria.
15. Prevention, C.-C. for D. C. and. CDC - Malaria - About Malaria - Disease. https://www.cdc.gov/malaria/about/disease.html (2019).
16. WHO. WHO | Fact Sheet: World Malaria Report 2015. *WHO* http://www.who.int/malaria/media/world-malaria-report-2015/en/ (2015).
17. WHO. WHO | World malaria report 2018. *WHO* http://www.who.int/malaria/publications/world-malaria-report-2018/en/ (2018).
18. The Global Fund. *Results Report 2021*. (2021).
19. WHO. *World malaria report 2021*. (2021).
20. Beier, J. C., Davis, J. R., Vaughan, J. A., Noden, B. H. & Beier, M. S. Quantitation of Plasmodium falciparum sporozoites transmitted in vitro by experimentally infected Anopheles gambiae and Anopheles stephensi. *Am J Trop Med Hyg* **44**, 564–570 (1991).
21. Beier, J. C. *et al.* Quantitation of malaria sporozoites transmitted in vitro during salivation by wild Afrotropical Anopheles. *Med Vet Entomol* **5**, 71–79 (1991).
22. Hopp, C. S. *et al.* Longitudinal analysis of Plasmodium sporozoite motility in the dermis reveals component of blood vessel recognition. *Elife* **4**, (2015).
23. Yamauchi, L. M., Coppi, A., Snounou, G. & Sinnis, P. Plasmodium sporozoites trickle out of the injection site. *Cell Microbiol* **9**, 1215–1222 (2007).
24. Vaughan, A. M. *et al.* Complete Plasmodium falciparum liver-stage development in liver-chimeric mice. *J Clin Invest* **122**, 3618–3628 (2012).
25. Sturm, A. *et al.* Manipulation of host hepatocytes by the malaria parasite for delivery into liver sinusoids. *Science* **313**, 1287–1290 (2006).

26. Cowman, A. F., Healer, J., Marapana, D. & Marsh, K. Malaria: Biology and Disease. *Cell* **167**, 610–624 (2016).

27. Birkholtz, L.-M., Bornman, R., Focke, W., Mutero, C. & de Jager, C. Sustainable malaria control: transdisciplinary approaches for translational applications. *Malar J* **11**, 431 (2012).

28. Reuling, I. J. *et al.* A randomized feasibility trial comparing four antimalarial drug regimens to induce Plasmodium falciparum gametocytemia in the controlled human malaria infection model. *Elife* **7**, e31549 (2018).

29. Collins, K. A. *et al.* A controlled human malaria infection model enabling evaluation of transmission-blocking interventions. *J Clin Invest* **128**, 1551–1562 (2018).

30. Michalakis, Y. & Renaud, F. Malaria: Evolution in vector control. *Nature* **462**, 298–300 (2009).

31. Nussenzweig, R., Vanderberg, J. & Most, H. Protective immunity produced by the injection of x-irradiated sporozoites of Plasmodium berghei. IV. Dose response, specificity and humoral immunity. *Mil Med* **134**, 1176–1182 (1969).

32. Vanderberg, J., Nussenzweig, R. & Most, H. Protective immunity produced by the injection of x-irradiated sporozoites of Plasmodium berghei. V. In vitro effects of immune serum on sporozoites. *Mil Med* **134**, 1183–1190 (1969).

33. Draper, S. J. *et al.* Malaria Vaccines: Recent Advances and New Horizons. *Cell Host Microbe* **24**, 43–56 (2018).

34. Nussenzweig, R. S., Vanderberg, J., Most, H. & Orton, C. Protective immunity produced by the injection of x-irradiated sporozoites of plasmodium berghei. *Nature* **216**, 160–162 (1967).

35. Yoshida, N., Nussenzweig, R. S., Potocnjak, P., Nussenzweig, V. & Aikawa, M. Hybridoma produces protective antibodies directed against the sporozoite stage of malaria parasite. *Science* **207**, 71–73 (1980).

36. Clyde, D. F., Most, H., McCarthy, V. C. & Vanderberg, J. P. Immunization of man against sporozite-induced falciparum malaria. *Am J Med Sci* **266**, 169–177 (1973).

37. Cockburn, I. A. & Seder, R. A. Malaria prevention: from immunological concepts to effective vaccines and protective antibodies. *Nat. Immunol.* **19**, 1199–1211 (2018).

38. Draper, S. J. *et al.* Malaria Vaccines: Recent Advances and New Horizons. *Cell Host Microbe* **24**, 43–56 (2018).

39. Wardemann, H. & Murugan, R. From human antibody structure and function towards the design of a novel Plasmodium falciparum circumsporozoite protein malaria vaccine. *Curr. Opin. Immunol.* **53**, 119–123 (2018).

40. Weedall, G. D., Preston, B. M. J., Thomas, A. W., Sutherland, C. J. & Conway, D. J. Differential evidence of natural selection on two leading sporozoite stage malaria vaccine candidate antigens. *Int J Parasitol* **37**, 77–85 (2007).

41. Gandhi, K. *et al.* Next generation sequencing to detect variation in the Plasmodium falciparum circumsporozoite protein. *Am J Trop Med Hyg* **86**, 775–781 (2012).

42. Bailey, J. A. *et al.* Use of massively parallel pyrosequencing to evaluate the diversity of and selection on Plasmodium falciparum csp T-cell epitopes in Lilongwe, Malawi. *J Infect Dis* **206**, 580–587 (2012).

43. Aragam, N. R. *et al.* Diversity of T cell epitopes in Plasmodium falciparum circumsporozoite protein likely due to protein-protein interactions. *PLoS One* **8**, e62427 (2013).

44. Zhao, J., Bhanot, P., Hu, J. & Wang, Q. A Comprehensive Analysis of Plasmodium Circumsporozoite Protein Binding to Hepatocytes. *PLOS ONE* **11**, e0161607 (2016).

45. Doud, M. B. *et al.* Unexpected fold in the circumsporozoite protein target of malaria vaccines. *Proc Natl Acad Sci U S A* **109**, 7817–7822 (2012).

46. Mohamed, N. S. *et al.* Assessment of genetic diversity of Plasmodium falciparum circumsporozoite protein in Sudan: the RTS,S leading malaria vaccine candidate. *Malar J* **20**, 436 (2021).

47. Huang, H.-Y. *et al.* Genetic polymorphism of Plasmodium falciparum circumsporozoite protein on Bioko Island, Equatorial Guinea and global comparative analysis. *Malar J* **19**, 245 (2020).

48. Lê, H. G. *et al.* Genetic polymorphism and natural selection of circumsporozoite surface protein in Plasmodium falciparum field isolates from Myanmar. *Malar. J.* **17**, 361 (2018).

49. Zeeshan, M. *et al.* Genetic variation in the Plasmodium falciparum circumsporozoite protein in India and its relevance to RTS,S malaria vaccine. *PLoS One* **7**, e43430 (2012).

50. Kisalu, N. K. *et al.* A human monoclonal antibody prevents malaria infection by targeting a new site of vulnerability on the parasite. *Nat. Med.* **24**, 408–416 (2018).

51. Bowman, S. *et al.* The complete nucleotide sequence of chromosome 3 of Plasmodium falciparum. *Nature* **400**, 532–538 (1999).

52. Hall, N. *et al.* Sequence of Plasmodium falciparum chromosomes 1, 3-9 and 13. *Nature* **419**, 527–531 (2002).

53. Oyen, D. *et al.* Cryo-EM structure of P. falciparum circumsporozoite protein with a vaccine-elicited antibody is stabilized by somatically mutated inter-Fab contacts. *Sci Adv* **4**, eaau8529 (2018).

54. AlphaFold Protein Structure Database. https://alphafold.ebi.ac.uk/entry/Q7K740.

55. Kojin, B. B. & Adelman, Z. N. The Sporozoite's Journey Through the Mosquito: A Critical Examination of Host and Parasite Factors Required for Salivary Gland Invasion. *Front. Ecol. Evol.* **7**, (2019).

56. Aly, A. S. I., Vaughan, A. M. & Kappe, S. H. I. Malaria Parasite Development in the Mosquito and Infection of the Mammalian Host. *Annu Rev Microbiol* **63**, 195–221 (2009).

57. Sidjanski, S. P., Vanderberg, J. P. & Sinnis, P. Anopheles stephensi salivary glands bear receptors for region I of the circumsporozoite protein of Plasmodium falciparum. *Mol. Biochem. Parasitol.* **90**, 33–41 (1997).

58. Myung, J. M., Marshall, P. & Sinnis, P. The Plasmodium circumsporozoite protein is involved in mosquito salivary gland invasion by sporozoites. *Mol. Biochem. Parasitol.* **133**, 53–59 (2004).

59. Ancsin, J. B. & Kisilevsky, R. A binding site for highly sulfated heparan sulfate is identified in the N terminus of the circumsporozoite protein: significance for malarial sporozoite attachment to hepatocytes. *J. Biol. Chem.* **279**, 21824–21832 (2004).

60. Zhao, J., Bhanot, P., Hu, J. & Wang, Q. A Comprehensive Analysis of Plasmodium Circumsporozoite Protein Binding to Hepatocytes. *PLOS ONE* **11**, e0161607 (2016).

61. Cerami, C. *et al.* The basolateral domain of the hepatocyte plasma membrane bears receptors for the circumsporozoite protein of Plasmodium falciparum sporozoites. *Cell* **70**, 1021–1033 (1992).

62. Frevert, U. *et al.* Malaria circumsporozoite protein binds to heparan sulfate proteoglycans associated with the surface membrane of hepatocytes. *J. Exp. Med.* **177**, 1287–1298 (1993).

63. Sinnis, P. *et al.* Structural and functional properties of region II-plus of the malaria circumsporozoite protein. *J. Exp. Med.* **180**, 297–306 (1994).

64. Tewari, R., Spaccapelo, R., Bistoni, F., Holder, A. A. & Crisanti, A. Function of region I and II adhesive motifs of Plasmodium falciparum circumsporozoite protein in sporozoite motility and infectivity. *J. Biol. Chem.* **277**, 47613–47618 (2002).

65. Coppi, A., Pinzon-Ortiz, C., Hutter, C. & Sinnis, P. The Plasmodium circumsporozoite protein is proteolytically processed during cell invasion. *J. Exp. Med.* **201**, 27–33 (2005).

66. Coppi, A. *et al.* Heparan Sulfate Proteoglycans Provide a Signal to Plasmodium Sporozoites to Stop Migrating and Productively Invade Cells. *Cell Host Microbe* **2**, 316–327 (2007).

67. Herrera, R. *et al.* Reversible Conformational Change in the Plasmodium falciparum Circumsporozoite Protein Masks Its Adhesion Domains. *Infection and Immunity* **83**, 3771–3780 (2015).

68. Coppi, A. *et al.* The malaria circumsporozoite protein has two functional domains, each with distinct roles as sporozoites journey from mosquito to mammalian host. *J Exp Med* **208**, 341–356 (2011).

69. Marti, M., Good, R. T., Rug, M., Knuepfer, E. & Cowman, A. F. Targeting Malaria Virulence and Remodeling Proteins to the Host Erythrocyte. *Science* **306**, 1930–1933 (2004).

70. Singh, A. P. *et al.* Plasmodium circumsporozoite protein promotes the development of the liver stages of the parasite. *Cell* **131**, 492–504 (2007).

71. Boddey, J. A., Moritz, R. L., Simpson, R. J. & Cowman, A. F. Role of the Plasmodium Export Element in Trafficking Parasite Proteins to the Infected Erythrocyte. *Traffic* **10**, 285–299 (2009).

72. Chang, H. H. *et al.* N-terminal processing of proteins exported by malaria parasites. *Mol. Biochem. Parasitol.* **160**, 107–115 (2008).

73. Gibson, K. D. & Scheraga, H. A. Predicted conformations for the immunodominant region of the circumsporozoite protein of the human malaria parasite Plasmodium falciparum. *Proc Natl Acad Sci U S A* **83**, 5649–5653 (1986).

74. Guy, A. J. *et al.* Insights into the Immunological Properties of Intrinsically Disordered Malaria Proteins Using Proteome Scale Predictions. *PLoS ONE* **10**, e0141729 (2015).

75. Patra, A. P., Sharma, S. & Ainavarapu, S. R. K. Force Spectroscopy of the Plasmodium falciparum Vaccine Candidate Circumsporozoite Protein Suggests a Mechanically Pliable Repeat Region. *J. Biol. Chem.* **292**, 2110–2119 (2017).

76. Plassmeyer, M. L. *et al.* Structure of the Plasmodium falciparum circumsporozoite protein, a leading malaria vaccine candidate. *J. Biol. Chem.* **284**, 26951–26963 (2009).

77. Zavala, F., Cochrane, A. H., Nardin, E. H., Nussenzweig, R. S. & Nussenzweig, V. Circumsporozoite proteins of malaria parasites contain a single immunodominant region with two or more identical epitopes. *J. Exp. Med.* **157**, 1947–1957 (1983).

78. Julien, J.-P. & Wardemann, H. Antibodies against Plasmodium falciparum malaria at the molecular level. *Nat. Rev. Immunol.* **19**, 761–775 (2019).

79. Oyen, D. *et al.* Structural basis for antibody recognition of the NANP repeats in Plasmodium falciparum circumsporozoite protein. *Proc. Natl. Acad. Sci. U.S.A.* **114**, E10438–E10445 (2017).

80. Ghasparian, A., Moehle, K., Linden, A. & Robinson, J. A. Crystal structure of an NPNA-repeat motif from the circumsporozoite protein of the malaria parasite Plasmodium falciparum. *Chem. Commun. (Camb.)* 174–176 (2006) doi:10.1039/b510812h.

81. Dyson, H. J., Satterthwait, A. C., Lerner, R. A. & Wright, P. E. Conformational preferences of synthetic peptides derived from the immunodominant site of the circumsporozoite protein of Plasmodium falciparum by 1H NMR. *Biochemistry* **29**, 7828–7837 (1990).

82. March, S. *et al.* Micropatterned coculture of primary human hepatocytes and supportive cells for the study of hepatotropic pathogens. *Nat Protoc* **10**, 2027–2053 (2015).

83. Hollingdale, M. R., Nardin, E. H., Tharavanij, S., Schwartz, A. L. & Nussenzweig, R. S. Inhibition of entry of Plasmodium falciparum and P. vivax sporozoites into cultured cells; an in vitro assay of protective antibodies. *J. Immunol.* **132**, 909–913 (1984).

84. Kisalu, N. K. *et al.* A human monoclonal antibody prevents malaria infection by targeting a new site of vulnerability on the parasite. *Nat. Med.* **24**, 408–416 (2018).

85. Wang, L. T. *et al.* A Potent Anti-Malarial Human Monoclonal Antibody Targets Circumsporozoite Protein Minor Repeats and Neutralizes Sporozoites in the Liver. *Immunity* **53**, 733-744.e8 (2020).

86. Amino, R. *et al.* Quantitative imaging of Plasmodium transmission from mosquito to mammal. *Nature Medicine* **12**, 220–224 (2006).

87. Sidjanski, S. & Vanderberg, J. P. Delayed migration of Plasmodium sporozoites from the mosquito bite site to the blood. *Am. J. Trop. Med. Hyg.* **57**, 426–429 (1997).

88. Medica, D. L. & Sinnis, P. Quantitative Dynamics of Plasmodium yoelii Sporozoite Transmission by Infected Anopheline Mosquitoes. *Infection and Immunity* **73**, 4363–4369 (2005).

89. Matsuoka, H., Yoshida, S., Hirai, M. & Ishii, A. A rodent malaria, Plasmodium berghei, is experimentally transmitted to mice by merely probing of infective mosquito, Anopheles stephensi. *Parasitol Int* **51**, 17–23 (2002).

90. Shin, S. C., Vanderberg, J. P. & Terzakis, J. A. Direct infection of hepatocytes by sporozoites of Plasmodium berghei. *J. Protozool.* **29**, 448–454 (1982).

91. Frevert, U. *et al.* Malaria circumsporozoite protein binds to heparan sulfate proteoglycans associated with the surface membrane of hepatocytes. *J. Exp. Med.* **177**, 1287–1298 (1993).

92. Ishino, T., Yano, K., Chinzei, Y. & Yuda, M. Cell-passage activity is required for the malarial parasite to cross the liver sinusoidal cell layer. *PLoS Biol.* **2**, E4 (2004).

93. Ishino, T., Chinzei, Y. & Yuda, M. A Plasmodium sporozoite protein with a membrane attack complex domain is required for breaching the liver sinusoidal cell layer prior to hepatocyte infection. *Cell. Microbiol.* **7**, 199–208 (2005).

94. Baer, K. *et al.* Kupffer cells are obligatory for Plasmodium yoelii sporozoite infection of the liver. *Cell Microbiol* **9**, 397–412 (2007).

95. Tavares, J. *et al.* Role of host cell traversal by the malaria sporozoite during liver infection. *J. Exp. Med.* **210**, 905–915 (2013).

96. Yang, A. S. P. *et al.* Cell Traversal Activity Is Important for Plasmodium falciparum Liver Infection in Humanized Mice. *Cell Rep* **18**, 3105–3116 (2017).

97. Amino, R. *et al.* Host cell traversal is important for progression of the malaria parasite through the dermis to the liver. *Cell Host Microbe* **3**, 88–96 (2008).

98. Aliprandini, E. *et al.* Cytotoxic anti-circumsporozoite antibodies target malaria sporozoites in the host skin. *Nat Microbiol* **3**, 1224–1233 (2018).

99. Vanderberg, J., Nussenzweig, R. & Most, H. Protective immunity produced by the injection of x-irradiated sporozoites of Plasmodium berghei. V. In vitro effects of immune serum on sporozoites. *Mil Med* **134**, 1183–1190 (1969).

100. Cochrane, A. H., Aikawa, M., Jeng, M. & Nussenzweig, R. S. Antibody-induced ultrastructural changes of malarial sporozoites. *J. Immunol.* **116**, 859–867 (1976).

101. Vanderberg, J. P. Studies on the motility of Plasmodium sporozoites. *J. Protozool.* **21**, 527–537 (1974).

102. Vanderberg, J. P. & Frevert, U. Intravital microscopy demonstrating antibody-mediated immobilisation of Plasmodium berghei sporozoites injected into skin by mosquitoes. *International Journal for Parasitology* **34**, 991–996 (2004).

103. Flores-Garcia, Y. *et al.* Antibody-Mediated Protection against *Plasmodium* Sporozoites Begins at the Dermal Inoculation Site. *mBio* **9**, e02194-18, /mbio/9/6/mBio.02194-18.atom (2018).

104. Hopp, C. S. *et al.* Comparative intravital imaging of human and rodent malaria sporozoites reveals the skin is not a species-specific barrier. *EMBO Mol Med* **13**, e11796 (2021).

105. Kebaier, C., Voza, T. & Vanderberg, J. Kinetics of mosquito-injected Plasmodium sporozoites in mice: fewer sporozoites are injected into sporozoite-immunized mice. *PLoS Pathog.* **5**, e1000399 (2009).

106. Espinosa, D. A. *et al.* Proteolytic Cleavage of the Plasmodium falciparum Circumsporozoite Protein Is a Target of Protective Antibodies. *J. Infect. Dis.* **212**, 1111–1119 (2015).

107. Kurtovic, L. *et al.* Human antibodies activate complement against Plasmodium falciparum sporozoites, and are associated with protection against malaria in children. *BMC Med* **16**, 61 (2018).

108. Kurtovic, L. *et al.* Induction and decay of functional complement-fixing antibodies by the RTS,S malaria vaccine in children, and a negative impact of malaria exposure. *BMC Med* **17**, 45 (2019).

109. Behet, M. C. *et al.* The Complement System Contributes to Functional Antibody-Mediated Responses Induced by Immunization with Plasmodium falciparum Malaria Sporozoites. *Infect. Immun.* **86**, (2018).

110. Zenklusen, I. *et al.* Immunization of Malaria-Preexposed Volunteers With PfSPZ Vaccine Elicits Long-Lived IgM Invasion-Inhibitory and Complement-Fixing Antibodies. *J Infect Dis* **217**, 1569–1578 (2018).

111. Winkel, B. M. F. *et al.* Plasmodium sporozoites induce regulatory macrophages. *PLoS Pathog* **16**, e1008799 (2020).

112. Feng, G. *et al.* Mechanisms and targets of Fcγ-receptor mediated immunity to malaria sporozoites. *Nat Commun* **12**, 1742 (2021).

113. Suscovich, T. J. *et al.* Mapping functional humoral correlates of protection against malaria challenge following RTS,S/AS01 vaccination. *Sci Transl Med* **12**, (2020).

114. Seguin, M. C., Ballou, W. R. & Nacy, C. A. Interactions of Plasmodium berghei sporozoites and murine Kupffer cells in vitro. *J Immunol* **143**, 1716–1722 (1989).

115. Rodriguez, M., Lustigman, S., Montero, E., Oksov, Y. & Lobo, C. A. PfRH5: a novel reticulocyte-binding family homolog of plasmodium falciparum that binds to the erythrocyte, and an investigation of its receptor. *PLoS One* **3**, e3300 (2008).

116. Chen, L. *et al.* An EGF-like protein forms a complex with PfRh5 and is required for invasion of human erythrocytes by Plasmodium falciparum. *PLoS Pathog* **7**, e1002199 (2011).

117. Dreyer, A. M. *et al.* Passive immunoprotection of Plasmodium falciparum-infected mice designates the CyRPA as candidate malaria vaccine antigen. *J Immunol* **188**, 6225–6237 (2012).

118. Ragotte, R. J., Higgins, M. K. & Draper, S. J. The RH5-CyRPA-Ripr Complex as a Malaria Vaccine Target. *Trends Parasitol* **36**, 545–559 (2020).

119. Galaway, F., Yu, R., Constantinou, A., Prugnolle, F. & Wright, G. J. Resurrection of the ancestral RH5 invasion ligand provides a molecular explanation for the origin of P. falciparum malaria in humans. *PLoS Biol* **17**, e3000490 (2019).

120. Wright, K. E. *et al.* Structure of malaria invasion protein RH5 with erythrocyte basigin and blocking antibodies. *Nature* **515**, 427–430 (2014).

121. Crosnier, C. *et al.* Basigin is a receptor essential for erythrocyte invasion by Plasmodium falciparum. *Nature* **480**, 534–537 (2011).

122. Chen, L. *et al.* Structural basis for inhibition of erythrocyte invasion by antibodies to Plasmodium falciparum protein CyRPA. *Elife* **6**, e21347 (2017).

123. Favuzza, P. *et al.* Structure of the malaria vaccine candidate antigen CyRPA and its complex with a parasite invasion inhibitory antibody. *Elife* **6**, e20383 (2017).

124. Wong, W. *et al.* Structure of Plasmodium falciparum Rh5-CyRPA-Ripr invasion complex. *Nature* **565**, 118–121 (2019).

125. Gilson, P. R. & Crabb, B. S. Morphology and kinetics of the three distinct phases of red blood cell invasion by Plasmodium falciparum merozoites. *Int J Parasitol* **39**, 91–96 (2009).

126. Cowman, A. F., Tonkin, C. J., Tham, W.-H. & Duraisingh, M. T. The Molecular Basis of Erythrocyte Invasion by Malaria Parasites. *Cell Host Microbe* **22**, 232–245 (2017).

127. Reddy, K. S. *et al.* Multiprotein complex between the GPI-anchored CyRPA with PfRH5 and PfRipr is crucial for Plasmodium falciparum erythrocyte invasion. *Proc Natl Acad Sci U S A* **112**, 1179–1184 (2015).

128. Volz, J. C. *et al.* Essential Role of the PfRh5/PfRipr/CyRPA Complex during Plasmodium falciparum Invasion of Erythrocytes. *Cell Host Microbe* **20**, 60–71 (2016).

129. Srinivasan, P. *et al.* Binding of Plasmodium merozoite proteins RON2 and AMA1 triggers commitment to invasion. *Proc Natl Acad Sci U S A* **108**, 13275–13280 (2011).

130. Healer, J., Crawford, S., Ralph, S., McFadden, G. & Cowman, A. F. Independent translocation of two micronemal proteins in developing Plasmodium falciparum merozoites. *Infect Immun* **70**, 5751–5758 (2002).

131. Keeley, A. & Soldati, D. The glideosome: a molecular machine powering motility and host-cell invasion by Apicomplexa. *Trends Cell Biol* **14**, 528–532 (2004).

132. Cowman, A. F. & Crabb, B. S. Invasion of red blood cells by malaria parasites. *Cell* **124**, 755–766 (2006).

133. Tran, T. M. *et al.* Naturally acquired antibodies specific for Plasmodium falciparum reticulocyte-binding protein homologue 5 inhibit parasite growth and predict protection from malaria. *J Infect Dis* **209**, 789–798 (2014).

134. Chiu, C. Y. H. *et al.* Association of antibodies to Plasmodium falciparum reticulocyte binding protein homolog 5 with protection from clinical malaria. *Front Microbiol* **5**, 314 (2014).

135. Healer, J. *et al.* Neutralising antibodies block the function of Rh5/Ripr/CyRPA complex during invasion of Plasmodium falciparum into human erythrocytes. *Cell. Microbiol.* **21**, e13030 (2019).

136. Richards, J. S. *et al.* Identification and prioritization of merozoite antigens as targets of protective human immunity to Plasmodium falciparum malaria for vaccine and biomarker development. *J Immunol* **191**, 795–809 (2013).

137. Partey, F. D. *et al.* Kinetics of antibody responses to PfRH5-complex antigens in Ghanaian children with Plasmodium falciparum malaria. *PLoS One* **13**, e0198371 (2018).

138. Osier, F. H. *et al.* New antigens for a multicomponent blood-stage malaria vaccine. *Sci Transl Med* **6**, 247ra102 (2014).

139. Douglas, A. D. *et al.* The blood-stage malaria antigen PfRH5 is susceptible to vaccine-inducible cross-strain neutralizing antibody. *Nat Commun* **2**, 601 (2011).

140. Malkin, E. M. *et al.* Phase 1 clinical trial of apical membrane antigen 1: an asexual blood-stage vaccine for Plasmodium falciparum malaria. *Infect Immun* **73**, 3677–3685 (2005).

141. Douglas, A. D. *et al.* A PfRH5-based vaccine is efficacious against heterologous strain blood-stage Plasmodium falciparum infection in aotus monkeys. *Cell Host Microbe* **17**, 130–139 (2015).

142. Mahdi Abdel Hamid, M. *et al.* Vaccination with Plasmodium knowlesi AMA1 formulated in the novel adjuvant co-vaccine HT^{TM} protects against blood-stage challenge in rhesus macaques. *PLoS One* **6**, e20547 (2011).

143. Stephens, R. *et al.* Malaria-specific transgenic CD4(+) T cells protect immunodeficient mice from lethal infection and demonstrate requirement for a protective threshold of antibody production for parasite clearance. *Blood* **106**, 1676–1684 (2005).

144. Douglas, A. D. *et al.* A defined mechanistic correlate of protection against Plasmodium falciparum malaria in non-human primates. *Nat Commun* **10**, 1953 (2019).

145. Alanine, D. G. W. *et al.* Human Antibodies that Slow Erythrocyte Invasion Potentiate Malaria-Neutralizing Antibodies. *Cell* **178**, 216-228.e21 (2019).

146. Douglas, A. D. *et al.* Neutralization of Plasmodium falciparum merozoites by antibodies against PfRH5. *J Immunol* **192**, 245–258 (2014).

147. Favuzza, P. *et al.* Generation of Plasmodium falciparum parasite-inhibitory antibodies by immunization with recombinantly-expressed CyRPA. *Malar J* **15**, 161 (2016).

148. Saunders, K. O. *et al.* Sustained Delivery of a Broadly Neutralizing Antibody in Nonhuman Primates Confers Long-Term Protection against Simian/Human Immunodeficiency Virus Infection. *J Virol* **89**, 5895–5903 (2015).

149. Schiller, Z. A. *et al.* Blocking Borrelia burgdorferi transmission from infected ticks to nonhuman primates with a human monoclonal antibody. *J Clin Invest* **131**, 144843 (2021).

150. Bustamante, L. Y. *et al.* Synergistic malaria vaccine combinations identified by systematic antigen screening. *Proc Natl Acad Sci U S A* **114**, 12045–12050 (2017).

151. Illingworth, J. J. *et al.* Functional Comparison of Blood-Stage Plasmodium falciparum Malaria Vaccine Candidate Antigens. *Front Immunol* **10**, 1254 (2019).

152. Gordon, D. M. *et al.* Safety, immunogenicity, and efficacy of a recombinantly produced Plasmodium falciparum circumsporozoite protein-hepatitis B surface antigen subunit vaccine. *J Infect Dis* **171**, 1576–1585 (1995).

153. Stoute, J. A. *et al.* A preliminary evaluation of a recombinant circumsporozoite protein vaccine against Plasmodium falciparum malaria. RTS,S Malaria Vaccine Evaluation Group. *N. Engl. J. Med.* **336**, 86–91 (1997).

154. RTS,S Clinical Trials Partnership. Efficacy and safety of RTS,S/AS01 malaria vaccine with or without a booster dose in infants and children in Africa: final results of a phase 3, individually randomised, controlled trial. *Lancet* **386**, 31–45 (2015).

155. White, M. T. *et al.* Immunogenicity of the RTS,S/AS01 malaria vaccine and implications for duration of vaccine efficacy: secondary analysis of data from a phase 3 randomised controlled trial. *Lancet Infect Dis* **15**, 1450–1458 (2015).

156. White, M. T. *et al.* A combined analysis of immunogenicity, antibody kinetics and vaccine efficacy from phase 2 trials of the RTS,S malaria vaccine. *BMC Med* **12**, 117 (2014).

157. Bejon, P. *et al.* Efficacy of RTS,S malaria vaccines: individual-participant pooled analysis of phase 2 data. *Lancet Infect Dis* **13**, 319–327 (2013).

158. Sotiriades, D. *Grece Med* 27 (1917).

159. Cohen, S., McGREGOR, I. A. & Carrington, S. Gamma-globulin and acquired immunity to human malaria. *Nature* **192**, 733–737 (1961).

160. Edozien, J. C., Gilles, H. M. & Udeozo, I. O. K. ADULT AND CORD-BLOOD GAMMA-GLOBULIN AND IMMUNITY TO MALARIA IN NIGERIANS. *The Lancet* **280**, 951–955 (1962).

161. McGregor, I. A., Carrington, S. P. & Cohen, S. Treatment of east african P. falciparum malaria with west african human γ-globulin. *Transactions of the Royal Society of Tropical Medicine and Hygiene* **57**, 170–175 (1963).

162. Sabchareon, A. *et al.* Parasitologic and clinical human response to immunoglobulin administration in falciparum malaria. *Am. J. Trop. Med. Hyg.* **45**, 297–308 (1991).

163. Taylor, T. E. *et al.* Intravenous immunoglobulin in the treatment of paediatric cerebral malaria. *Clin Exp Immunol* **90**, 357–362 (1992).

164. Kang, T. H. & Jung, S. T. Boosting therapeutic potency of antibodies by taming Fc domain functions. *Exp. Mol. Med.* **51**, 1–9 (2019).

165. Mackness, B. C. *et al.* Antibody Fc engineering for enhanced neonatal Fc receptor binding and prolonged circulation half-life. *MAbs* **11**, 1276–1288 (2019).

166. Ko, S.-Y. *et al.* Enhanced neonatal Fc receptor function improves protection against primate SHIV infection. *Nature* **514**, 642–645 (2014).

167. Gaudinski, M. R. *et al.* Safety and pharmacokinetics of the Fc-modified HIV-1 human monoclonal antibody VRC01LS: A Phase 1 open-label clinical trial in healthy adults. *PLoS Med.* **15**, e1002493 (2018).

168. Gaudinski, M. R. *et al.* A Monoclonal Antibody for Malaria Prevention. *N Engl J Med* **385**, 803–814 (2021).

169. Lyke, K. E. *et al.* Attenuated PfSPZ Vaccine induces strain-transcending T cells and durable protection against heterologous controlled human malaria infection. *Proc Natl Acad Sci U S A* **114**, 2711–2716 (2017).

170. Seder, R. A. *et al.* Protection against malaria by intravenous immunization with a nonreplicating sporozoite vaccine. *Science* **341**, 1359–1365 (2013).

171. Tan, J. *et al.* Functional human IgA targets a conserved site on malaria sporozoites. *Sci Transl Med* **13**, eabg2344 (2021).

172. Tran, T. M. *et al.* An intensive longitudinal cohort study of Malian children and adults reveals no evidence of acquired immunity to Plasmodium falciparum infection. *Clin Infect Dis* **57**, 40–47 (2013).

173. Minassian, A. M. *et al.* Reduced blood-stage malaria growth and immune correlates in humans following RH5 vaccination. *Med (N Y)* **2**, 701-719.e19 (2021).

174. Espinosa, D. A. *et al.* Robust antibody and CD8+ T-cell responses induced by P. falciparum CSP adsorbed to cationic liposomal adjuvant CAF09 confer sterilizing immunity against experimental rodent malaria infection. *NPJ Vaccines* **2**, (2017).

175. Delemarre-van de Waal, H. A. & de Waal, F. C. [A 2d patient with tropical malaria contracted in a natural way in the Netherlands]. *Ned Tijdschr Geneeskd* **125**, 375–377 (1981).

176. Flores-Garcia, Y. *et al.* Optimization of an in vivo model to study immunity to Plasmodium falciparum pre-erythrocytic stages. *Malar. J.* **18**, 426 (2019).

177. Sattabongkot, J. *et al.* Establishment of a human hepatocyte line that supports in vitro development of the exo-erythrocytic stages of the malaria parasites Plasmodium falciparum and P. vivax. *Am. J. Trop. Med. Hyg.* **74**, 708–715 (2006).

178. Wang, L. T. *et al.* A Potent Anti-Malarial Human Monoclonal Antibody Targets Circumsporozoite Protein Minor Repeats and Neutralizes Sporozoites in the Liver. *Immunity* (2020) doi:10.1016/j.immuni.2020.08.014.

179. Wang, J.-Y. *et al.* Improved expression of secretory and trimeric proteins in mammalian cells via the introduction of a new trimer motif and a mutant of the tPA signal sequence. *Appl Microbiol Biotechnol* **91**, 731–740 (2011).

180. Durocher, Y., Perret, S. & Kamen, A. High-level and high-throughput recombinant protein production by transient transfection of suspension-growing human 293-EBNA1 cells. *Nucleic Acids Res* **30**, E9 (2002).

181. Carbonetti, S. *et al.* A method for the isolation and characterization of functional murine monoclonal antibodies by single B cell cloning. *J Immunol Methods* **448**, 66–73 (2017).

182. Kennedy, M. *et al.* A rapid and scalable density gradient purification method for Plasmodium sporozoites. *Malar J* **11**, 421 (2012).

183. Holm, S. A Simple Sequentially Rejective Multiple Test Procedure. *Scandinavian Journal of Statistics* **6**, 65–70 (1979).

184. Hothorn, T., Hornik, K., Wiel, M. A. van de & Zeileis, A. Implementing a Class of Permutation Tests: The coin Package. *Journal of Statistical Software* **28**, 1–23 (2008).

185. Raghunandan, R. *et al.* Characterization of two in vivo challenge models to measure functional activity of monoclonal antibodies to Plasmodium falciparum circumsporozoite protein. *Malar. J.* **19**, 113 (2020).

186. Kosmidis, I. & Firth, D. Bias reduction in exponential family nonlinear models. *Biometrika* **96**, 793–804 (2009).

187. R Core Team. R: The R Project for Statistical Computing. https://www.r-project.org/.

188. Bates, D., Mächler, M., Bolker, B. & Walker, S. Fitting Linear Mixed-Effects Models Using lme4. *Journal of Statistical Software* **67**, 1–48 (2015).

189. Gelman, A. *et al. arm: Data Analysis Using Regression and Multilevel/Hierarchical Models*. (2020).

190. Wickham, H. *et al.* Welcome to the Tidyverse. *Journal of Open Source Software* **4**, 1686 (2019).

191. Wilke, C. O. *cowplot: Streamlined Plot Theme and Plot Annotations for 'ggplot2'*. (2019).

192. Williams, C. J. *et al.* MolProbity: More and better reference data for improved all-atom structure validation. *Protein Sci* **27**, 293–315 (2018).

193. Chevalier, A. *et al.* Massively parallel de novo protein design for targeted therapeutics. *Nature* **550**, 74–79 (2017).

194. Foquet, L. *et al.* Molecular detection and quantification of Plasmodium falciparum-infected human hepatocytes in chimeric immune-deficient mice. *Malar. J.* **12**, 430 (2013).

195. McCall, M. B. B. *et al.* Infectivity of Plasmodium falciparum sporozoites determines emerging parasitemia in infected volunteers. *Sci Transl Med* **9**, (2017).

196. Alcoser, S. Y. *et al.* Real-time PCR-based assay to quantify the relative amount of human and mouse tissue present in tumor xenografts. *BMC Biotechnol* **11**, 124 (2011).

197. Kisalu, N. K. *et al.* Enhancing durability of CIS43 monoclonal antibody by Fc mutation or AAV delivery for malaria prevention. *JCI Insight* **6**, 143958 (2021).

198. Greenfield, E. A. Single-Cell Cloning of Hybridoma Cells by Limiting Dilution. *Cold Spring Harb Protoc* **2019**, (2019).

199. March, S. *et al.* A microscale human liver platform that supports the hepatic stages of Plasmodium falciparum and vivax. *Cell Host Microbe* **14**, 104–115 (2013).

200. McNamara, H. A. *et al.* Up-regulation of LFA-1 allows liver-resident memory T cells to patrol and remain in the hepatic sinusoids. *Sci Immunol* **2**, (2017).

201. Zhu, J. *et al.* Mining the antibodyome for HIV-1–neutralizing antibodies with next-generation sequencing and phylogenetic pairing of heavy/light chains. *Proc Natl Acad Sci U S A* **110**, 6470–6475 (2013).

202. Ye, J., Ma, N., Madden, T. L. & Ostell, J. M. IgBLAST: an immunoglobulin variable domain sequence analysis tool. *Nucleic Acids Res* **41**, W34-40 (2013).

203. Katoh, K. & Standley, D. M. MAFFT multiple sequence alignment software version 7: improvements in performance and usability. *Mol Biol Evol* **30**, 772–780 (2013).

204. Felsenstein, J. PHYLIP-Phylogeny Inference Package (Version 3.2). *Cladistics* **5**, 164–166 (1989).

205. Kabsch, W. XDS. *Acta Cryst D* **66**, 125–132 (2010).

206. Winn, M. D. *et al.* Overview of the CCP4 suite and current developments. *Acta Crystallogr D Biol Crystallogr* **67**, 235–242 (2011).

207. Liebschner, D. *et al.* Macromolecular structure determination using X-rays, neutrons and electrons: recent developments in Phenix. *Acta Cryst D* **75**, 861–877 (2019).

208. Emsley, P., Lohkamp, B., Scott, W. G. & Cowtan, K. Features and development of Coot. *Acta Cryst D* **66**, 486–501 (2010).

209. Flores-Garcia, Y. *et al.* The P. falciparum CSP repeat region contains three distinct epitopes required for protection by antibodies in vivo. *PLoS Pathog* **17**, e1010042 (2021).

210. Collins, K. A., Snaith, R., Cottingham, M. G., Gilbert, S. C. & Hill, A. V. S. Enhancing protective immunity to malaria with a highly immunogenic virus-like particle vaccine. *Sci Rep* **7**, 46621 (2017).

211. Alving, C. R., Peachman, K. K., Matyas, G. R., Rao, M. & Beck, Z. Army Liposome Formulation (ALF) family of vaccine adjuvants. *Expert Rev Vaccines* **19**, 279–292 (2020).

212. Cho, H. *et al.* Bispecific antibodies targeting distinct regions of the spike protein potently neutralize SARS-CoV-2 variants of concern. *Sci Transl Med* **13**, eabj5413 (2021).

213. Tan, J. *et al.* A public antibody lineage that potently inhibits malaria infection through dual binding to the circumsporozoite protein. *Nat. Med.* **24**, 401–407 (2018).

214. Draper, S. J. & Higgins, M. K. A new site of attack for a malaria vaccine. *Nat. Med.* **24**, 382–383 (2018).

215. Oyen, D. *et al.* Structure and mechanism of monoclonal antibody binding to the junctional epitope of Plasmodium falciparum circumsporozoite protein. *PLoS Pathog.* **16**, e1008373 (2020).

216. National Institute of Allergy and Infectious Diseases (NIAID). First human trial of monoclonal antibody to prevent malaria opens. *National Institutes of Health (NIH)* https://www.nih.gov/news-events/news-releases/first-human-trial-monoclonal-antibody-prevent-malaria-opens (2020).

217. National Institute of Allergy and Infectious Diseases (NIAID). *VRC 612: A Phase 1, Dose Escalation, Open-Label Clinical Trial With Experimental Controlled Human Malaria Infections (CHMI) to Evaluate Safety and Protective Efficacy of an Anti-Malaria Human Monoclonal Antibody,VRC-MALMAB0100-00-AB (CIS43LS), in Healthy, Malaria-Naive Adults*. https://clinicaltrials.gov/ct2/show/NCT04206332 (2020).

218. Johnson, M. Harnessing anti-idiotypic antibody alternatives to advance biotherapeutic pharmacokinetic assays. *Bioanalysis* **12**, 125–128 (2020).

219. Imkeller, K. *et al.* Antihomotypic affinity maturation improves human B cell responses against a repetitive epitope. *Science* **360**, 1358–1362 (2018).

220. Triller, G. *et al.* Natural Parasite Exposure Induces Protective Human Anti-Malarial Antibodies. *Immunity* **47**, 1197-1209.e10 (2017).

221. Rosenberg, R., Wirtz, R. A., Schneider, I. & Burge, R. An estimation of the number of malaria sporozoites ejected by a feeding mosquito. *Trans. R. Soc. Trop. Med. Hyg.* **84**, 209–212 (1990).

222. Ponnudurai, T., Lensen, A. H., van Gemert, G. J., Bolmer, M. G. & Meuwissen, J. H. Feeding behaviour and sporozoite ejection by infected Anopheles stephensi. *Trans. R. Soc. Trop. Med. Hyg.* **85**, 175–180 (1991).

223. Foquet, L. *et al.* Plasmodium falciparum Liver Stage Infection and Transition to Stable Blood Stage Infection in Liver-Humanized and Blood-Humanized FRGN KO Mice Enables

Testing of Blood Stage Inhibitory Antibodies (Reticulocyte-Binding Protein Homolog 5) In Vivo. *Front Immunol* **9**, 524 (2018).

224. Ko, S.-Y. *et al.* Enhanced neonatal Fc receptor function improves protection against primate SHIV infection. *Nature* **514**, 642–645 (2014).
225. Sällberg, M., Hughes, J., Jones, J., Phillips, T. R. & Milich, D. R. A malaria vaccine candidate based on a hepatitis B virus core platform. *Intervirology* **45**, 350–361 (2002).
226. Scally, S. W. *et al.* Rare PfCSP C-terminal antibodies induced by live sporozoite vaccination are ineffective against malaria infection. *J. Exp. Med.* **215**, 63–75 (2018).
227. Mota, M. M. *et al.* Migration of Plasmodium sporozoites through cells before infection. *Science* **291**, 141–144 (2001).
228. Scally, S. W. & Julien, J.-P. Peek-Peak-Pique: Repeating Motifs of Subtle Variance Are Targets for Potent Malaria Antibodies. *Immunity* **48**, 851–854 (2018).
229. Murugan, R. *et al.* Evolution of protective human antibodies against Plasmodium falciparum circumsporozoite protein repeat motifs. *Nat. Med.* **26**, 1135–1145 (2020).
230. Rodríguez-Galán, A. *et al.* An in vitro assay to measure antibody-mediated inhibition of P. berghei sporozoite invasion against P. falciparum antigens. *Sci Rep* **7**, 17011 (2017).
231. Tavares, J. *et al.* Role of host cell traversal by the malaria sporozoite during liver infection. *J. Exp. Med.* **210**, 905–915 (2013).
232. Sidjanski, S. & Vanderberg, J. P. Delayed migration of Plasmodium sporozoites from the mosquito bite site to the blood. *Am. J. Trop. Med. Hyg.* **57**, 426–429 (1997).
233. Krettli, A. U. & Miller, L. H. Malaria: a sporozoite runs through it. *Curr. Biol.* **11**, R409-412 (2001).

234. Frischknecht, F. & Matuschewski, K. Plasmodium Sporozoite Biology. *Cold Spring Harb Perspect Med* **7**, (2017).

235. Julien, J.-P. & Wardemann, H. Antibodies against Plasmodium falciparum malaria at the molecular level. *Nat. Rev. Immunol.* **19**, 761–775 (2019).

236. Murugan, R. *et al.* Clonal selection drives protective memory B cell responses in controlled human malaria infection. *Sci Immunol* **3**, (2018).

237. Murugan, R. *et al.* Evolution of protective human antibodies against Plasmodium falciparum circumsporozoite protein repeat motifs. *Nat. Med.* (2020) doi:10.1038/s41591-020-0881-9.

238. Tan, J., Piccoli, L. & Lanzavecchia, A. The Antibody Response to Plasmodium falciparum: Cues for Vaccine Design and the Discovery of Receptor-Based Antibodies. *Annu. Rev. Immunol.* **37**, 225–246 (2019).

239. Zhou, T. *et al.* Structural basis for broad and potent neutralization of HIV-1 by antibody VRC01. *Science* **329**, 811–817 (2010).

240. Ghasparian, A., Moehle, K., Linden, A. & Robinson, J. A. Crystal structure of an NPNA-repeat motif from the circumsporozoite protein of the malaria parasite Plasmodium falciparum. *Chem. Commun. (Camb.)* 174–176 (2006) doi:10.1039/b510812h.

241. Pholcharee, T. *et al.* Structural and biophysical correlation of anti-NANP antibodies with in vivo protection against P. falciparum. *Nat Commun* **12**, 1063 (2021).

242. Swindells, M. B. *et al.* abYsis: Integrated Antibody Sequence and Structure-Management, Analysis, and Prediction. *J Mol Biol* **429**, 356–364 (2017).

243. Shi, Y. P. *et al.* Natural antibody responses against the non-repeat-sequence-based B-cell epitopes of the Plasmodium falciparum circumsporozoite protein. *Infect. Immun.* **61**, 2425–2433 (1993).

244. Lopez, J. A. *et al.* Recognition of synthetic 104-mer and 102-mer peptides corresponding to N- and C-terminal nonrepeat regions of the Plasmodium falciparum circumsporozoite protein by sera from human donors. *Am. J. Trop. Med. Hyg.* **55**, 424–429 (1996).

245. Roggero, M. A. *et al.* Synthesis and immunological characterization of 104-mer and 102-mer peptides corresponding to the N- and C-terminal regions of the Plasmodium falciparum CS protein. *Molecular Immunology* **32**, 1301–1309 (1995).

246. Del Giudice, G. *et al.* Immunogenicity of a non-repetitive sequence of Plasmodium falciparum circumsporozoite protein in man and mice. *Immunology* **63**, 187–191 (1988).

247. Bongfen, S. E. *et al.* The N-terminal domain of Plasmodium falciparum circumsporozoite protein represents a target of protective immunity. *Vaccine* **27**, 328–335 (2009).

248. Rathore, D. *et al.* An immunologically cryptic epitope of Plasmodium falciparum circumsporozoite protein facilitates liver cell recognition and induces protective antibodies that block liver cell invasion. *J. Biol. Chem.* **280**, 20524–20529 (2005).

249. Thai, E. *et al.* A high-affinity antibody against the CSP N-terminal domain lacks Plasmodium falciparum inhibitory activity. *J Exp Med* **217**, (2020).

250. Roggero, M. A. *et al.* Synthesis and immunological characterization of 104-mer and 102-mer peptides corresponding to the N- and C-terminal regions of the Plasmodium falciparum CS protein. *Molecular Immunology* **32**, 1301–1309 (1995).

251. Chaudhury, S. *et al.* The biological function of antibodies induced by the RTS,S/AS01 malaria vaccine candidate is determined by their fine specificity. *Malar J* **15**, (2016).

252. Dobaño, C. *et al.* Concentration and avidity of antibodies to different circumsporozoite epitopes correlate with RTS,S/AS01E malaria vaccine efficacy. *Nat Commun* **10**, 2174 (2019).

253. Chaudhury, S. *et al.* Breadth of humoral immune responses to the C-terminus of the circumsporozoite protein is associated with protective efficacy induced by the RTS,S malaria vaccine. *Vaccine* (2021) doi:10.1016/j.vaccine.2020.12.055.

254. Suscovich, T. J. *et al.* Mapping functional humoral correlates of protection against malaria challenge following RTS,S/AS01 vaccination. *Sci Transl Med* **12**, (2020).

255. Chaudhury, S. *et al.* Delayed fractional dose regimen of the RTS,S/AS01 malaria vaccine candidate enhances an IgG4 response that inhibits serum opsonophagocytosis. *Sci Rep* **7**, 7998 (2017).

256. Ubillos, I. *et al.* Baseline exposure, antibody subclass, and hepatitis B response differentially affect malaria protective immunity following RTS,S/AS01E vaccination in African children. *BMC Med* **16**, 197 (2018).

257. Neafsey, D. E. *et al.* Genetic Diversity and Protective Efficacy of the RTS,S/AS01 Malaria Vaccine. *N. Engl. J. Med.* **373**, 2025–2037 (2015).

258. Pringle, J. C. *et al.* RTS,S/AS01 malaria vaccine mismatch observed among Plasmodium falciparum isolates from southern and central Africa and globally. *Sci Rep* **8**, 6622 (2018).

259. Kwong, P. D. *et al.* HIV-1 evades antibody-mediated neutralization through conformational masking of receptor-binding sites. *Nature* **420**, 678–682 (2002).

260. Mendoza, P. *et al.* Combination therapy with anti-HIV-1 antibodies maintains viral suppression. *Nature* **561**, 479–484 (2018).

261. Ramirez Valdez, K. P. *et al.* Complementary and synergistic activities of anti-V3, CD4bs and CD4i antibodies derived from a single individual can cover a wide range of HIV-1 strains. *Virology* **475**, 187–203 (2015).

262. Wu, X. *et al.* Rational design of envelope identifies broadly neutralizing human monoclonal antibodies to HIV-1. *Science* **329**, 856–861 (2010).

263. Stewart, M. J. & Vanderberg, J. P. Malaria sporozoites release circumsporozoite protein from their apical end and translocate it along their surface. *J. Protozool.* **38**, 411–421 (1991).

264. Murphy, K. P., Bhakuni, V., Xie, D. & Freire, E. Molecular basis of co-operativity in protein folding. III. Structural identification of cooperative folding units and folding intermediates. *J Mol Biol* **227**, 293–306 (1992).

265. Gómez, J., Hilser, V. J., Xie, D. & Freire, E. The heat capacity of proteins. *Proteins* **22**, 404–412 (1995).

266. Alanine, D. G. W. *et al.* Human Antibodies that Slow Erythrocyte Invasion Potentiate Malaria-Neutralizing Antibodies. *Cell* **178**, 216-228.e21 (2019).

267. Lyke, K. E. *et al.* Attenuated PfSPZ Vaccine induces strain-transcending T cells and durable protection against heterologous controlled human malaria infection. *Proc Natl Acad Sci U S A* **114**, 2711–2716 (2017).

268. Herrera, R. *et al.* Reversible Conformational Change in the Plasmodium falciparum Circumsporozoite Protein Masks Its Adhesion Domains. *Infection and Immunity* **83**, 3771–3780 (2015).

269. McNamara, H. A. *et al.* Antibody Feedback Limits the Expansion of B Cell Responses to Malaria Vaccination but Drives Diversification of the Humoral Response. *Cell Host Microbe* **28**, 572-585.e7 (2020).

270. Mulangu, S. *et al.* A Randomized, Controlled Trial of Ebola Virus Disease Therapeutics. *N Engl J Med* **381**, 2293–2303 (2019).

271. Weinreich, D. M. *et al.* REGN-COV2, a Neutralizing Antibody Cocktail, in Outpatients with Covid-19. *N Engl J Med* **384**, 238–251 (2021).

272. Moorthy, V. S. & Ballou, W. R. Immunological mechanisms underlying protection mediated by RTS,S: a review of the available data. *Malar J* **8**, 312 (2009).

273. Tran, T. M. *et al.* A Molecular Signature in Blood Reveals a Role for p53 in Regulating Malaria-Induced Inflammation. *Immunity* **51**, 750-765.e10 (2019).

274. Sheehy, S. H. *et al.* Phase Ia clinical evaluation of the Plasmodium falciparum blood-stage antigen MSP1 in ChAd63 and MVA vaccine vectors. *Mol Ther* **19**, 2269–2276 (2011).

275. Zavala, F., Cochrane, A. H., Nardin, E. H., Nussenzweig, R. S. & Nussenzweig, V. Circumsporozoite proteins of malaria parasites contain a single immunodominant region with two or more identical epitopes. *J. Exp. Med.* **157**, 1947–1957 (1983).

Appendices

rPfCSP Construct	MW (Da)	Ext. Coeff. ($M^{-1}cm^{-1}$)	Abs 0.1% (=1 g/l)
WT	41500.81	29910	0.721
ΔABCD	41384.65	29910	0.723
ΔABC	41413.69	29910	0.722
ΔABD	41413.69	29910	0.722
ΔACD	41413.69	29910	0.722
ΔBCD	41413.69	29910	0.722
ΔAB	41442.73	29910	0.722
ΔAC	41442.73	29910	0.722
ΔAD	41442.73	29910	0.722
ΔBC	41442.73	29910	0.722
ΔBD	41442.73	29910	0.722
ΔCD	41442.73	29910	0.722
ΔA	41471.77	29910	0.721
ΔB	41471.77	29910	0.721
ΔC	41471.77	29910	0.721
ΔD	41471.77	29910	0.721

Appendix 1: rPfCSP NVDP repeat mutants molecular attributes. Molecular weight (MW), extinction coefficient (ext. coeff.), and absorbance (Abs) assuming all pairs of Cys residues are reduced for the sixteen constructs in Figure 3.13 calculated using ExPASy ProtParam.

mAb	Description of mAb-Bound SPZ Morphologies
VRC01	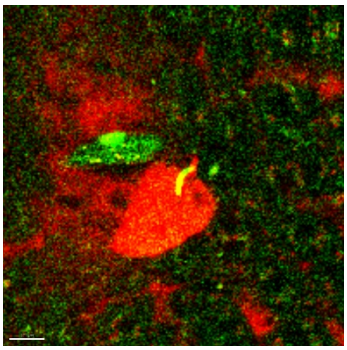 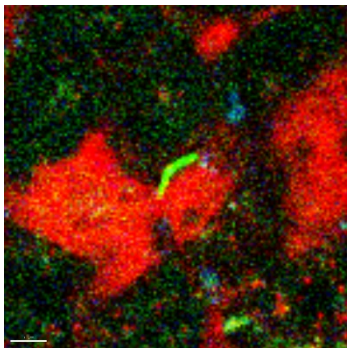 *SPZ are long, crescentic, and highly motile. They migrate freely between and through the liver stroma and hepatocytes. SPZ fluorescence is high, and they maintain a smooth surface.*
CIS43	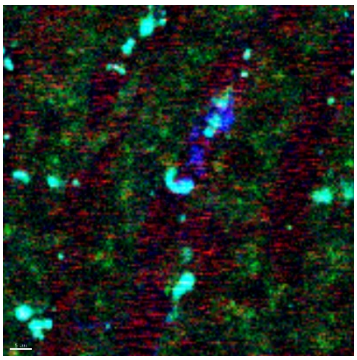 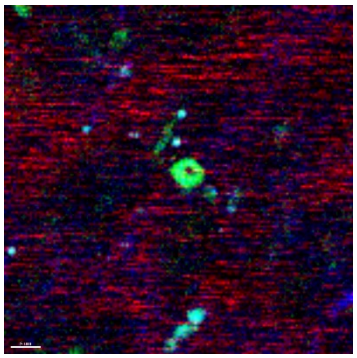 *SPZ bend into a circular morphology, seeming to wrap upon themselves and the leading edges become rounded. Most SPZ motility is lost, and few seem to escape the vasculature. The ability to traverse is also inhibited. Many of the parasites remain bound by antibody within the hepatocyte but are still able to traverse or establish active infection.*
L9	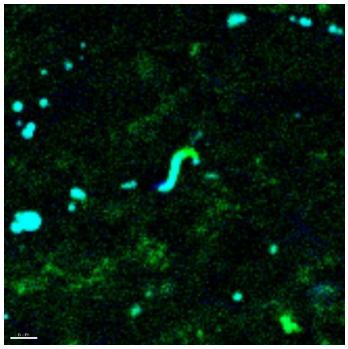 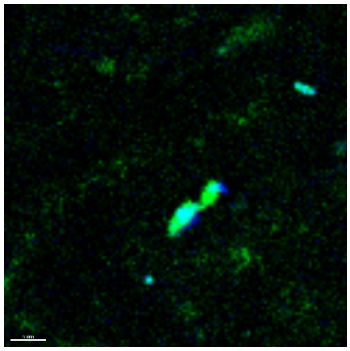 *SPZ change morphology substantially. The surface becomes ruffled and PfCSP seems to shed and collect at the tip of the parasite. The parasite develops kinks within its structure and bends sharply along its borders. It loses its normal wavy or straight morphology.*
mAb10	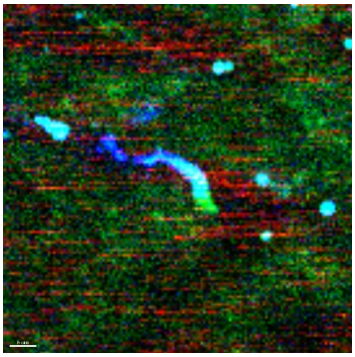 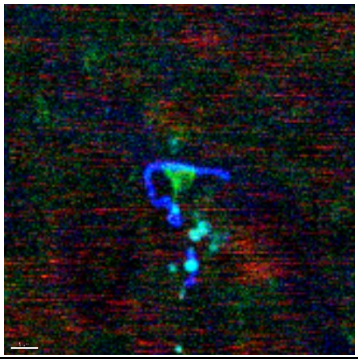 *SPZ seem to become elongated. The bound PfCSP sheds off from the non-leading end. They lose motility and become ruffled. Many SPZ remain bound by antibody within the hepatocyte but are still able to traverse or establish active infection.*
MGU12	*The parasite sheds PfCSP as it enters hepatocytes; however, it does not continue to be bound by antibody. Instead, it leaves the shed PfCSP outside the hepatocyte, and*

	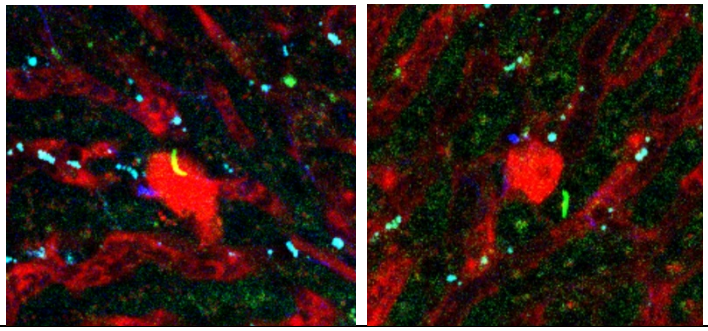	*continues to traverse with little binding to mAb. SPZ appearance is smooth, and its shape is curved.*
1210	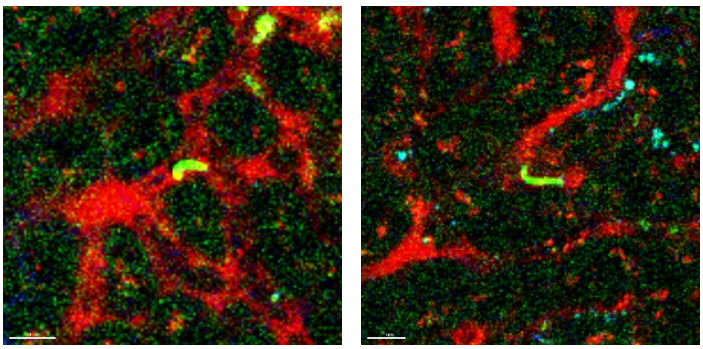	*SPZ appears shorter, curved, and smooth. Few phenotypic changes.*
311	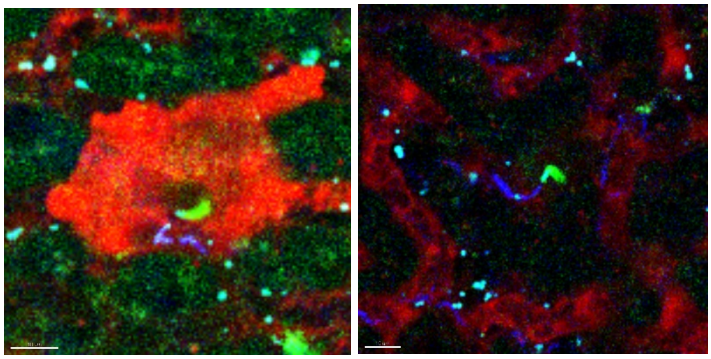	*SPZ become very smooth and curved. They also develop long tails of shed PfCSP. They maintain the ability to traverse hepatocytes; however, the ability to establish active infection is inhibited.*
317	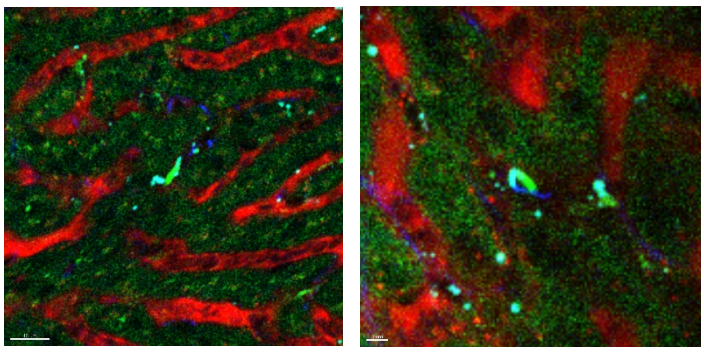	*SPZ become ruffled, kinked along their axis, and develop small shed PfCSP tails. As they enter hepatocytes, they commonly begin to fragment and cannot enter the hepatocyte completely. The mobility of the parasite is substantially inhibited and its ability to leave the vasculature is substantially inhibited.*

Appendix 2: Subjective observations of the effect of PfCSP mAbs on SPZ morphologies in the liver. Representative images of Pb-PfCSP-SPZ expressing GFP bound by indicated AF405-labeled PfCSP mAb in the livers of mice (scale bars: 10 μm). Subjective descriptions of the morphologies of mAb-bound SPZ are detailed; MGG4 was excluded from this analysis.

	apo-L9	$F10_HL9_K$-NANPNVDP	$L9_HF10_K$-NANPNVDP
X-ray Source	ALS 5.0.2	ALS 5.0.2	APS 19-ID
Data collection			
Space group	I222	$P12_11$	$P2_12_12_1$
Cell dimensions			
a, *b*, *c* (Å)	67.964, 117.67, 143.665	42.787, 84.944, 64.243	71.503, 85.817, 145.456
α, β, γ (°)	90, 90, 90	90, 103.23, 90	90, 90, 90
Resolution (Å)	35.92-2.98 (3.087-2.98)	41.65-1.89 (1.958-1.89)	42.91-2.23 (2.31-2.23)
R_{merge}[a]	0.018 (0.267)	0.022 (0.202)	0.042 (0.347)
<I/σ(I)>	18.27 (2.35)	12.92 (2.64)	9.36 (2.28)
$CC_{1/2}$	0.999 (0.831)	0.999 (0.908)	0.998 (0.711)
Completeness (%)	99.32 (100)	93.60 (67.83)	99.49 (97.82)
Redundancy	2.0 (2.0)	1.9 (1.7)	2.0 (2.0)
Refinement			
Resolution (Å)	35.92-2.98 (3.10-2.98)	41.65-1.89 (1.91-1.89)	42.91-2.23 (2.28-2.23)
No. unique reflections	12065 (1207)	33535 (2404)	44164 (4271)
R_{work}[b]/R_{free}[c]	19.89/25.00 (30.05/38.09)	16.11/20.40 (24.09/28.91)	18.90/23.84 (25.40/32.56)
No. atoms	3232	3584	7096
Protein	3229	3349	6658
Water	3	218	434
Ligand	0	17	4
B-factors (Å^2)	113.2	42.18	40.78
Protein	113.24	41.85	40.66
Water	72.34	46.07	42.54
Ligand		57.28	55.58
RMS bond length (Å)	0.006	0.015	0.003
RMS bond angle (°)	1.05	1.31	0.57
Ramachadran Plot Statistics[d]			
Residues	425	438	873
Most Favored region (%)	94.27	97.20	96.97
Allowed Region (%)	5.73	2.57	2.80
Disallowed Region (%)	0.00	0.23	0.23
Clashscore	14.42	2.41	2.44
PDB ID	**7RQP**	**7RQQ**	**7RQR**

Appendix 3: Data collection and refinement statistics for crystal structures. [a] $R_{merge} = [\sum_h\sum_i|I_h - I_{hi}|/\sum_h\sum_i I_{hi}]$ where I_h is the mean of I_{hi} observations of reflection *h*. Numbers in parenthesis represent highest resolution shell. [b] R_{factor} and [c] $R_{free} = \sum||F_{obs}| - |F_{calc}|| / \sum|F_{obs}|$ x 100 for 95% of recorded data (R_{factor}) or 5% data (R_{free}). [d] Calculated using Williams et al., 2018[192]